

Physics Division Annual Report 2006



About the Cover

Students and teachers from the first "Rickover High School Experience", a week long summer camp for top academic students from the Rickover Naval Academy, a magnet school in downtown Chicago. The school was held in the Physics Division and covered "hands on" experiments, lectures, tours, and career discussions. In future years the school will expand to cover Chemistry and Biology, and have participation from other schools.

About Argonne National Laboratory

Argonne is a U.S. Department of Energy laboratory managed by UChicago Argonne, LLC under contract DE-AC02-06CH11357. The Laboratory's main facility is outside Chicago, at 9700 South Cass Avenue, Argonne, Illinois 60439. For information about Argonne, see www.anl.gov.

Availability of This Report

This report is available, at no cost, at <http://www.osti.gov/bridge>. It is also available on paper to the U.S. Department of Energy and its contractors, for a processing fee, from:

U.S. Department of Energy
Office of Scientific and Technical Information
P.O. Box 62
Oak Ridge, TN 37831-0062
phone (865) 576-8401
fax (865) 576-5728
reports@adonis.osti.gov

Disclaimer

This report was prepared as an account of work sponsored by an agency of the United States Government. Neither the United States Government nor any agency thereof, nor UChicago Argonne, LLC, nor any of their employees or officers, makes any warranty, express or implied, or assumes any legal liability or responsibility for the accuracy, completeness, or usefulness of any information, apparatus, product, or process disclosed, or represents that its use would not infringe privately owned rights. Reference herein to any specific commercial product, process, or service by trade name, trademark, manufacturer, or otherwise, does not necessarily constitute or imply its endorsement, recommendation, or favoring by the United States Government or any agency thereof. The views and opinions of document authors expressed herein do not necessarily state or reflect those of the United States Government or any agency thereof, Argonne National Laboratory, or UChicago Argonne, LLC.

ANL-07/29

ARGONNE NATIONAL LABORATORY
9700 S. Cass Avenue
Argonne, Illinois 60439-4801

**PHYSICS DIVISION ANNUAL REPORT
2006**

Robert V. F. Janssens
Director

December 2007

Preceding Annual Reports

ANL-04/22 2003

ANL-05/61 2004

ANL-06/53 2005

Edited by Jeannie Glover

FOREWORD

This report highlights the activities of the Physics Division of Argonne National Laboratory in 2006. The Division's programs include the operation as a national user facility of ATLAS, the Argonne Tandem Linear Accelerator System, research in nuclear structure and reactions, nuclear astrophysics, nuclear theory, investigations in medium-energy nuclear physics as well as research and development in accelerator technology. The mission of nuclear physics is to understand the origin, evolution and structure of baryonic matter in the universe – the core of matter, the fuel of stars, and the basic constituent of life itself. The Division's research focuses on innovative new ways to address this mission.

The cover of this report illustrates a new initiative in the Division: the one-week summer school for high school students from the Rickover Naval Academy, a magnet school in the Chicago Public Schools system. This one-week program was organized by members of the Division with the aim of exposing the students to the potential and the excitement of a scientific career through active participation in a number of activities. The opportunities ranged from hands on experiments to lectures about contemporary physics issues, from presentations by scientists about their careers to tours of some of Argonne's main research facilities. The Division views education as a key part of its mission and as such is involved in many other programs at the undergraduate, graduate and post-doctoral levels, mostly coordinated by Argonne's Division of Educational Programs. This report also highlights efforts towards increasing the number and quality of minority students in science.

During 2006, progress towards the Californium Rare Ion Breeder Upgrade (CARIBU) has been brisk. This project, with a 2009 completion date, will enhance the research potential at ATLAS by making hundreds of neutron-rich nuclei available for research at energies in the vicinity of the Coulomb barrier. As this report shows, the design of most major components has been completed and the project is moving into the production phase.

Argonne also continues to lead in the development of new technical concepts required for an advanced exotic beam facility. Highlights of developments during 2006 are too numerous to be listed here, but include the initial operation of a new clean room and surface processing facility for superconducting cavities, a joint venture with Fermilab, full power tests of the prototype module of a cw RFQ for the high-power driver linac, and the construction of a dedicated facility for high-intensity tests of a large-scale prototype gas catcher.

Notable results from ATLAS include the discovery of the first excited state in ^{101}Sn , which provides the first experimental information on the energy separation between the neutron $d_{5/2}$ and $g_{7/2}$ single-particle orbits outside doubly-magic ^{100}Sn , and the completion of work related to the determination of the E1 component of the $^{12}\text{C}(\alpha,\gamma)^{16}\text{O}$ reaction rate at energies essential for nuclear astrophysics. The impact of the hindrance of fusion at extreme sub-barrier energies, a phenomenon discovered at ATLAS a few years ago, on reactions of importance in astrophysics such as $^{12}\text{C} + ^{12,13}\text{C}$, $^{12}\text{C} + ^{16}\text{O}$, and $^{16}\text{O} + ^{16}\text{O}$ has been quantified. High-precision mass measurements of neutron-rich fission fragments in the $A \sim 140$ region with the Canadian Penning Trap suggest that the neutron drip line may not be located as far out in neutron number as previously thought.

In medium-energy physics, preparations to search for an electric dipole moment in ^{225}Ra have advanced considerably: not only were ^{225}Ra atoms optically trapped, but the beneficial effect of blackbody radiation on the trap was discovered. Preparations are well underway for a super-Rosenbluth measurement of electron-proton elastic scattering. The ultimate goal of this program is the elucidation of the existing discrepancies between the results obtained with this technique and those derived from polarization transfer for the charge and magnetization distributions of the proton. Preliminary results from experiment E03-103 at Jefferson Laboratory indicate that the EMC effect in ^4He is nearly identical to that in ^{12}C , suggesting that the nuclear dependence of this effect scales with density rather than mass.

In nuclear theory, Green function quantum Monte Carlo calculations of the rms radii of the helium isotopes were extended to ^8He in preparation for an upcoming experiment. In an effort to account for the hindrance of fusion between complex nuclei, it was shown that this phenomenon can be understood in a coupled-channels approach by using an ion-ion potential in the entrance channel that has a shallow pocket, linked to nuclear incompressibility. At the level of quantum chromodynamics, important progress continues to be made using the Dyson-Schwinger equations. For example, a constraint on the convergence radius of chiral perturbation theory was developed and a prediction made for the ratio of the neutron electric and magnetic form factors. At the level of meson and baryon degrees of freedom, efforts to develop a dynamical coupled-channels model have progressed to the point where hadronic interactions have been determined from the fitting of pion-nucleon scattering data up to 2 GeV. The group also continues to play the lead role in directing the Excited Baryon Analysis Center at Jefferson Laboratory.

The progress that has been made in meeting the exciting intellectual challenges of modern Nuclear Physics reflects the talents and dedication of the staff of the Physics Division as well as that of the many visitors and students who bring so much to the research. The year 2006 was a particularly challenging one from the fiscal point of view, and this report is testimony to the resourcefulness of everyone. In particular, the Division owes a debt of gratitude to its Director during these challenging times, Don Geesaman. With vision and enthusiasm he kept the focus of everyone on the physics issues at hand.



Robert V. F. Janssens, Director

TABLE OF CONTENTS

	<u>Page</u>
I. LOW-ENERGY NUCLEAR PHYSICS RESEARCH	1
A. REACTIONS OF ASTROPHYSICAL IMPORTANCE	3
a.1. Expectations for ^{12}C and ^{16}O Induced Fusion Cross Sections at Energies of Astrophysical Interest	3
a.2. A New Measurement of the E1 Component of the $^{12}\text{C}(\alpha,\gamma)^{16}\text{O}$ Cross Section at Low Energies	4
a.3. The Branching Ratio of the Subthreshold 1^- State in the β -Decay of ^{16}N	7
a.4. Experiments to Further the Understanding of the Triple-Alpha Process in Hot Astrophysical Scenarios.....	8
a.5. Study of the $^{57}\text{Fe}(d,p)^{58}\text{Fe}$ Reaction in Inverse Kinematics as Surrogate to an (n,γ) Reaction	10
a.6. The Spin of the 2.645 MeV State in ^{20}Na	12
a.7. Improved Measurement of the ^{44}Ti Half-Life from a 14-Year Long Study	14
a.8. Ultra-Sensitive Detection of the p -Process Nuclide ^{146}Sm	17
B. WEAK INTERACTIONS	19
b.1. β -Decay of $^{69,70,71}\text{Kr}$	19
b.2. Progress at the Beta-Decay Paul Trap	19
b.3. Nuclear Structure Relevant to Neutrinoless Double Beta Decay: ^{76}Ge and ^{76}Se	21
C. SPECTROSCOPY OF VERY HEAVY ELEMENTS	25
c.1. Two-Quasiparticle States in ^{254}No and the Stability of Superheavy Nuclei.....	25
c.2. $K = 8^-$ Isomers and $K = 2^-$ Octupole Bands in ^{252}No and $N = 150$ Isotones	26
c.3. Octupole Strength in the $^{238,240,242}\text{Pu}$ Nuclei	28
c.4. Measurements of the ^{246}Cm Half-Life	30
D. STRUCTURE OF NUCLEI FAR FROM STABILITY	31
d.1. Neutron-Rich Nuclei.....	31
d.1.1. Is the Nuclear Spin-Orbit Interaction Changing with Neutron Excess?.....	31
d.1.2. Excited States in the Ca Isotopes Towards “Doubly-Magic” ^{54}Ca : β Decay of $^{51-53}\text{K}$	33
d.1.3. Shell Model States in Neutron-Rich Potassium Isotopes	34
d.1.4. Yrast Structure of Neutron-Rich ^{51}Ca	36

d.1.5.	One-Neutron Knockout in the Vicinity of the $N = 32$ Sub-Shell Closure: ${}^9\text{Be}({}^{57}\text{Cr}, {}^{56}\text{Cr} + \gamma)\text{X}$	38
d.1.6.	One-Particle Excitations Outside the ${}^{54}\text{Ti}$ Semi-Magic Core: The ${}^{55}\text{V}$ and ${}^{55}\text{Ti}$ Yrast Structures	38
d.1.7.	Structure of the Even-Even Neutron-Rich ${}^{56,58,60}\text{Cr}$ Isotopes	40
d.1.8.	Yrast Structures in the Neutron-Rich Isotopes ${}^{59,60}\text{Fe}$ and the Role of the $g_{9/2}$ Orbital	41
d.1.9.	Deep Inelastic Reaction Studies with Gammasphere: The Structure of ${}^{61}\text{Fe}$	41
d.1.10.	Deep Inelastic Reaction Studies with Gammasphere: The Structure of ${}^{64}\text{Fe}$	42
d.1.11.	Study of $N = 50$ Nuclei Near ${}^{78}\text{Ni}$ Using Deep Inelastic Reactions	43
d.1.12.	Structure of Neutron-Rich Zn Isotopes.....	45
d.1.13.	Beta-Decay Studies of Neutron-Rich Fission Products for Advanced Fuel Cycle Applications.....	47
d.1.14.	Multi-Quasiparticle K-Isomers in ${}^{174}\text{Lu}$ and Neutron-Rich ${}^{172,174}\text{Er}$	48
d.2.	Proton-Rich Nuclei	48
d.2.1.	Single-Neutron States in ${}^{101}\text{Sn}$	48
d.2.2.	Isospin Symmetry of Odd-Odd Mirror Nuclei: Identification of Excited States in ${}^{48}\text{Mn}$ and a Comparison to the Mirror Nucleus ${}^{48}\text{V}$	50
d.2.3.	Coulomb Shifts and Shape Changes in the Mass 70 Region	51
d.2.4.	Shapes and Triaxiality of ${}^{74}\text{Kr}$	52
d.2.5.	$T = 1$ States in ${}^{74}\text{Rb}$ and Their ${}^{74}\text{Kr}$ Analogs	52
d.2.6.	Mapping the Periphery of Deformation in the $A \sim 80$ Region: A Study of ${}^{83}\text{Nb}$	52
d.2.7.	Effect of a Triaxial Nuclear Shape on Proton Tunneling in ${}^{145}\text{Tm}$	53
d.2.8.	Multiple Band Structures in ${}^{169}\text{Ta}$	54
d.2.9.	Reflection-Asymmetric Tidal Waves in ${}^{220}\text{Th}$	54
E.	OTHER NUCLEAR STRUCTURE RESEARCH	57
e.1.	Rotational Damping, Ridges and the Quasicontinuum of γ Rays in ${}^{152}\text{Dy}$	57
e.2.	Rotational Damping, Ridges and the Quasicontinuum of γ Rays in ${}^{194}\text{Hg}$	58
e.3.	Understanding the Origin of Ergodic Superdeformed Bands	59
e.4.	Triaxial Strongly Deformed Bands in ${}^{163}\text{Tm}$	61
e.5.	Quantifying the Level of Isospin Mixing in the $A = 31$ Mirror Nuclei.....	63
F.	THE PHOBOS EXPERIMENT AT RHIC	67
f.1.	The Phobos Experiment at RHIC	67
f.1.1.	System Size, Energy, Pseudorapidity, and Centrality Dependence of Elliptic Flow	67
f.1.2.	Elliptic Flow Fluctuations in Au + Au Collisions at 200 GeV	68
f.1.3.	Identified Hadron Transverse Momentum Spectra in AuAu Collisions at 62.4 GeV	69

G.	REACTION MECHANISM STUDIES	71
g.1.	Radius-of-Curvature of the S Factor Maximum in Sub-Barrier Fusion Hindrance	71
H.	HIGH-PRECISION AND HIGH-SENSITIVITY EXPERIMENTS	75
h.1.	High-Precision Q -Value Measurements on Superalloyed Fermi Emitters	75
h.2.	Mass Measurements of Heavy Fission Fragments Using the CPT Mass Spectrometer	76
h.3.	A Bragg Scattering Method to Search for the Neutron Electric Dipole Moment	78
I.	DEVELOPMENT OF NEW EXPERIMENTAL EQUIPMENT	81
i.1.	HELIOS – A Solenoidal Spectrometer for Inverse Reactions	81
i.2.	A High Resolution Isobar Separator for the CARIBU Project	82
i.3.	GRETINA Progress	82
i.4.	Polarization Experiment at Lawrence Berkeley National Laboratory	82
i.5.	Digital Waveform Analysis of Signals from the Twin-Ionization Chamber	84
i.6.	Argonne Implantation-Decay Array – Status Report	85
i.7.	A Comparison of Performance of High Purity Germanium (HPGe) DSSDs with Different Electrode Technologies	87
i.8.	Development of a Portable Gamma Array, MISTI, for Homeland Security Use	90
i.9.	Gammasphere Operations	91
i.10.	Nuclear Target Development	91
J.	ATLAS USER PROGRAM	93
j.1.	ATLAS User Program	93
j.2.	Experiments Involving Outside Users	93
j.3.	Renovation of the ATLAS Data Room	97
II.	OPERATION AND DEVELOPMENT OF ATLAS	99
A.	OPERATION OF THE ACCELERATOR	101
a.1.	Operations Summary	101

B.	DEVELOPMENTS RELATED TO ATLAS	103
b.1.	Status of the ECR Ion Sources	103
b.1.1.	Refinement of the Sputter Technique	103
b.1.2.	Source Liner Development	104
b.2.	ATLAS Control System	104
b.2.1.	ATLAS Operations Databases and Communication Improvements	104
b.2.2.	ATLAS Hardware Upgrade Project	105
b.3.	ATLAS Electronics	106
b.3.1.	RF Amplifier Replacement	106
b.3.2.	Tandem Electronics Upgrade	106
b.4.	Slow Tuner System with High Slew Rate	107
b.5.	ATLAS Cryogenic System	108
b.5.1.	Installation of an Additional 2800 Refrigerator	108
b.6.	A 50-kV RF Chopper for In-Flight RIB Beams	110
b.7.	Californium Rare Ion Breeder Upgrade Project (CARIBU)	110
III.	ACCELERATOR PHYSICS AND EXOTIC BEAM TECHNOLOGY	117
A.	SUPERCONDUCTING RF	119
a.1.	Joint ANL/FNAL Superconducting Cavity Surface Processing Facility (SCSPF)	119
a.2.	Fast Mechanical Tuner Development for AEBL	120
a.3.	Cavities and Cryomodule for the ATLAS Upgrade	122
B.	BEAM DYNAMICS AND INJECTORS	125
b.1.	Development and Test of a Grid-Less Multi-Harmonic Buncher	125
b.2.	High Power Tests of a 57-MHz CW RFQ	126
b.3.	Production of a ^{209}Bi Beam in an All Permanent Magnet ECR Ion Source	127
b.4.	High Current Regime of an All Permanent Magnet ECR Ion Source	129
b.5.	Scintillator Screen Based CW Beam Emittance Measurements	129
b.6.	A Parallel 3D Poisson Solver in Cylindrical Coordinates	131
b.7.	Concept for an Ion LINAC for the Future Electron-Ion Collider	133
b.8.	Developments Related to the Low-Q Post-Accelerator	135
b.9.	Realistic Corrective Steering in the Front-End of the Fermilab Proton Driver Linac	137
b.10.	First Track Simulations of the SNS Linac	139
b.11.	Automatic Transverse Tuning of a Multiple-Charge-State Heavy-Ion Beam	142

C.	RARE ISOTOPE PRODUCTION AND SEPARATION	145
c.1.	Development of a Windowless Liquid Lithium Stripper.....	145
c.2.	Fragment Separator Design.....	149
c.3.	Effects of the Wedge Absorber in Fragment Separators	151
c.4.	Large Aperture Magnet Maps to Optics Maps	153
c.5.	Development of Uranium Carbide Material for High Power ISOL Applications	156
c.6.	A Study of the Cyclotron Gas Stopper Concept.....	158
c.7.	The High-Intensity AEBL/RIA Gas Catcher Test at ATLAS	159
IV.	MEDIUM-ENERGY NUCLEAR PHYSICS RESEARCH	163
A.	HADRON PROPERTIES.....	165
a.1.	Precision Measurements of the Proton Electromagnetic Form Factors and Two-Photon Exchange Effects	165
a.2.	Parity Violating Electron-Proton Scattering and the Strangeness Content of the Nucleon.....	166
a.3.	The Charged Pion Form Factor.....	167
a.4.	Duality and Separated Structure Functions of Nucleons and Nuclei.....	168
a.5.	Search for Additional Pentaquark States at JLab.....	169
B.	HADRONS IN THE NUCLEAR MEDIUM.....	171
b.1.	Measurement of the EMC Effect in Very Light Nuclei.....	171
b.2.	Search for the Onset of Color Transparency: JLab E02-110 Experiment	172
b.3.	Study of Color Transparency in Exclusive Vector Meson Electroproduction Off Nuclei: JLab E12-06-106 Experiment.....	174
b.4.	Search for Color Transparency in Pion Electroproduction.....	175
b.5.	Dynamics of Hadronization from Nuclear Semi-Inclusive Deep-Inelastic Scattering: JLab E02-104 Experiment.....	176
b.6.	Quark Propagation and Hadron Formation: JLab E12-06-117 Experiment	178
b.7.	Measurement of High Momentum Nucleons in Nuclei.....	180
b.8.	Short Range Correlations in Nuclei	180
b.9.	Mapping Out the Distribution of Super-Fast Quarks in Nuclei.....	181
C.	QUARK STRUCTURE OF MATTER.....	183
c.1.	Studies of Nucleon Spin Structure and Related Measurements of Deep-Inelastic Scattering at HERA	183
c.1.1.	Commissioning and Operation of the HERMES Recoil Detector.....	184
c.1.2.	Strange Quark Parton Distributions in the Proton from Semi-Inclusive Deep-Inelastic Scattering on the Deuteron	185
c.1.3.	Inclusive Longitudinal Spin Asymmetries for the Proton and Deuteron.....	186

c.1.4.	Collins and Sivers Asymmetries for Charged Pions and Kaons with a Transversely Polarized Target	187
c.1.5.	Transverse Target-Spin Asymmetries in Deeply-Virtual Compton Scattering at HERMES	188
c.1.6.	Determination of the Gluon Polarization from High- p_T Hadron Electroproduction.....	189
c.1.7.	Hadronization in Semi-Inclusive Deep-Inelastic Scattering on Nuclei	190
c.2.1.	Drell-Yan Measurements with 120 GeV Protons, FNAL E906	190
c.2.2.	Measurement of the Drell-Yan Angular Distributions	192
c.3.	12-GeV Proposal to Determine the d/u Ratio in the Proton at High x	193
D.	FUNDAMENTAL SYMMETRIES IN NUCLEI	195
d.1.	Laser Trapping of the Octupole-Deformed ^{225}Ra with Repumping by Black-Body Radiation.....	195
d.2.	Measurement of $\sin^2\theta_W$ Through Parity Violation in Deep-Inelastic Scattering (PV DIS) on Deuterium.....	197
E.	ATOMIC TRAP TRACE ANALYSIS	199
e.1.	Measuring the Nuclear Charge Radius of ^8He	199
e.2.	ATTA-3: The Next-Generation Instrument for ^{81}Kr -Dating.....	200
V.	THEORETICAL PHYSICS	201
A.	NUCLEAR DYNAMICS WITH SUBNUCLEONIC DEGREES OF FREEDOM	203
a.1.	Space-Time Variation of Strong Interactions and Fine Structure Constant	204
a.2.	Coulomb Problem for Vector Bosons.....	204
a.3.	Quark Deconfinement in Neutron Star Cores: The Effects of Spin-Down	205
a.4.	Quark Matter in Neutron Stars: An Aperçu.....	206
a.5.	Surface Structure of Quark Stars with Magnetic Fields	206
a.6.	Nucleosynthesis in Decompressing Neutron Star Matter	207
a.7.	Nucleon Weak and Strong Form Factors.....	208
a.8.	Dynamical Chiral Symmetry Breaking and a Critical Mass.....	209
a.9.	Studies of Meson Properties	210
a.10.	Schwinger Functions and Light-Quark Bound States.....	212
a.11.	Nucleon Electromagnetic Form Factors	213
a.12.	Semileptonic Decays of Heavy Ω Baryons in a Quark Model	215
a.13.	Ξ Baryons in a Constituent Quark Model.....	215
a.14.	Dynamical Coupled-Channel Model of πN Scattering in the $W \leq 2$ GeV Nucleon Resonance Region	215
a.15.	Extraction and Interpretation of $\gamma N \rightarrow \Delta$ Form Factors within a Dynamical Model	217

a.16.	Dynamical Coupled-Channel Analysis of π Electroproduction	218
a.17.	Speed-Plot and Time-Delayed Methods for Extracting Resonance Parameters.....	218
a.18.	On the Sign of the π - ρ - ω Coupling Constant.....	219
B.	NUCLEAR FORCES AND NUCLEAR SYSTEMS.....	221
b.1.	Quantum Monte Carlo Calculations of Light Nuclei Energies.....	222
b.2.	Scattering Methods for Quantum Monte Carlo Calculations	223
b.3.	Spectroscopic Factors and Cluster Form Factors of Light Nuclei.....	225
b.4.	Calculations of RMS Radii of Helium Isotopes	225
b.5.	Pair Counting, Pion-Exchange Forces, and the Structure of Light Nuclei	226
b.6.	Tensor Forces and the Ground State Structure of Nuclei	226
b.7.	Quantum Monte Carlo Calculations of Electroweak Transition Matrix Elements.....	227
b.8.	Quantum Monte Carlo Calculations of Isospin-Mixing Matrix Elements in ^8Be	228
b.9.	Dependence of Nuclear Binding on Hadronic Mass Variation	229
C.	NUCLEAR ASTROPHYSICS	231
c.1.	Sedimentation and Type I X-Ray Bursts at Low Accretion Rates	232
c.2.	Flame Evolution for the Deflagration Phase in Type Ia Supernova Simulations	233
c.3.	2-D Hydrodynamic Studies of Novae.....	234
c.4.	r -Process Synthesis of the Heaviest Elements.....	235
D.	NUCLEAR STRUCTURE AND HEAVY-ION REACTIONS.....	237
d.1.	Signature of Shallow Potentials in Deep Sub-Barrier Fusion Reactions.....	238
d.2.	Coupled-Channels Analysis of $^{16}\text{O} + ^{208}\text{Pb}$ Fusion Reactions.....	240
d.3.	Coupled-Channels Analysis of $^{48}\text{Ca} + ^{90,96}\text{Zr}$ Fusion Reactions.....	241
d.4.	Charge Radius and Dipole Response of ^{11}Li	243
d.5.	Mean Field and Many Body Wavefunctions	245
d.6.	Variational Approach to Configuration Interaction.....	246
d.7.	Neutron-Proton Pairing.....	246
d.8.	Energy Levels of the Heavy Elements.....	248
E.	ATOMIC THEORY AND FUNDAMENTAL QUANTUM MECHANICS	249
e.1.	Interactions of Photons with Matter.....	249
e.2.	Interactions of Charged Particles with Matter	250

e.3.	A Bragg Scattering Method to Search for the Neutron Electric Dipole Moment	250
e.4.	Quantum Theory Representations of Real and Complex Numbers.....	251
e.5.	Fields of Iterated Reference Frames Based on Quantum Theory Representations of Real and Complex Numbers.....	251
F.	OTHER ACTIVITIES	253
f.1.	Third ANL/MSU/INT/JINA Rare Isotope Accelerator Workshop	253
f.2.	Nineteenth Annual Midwest Theory Get-Together	253
VI.	OTHER EDUCATIONAL AND COMMUNITY OUTREACH ACTIVITIES	255
a.1.	Minority Program.....	255
b.1.	ANL Summer School Experience in Physics	256
	Staff Members of the Physics Division	257
	Publications	267
	Low-Energy Nuclear Physics Research.....	267
	Operation and Development of ATLAS and Accelerator Physics and Exotic Beam Technology	281
	Medium-Energy Nuclear Physics Research.....	283
	Theoretical Physics	285

I. LOW-ENERGY NUCLEAR PHYSICS RESEARCH

OVERVIEW



The low-energy nuclear research program is focused on the fundamental study of the many-body quantum system that is the atomic nucleus. Much recent interest in this field derives both from the many and strong interrelations this field has with fundamental studies of astrophysics and cosmology, as well as applications in medicine, energy generation, national security and defense. The nuclear physics is constantly evolving and recently a stronger emphasis has been placed on the study of nuclei far from stability – both on the neutron and proton-rich sides of the line of stability. The Argonne nuclear physics program is, therefore, concerned with many of the most pressing questions in the field. Some highlights are listed below:

- The study of reactions and nuclear structure of importance for the nucleosynthesis in stellar environments is a central part of the program, which for many studies uses the radioactive beams from the ATLAS in-flight facility. Recent work in this area includes studies of the $^{12}\text{C}(\alpha,\gamma)$ reaction – one of the most important reactions in nucleosynthesis – as well as the triple α -reaction, which produces the carbon that is essential for all known life forms.
- In weak interaction physics, a central question is whether the neutrino – now known to have mass – is its own antiparticle, which would allow neutrinoless double beta decays, $0\nu\beta\beta$, in $0^+ \rightarrow 0^+$ transitions. Such transitions have not yet been conclusively identified, but even if they were, the interpretation of the transition strength in terms of the neutrino mass depends sensitively on the occupation of valence orbits in both the parent and daughter nucleus. A program to experimentally determine these properties in the relevant nuclei near ^{76}Ge has been undertaken in collaboration with Yale University and the Research Center for Nuclear Physics, Osaka.
- Efforts in the study of heavy elements are aimed at understanding the single particle structure in transfermium nuclei, in particular the orbits that are associated with the expected spherical shell gaps in super-heavy nuclei. Two recent studies have identified the location of the $[521]_{1/2}$ proton orbital and the 2-qp $\{[734]9/2, [624]7/2\}$ neutron configuration in ^{254}No and ^{252}No , respectively. These findings provide important experimental information for improving theoretical models used to predict the stability of nuclei in the super-heavy region.
- The study of nuclei far from the stability is a central theme in modern nuclear structure research. The neutron-rich nuclei offer a rich area for studies of possible changes in the spin-orbit strength, the development of a new “sub-shell” at $N = 32-34$, and the use of the deep-inelastic reaction to reach very neutron-rich nuclei, *e.g.*, the doubly-magic ^{78}Ni .

- The nuclei along the $N = Z$ line offers the opportunity to study n - p pairing and the isospin mirror symmetry, and recently a glimpse of the single neutron structure outside the ^{100}Sn doubly-closed shell has been obtained – a long anticipated achievement.
- Interesting dynamical features in the continuum γ -ray emission during the spin-down of super-deformed ^{152}Dy and ^{194}Hg have been discovered, which give rise to rotational damping in these systems and as well as ergodic rotational bands in ^{194}Hg .
- A small, but successful, effort is devoted to the study of heavy-ion fusion at deep sub-barrier energies, where a hindrance of the fusion probability was previously discovered. The present focus in this work is on the characterization of this phenomenon and extension of experiments to lighter systems, some of which play a strong role in carbon and oxygen burning in Type Ia supernovae explosions. The study of relativistic heavy-ion collisions with the PHOBOS collaboration at RHIC is in the process of phasing out with the publications of the final results from this work.
- A number of exciting technical developments have been progressing over the past year. Chief among them is the construction of the CARIBU radioactive ion injector at the ATLAS facility. When complete, this system will provide a wide range of very neutron-rich beams derived from ^{252}Cf fission fragments, albeit at low intensity, which will enable the study of, *e.g.*, the single particle structure near doubly-magic ^{132}Sn as well as a wide range of both lighter and heavier neutron-rich nuclei. In order to take advantage of these beams, a novel, high-acceptance spectrometer, HELIOS, is being constructed, which is designed for studying light-ion transfer reactions in inverse kinematics with such beams.
- Other important technical developments include the Argonne contribution to the GRETINA γ -tracking array, completion of the Argonne Implantation – Decay Array (AIDA), using planar HPGe detectors for polarization measurements, and the development of portable γ -ray detector systems for Homeland Security applications.



A. REACTIONS OF ASTROPHYSICAL IMPORTANCE

The study of nuclear processes and quantum states which are of relevance for the energy production and the synthesis of heavier elements in stars and explosive stellar processes, such as Type Ia supernovae, gamma-ray bursts, etc., are critical components of the ATLAS research program.

a.1. Expectations for ^{12}C and ^{16}O Induced Fusion Cross Sections at Energies of Astrophysical Interest (C. L. Jiang, K. E. Rehm, B. B. Back, and R. V. F. Janssens)

Fusion reactions between light heavy-ions such as ^{12}C and ^{16}O play an important role in the history of stellar evolution, especially in the interior of highly developed stars (like carbon and oxygen burnings, type Ia supernovae, etc.), where these reactions are important routes for the production of heavier nuclei. Although these processes occur in explosive scenarios at high temperatures, the Gamow energies are still extremely low, resulting in very small cross sections, which in many cases are not yet experimentally accessible. One has, therefore, to rely on phenomenological extrapolation methods, *e.g.*, optical model calculations, which are often used to analyze fusion reactions of light heavy-ion systems. Extrapolations based on the optical model analysis give astrophysical S factors that increase continuously while the energy decreases. This result is somewhat at variance with the data. Instead, a maximum of the S factor has been recently observed in many medium-heavy systems where it was interpreted as a new fusion hindrance effect occurring at extreme sub-barrier energies.¹ It was concluded in a systematic study (see Ref. 2) that there may be a hindrance behavior for light heavy-ion fusion reactions too. We have, therefore, studied the effect of the hindrance behavior for lighter systems, using the systematics obtained from the fusion reactions of both heavier and lighter nuclei.² This effect will introduce a substantial change in the extrapolated S factor and consequently also in the calculated astrophysical reaction rates. The extrapolations for three reactions $^{12}\text{C} + ^{12}\text{C}$, $^{12}\text{C} + ^{16}\text{O}$ and $^{16}\text{O} + ^{16}\text{O}$ are reexamined in the present study.

For example, the fusion reaction $^{16}\text{O} + ^{16}\text{O}$, a temperature of $T_9 = 3$ corresponds to an effective energy of ~ 7 MeV, which is about the energy of the lowest data point measured so far. The calculated reaction rates for three extrapolations are presented in Fig. I-1a, *i.e.*, Hulke *et al.*, (dot-dashed line³), Fowler

et al. (dashed line⁴) and the present analysis (solid line). Here the rate of Hulke *et al.* is higher than that of Fowler *et al.* reflecting the fact that Hulke's $S(E)$ factor is always higher. The difference between the two rates is about a factor of 5 at lower temperatures, and decreases to a factor of 2 at higher temperatures. The results from the present extrapolation which includes the fusion hindrance behavior, are much smaller than the other two, except at temperatures above $T_9 \sim 2$, consistent with the difference in the S factors discussed above.

The relations of reaction rates calculated for the fusion reactions $^{12}\text{C} + ^{16}\text{O}$ and $^{12}\text{C} + ^{12}\text{C}$ for the previous and present extrapolation are similar to $^{16}\text{O} + ^{16}\text{O}$.

The ratios of reaction rates calculated from the present extrapolation to Fowler's compilation⁴ for the three fusion reactions $^{12}\text{C} + ^{12}\text{C}$, $^{12}\text{C} + ^{16}\text{O}$ and $^{16}\text{O} + ^{16}\text{O}$ are summarized in Fig. I-1b as red, black and light-blue bands, respectively. Obviously, the influence of fusion hindrance is more pronounced for the reaction $^{16}\text{O} + ^{16}\text{O}$. At a temperature of $T_9 \sim 1.0$ the ratios differ by factors of up to 100. For the reactions $^{12}\text{C} + ^{16}\text{O}$ and $^{12}\text{C} + ^{12}\text{C}$, the differences of the ratios are in the range 1.5-3 and 1-5, respectively. At lower temperatures, the differences increase rapidly.

Since the physical nature of fusion hindrance at extreme low energies is still a matter of debate, many questions need to be answered by future experiments and better theoretical treatments. The extrapolation method presented in this paper is only a first step which hopefully will trigger future fusion measurements as well as theoretical studies of these important light heavy-ion systems and improves our understanding of the reaction mechanism at extremely low energies. The detailed result of the present study has been published in Ref. 5.

¹C. L. Jiang *et al.*, Phys. Rev. Lett. **89**, 052701 (2002); Phys. Rev. C **69**, 014604 (2004); Phys. Rev. Lett. **93**, 012701 (2004); Phys. Rev. C **71**, 044613 (2005); Phys. Lett. **B540**, 18 (2006).

²C. L. Jiang *et al.*, Phys. Rev. C **73**, 014613 (2006).

³G. Hulke *et al.*, Z. Phys. **A297**, 161 (1980).

⁴W. Fowler, G. Caughlan, and B. Zimmerman, Annu. Rev. Astrophys. **13**, 69 (1975).

⁵C. L. Jiang *et al.*, Phys. Rev. C **75**, 015803 (2007).

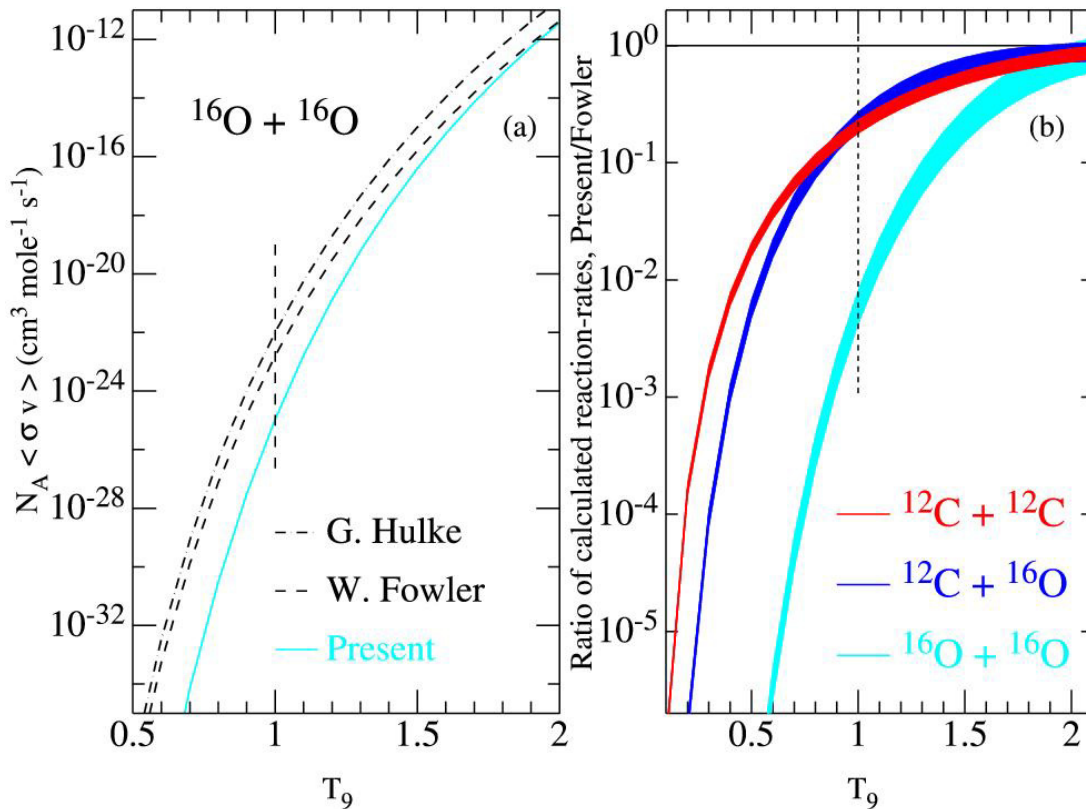


Fig. I-1. (a) Calculated fusion reaction rates for the system $^{16}\text{O} + ^{16}\text{O}$. (b) Ratio of calculated reactions rates (present to Fowler's) for systems $^{16}\text{O} + ^{16}\text{O}$, $^{12}\text{C} + ^{16}\text{O}$ and $^{12}\text{C} + ^{12}\text{C}$.

a.2. A New Measurement of the E1 Component of the $^{12}\text{C}(\alpha,\gamma)^{16}\text{O}$ Cross Section at Low Energies (X. D. Tang, K. E. Rehm, I. Ahmad, J. Greene, A. Hecht, D. Henderson, R. V. F. Janssens, C. L. Jiang, D. Kahl, F. Moore, M. Notani, R. C. Pardo, N. Patel, G. Savard, J. P. Schiffer, S. Sinha, B. Shumard, M. Paul,* A. Champagne,† C. Brune,‡ L. Jisonna,§ R. E. Segel,§ and A. Wuosmaa¶)

Measurements of the β -delayed α decay of ^{16}N provide the tightest constraints for determining the E1 component of the α -capture reaction $^{12}\text{C}(\alpha,\gamma)^{16}\text{O}$. In these experiments S_{E1} is extracted from the height of a small satellite peak in the α -energy spectrum. This peak, which originates from the interference between the subthreshold 1^- state at $E_x = 7.117$ MeV and the higher-lying 1^- state at $E_x = 9.585$ MeV, has been

studied by several groups in the past,^{1,2} all of them using Si surface barrier detectors. These detectors are sensitive to β particles, have dead layers and are prone to deterioration effects during long measurements.

Because of the importance of the $^{12}\text{C}(\alpha,\gamma)^{16}\text{O}$ reaction in nuclear astrophysics, we have remeasured the ^{16}N decay using a different approach. To reduce the

sensitivity to electrons from the beta decay we have developed an array of high acceptance ionization chambers of minimal thickness to be used for the coincident detection of ^{12}C and α particles following the ^{16}N decay. Special emphasis has been put on measuring backgrounds simultaneously using the identical geometry. A schematic of the setup and a description of the procedure used in the experiments were given in last year's annual report.

Figure I-2 shows the coincident events measured in the upstream and downstream parts of the detector. On the left the decay events of ^{16}N implanted into a $17\ \mu\text{g}/\text{cm}^2$ thick carbon foil are presented, while on the right a background spectrum for the same detector is shown.

The two groups with the highest count rate seen in the left part of Fig. I-2 correspond to ^{12}C - α coincidences in the up- and down-stream detectors, respectively. The two groups exhibit a tail caused by energy-loss straggling of the low energy ^{12}C particles in the carbon foil. The groups observed close to the y-axis are caused by ^{16}N decays, where either the ^{12}C or the α particle is stopped in the target frame, so that only part of the corresponding energy is detected. In a first pass of the analysis we discuss the events in the lower right part of the spectrum which are not effected by the target frame. The resulting α spectrum is shown in Fig. I-3. The insert in Fig. I-3 shows a comparison of the low-energy part of our spectrum with the results from earlier experiments, given by the dashed¹ and solid² lines.

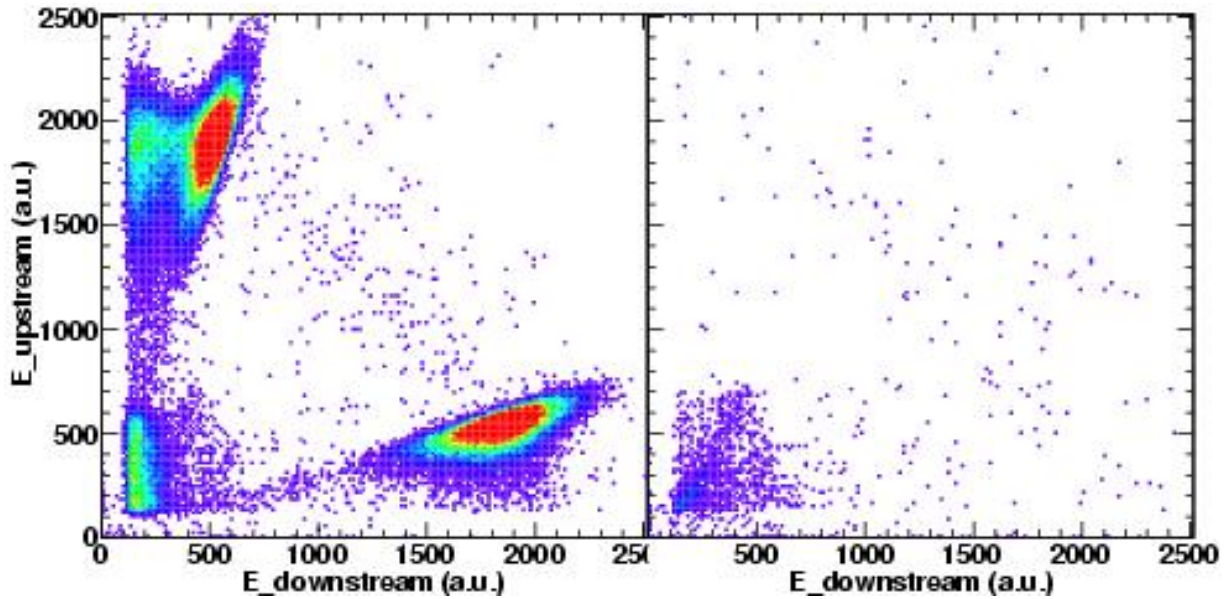


Fig. I-2. (Left) coincident energy spectrum, measured with one of the twin-ionization chambers for a foil with implanted ^{16}N particles. (Right) same as above, but for a non-implanted foil.

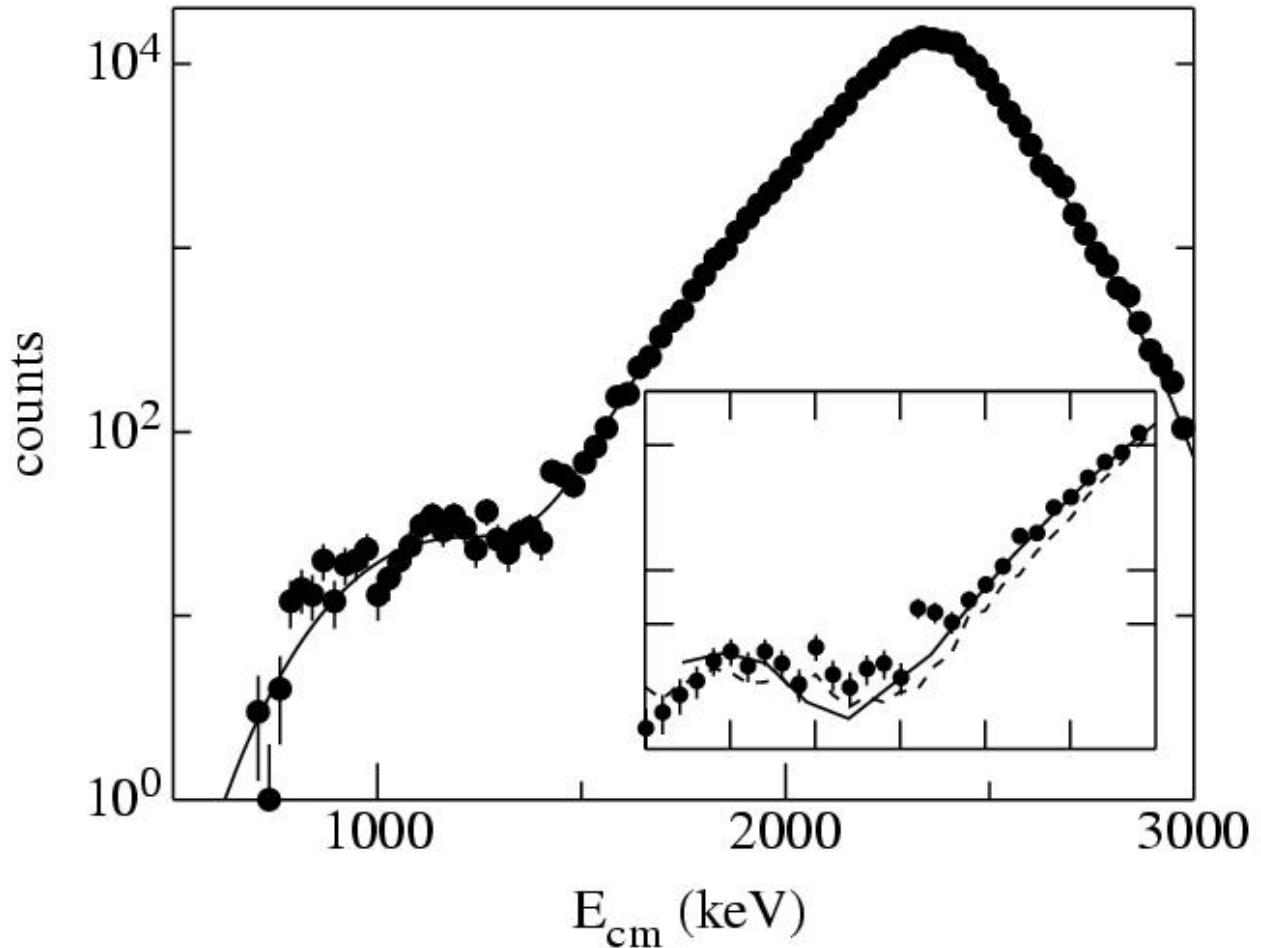


Fig. I-3. Summed α spectrum in comparison with an R-matrix fit. The insert shows the low-energy part of the spectrum together with the previous results. (dashed line: Ref. 1, solid line: Ref. 2).

Extracting the relevant S -factor S_{EI} from the data is usually done using the R-matrix formalism with a least-squares fit to data from the β -delayed α decay of ^{16}N , in combination with experimental results of the capture reaction $^{12}\text{C}(\alpha,\gamma)^{16}\text{O}$, performed at higher energies, as well as with phase shift parameters obtained from elastic scattering $^{12}\text{C}(\alpha,\alpha)$. There are a large number of free parameters (~ 14) which in some cases show strong correlations. We have used the R-matrix program from Ref. 2 together with the same phase shift and capture data. From this fit we obtain $S_{EI} = 74 \pm 21$ keVb, including a systematic uncertainty of 10 keVb, which is dominated by the ± 5 keV uncertainty of the energy calibration.

There are new data available for some of the other inputs used in the fits. With the phase shifts of Ref. 3, which are not yet available in tabulated form, the S_{EI} value increases to about 88 ± 18 keVb. A similar

sensitivity of S_{EI} was observed when the β -branching ratio of the sub-threshold 1^- state was increased by about 10%, as suggested by a recent experiment (see following contribution). Using the newest set of α capture data,^{4,6} however, does not change S_{EI} appreciably. The results of the fits are summarized in Table I-1. A paper describing these results has been published in Phys. Rev. Lett.⁷

We are presently analyzing the full data set, which requires a cut in the emission angle of the ^{12}C and α particles. A paper with the whole data set, including a detailed description of the twin-ionization chambers is under preparation. The strong sensitivities to the fit parameters indicate that improved measurements for all input parameters as well as a better theoretical description are needed in order to reduce the uncertainties in the $^{12}\text{C}(\alpha,\gamma)^{16}\text{O}$ reaction rate.

Table I-1. S_{EI} values obtained from R-matrix fits with different input parameters. See text for details.

Source of ^{16}N data	S_{EI} (keVb)	χ^2	Other data used in fit
Ref.1	79 ± 21	1.6	
This work	74 ± 21	2	Standard input
	88 ± 18	2.9	Phase shift from [3]
	70 ± 20	2	New β -branching ratio
	73 ± 21	1.7	(α, γ) data from [4-6]
	85 ± 18	2.7	Data from [3-6]

*The Hebrew University of Jerusalem, Israel, †University of North Carolina, ‡Ohio University, §Northwestern University, ¶Western Michigan University.

¹R. Azuma *et al.*, Phys. Rev. C **50**, 1194 (1994), L. Buchmann *et al.*, Phys. Rev. Lett. **70**, 726 (1993).

²Z. Zhao *et al.*, Phys. Rev. Lett. **70**, 2066 (1993).

³L. Buchmann and C. Barnes, Nucl. Phys. **A777**, 254 (2006).

⁴R. Kunz *et al.*, Phys. Rev. Lett. **86**, 3244 (2001).

⁵R. Kunz *et al.*, Astrophys. J. **567**, 643 (2002).

⁶M. Assunção *et al.*, Phys. Rev. C **73**, 055801 (2006).

⁷X. D. Tang *et al.*, Phys. Rev. Lett. **99**, 052502 (2007).

a.3. The Branching Ratio of the Subthreshold 1^- State in the β -Decay of ^{16}N (K. E. Rehm, X. D. Tang, G. Savard, M. P. Carpenter, J. P. Greene, R. V. F. Janssens, C. L. Jiang, T. Lauritsen, C. J. Lister, M. Notani, N. Patel, R. C. Pardo, J. P. Schiffer, S. Zhou, and M. Paul*)

In the last three years we have been involved in an experiment to study the $^{12}\text{C}(\alpha, \gamma)^{16}\text{O}$ reaction, which has often been called the most important reaction in nuclear astrophysics. In this experiment we measured the beta-delayed α decay of ^{16}N , using a new setup of high-efficiency twin-ionization chambers. The final error in determining the astrophysically important S_{EI} of the $^{12}\text{C}(\alpha, \gamma)^{16}\text{O}$ reaction has contributions coming from the statistics as well as from systematic uncertainties. The three main contributions to the systematic uncertainties originate from the energy calibration of the α spectrum, from the $^{17,18}\text{N}$ contaminations in the beam and from the β -branching ratio, populating the two 1^- states in ^{16}O .

Because of the strong dependence on the α energy calibration, special emphasis has been put in our experiment on obtaining good energy calibrations. In order to bracket the main alpha peak from the decay of ^{16}N , we have produced a "sandwich" source consisting of layers of $10 \mu\text{g}/\text{cm}^2$ thick ^6LiF and ^{10}B , evaporated on the two sides of a $17 \mu\text{g}/\text{cm}^2$ thick carbon target. From this, alpha lines of 2.056, 1.776 and 1.472 MeV were obtained, with thermal neutrons from a PuBe source, through the (n, α) reaction. The thickness of these foils was determined with a ^{228}Th source using the

split pole spectrograph. The stability of the ionization chamber calibration during a two-week long run was checked during the experiment with daily ^{10}B calibrations and was found to be better than ± 2 keV. In addition, pulser calibrations and linearity tests have been performed before and after the experiment. With all these tests we obtained for the whole run an energy calibration with an accuracy of ± 5 keV, which is a factor of four better than the energy calibration obtained in Ref. 1. Because of the ^{16}N production technique used in this experiment, we do not have to apply a correction for the presence of $^{17,18}\text{N}$ components in the beam.

The next highest systematic uncertainty comes from the branching ratio populating the two 1^- states in ^{16}O . We have, therefore, performed an experiment at Gammasphere to reduce the uncertainty of the β -branching ratio of the sub-threshold 1^- state in ^{16}O at 7116.9 keV that was previously measured to be 4.8(4)%.

The β -decay of ^{16}N proceeds mainly to the 3^- state at 6129.9 keV, which has a precisely determined beta branching ratio of 66.2(6)%. The 3^- as well as the sub-

threshold 1^- states decay almost exclusively by emission of a single high-energy gamma ray and the beta branching ratio to the 7116.9 keV state can then be

$$\frac{BR(6129)}{BR(7116)} = \frac{N_\gamma(6129) \varepsilon_\gamma(7116)}{N_\gamma(7116) \varepsilon_\gamma(6129)} \quad (1)$$

where $BR(E)$ is the direct beta feeding to the state at excitation energy, E , $N_\gamma(E)$ is the number of gamma rays detected at that energy and $\varepsilon_\gamma(E)$ is the detector efficiency at that gamma ray energy.

determined from the relative intensities of the 7116.9 keV and 6129.9 keV gamma rays emitted in the decay of ^{16}N :

For the case of ^{16}N the efficiencies, ε_γ can be obtained from the ratio between the coincident counts $N_{\gamma\gamma}$ populating and depopulating the level of interest and the number of counts N_γ , populating the level, *e.g.*,

$$\frac{N_{\gamma\gamma}(6129-2741)}{N_\gamma(2741)} = \frac{\varepsilon_\gamma(6129)\varepsilon_\gamma(2741)}{\varepsilon_\gamma(2741)} = \varepsilon_\gamma(6129) \quad (2)$$

Combining equations (1) and (2) we obtain

$$\frac{BR(6129)}{BR(7116)} = \frac{N_\gamma(6129) N_{\gamma\gamma}(7116-1754) N_\gamma(2741)}{N_\gamma(7116) N_{\gamma\gamma}(6129-2741) N_\gamma(1754)} \quad (3)$$

Corrections to equation (3) due to side feeding and angular correlation effects are smaller than 1%.

The experiment was performed with a 1-2 nA 28 MeV ^{15}N beam bombarding a 10 mg/cm² thick Ti foil, which was loaded with deuterium. The ^{16}N products, produced via the $d(^{15}\text{N}, ^{16}\text{N})p$ reaction, were stopped in the target. A measurement cycle consisted of a 7 s long

production period followed by a 7 s counting period. The gamma decays were detected with the 100 individual detectors of Gammasphere. From the analysis of the spectra and using Eq. 3 a new preliminary value for the beta branching ratio of the sub-threshold 1^- state of $BR = 5.1(1)\%$ has been obtained.

*The Hebrew University of Jerusalem, Israel.

¹R. E. Azuma *et al.*, Phys. Rev. C **50**,1194 (1994).

a.4. Experiments to Further the Understanding of the Triple-Alpha Process in Hot Astrophysical Scenarios (N. Patel, U. Greife, K. E. Rehm, C. L. Jiang, D. Henderson, M. Notani, and X. D. Tang)

The elements beyond the stability gaps at $A = 5$ and $A = 8$ rely in their production on the triple-alpha process, which in two steps *via* the reactions $\alpha(\alpha,\gamma)^8\text{Be}$ (through the short-lived ^8Be ground state) and $^8\text{Be}(\alpha,\gamma)^{12}\text{C}$ synthesizes one crucial element of life. The great story of the universe would not have produced Carbon-based life forms if the latter reaction had not conveniently located in the Gamow window of the Helium burning Red Giant stars, an s-wave resonance combining the three alpha particles to ^{12}C . Considering the importance of Carbon nucleosynthesis, it is quite surprising how unexplored the region of excited states above the $^8\text{Be}(\alpha,\gamma)^{12}\text{C}$ threshold has been (since the

early experiments in the 1950's – 60's)¹⁻⁶ until recently the Aarhus/Jyvaskylä group has undertaken and published⁷⁻¹¹ several experiments looking at the alpha emission from states in ^{12}C populated by beta decay of ^{12}B and ^{12}N . These new measurements require a rethinking of the level structure in ^{12}C above the astrophysically most relevant level at 7.654 MeV (0^+).

In addition to the 1990 edition of Ajzenberg-Selove¹² of excited states, the recent NACRE compilation¹³ assumes a 2^+ resonance at 9.117 MeV ($\Gamma_\alpha = 0.56$ MeV)¹⁴ for which no experimental evidence exists. Other publications [*e.g.* 15] prefer to limit their

range of astrophysical temperatures to where they think that only the well known 7.65 MeV level is relevant. In explosive scenarios like supernovae, where the temperatures up to several 10^9 K are achieved, taking only the 7.65 MeV resonance into account is not sufficient and the inclusion of either the theoretically predicted 2^+ state¹³ or experimentally inferred states⁷ has a significant effect. The ^{12}N and ^{12}B decay experiments performed at Jyväskylä and CERN/ISOLDE clearly show a broad resonance structure above the 7.65 MeV state. The group performed detailed R-matrix calculations of the different ways this resonance could interfere with the state at 7.65 MeV and conclude that their spectrum could not be explained by the 2^+ resonance theoretically predicted¹⁴ and used in the NACRE compilation.¹³ The assumption of a 0^+ state and its interference with the

7.65 MeV level is shown to yield a more satisfactory fit.

In order to improve the earlier experiments we have developed a new detector system that will be used for the studies of the triple alpha decay of high-lying states in ^{12}C . Stopping the ^{12}B (^{12}N) beam in a catcher foil and measuring the triple α decay in an array of Si strip detectors suffers from efficiency corrections that need to be applied especially for decays with lower energies. Stopping the beam in a Si detector and measuring the subsequent α decay, as done, *e.g.*, in our earlier ^8B experiment, results in " β -summing effects" that need to be corrected in the analysis. We have, therefore, developed a new detector system consisting of a pair of twin-ionization chambers (IC), filled with P10 counting gas. The system is shown in Fig. I-4.

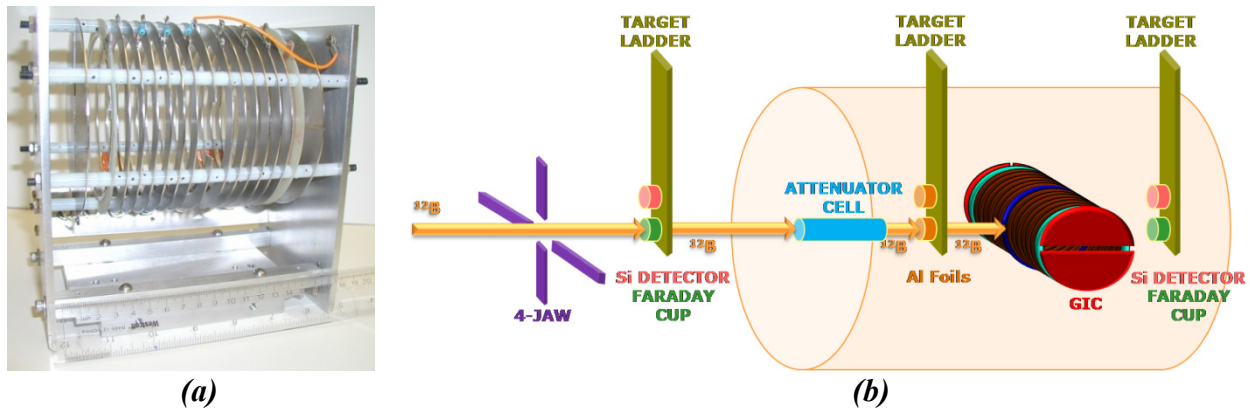


Fig. I-4. (a) Twin Frisch gridded ionization chamber (GIC) and (b) the schematic of the experimental setup.

A 72 MeV ^{12}B beam, produced *via* the $d(^{11}\text{B}, ^{12}\text{B})p$ reaction in a cryogenically cooled gas cell, enters the ionization chamber after passing through an attenuator cell where its energy is reduced so that the ^{12}B ions are stopped in the center of the IC. The short half-life of ^{12}B (~ 20 ms) eliminates the need for a stopping foil and, thus, no energy corrections are needed. In phase I of the experiment we have investigated the technique of stopping the ^{12}B ions in the center of the IC. For this the beam-left anode of the IC was subdivided into an

upstream and a downstream part. At a low pressure in the attenuator most of the energy from the triple α decay of ^{12}C is deposited in the downstream half of the anode, while at a higher pressure the energy is mainly deposited in the upstream half. The results are shown in Fig. I-5. In this experiment the optimum pressure for the attenuator was found to be 100 Torr. Experiments to use this detector system for measuring the triple α decay are under way.

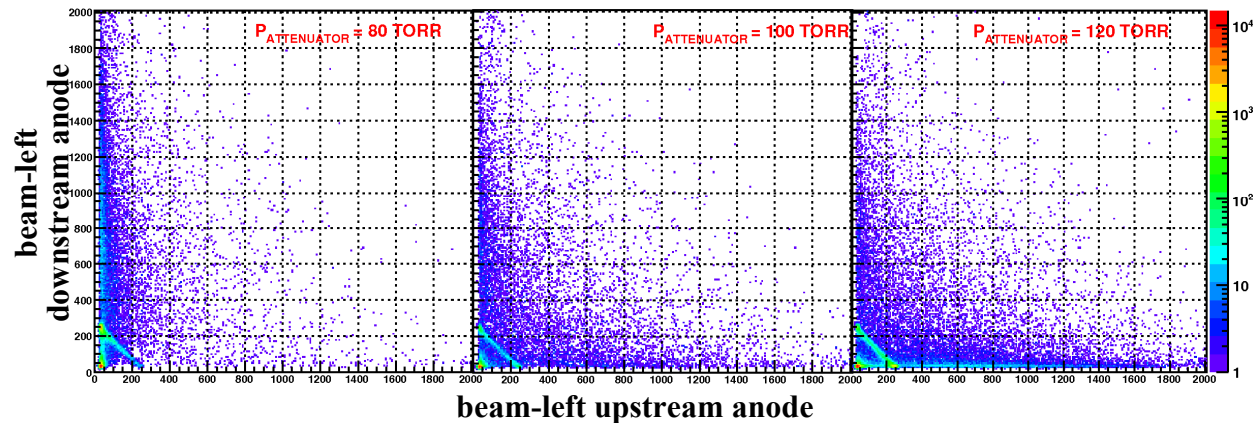


Fig. I-5. Spectra of the energy deposited in the upstream and downstream part of the twin-ionization chamber for different pressures in the attenuator cell. The pressure in the IC was 250 Torr.

¹D. N. F. Dubar *et al.*, Phys. Rev. **92**, 649 (1953).

²C. W. Cook *et al.*, Phys. Rev. **107**, 508 (1957).

³C. W. Cook *et al.*, Phys. Rev. **111**, 567 (1958).

⁴R. W. Peterson and N. W. Glass, Phys. Rev. **130**, 292 (1963).

⁵W. C. Olsen *et al.*, Nucl. Phys. **61**, 625 (1965).

⁶D. Schwalm and B. Povh, Nucl. Phys. **89**, 401 (1966).

⁷H. O. U. Fynbo *et al.*, Nature **433**, 136 (2005).

⁸C. Au. Diget *et al.*, Nucl. Phys. **A760**, 3 (2005).

⁹H. O. U. Fynbo *et al.*, Nucl. Phys. **A718**, 541c (2003).

¹⁰H. O. U. Fynbo *et al.*, Phys. Rev. Lett. **91**, 082502 (2003).

¹¹H. O. U. Fynbo *et al.*, Eur. J. Phys. **A15**, 135 (2002).

¹²F. Ajzenberg-Selove, Nucl. Phys. **A506**, 1 (1990).

¹³C. Angulo *et al.*, Nucl. Phys. **A656**, 3 (1999).

¹⁴P. Descouvemont and D. Baye, Phys. Rev. C **36**, 54 (1987).

¹⁵K. Langanke, M. Wiescher, and F. K. Thielemann, Z. Phys. **A324**, 147 (1986).

a.5. Study of the $^{57}\text{Fe}(d,p)^{58}\text{Fe}$ Reaction in Inverse Kinematics as Surrogate to an (n,γ) Reaction (K. E. Rehm, X. D. Tang, I. Ahmad, J. P. Greene, D. J. Henderson, C. L. Jiang, R. C. Pardo, R. Scott, D. Seweryniak, R. Vondrasek, M. Paul,* P. Collon,† B. Ingel,* Y. Kashiv,* ‡ H. Nassar,* and A. Wuosmaa§)

The nuclide ^{60}Fe is thought to be predominantly produced in core-collapse supernovae (CCSN) by an (n,γ) reaction on the radioactive nucleus ^{59}Fe ($t_{1/2}(\text{g.s.}) = 45.1$ days). The observation of two lines (1173 keV and 1333 keV) in the decay of ^{60}Fe through ^{60}Co (1173 keV and 1333 keV) has been very recently reported by the Integral mission.¹ Further measurements are hoped to reveal subtle differences in the sources of the two isotopes (mass, metallicity of star, depth within the star and effect of the final explosion). Independently, a signal of live ^{60}Fe measured in a deep-sea crust² was interpreted as resulting from the direct deposition on Earth of ejecta

from a close-by supernova (estimated to have been ~ 20 pc away and ~ 3 Myr ago). These first experimental results emphasize the importance of ^{60}Fe as an observable from CCSN's and of the understanding of its nucleosynthesis. No experimental information exists on the $^{59}\text{Fe}(n,\gamma)^{60}\text{Fe}$ reaction at stellar temperatures.

In order to study the possible relation between (d,p) and (n,γ) reactions in this region of nuclides (see *e.g.* Ref. 3), we investigated the reaction $^{57}\text{Fe}(d,p)^{58}\text{Fe}$ in inverse kinematics with a ^{57}Fe beam at a laboratory incident energy of 500 MeV on a CD_2 target. The

energy allows us to populate neutron unbound states in ^{58}Fe , also available in the neutron capture reaction $^{57}\text{Fe}(n,\gamma)^{58}\text{Fe}$ (Fig. I-6). The detection system is illustrated in Fig. I-7. A thick absorber (Au) had to be

used in order to slow down forward-recoiling ^{58}Fe ions so as to match the electric rigidity acceptance of the FMA (Fig. I-7).

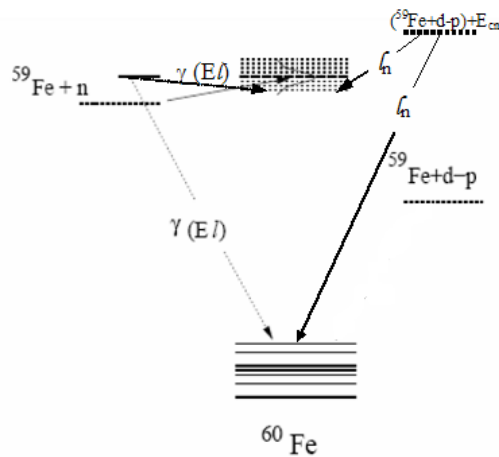


Fig. I-6. Schematic diagram of (n,γ) and (d,p) reactions.

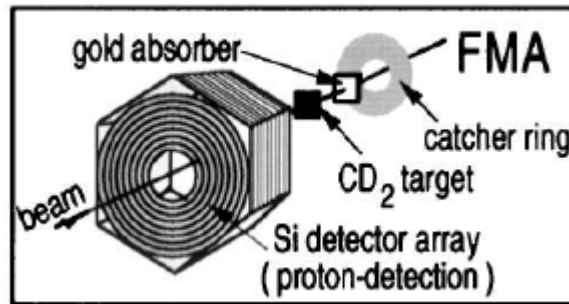


Fig. I-7. Schematic diagram of the detection system for the study of the $d(^{57}\text{Fe},p)^{58}\text{Fe}$. Protons are detected at back angles in a double-sided Si strip detector and forward recoils in the FMA.

Figure I-8 shows the proton singles spectrum measured in the Si detector, showing population of discrete low-lying states; interestingly, most of the states identified are 2^+ states. Population of highly-excited states near and above the neutron separation energy ($S_n = 6.1$ MeV) are also strongly populated. However, owing to the thick absorber and the resulting angular scattering, the efficiency of coincidences between forward recoils (FMA) and protons (DSSD) was very

low in this experiment and did not allow us to collect significant statistics on high-lying states. Moreover, the detection of neutron-unbound states requires the detection of a ^{57}Fe forward recoil and its discrimination from the high-intensity scattered beam. Use of a Ti absorber instead of Au is expected to improve the conditions. Alternative methods of detection of the forward-recoils (magnetic spectrograph, gas-filled magnet) are being also considered.

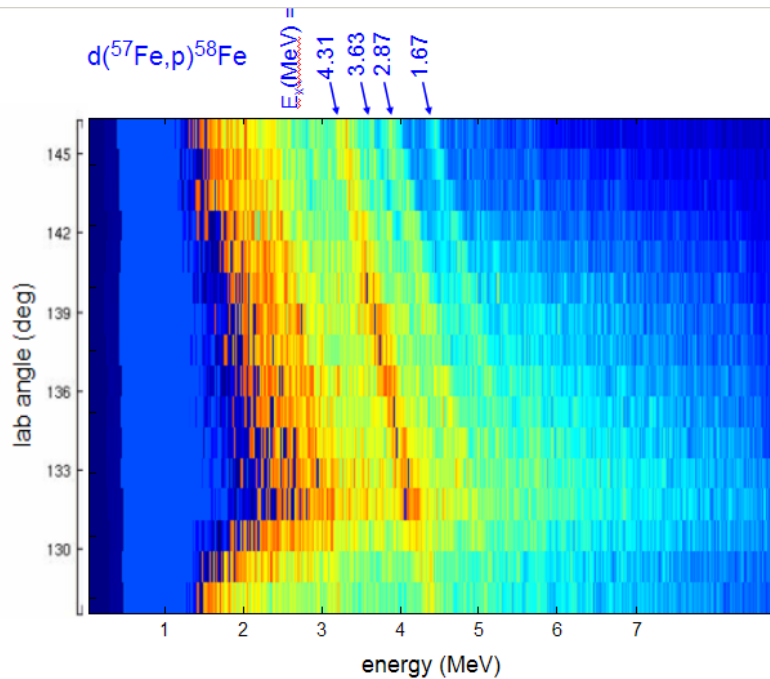


Fig. I-8. Angle vs. energy of protons detected in the backward double-sided Si strip detector. Kinematic lines corresponding to states identified in ^{58}Fe are shown.

*The Hebrew University of Jerusalem, Israel, †University of Notre Dame, ‡University of Chicago, §Western Michigan University.

¹M. J. Harris *et al.*, arXiv: astro-ph/0502219, (2005).

²K. Knie *et al.*, Phys. Rev. Lett. **93** 171103, (2004).

³P. G. Hansen and J. A. Tostevin, Ann. Rev. Nucl. Part. Sci. **53**, 219 (2003).

a.6. The Spin of the 2.645 MeV State in ^{20}Na (K. E. Rehm, J. Greene, D. Henderson, R. V. F. Janssens, C. L. Jiang, M. Notani, R. C. Pardo, J. P. Schiffer, X. D. Tang, L. Jisonna,* R. E. Segel,* M. Paul,† and A. Wuosmaa‡)

The 2.645-MeV state in ^{20}Na , the first level above the $^{19}\text{Ne} + p$ threshold, plays an important role in the $^{19}\text{Ne}(p,\gamma)^{20}\text{Na}$ reaction rate and, thus, in the breakout from the hot CNO cycle into the rp -process, which occurs in various hydrogen-rich stellar environments. However, this reaction rate is still uncertain by 2-3 orders of magnitude. This uncertainty has its origin in the two possible spin-parity assignments that have been proposed for this state in the literature. In Ref. 1, this state has been given a 1^+ assignment based on measurements of angular distributions of the $^{20}\text{Ne}(^3\text{He},t)$ reaction. The 1^+ assignment, however, has been questioned² because it requires an unusually large Coulomb shift and, therefore, the authors of Ref. 2 have assigned a spin-parity of 3^+ to this level.

Because of its importance for the breakout from the hot CNO cycle in novae, several attempts have recently been made to determine the spin-parity of this state.^{3,4} In Ref. 3, the structure of ^{20}Na was studied using a heavy ion fusion reaction ($^{10}\text{B} + ^{12}\text{C}$), but only the level structure below the proton threshold could be measured. A recent direct study of the $^{19}\text{Ne}(p,\gamma)^{20}\text{Na}$ reaction using a recoil mass separator could only give an upper limit for the resonance strength.⁴

We have performed a coincidence experiment to determine the branching ratio Γ_p/Γ_γ for the 2.645 MeV and 2.849 MeV states. These states, which lie above the proton threshold and can, therefore, decay either by γ or by proton emission, were populated *via* the $^3\text{He}(^{20}\text{Ne},t)^{20}\text{Na}$ reaction with a 160 MeV ^{20}Ne beam

bombarding a $\sim 50 \mu\text{g}/\text{cm}^2$ gas cell target filled with ^3He and cooled to LN_2 temperatures. The outgoing tritons were detected in a $40 \times 40 \text{ mm}^2$ double-sided Si strip detector. The coincident heavy recoils ^{20}Na (following γ -decay) or ^{19}Ne (following proton decay) were identified according to mass and nuclear charge in the focal plane detector of the Enge split-pole spectrograph. Due to the advantages of inverse kinematics this technique has a high detection efficiency.

Figure I-9 shows Q -value spectra obtained from the angle and energy of the tritons detected in the position-sensitive Si detector, in coincidence with ^{20}Na (blue) and ^{19}Ne (magenta) detected in the spectrograph. Because of the particle threshold at 2.199 MeV, the tritons in coincidence with ^{20}Na mainly populate states below 2 MeV, while the spectrum in coincidence with ^{19}Ne shows only states above $E_x \sim 2.5$ MeV. The locations of various levels in ^{20}Na are indicated by the arrows. Considerable effort has been devoted to study the backgrounds in these spectra. The requirement of a triton-heavy-recoil coincidence leads to a background suppression of three orders of magnitude. This is sufficient for the ^{20}Na spectrum which gives us confidence that the events above $E_x \sim 2$ MeV are free of background. A source of background in the ^{19}Ne

Q -value spectrum is proton- ^{19}Ne coincidences from the decay of proton-unbound ^{20}Na excited states. The Si strip detector could not distinguish protons from tritons and because the protons are from a three-body final state they are spread over a wide range of energy and angle. This, in turn, leads to events scattered throughout the ^{19}Ne Q -value spectrum including the region in ^{20}Na where proton decay to ^{19}Ne is energetically forbidden.

From the spectra shown in Fig. I-9 we can obtain estimates for the ratio Γ_p/Γ_γ . Predictions for Γ_p/Γ_γ for the states at $E_x = 2.646$ MeV and 2.849 MeV taken from the literature are given in Table I-2. While the restrictions on Γ_p/Γ_γ are of little help in choosing between the 1^+ and 3^+ possibilities for the 2.645 MeV state, the ratio for the two spin possibilities (3^+ and 3^-) for the 2.849 MeV state differ by almost a factor of 200. Even with the limited statistics that were achieved in this experiment the experimental ratios obtained in this measurement favor a 3^+ assignment for the 2.849 MeV state, leaving the spin-parity of 1^+ for the 2.645 MeV state. In order to finalize the limits which can be given to Γ_p/Γ_γ the efficiency of the experimental setup needs to be calculated. For this Monte Carlo calculations are presently being performed.

Table I-2. Calculated branching ratios Γ_p/Γ_γ from the reported resonance parameters taken from the literature for the 2.645 MeV and the 2.849 MeV states in ^{20}Na .

E_x (MeV)	E_r (keV)	J^π	Γ_p/Γ_γ
2.645	0.446	1^+	8.9^1
		3^+	$\leq 28.9^5$
2.849	0.650	3^+	2445^1
		3^-	13.5^2

*Northwestern University, †The University of Jerusalem, Israel, ‡Western Michigan University.

¹L. O. Lamm *et al.*, Nucl. Phys. **A510**, 503(1990).

²B. A. Brown *et al.*, Phys. Rev. C **48**, 1456(1993).

³D. Seweryniak *et al.*, Phys. Lett. **B590**, 170(2004).

⁴M. Couder *et al.*, Phys. Rev. C **69**, 022801 (2004).

⁵T. Fortune *et al.*, Phys. Rev. C **61**, 057303 (2000).

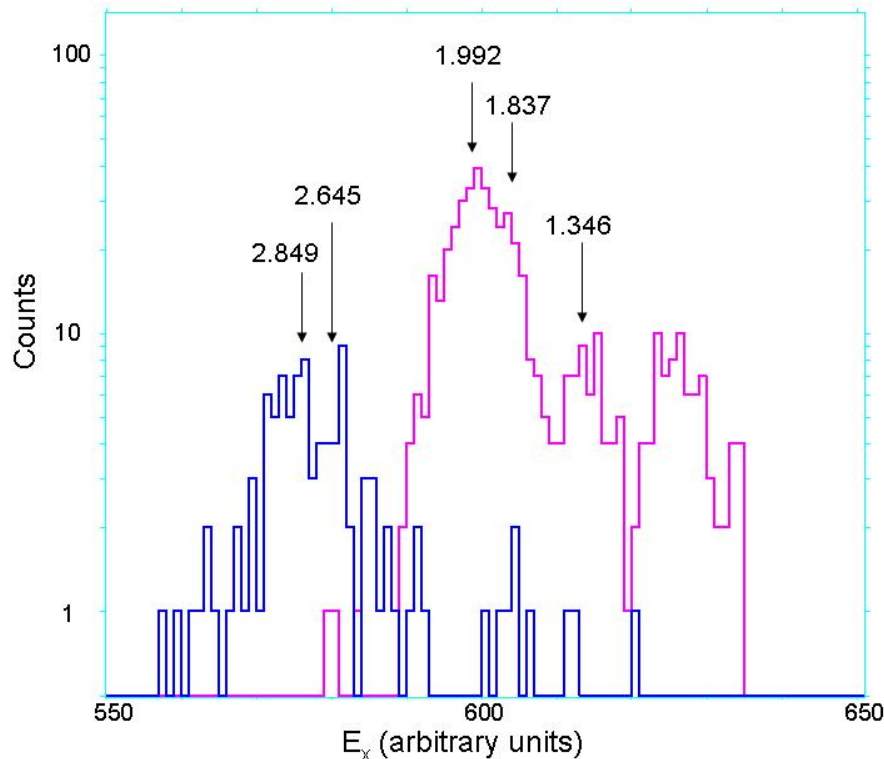


Fig. I-9. Q -value spectra for tritons coincident with ^{20}Na (magenta) and ^{19}Ne (blue) for ^{20}Na states in the excitation energy region $E_x = 0.5\text{-}3\text{ MeV}$.

a.7. Improved Measurement of the ^{44}Ti Half-Life from a 14-Year Long Study (I. Ahmad, J. P. Greene, E. F. Moore, S. Ghelberg,* A. Ofan,* M. Paul,* and W. Kutschera†)

The half-life of ^{44}Ti has been determined by following the decay of ^{44}Ti and ^{60}Co for 14 years. Mixed sources containing ^{44}Ti and ^{60}Co , and pure sources of ^{44}Ti and ^{60}Co were prepared and their gamma-ray spectra were measured with Ge spectrometers once or twice a year. Measurements were performed at Argonne and at The Hebrew University of Jerusalem. Special efforts were made to check for systematic errors and these were found to be negligible within the quoted uncertainty.

The half-life values at Argonne were determined from the ratios of the counts in the 1157.0 keV peak and the 1173.2- and 1332.5 keV gamma ray peaks. These ratios were fitted as a function of the time since the beginning of the experiment with an exponential function. The slope of the fit gives the difference between the decay constants of ^{60}Co and ^{44}Ti

($\lambda^{60}\text{Co} - \lambda^{44}\text{Ti}$). The half-life was determined by using $5.2711 \pm 0.0004\text{ yr}$ for the ^{60}Co half-life. An example of the fit is shown in Fig. I-10. The data obtained from spectra measured at source-to-detector distances of 5.2 cm and 10.2 cm were used. In addition, half-life values were determined from the spectra of the mixed source and the spectra of the pure ^{44}Ti and ^{60}Co sources. At The Hebrew University of Jerusalem, only the mixed source was used and the measurements were made at one distance. The half-life values determined from these measurements are given in Table I-3. The weighted average of all the data set gives a half-life of $58.9 \pm 0.2\text{ yr}$. In order to include possible systematic uncertainty, we have increased the error to 0.3 yr giving a final value of $58.9 \pm 0.3\text{ yr}$. The results of this study were published.¹

Table I-3. Summary of ^{44}Ti half-life measurements. All values except those given in the last line were measured at Argonne.

Source	Distance	Number of data points	Half-life from 1157/1173 ratio ^a	χ^2/DOF^b	Half-life from 1157/1333 ratio ^a	χ^2/DOF^b
Measurements at Argonne						
Mixed ^{44}Ti + ^{60}Co	5.2 cm	22	58.8 ± 0.4 yr	0.97	59.0 ± 0.3 yr	1.03
Mixed ^{44}Ti + ^{60}Co	10.2 cm	19	58.7 ± 0.5 yr	1.5	58.8 ± 0.4 yr	0.95
Pure ^{44}Ti and pure ^{60}Co	5.2 cm	18	59.0 ± 0.5 yr	2.1	59.4 ± 0.6 yr	3.5
Pure ^{44}Ti and pure ^{60}Co	10.2 cm	15	58.5 ± 0.6 yr	1.8	59.2 ± 0.6 yr	2.3
Measurements at HU						
Mixed ^{44}Ti + ^{60}Co	6.7 cm	18	58.4 ± 0.5 yr	1.2	59.0 ± 0.7 yr	0.8

^a 1σ uncertainties are given. The weighted average of all above numbers give a value of 58.9 ± 0.2 yr.

^bDOF = degree of freedom.

*The Hebrew University of Jerusalem, Israel, †University of Vienna, Austria.

¹I. Ahmad *et al.*, Phys. Rev. C **74**, 065803 (2006).

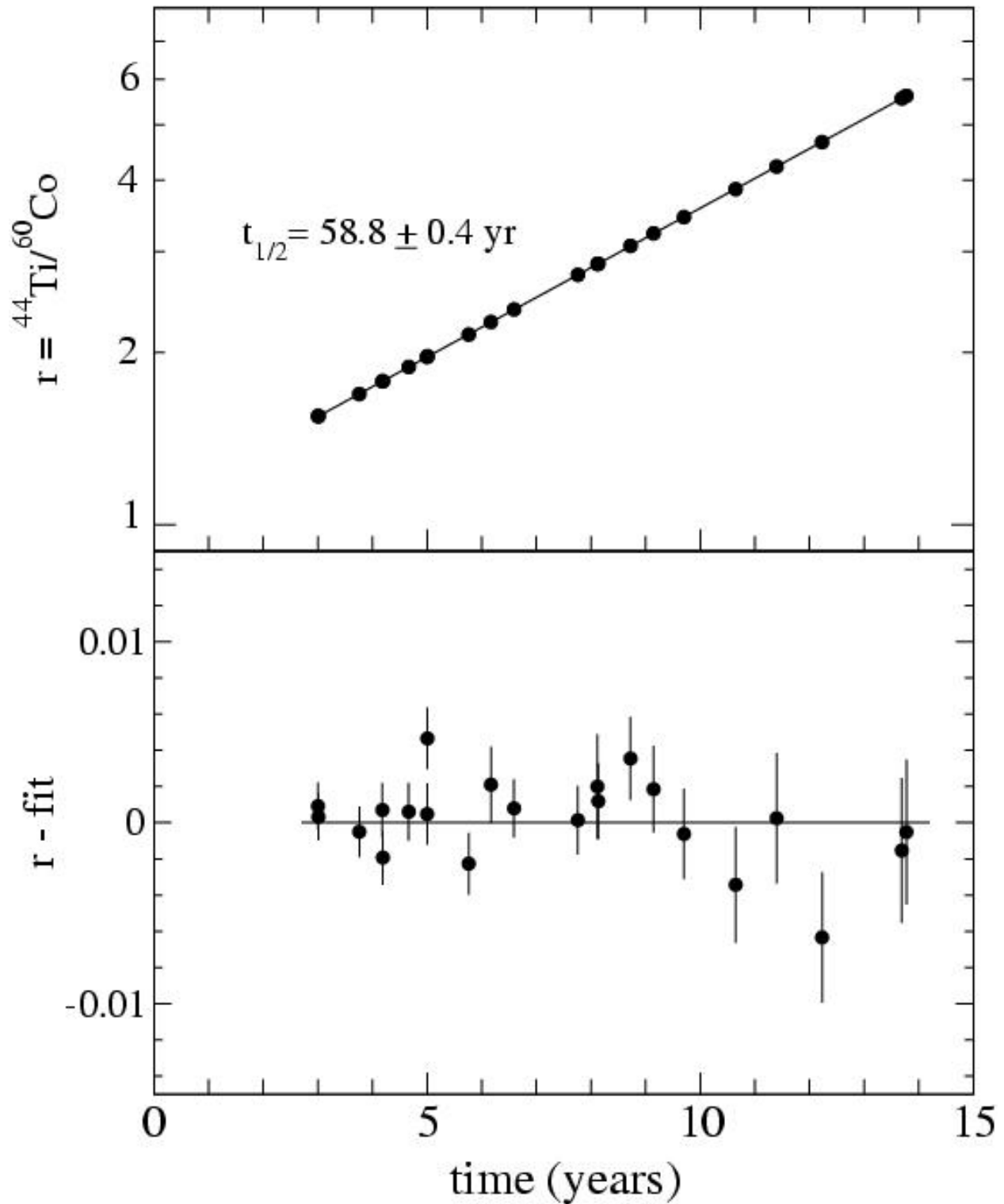


Fig. I-10. Semi-logarithmic plot of the ratios of the areas of the 1157.0 keV peak of ${}^{44}\text{Ti}$ and the 1173.2 keV of ${}^{60}\text{Co}$ peak against the time of measurement for the Argonne data. The line represents the best fit to data points and gives a half-life value of $58.8 \pm 0.4 \text{ yr}$. The bottom figure shows the difference between the measured data points and the values calculated by the fit.

a.8. Ultra-Sensitive Detection of the p -Process Nuclide ^{146}Sm (I. Ahmad, J. P. Greene, D. J. Henderson, C. L. Jiang, M. Notani, R. C. Pardo, N. Patel, K. E. Rehm, R. Scott, R. Vondrasek, N. Kinoshita,* T. Hashimoto,* T. Nakanishi,* A. Yokoyama,* H. Amakawa,† T. Mitsugashira,‡ T. Ohtsuki,§ N. Takahashi,¶ L. Jisonna,|| P. Collon,** D. Robertson,** C. Schmitt,** X. D. Tang,** Y. Kashiv,†† H. Nassar,†† and M. Paul††)

Among the very few p -process nuclides (see Ref. 1 for a review), ^{146}Sm is especially interesting in view of its half-life ($t_{1/2} = 1.03 \times 10^8 \text{ yr}$)²⁻⁵ and evidence for live ^{146}Sm in the Early-Solar System, established by isotopic anomalies of Nd in meteoritic material.⁶ Earth crust samples themselves display an interesting anomaly in their $^{142}\text{Nd}/\text{Nd}$ isotopic abundance compared to bulk meteoritic material (chondrites), tentatively interpreted as resulting from fractionation between Sm and Nd due to subtle differences in their geochemical properties during planet differentiation.^{7,8} The α decay of ^{146}Sm to ^{142}Nd constitutes in this case a Solar-System clock for such planetary processes, enhancing the importance of an accurate knowledge of the ^{146}Sm half-life value. This work is devoted to the development of a high-sensitivity direct detection method based on accelerator mass spectrometry (AMS). A first application will be a new determination of the ^{146}Sm half-life. The measurement will be performed using the relation $t_{146} = (A_{147}/A_{146})(N_{146}/N_{147})t_{147}$, where N_{146} (N_{147}) represent respectively the number of ^{146}Sm (^{147}Sm) atoms in a sample measured by AMS (ICP-MS), A_{146} (A_{147}) their respective α activities and t_{147} the accurately known ^{147}Sm α half-life

$$((1.17 \pm 0.02) \times 10^{11} \text{ yr}).^9$$

^{146}Sm samples were produced by activation of enriched ^{147}Sm targets *via* (γ, n), ($n, 2n$) and ($p, 2n$) reactions, the latter followed by electron capture. Sm was then purified and ^{147}Sm and ^{146}Sm α -counted at Kanazawa University (Japan). The experimental method used involves: (i) use of sputter cathodes (reduced Sm metal) in the ECR-II ion source; (ii) tuning of the accelerator system with $^{80}\text{Kr}^{12+}$ (pilot beam) and/or $^{147}\text{Sm}^{22+}$ and scaling the ATLAS beam line components by the small ratio of m/q 's for $^{146}\text{Sm}^{22+}$; and (iii) detection of ^{146}Sm in the gas-filled Enge split-pole spectrograph (10 Torr N_2) used to disperse the isobaric ^{146}Sm and ^{146}Nd (and other background) components.¹⁰ Figure I-11 shows α -radioactivity and AMS identification spectra measured in our experiment.

Figure I-11 demonstrates for the first time the successful identification of ^{146}Sm and its separation from stable ^{146}Nd by AMS. Efforts towards the measurement of the $^{146}\text{Sm}/^{147}\text{Sm}$ absolute isotopic ratios in the irradiated targets and a new determination of the ^{146}Sm half-life are underway.

*Kanazawa University, Ishikawa, Japan, †The University of Tokyo, Japan, ‡Tohoku University, Ibaraki, Japan, §Tohoku University, Miyagi, Japan, ¶Osaka University, Japan, ||Northwestern University, **University of Notre Dame, ††The Hebrew University of Jerusalem, Israel.

¹M. Arnould and S. Goriely, *Phys. Rep.* **384**, 1-84 (2003).

²D. C. Dunlavey and G. T. Seaborg, *Phys. Rev.* **92**, 206 (1953).

³M. Nurmi *et al.*, *Ann. Acad. Sci. Fenn. A* **VI**, 148 (1964).

⁴A. M. Friedman *et al.*, *Radiochim. Acta* **5**, 192-194 (1966).

⁵F. Meissner *et al.*, *Z. Phys.* **A327**, 171-174 (1987).

⁶S. B. Jacobsen and G. J. Wasserburg, *Earth Planet. Sci. Lett.* **67**, 137 (1984).

⁷M. Boyet and R. W. Carlson, *EPSL* **250**, 254-268 (2006).

⁸R. Andreasen and M. Sharma, *Science* **314**, 806 (2006).

⁹N. Kinoshita *et al.*, *J. Nucl. Radiochem. Sci.* **4**, 5 (2003).

¹⁰M. Paul *et al.*, *Nucl. Phys.* **A746**, 613 (2004), *Nucl. Instrum. Methods* **A277**, 418 (1989).

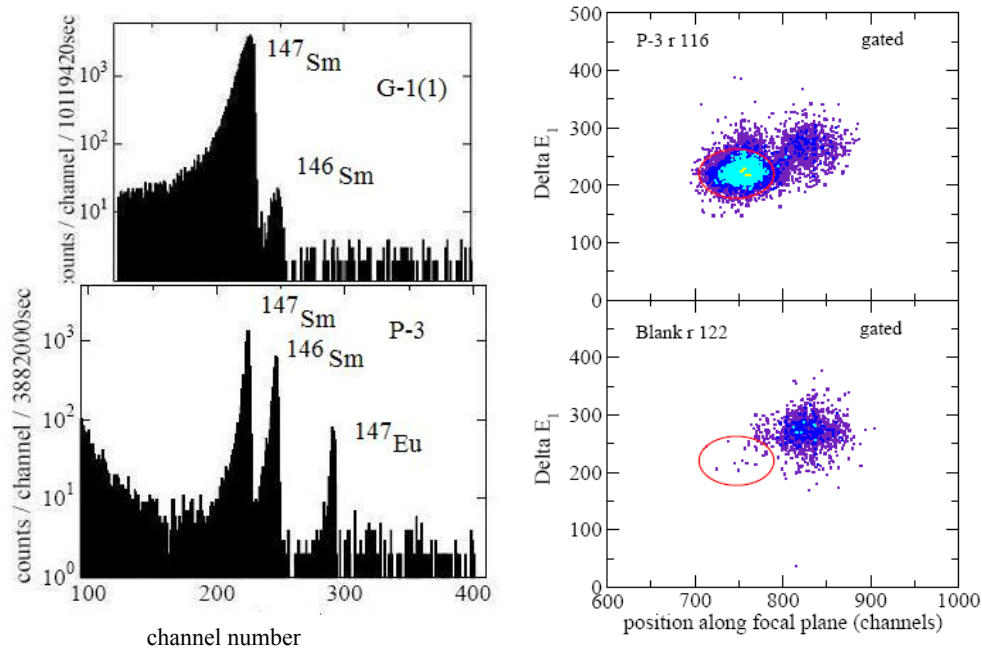


Fig. I-11. Left: α -spectra measured for the (γ, n) (top) and $(p, 2n)$ followed by electron capture (bottom) irradiated ^{147}Sm target. The groups corresponding to ^{147}Sm and ^{146}Sm (and an additional ^{147}Eu group produced in the proton activation) are observed; Right: spectra of energy-loss signal (ΔE_i) vs. position gated by a software window on ^{146}Sm events. The counts observed for the blank spectrum (right bottom) are attributed to a memory effect in the ion source and correspond to a ratio $^{146}\text{Sm}/^{147}\text{Sm}$ of 3×10^{-12} . Interestingly, Sm is observed to have a stopping power smaller than Nd in the measured energy range, in agreement with a SRIM 2006 calculation.

B. WEAK INTERACTIONS

Nuclear decays constitute an essential tool for studying the fundamental properties of the weak interaction. Several studies relating to this work are carried out at ATLAS and at other laboratories. One study involves a search for scalar currents in weak decays – in violation of the Standard Model – in the super-allowed $0+ 0+$ transitions by measuring the $\beta\nu$ angular correlation of ^{14}O nuclei stored in a Paul trap. Another important study is the determination of the nuclear structure relevant for the interpretation of potential observation of neutrino-less double beta in ^{76}Ge . The observation of this decay mode would establish the Majorana nature of neutrinos and their mass could be derived once the nuclear structure is sufficiently well known to compute the relevant transition matrix elements.

b.1. β -Decay of $^{69,70,71}\text{Kr}$ (C. J. Lister, S. M. Fischer, M. P. Carpenter, S. Gros, G. Savard, J. Clark,* and B. Blank†)

The β -decays of $N < Z$ Krypton isotopes are all interesting. $^{71}\text{Kr} \rightarrow ^{71}\text{Br}$ tests Mirror Symmetry. It is known already to have the largest non-analog branch known between mirror pairs. $^{70}\text{Kr} \rightarrow ^{70}\text{Br}$ is ideal for seeking low-lying $J = 0, 1$ states in ^{70}Br which are key for quantifying the difference in $T = 1$ and $T = 0$ pairing. $^{69}\text{Kr} \rightarrow ^{69}\text{Br}$ is a “Trojan Horse” as the subsequent $^{69}\text{Br} \rightarrow ^{68}\text{Se} + p$ breakup allows the mass of ^{69}Br to be inferred from the known ^{68}Se mass and the observation of the decay proton.

This experiment cannot be done at ANL as the production cross sections in fusion-evaporation are too small. It is also not possible at MSU using fragmentation, as a velocity filter (which is still under construction) is needed to remove very strong contaminants from the cocktail beam. However, at GANIL in France, this experiment is feasible using the LISE spectrometer. In collaboration with Bertram Blank from Bordeaux, we proposed the study in 2006 and now have got the beam time allocated for a run in November 2007.

*Yale University, †University of Bordeaux, France.

b.2. Progress at the Beta-Decay Paul Trap (N. D. Scielzo,* G. Savard,† S. Caldwell,† J. Fallis,‡ L. Gang,§ A. A. Hecht,¶ D. Lascar,|| A. Levand, H. Sharma,‡ I. Tanihata, A. Villari,** B. J. Zabransky, J. A. Clark,†† S. Gulick,‡‡ R. Segel,§§ and K. S. Sharma¶¶)

The development of the BPT program has continued with initial loadings with ^{14}O isotopes and test measurements of the beta-gamma correlation in its decay for the planned scalar current search experiment to be performed. The ^{14}O isotopes were produced with the $p(^{14}\text{N}, ^{14}\text{O})$ reaction, transported through the Enge spectrograph and stopped in the gas catcher where they were cooled and extracted for transport and accumulation in the gas cooler modified to operate at the higher frequencies required for very light ions. The ^{14}O ions extracted from the cooler were transported to the new isobar separator where they were purified and

accumulated before transfer to the BPT where further accumulation was implemented. Although issues with lifetime of the ions in the traps and the gas catcher were encountered because of vacuum failures occurring at short intervals before the runs, it was possible to obtain first beta-gamma angular correlation data from trapped radioactive ions inside the BPT. A spectra of beta-coincident gamma rays detected in the high-purity germanium detectors surrounding the BPT is shown in Fig. I-12. The spectra is extremely clean with only the 2313 keV gamma ray of interest and 511 keV annihilation radiation detected.

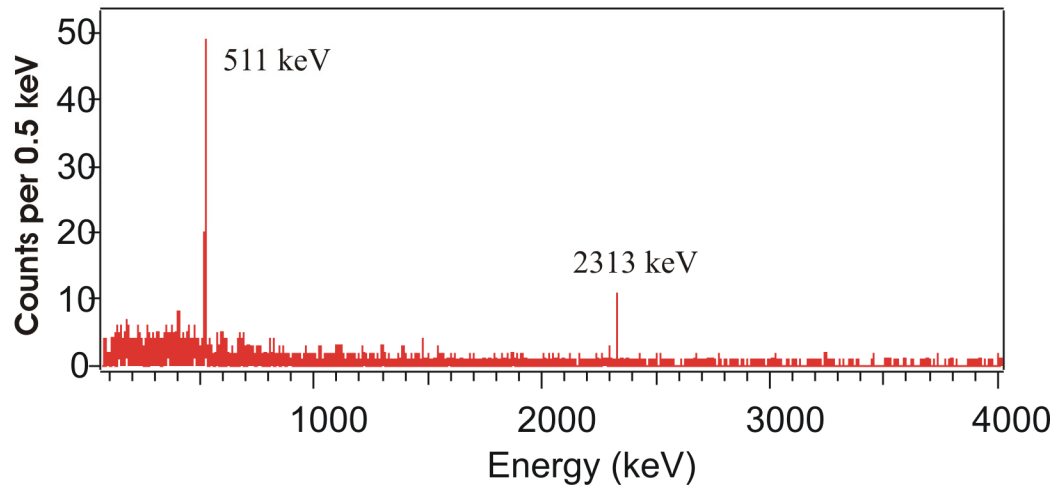


Fig. I-12. Gamma ray energy spectrum observed in coincidence with betas from the pure ^{14}O radioactive ion sample trapped in the BPT.

This initial correlation measurement was hampered by the limited lifetime of the radioactive ions inside the BPT which resulted in part of the sample decaying from the walls of the trap, not the trap centered. After determining experimentally that this was a gas purity issue and not an ion optical injection issue, it was still possible to subtract this contribution (at a severe loss in statistics) and observe the effect of the beta-neutrino

correlation as shown in Fig. I-13. The observed energy shifts are in agreement with the expected values in the Standard Model for a pure vector transition. This measurement was performed with only part of the silicon array in operation and under poor vacuum conditions. Both conditions have been cured and a higher statistics run is expected to follow.

*Argonne National Laboratory and Lawrence Livermore National Laboratory, †Argonne National Laboratory and University of Chicago, ‡Argonne National Laboratory and University of Manitoba, Canada, §Argonne National Laboratory and McGill University, Quebec, Canada, ¶Argonne National Laboratory and University of Maryland, ||Argonne National Laboratory and Northwestern University, **GANIL, Caen, France, ††Yale University, ‡‡McGill University, Quebec, Canada, §§Northwestern University, ¶¶University of Manitoba, Canada

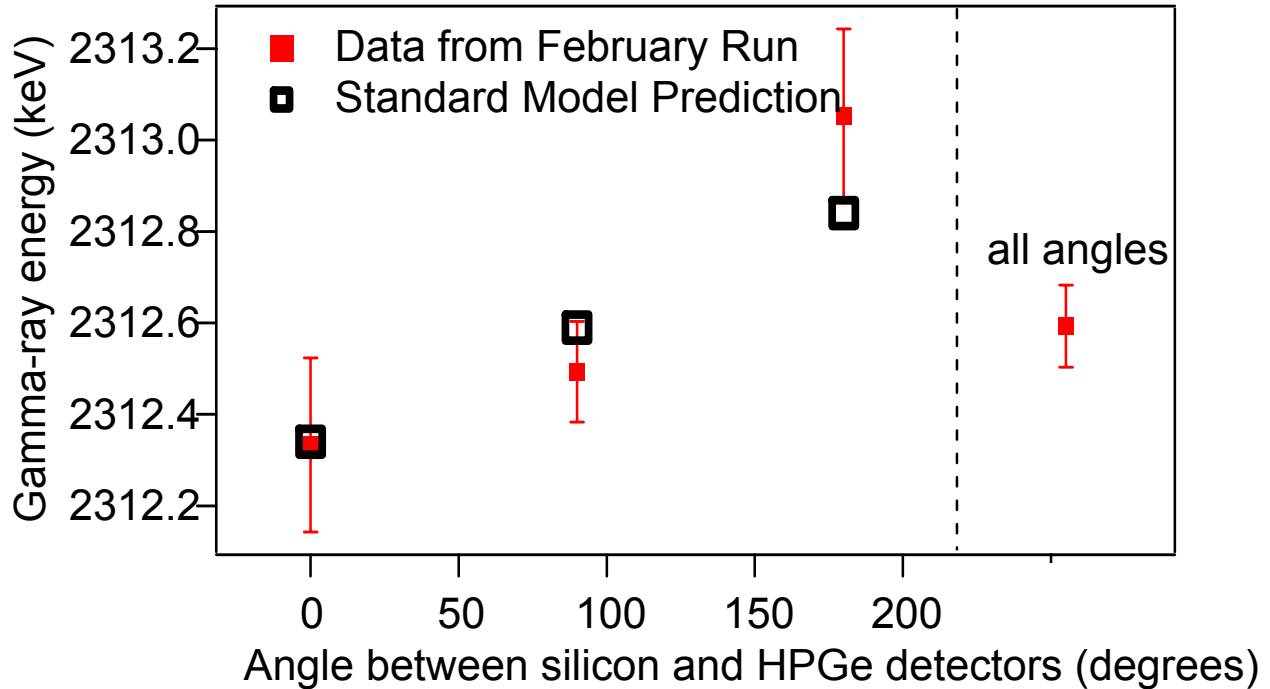


Fig. I-13. Doppler shifted gamma-ray energies as a function of the angle between the beta and gamma ray detected. The black squares are the shifts expected using the Standard Model predictions for a pure Fermi decay.

b.3. Nuclear Structure Relevant to Neutrinoless Double Beta Decay: ^{76}Ge and ^{76}Se

(J. P. Schiffer, S. Gros, C. L. Jiang, K. E. Rehm, X. D. Tang, S. J. Freeman,*
 J. A. Clark,† C. Deibel,† C. R. Fitzpatrick,* A. Heinz,† D. Hirata,§ B. P. Kay,*
 A. Parikh,† P. D. Parker,† A. C. C. Villari,‡ V. Werner,† and C. Wrede†)

The possibility of observing neutrinoless 2β decay¹ would offer the opportunity of determining the neutrino mass *if* the nuclear matrix element were known. Because theoretical calculations are uncertain, measurements of the occupations of valence orbits with nucleons active in the decay can be important. The occupation of valence neutron orbits in ^{76}Ge and ^{76}Se were determined by precisely measuring cross sections for both neutron-adding and removing transfer reactions. Our results indicate that the Fermi surface is much more diffuse than in theoretical (QRPA) calculations and that the populations of at least three orbits change significantly in the process -- by contrast in the calculations the changes are confined primarily to one orbit.

What unquestionably matters to the matrix element is knowing the population of the valence orbits of nucleons that switch from neutrons to protons. We have, therefore, undertaken a set of measurements to determine this quantity experimentally, and report here

on results focusing on the valence neutron populations and the differences in these populations for ^{76}Ge and ^{76}Se . In a previous experiment we determined that the neutron pair correlations in these two nuclei are quantitatively very similar.²

In the present measurement the Macfarlane-French sum rules were used with the measured sums of spectroscopic factors for neutron-adding and neutron-removing reactions. The active orbits for neutrons in these nuclei, with 42 and 44 neutrons, are $p_{3/2}$, $f_{5/2}$, $p_{1/2}$, and $g_{9/2}$. We took care to measure the absolute cross sections for the neutron-adding (d,p) and (α , ^3He), as well as for the neutron-removing (p,d) and (^3He , α) reactions at or near the peaks of the angular distributions for each l -value.

The measurement was carried out at the Yale tandem accelerator with the particles identified with the Enge spectrograph and gas-filled focal-plane detector backed by a scintillator. The target thicknesses together with

the spectrometer solid angle and beam current measurements were calibrated by measuring Rutherford scattering at an energy low enough to assure pure Coulomb scattering. Most of these reactions have been measured previously, but we show the angle-dependence in Fig. I-14, where all the ratios indicate

consistency with previously determined spins. While our primary purpose was to obtain accurate relative cross sections, a possible candidate for the missing $5/2^-$ state in ^{77}Ge was identified. The finite-range DWBA program PTOLEMY was used in the extraction of spectroscopic factors.

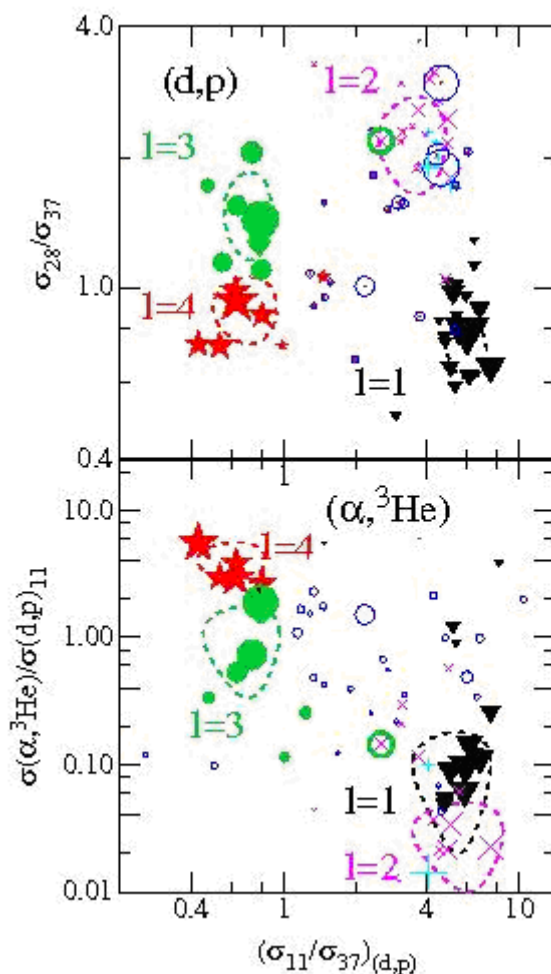


Fig. I-14. The ratios of cross sections are shown for different angles and reactions. The data on top are from (d,p) reactions. The data in the bottom panel are from a combination of the $(\alpha, ^3\text{He})$ and the (d,p) experiments. The symbols, one for each state, indicate the l -value assignments from previous work: triangles (black) are $l = 1$, circles (green) are $l = 3$, and stars (red) are $l = 4$. In addition, states not included in the analysis, are $l = 2$ transitions indicated by x 's and $l = 0$ by $+$ signs. States with unknown l -values are indicated by hollow circles (in blue). The size of the symbols is a rough measure of the cross sections. The dashed lines indicate the loci of the ratios for well-established l -values. The x surrounded by a (green) circle in the lower box, between the $l = 2$ and 3 islands is the 500-keV $5/2 \pm 5/2^-$ doublet ^{77}Ge .

To circumvent the issue of absolute spectroscopic factors we normalized the sums by requiring that the summed strengths for neutron-adding and neutron-removing spectroscopic factors, the vacancies and occupancies can, therefore, add up to the $(2J + 1)$

degeneracy of the orbits. The normalization factors for the $l = 1, 3$, and 4 transitions are 0.56, 0.55, and 0.62 respectively with rms fluctuations among the targets of 1, 12, and 6%. These values are consistent with the spectroscopic factors expected from short-range

correlations.

The results are summarized in Table I-4. Data with ^{74}Ge and ^{78}Se were obtained in parallel as a check. The constancy of the sums is a measure of the validity of the procedure. The occupancy is determined both from the neutron adding and the neutron removing reactions, but since the latter is smaller it is likely to be more accurate. The weighted mean of the two numbers is given in the last column.

While the estimates of uncertainties depend on some ambiguities in the DWBA sensitivity to distorting parameters and the possibility of missed states, and,

therefore, need to be taken with caution, there are several checks that give us some confidence in them.

- The normalization factors obtained for each target separately are relatively constant, and so are those obtained for $l = 3$ and 4 transitions separately.
- The summed neutron-removal and adding strengths for $^{74,76}\text{Ge}$ $^{76,78}\text{Se}$ are consistent with the expected value of 22.0 using two overall normalization numbers for all four targets.
- As an independent result, the neutron vacancies expected for the four nuclei are 8, 6, 8, and 6 respectively, while the observed values are 7.3, 6.1, 8.1 and 5.8, in very good agreement.

Table I-4. Summary of results.

l-value Target	Holes	Particles	Holes + Particles	Adopted Occupancy
l = 1 ($1/2^- + 3/2^-$)				
^{74}Ge	1.10			4.9
^{76}Ge	1.07	4.94	6.06	4.95(.2)
^{76}Se	1.56	4.63	5.93	4.42(.2)
^{78}Se	0.90			5.1
l = 3 ($5/2^-$)				
^{74}Ge	1.93	4.25	6.18	4.1
^{76}Ge	1.13	3.82	4.95	4.5(0.4)
^{76}Se	2.13	3.46	5.60	3.7(0.4)
^{78}Se	2.37	4.43	6.80	3.9
l = 4 ($9/2^+$)				
^{74}Ge	4.43	5.88	10.31	5.67
^{76}Ge	3.45	6.34	9.80	6.47(0.3)
^{76}Se	4.41	6.11	10.53	5.76(0.3)
^{78}Se	2.84	7.36	10.20	7.23

As to orbits beyond the closed shell at $N = 50$ that may have some occupancy, we have some limits from the neutron-removal reaction on ^{76}Se , which suggests that perhaps about 0.2 neutrons are in the $1d_{5/2}$ orbit. The difference in the occupancy of orbits in ^{76}Ge and ^{76}Se is 0.4 ± 0.2 in $1p$, 0.7 ± 0.3 in $0g_{9/2}$ and $0.7 \pm .4$ in $0f_{5/2}$, and is plotted in Fig. I-15 along with the QRPA calculations³ in the figure.

There are significantly more vacancies in the $1p$ and

especially in the $0f_{5/2}$ orbits in the data than in the calculations. For the neutrinoless double-beta decay experiments it is the **changes** in occupancy that are important and so, in the lower part of Fig. I-15 we show the differences between ^{76}Ge and ^{76}Se . From this it is very clear that while the QRPA results indicate that the predicted changes between the two nuclei are mostly in the $0g_{9/2}$ orbit, the experiment shows quite clearly that the changes in the $1p$ and $0f_{5/2}$ orbits are much larger than predicted.

*University of Manchester, United Kingdom, †Yale University, ‡GANIL, Caen, France, §GANIL, Caen, France and The Open University, Milton Keynes, United Kingdom.

¹S. R. Elliott and P. Vogel, Ann. Rev. Nucl. Part. Sci. **52**, 115 (2002).

²S. J. Freeman *et al.*, Phys. Rev. C **75**, 051301 (2007).

³V. A. Rodin and A. Faessler, private communication, calculated within the method of QRPA and RQRPA as described in V. A. Rodin, A. Faessler, F. Simkovic, and P. Vogel, Phys. Rev. C **68**, 044302 (2003) and Nucl. Phys. A**766**, 107 (2006).

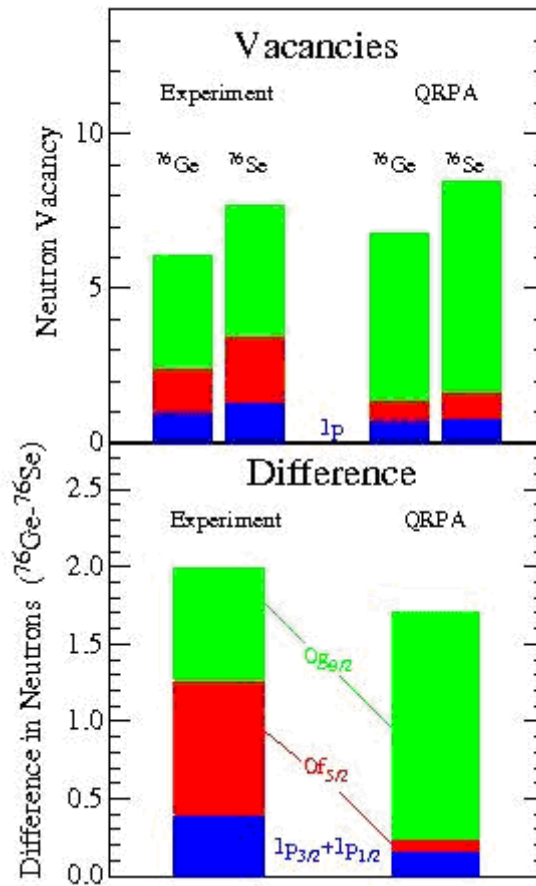


Fig. 1-15. The deduced neutron vacancies for ⁷⁶Ge and ⁷⁶Se are shown in the three active valence orbits and compared to those from the QRPA calculations of Ref. 3. The naive shell closure should give 6 and 8 vacancies for these two nuclei. The lower part of the figure shows the differences in these occupations (expected to be 2.0), again compared to the QRPA calculation.

C. SPECTROSCOPY OF VERY HEAVY ELEMENTS

Recent improvements in detection efficiency and production rate have enabled an important experimental program on the spectroscopy of trans-fermium nuclei. The aim of this program is to determine the location of single particle and 2-quasiparticle states in deformed No nuclei in order to help pin down the level spacing and, therefore, the stability of spherical super-heavy nuclei. Detailed nuclear structure properties of slightly lighter nuclei are also studied.

c.1. Two-Quasiparticle States in ^{254}No and the Stability of Superheavy Nuclei

(T. L. Khoo, D. Seweryniak, I. Ahmad, B. Back, R. Blinstrup, M. P. Carpenter, J. Chapman, C. N. Davids, R. V. F. Janssens, F. G. Kondev, T. Lauritsen, C. J. Lister, E. F. Moore, D. Peterson, S. F. Zhu, S. K. Tandel,* G. Mukherjee,*[†] P. A. Butler,[‡] P. Chowdhury,* P. T. Greenlees,[§] A. A. Hecht,[†][¶] A. Heinz,^{||} R.-D. Herzberg,[‡] P. Ikin,[‡] G. D. Jones,[‡] P. Reiter,^{**} U. S. Tandel,* and X. F. Wang[†],^{††})

A central question in the study of superheavy nuclei is the location of the magic gaps. Models predict gaps with significantly different locations in Z and N as a consequence of different single-particle energies. Hence, discriminating tests of the models can be made by checking the predicted energies against experimental values. In this manner, 2-quasiparticle (qp) states in shell-stabilized nuclei probe the levels that govern the stability of superheavy nuclei, test 2-qp energies from theory and, thereby, check their predictions of magic gaps.

We have identified in ^{254}No ($Z = 102$) 2- and 4-qp isomers, with quantum numbers $K^\pi = 8^-$ and (14^+) , and a low-energy 2-qp $K^\pi = 3^+$ state. It is significant that a constituent of the $K^\pi = 3^+$ configuration is the $[521]1/2$ orbit, from the spherical $f_{5/2}$ shell, which lies above a $Z = 114$ gap that appears with Woods-Saxon (WS) single-particle energies. The use of WS single-particle energies reproduces the experimental proton 2-qp energies in ^{254}No . The WS potential also systematically reproduces the 1-qp energies in odd-A heavy nuclei.¹ These results indicate that WS energies are valid for Z up to 102 and suggest that a proton gap would occur

at $Z = 114$ -- if the WS potential continues to describe the proton energy levels of nuclei with $Z > 102$. In contrast, there are shortcomings in the 2-qp energies from self-consistent mean-field theories, with corresponding deviations in 1-qp energies in neighboring odd-A nuclei. Therefore, their predictions of magic gaps at $Z = 120$ and 126 should be viewed with reservations. The parameters of the interactions used in self-consistent mean-field SHFB and RMF models have been adjusted to fit bulk properties of closed-shell nuclei. Thus, the success of their single-particle energies is impressive, but definitely do require improvements,² *e.g.* a lowering of the proton $i_{13/2}$ orbit, to reproduce *all* measured 1- and 2-qp energies. To preserve the virtue of self-consistency when extrapolating to the heaviest nuclei, there is a need for a new interaction designed for this purpose.

In summary, spectroscopic measurements of 2-qp states in ^{254}No provide the first experimental information on the proton magic shell gap for superheavy nuclei by discriminating among the theories that make predictions on the gap. This work has been published in Physical Review Letters.²

*University of Massachusetts-Lowell, [†]Argonne National Laboratory, [‡]University of Liverpool, United Kingdom, [§]University of Jyväskylä, Finland, [¶]University of Maryland, ^{||}Yale University, ^{**}Universität zu Köln, Germany, ^{††}University of Notre Dame.

¹R. Chasman *et al.*, Rev. Mod. Phys. **49**, 833 (1978); A. Parkhomenko and A. Sobiczewski, Acta Phys. Pol. **B35**, 2447 (2004), *ibid.* **B36**, 3115 (2005).

²S. K. Tandel *et al.*, Phys. Rev. Lett. **97**, 082502/1-4 (2006).

c.2. $K = 8^-$ Isomers and $K = 2^-$ Octupole Bands in ^{252}No and $N = 150$ Isotones

(A. Robinson, T. L. Khoo, I. Ahmad, D. Seweryniak, S. Gros, D. Peterson, B. B. Back, M. P. Carpenter, C. N. Davids, J. P. Greene, A. Hecht, R. V. F. Janssens, F. G. Kondev, T. Lauritsen, C. J. Lister, E. F. Moore, S. Zhu, S. K. Tandel,* P. Chowdhury,* U. Tandel,* A. Heinz,† X. Wang,‡ P. A. Butler,§ R. Herzberg,§ G. Jones,§ S. Eeckhaudt,¶ P. T. Greenlees,¶ R. Julin,¶ M. Leino,¶ J. Uusitalo,¶ P. Reiter,|| and G. Mukherjee**)

In shell-stabilized heavy nuclei around ^{254}No , many of the orbitals around the Fermi level have large projections of their spin along the symmetry axis so that high- K isomers should be common. The isomers, which can be studied in a quiet environment far from the target, provide opportunities to investigate the excited configurations of nuclei populated with sub-microbarn cross sections, not only of the isomers, but also of lower-lying rotational bands fed in the isomeric decays. The occurrence of K isomers reveals the applicability of K -selection rules, indicating that K is a good quantum number and that the nucleus has a prolate shape with axial symmetry. The energies of 2-quasiparticle states provide incisive tests of theories. An example is the $K = 8^-$ isomer at 1296 keV in ^{254}No which decays to a $K = 3^+$ band. The energies of the $K = 3^+$, 8^- states, which are built on proton configurations, reveal that Woods-Saxon proton single-particle energies are accurate for Z up to at least 102. In ^{252}No , 2-quasiparticle energies calculated with the Woods-Saxon potential also suggest a $K = 8^-$ isomer, but built instead on neutron states, at a lower energy of 1.01 MeV. Hence, detection of this predicted isomer constitutes a test of the Woods-Saxon single-particle energies.

The $^{206}\text{Pb}(^{48}\text{Ca},2n)$ reaction was used to populate states in ^{252}No . The nuclides were transported and uniquely identified by the Fragment Mass Analyzer (FMA). The nuclides were implanted into individual $1 \times 1 \text{ mm}^2$ pixels of a double-sided Si strip detector. Time and spatial correlations then identified the decay of an isomer, *i.e.*, in each pixel, a delayed coincidence between the implant and an electron signal, with sum energy 100-500 keV. Gamma rays from the isomer were detected in prompt coincidence with the delayed electron signal. In this manner, an isomer was discovered in ^{252}No , with a half-life of 109 ms and

quantum numbers $I, K^\pi = 8, 8^-$. It decays *via* multiple pathways into a $K^\pi = 2^-$ octupole vibrational band. The decay scheme of the isomer is shown in Fig. I-16, together with that of the isotone ^{246}Cm .¹⁻² The two decay schemes are very similar.

The energies of $IK^\pi = 22^-$ and 88^- states in the $N = 150$ isotones are displayed in Fig. I-17. They span an impressively wide range of $Z = 94-102$, especially for such heavy nuclei. The 8^- energies are rather constant (within 75 keV), which suggests that the 8^- state has a neutron configuration – as expected. Similarly, the energies of the 2^- octupole band head are constant within 90 keV. A striking exception is the 2^- energy in ^{248}Cf , where there is a pronounced minimum. For the 8^- states, we propose a neutron 2-qp configuration $\{[734]9/2, [624]7/2\}$. The calculated energies for this configuration, based on Woods-Saxon single-particle energies and a Lipkin-Nogami prescription for pairing, are 170-260 keV lower than the measured ones, but within the model uncertainty of ~ 300 keV. The deep minimum at $Z = 98$ is due to the nearly degenerate proton orbitals $7/2[633]$ and $3/2[521]$ (Ref. 5), which constitute a low-lying 2-qp proton state. Only in ^{248}Cf is there a confluence of low-lying proton and neutron 2^- 2-qp states, increasing the octupole collectivity and, thereby, lowering the vibrational energy. Quasiparticle (QRPA) calculations for octupole vibrations have been performed using single-particle energies given by a modified Nilsson potential, which approximate those from the Woods-Saxon potential. The trend with Z of the $K = 2^-$ energies, including the minimum at $Z = 98$, is reproduced by the QRPA calculations. All calculated energies are higher by ~ 200 keV. This difference is not significant since the calculated energies are very sensitive to the magnitude of the octupole force, *e.g.*, a 2% reduction would give agreement with the experiment.

*University of Massachusetts-Lowell, †Yale University, ‡University of Notre Dame, §University of Liverpool, United Kingdom, ¶University of Jyväskylä, Finland, ||Universität zu Köln, Germany, **Variable Energy Cyclotron Center, Kolkata, India.

¹K. Moody *et al.*, *Z. Phys. A - Atomic Nuclei* **328**, 417 (1987).

²I. Ahmad, in *Proc. Frontiers in Nuclear Physics*, Dubna, p. 31 (1995).

³S. W. Yates, A. M. Friedman, and I. Ahmad, Phys. Rev. C **12**, 442 (1975).

⁴T. Greenlees *et al.*, private communication (2006).

⁵I. Ahmad *et al.*, Phys. Rev. C **71**, 054305 (2005).

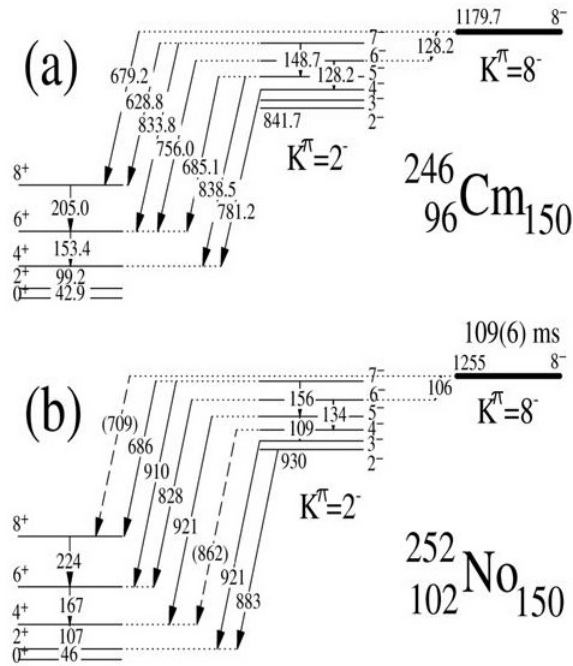


Fig. I-16. Decay schemes of the $K^\pi = 8^-$ isomers in the $N = 150$ isotones, ^{246}Cm and ^{252}No .

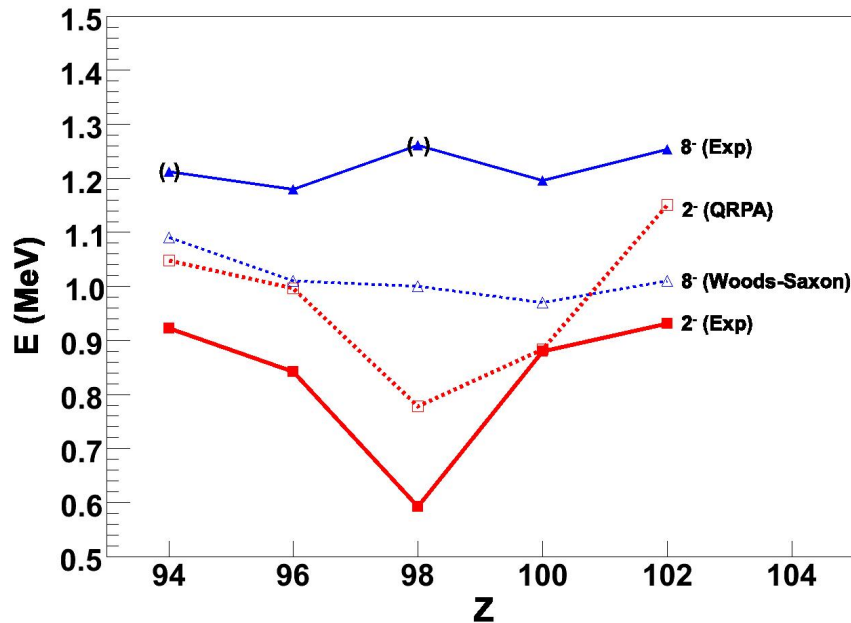


Fig. I-17. Energies of the $K^\pi = 8^-$ isomers (blue) and 2^- octupole bands (red) in $N = 150$ isotones with $Z = 94-102$ from experiment (filled symbols) and theory (open symbols). The data for ^{244}Pu , ^{246}Cm , ^{248}Cf and ^{250}Fm are from Ref. 1-4. Based on the published data^{1,3} we have made assignments of 8^- states in ^{244}Pu and ^{248}Cf .

c.3. Octupole Strength in the ^{238,240,242}Pu Nuclei (R. V. F. Janssens, S. Zhu, M. P. Carpenter, I. Ahmad, J. P. Greene, T. L. Khoo, T. Lauritsen, C. J. Lister, D. Seweryniak, F. G. Kondev,* X. Wang,† U. Garg,† I. Wiedenhöver,‡ A. Bernstein,‡ P. Wilson,‡ E. Diffenderfer,‡ C. Teal,‡ A. Larabee,§ B. Meredith,§ and S. Freeman||)

Octupole correlations have attracted much attention over the years, and the actinide nuclei remain an interesting source of information because they offer the possibility to investigate the interplay between collective rotation and octupole degrees of freedom. Sheline and Riley¹ recently pointed out that a deep depression of the excitation energies of the lowest 1^- states occurs in the region of neutron numbers from 132 to 140 for Ra and Th nuclei, where strong octupole correlations lead to the stable octupole deformation. Moreover, a smaller depression was found at neutron numbers of 144 and 146 for Pu isotopes, *i.e.* ^{238,240}Pu. This observation is consistent with an earlier suggestion by I. Wiedenhöver *et al.*² that, in the lightest Pu isotopes, strong octupole correlations lead to the absence (239, 240) or delay in frequency (238) of the strong proton alignment observed in the heavier (241, 242, 243, 244) Pu isotopes.

The present work focuses on the octupole correlations in 3 even even ($A = 238, 240, 242$) Pu nuclei. A series of "unsafe" Coulomb excitation experiments as well as 1 neutron transfer measurements has been carried out with Gammasphere at ATLAS. The so called "unsafe" Coulomb excitation technique (beam energy is about 15% above Coulomb barrier) was used in order to enhance the feeding of the highest spin states. Billions of events with fold 3 or higher were collected. In the subsequent data analysis, the raw data were converted into both the traditional RADWARE format (Cube and Hypercube) and the latest BLUE database format.

For ²³⁸Pu, only the yrast and octupole vibrational bands are seen in the level scheme resulting from our data analysis (see Fig. I-18) since this data is from the weak 1 neutron pick up channel in reactions of a ²⁰⁷Pb beam with a ²³⁹Pu target. Both bands are extended towards higher spin by 2 more levels, which are critical, therefore, the obtained alignment plot better indicates that the expected "back bending" is delayed at least up to $\hbar\omega \sim 0.3$ MeV. It is also noteworthy that the levels in the yrast and octupole bands are interleaved at the highest spins.

In ²⁴⁰Pu, the key $(I + 1)^+ \rightarrow I^-$ E1 linking transitions have been established at high spin. This can be viewed as solid evidence for an octupole rotor. The investigation of the branching ratios, between the inter- and in-band transitions, also supports the conclusion of a stable octupole deformation at high spin. This is in agreement with theoretical predictions by Jolos and von Brentano.^{3,4}

In ²⁴²Pu, the yrast and 5 excited bands (1 of positive and 4 of negative parity) were observed. One of the most notable differences between ²⁴²Pu and ²⁴⁰Pu is that in ²⁴²Pu all excited bands decay to the yrast band. The so called "back bending" occurs at $\hbar\omega \sim 0.25$ MeV, and no pattern of interleaved states with alternating spin and parity is observed.

Detailed calculations are being performed currently, hence, a complete interpretation of the experimental results is still under discussion.

*Nuclear Engineering Division, Argonne National Laboratory, †University of Notre Dame, ‡Florida State University, §Greenville College, ||University of Manchester, United Kingdom.

¹R. K. Sheline and M. A. Riley, Phys. Rev. C **61**, 057301 (2000).

²I. Wiedenhöver *et al.*, Phys. Rev. Lett. **83**, 2143 (1999).

³R. V. Jolos and P. von Brentano, Phys. Rev. C **49**, R2301 (1994).

⁴R. V. Jolos and P. von Brentano, Nucl. Phys. **A587**, 377 (1995).

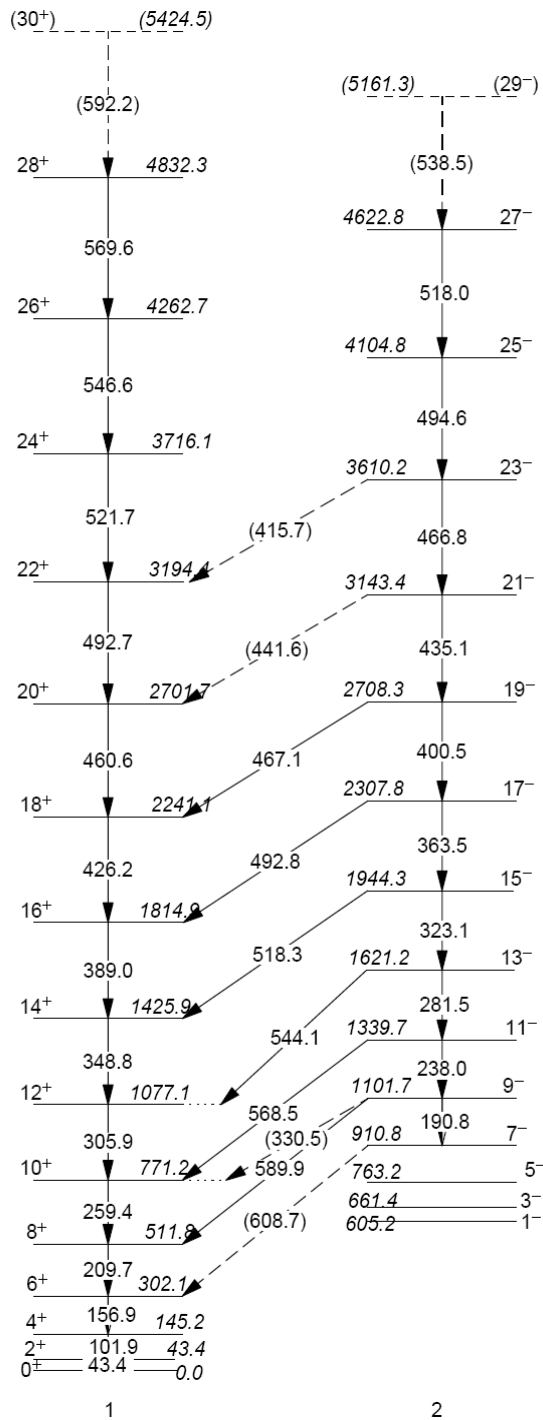


Fig. I-18. Partial level scheme of ^{238}Pu .

c.4. Measurements of the ^{246}Cm Half-Life (I. Ahmad, F. G. Kondev, J. P. Greene, M. A. Kellett,* and L. L. Nichols*)

Precise half-life values of actinide nuclei and their decay properties are needed for proper handling of the radioactive waste generated in reactors. Long half-lives are difficult to measure and, hence, it is important to use different techniques to reduce systematic uncertainties. One method which has not been much used in the past is the measurement of the daughter activity in the presence of the parent. We have determined the ^{246}Cm half-life by measuring the activity of ^{246}Cm in a sample of ^{250}Cf after it has decayed several half-lives. A thin source of ^{250}Cf was prepared

in the 1970s with an electromagnetic isotope separator and allowed to decay. The alpha spectra of this source was measured with a PIPS Si detector. An example of the alpha spectrum is shown in Fig. I-19. Using the ratio of the alpha activities of ^{246}Cm and ^{250}Cf and the decay time and the half-life of ^{250}Cf ($13.08 \pm .09$ yr), the half-life of ^{246}Cm was determined to be 4706 ± 40 yr. This is in agreement with previously measured precise values of ^{246}Cm . The results of this study were published.¹

*International Atomic Energy Agency, Vienna, Austria.

¹F. G. Kondev *et al.*, *Appl. Radiat. Isot.* **65**, 335 (2007).

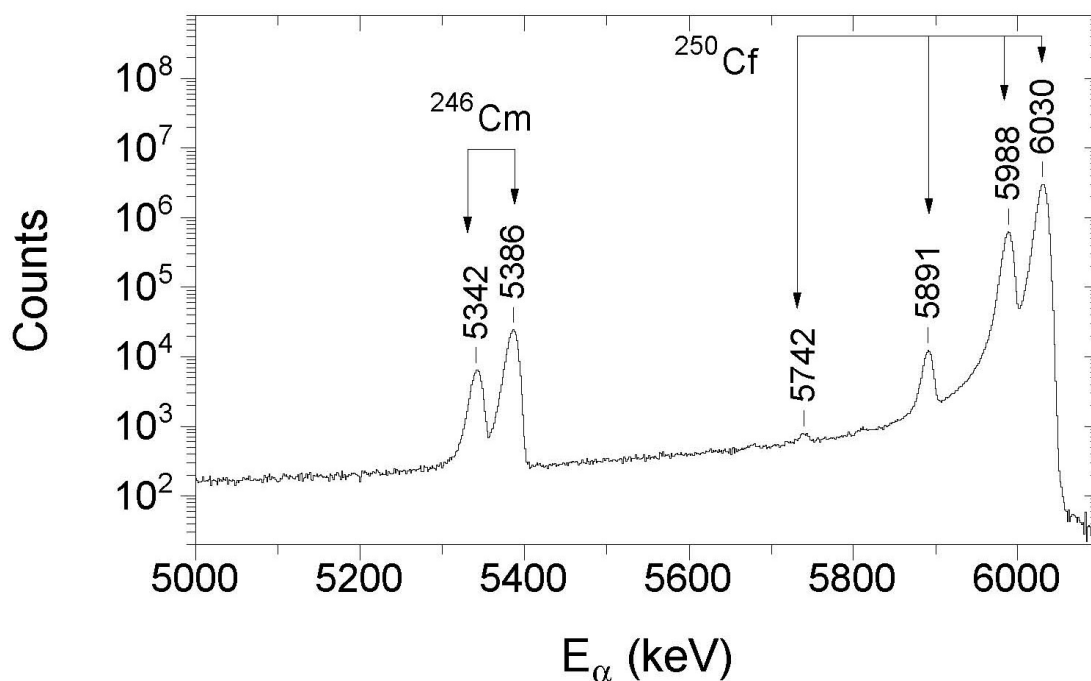


Fig. I-19. The α -particle spectrum of a mass-separated ^{250}Cf source measured with a 25-mm^2 PIPS detector at a source-to-detector geometry of 0.23%.

D. STRUCTURE OF NUCLEI FAR FROM STABILITY

The study of nuclei far from stability is a central focus of modern nuclear physics research. A recent success was the identification of the first excited state in ^{101}Sn , which represents a single neutron orbit outside the doubly-magic ^{100}Sn core. Other studies are attempting to reach the doubly-magic ^{78}Ni nucleus on the neutron-rich side using the deep-inelastic reaction mechanism. A wide range of studies are pursued which aim to reveal the changes in shell structure and shapes of nuclei away from the line of β -stability using beams from ATLAS and other facilities.

d.1. Neutron-Rich Nuclei

d.1.1. Is the Nuclear Spin-Orbit Interaction Changing with Neutron Excess?

(J. P. Schiffer, K. E. Rehm, B. P. Kay,* S. J. Freeman,* J. A. Clark,† C. Deibel,* A. Heinz,† A. Parikh,† P. D. Parker,* and C. Wrede*)

The single-particle character of nuclei underlies much of our understanding of nuclear structure. The states formed by a proton outside the closed shell of 50 protons, the $g_{7/2}$ - $h_{11/2}$ separation in particular, was studied with the (α,t) reaction on all the stable, even Sn isotopes in 2004 to demonstrate that the difference between major single-particle states was changing drastically with neutron excess.¹ This result has been explained by Otsuka² by the effect of the tensor part of the nucleon-nucleon interaction as the $h_{11/2}$ neutron orbit is filling in the Sn isotopes. This explanation also seems to account, at least qualitatively, for the observed changes in single-particle states, and even shell structure, in light nuclei away from the region of stability.³

An experiment to obtain quantitative information on neutron single-particle states in heavy nuclei, outside $N = 82$, was carried out on the separation between the $i_{13/2}$ and $h_{9/2}$ single-neutron states. The measurement was carried out at the Yale tandem using the $(\alpha,^3\text{He})$ reaction, that is particularly suited for measurements

with high orbital-angular-momentum transfer. Targets were a problem because the available stable $N = 82$ targets are ^{136}Xe , ^{138}Ba , ^{140}Ce , ^{142}Nd , and ^{144}Sm . Xenon is a gas and, therefore, difficult to use as a target, while the metallic targets all oxidize quickly. With some care these difficulties have been overcome.

The single-particle states are all fragmented into two components, apparently due to the proximity of the $9/2^-$ and $13/2^+$ states formed by coupling an $f_{7/2}$ neutron to the 2^+ or 3^- vibration in these nuclei. The centroids of the single-particle states were observed, and the trends in the separation show a behavior that is similar to that predicted by the tensor matrix elements, when the protons are filling the $0g_{7/2}$ and $1d_{5/2}$ orbits.³ The results are shown in Fig. I-20.

In addition, from the spectroscopic factors, the mixing matrix elements to the weak coupling states could be extracted, and these were found to be remarkably constant. These are listed in Table I-5.

Table I-5. Mixing Matrix Elements in $N = 83$ Nuclei.

	$h_{9/2} - 2^+ \otimes f_{7/2}$	$i_{13/2} - 3^- \otimes f_{7/2}$
^{139}Ba	162 ± 6 keV	629 ± 17 keV
^{141}Ce	151 ± 5 keV	632 ± 34 keV
^{143}Nd	145 ± 2 keV	686 ± 16 keV
^{145}Sm	162 ± 4 keV	725 ± 9 keV
Average (rms)	150 keV (9)	698 keV (50)

*University of Manchester, United Kingdom, †Yale University.

¹J. P. Schiffer *et al.*, Phys. Rev. Lett. **92**, 162501 (2004).

²T. Otsuka *et al.*, Phys. Rev. Lett. **95**, 232502 (2005).

³A. Ozawa *et al.*, Phys. Rev. Lett. **84**, 5493 (2000).

⁴B. H. Wildenthal *et al.*, Phys. Rev. C **3**, 1199 (1971).

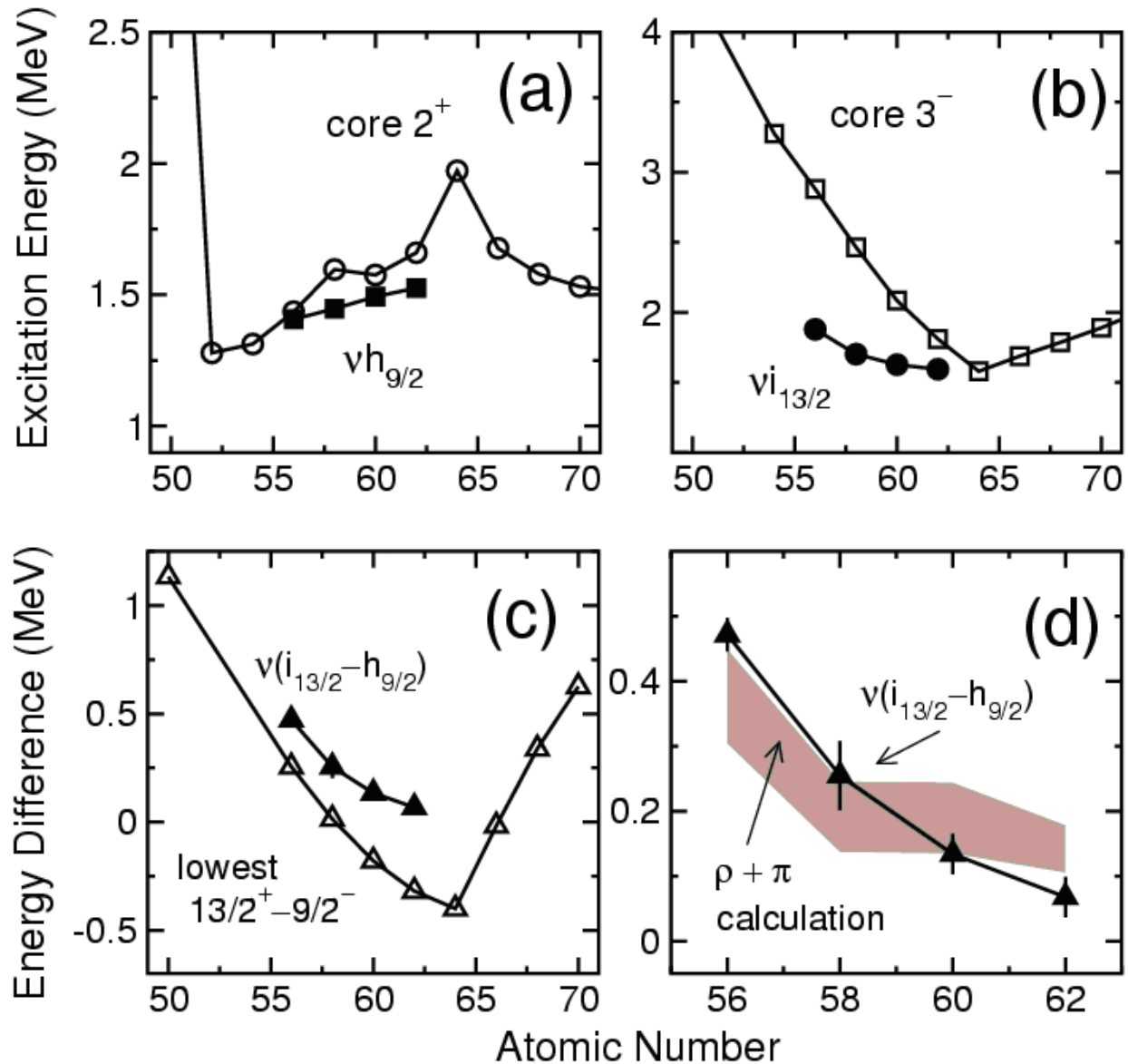


Fig. I-20. The top two boxes show the energy dependence of the single-particle states determined in the present experiment for $N = 83$ systems (solid symbols), compared to the energies of the vibrational states in the core $N = 82$ nuclei (open symbols), for the $h_{9/2}$ and $i_{13/2}$ states respectively in (a) and (b). In (c) the energy splitting between these two centroid energies from the present work is shown in solid symbols while the open symbols show the separation between the lowest states with these quantum numbers in all $N = 83$ nuclei. In (d) the present results are again shown with the colored band representing the results with the tensor interaction. The width of this band represents the experimental uncertainty⁴ in the proton occupation numbers.

d.1.2. Excited States in the Ca Isotopes Towards “Doubly-Magic” ^{54}Ca : β Decay of $^{51-53}\text{K}$ (R. V. F. Janssens, S. Zhu, M. P. Carpenter, F. G. Kondev, X. Wang, R. Broda,* B. Fornal,* P. Mantica,† J. Pereira,† J. Stoker,† J. Pinter,† G. C. Ball,‡ G. Hackman,‡ A. Andreyev,‡ A. C. Morton,‡ C. Pearson,‡ S. C. Ravuri,‡ C. Svensson,§ P. E. Garrett,§ D. Bandyopadhyay,§ G. F. Grinyer,§ B. Hyland,§ A. A. Phillips,§ M. A. Schumaker,§ J. C. Waddington,¶ R. A. E. Austin,|| J. J. Ressler,** J. Kozemczak,†† and A. Larabee††)

Shell model calculations with the new GXPF1 *pf* shell interaction¹ have suggested the development of significant sub-shell gaps at $N = 32$ and $N = 34$ in the Ca isotopes. These new gaps in these neutron-rich nuclei are believed to be the result of a reduced proton $f_{7/2}$ – neutron $f_{5/2}$ monopole interaction as protons are removed from the $f_{7/2}$ orbital, when the proton number decreases from $Z = 28$ (Ni) to $Z = 20$ (Ca). Confirmation of the $N = 32$ sub-shell gap has already been achieved in the Ti and Cr isotopic chains, based on the results of beta-decay measurements, high-spin state studies following deep inelastic reactions and $B(E2)$ transition strengths through Coulomb excitation of intermediate energy fragments.²⁻⁴ However, there is no evidence for a $N = 34$ shell closure in ^{56}Ti and ^{58}Cr . For example, the energy of the first excited 2^+ state in ^{56}Ti ⁵ falls midway between the shell model predictions with the GXPF1 Hamiltonian, where a shell closure is expected, and those with the KB3G interaction, where this gap is absent. However, the presence of a $N = 34$ shell gap at ^{54}Ca , where the proton $f_{7/2}$ shell is empty, cannot be ruled out. In fact, the latest calculations with a modified GXPF1 interaction, labeled GXPF1A, still predict a gap at $N = 34$ in the Ca isotopic chain.^{3,6} Systematic data on the approach to the proposed ^{54}Ca “doubly-magic” nucleus are critical to test the latest

shell model predictions. To put it simply, with the $Z = 20$ proton shell closed, the neutron-rich calcium isotopes provide a unique opportunity to delineate neutron shell structure above $N = 28$. Specifically, information on the ordering and on the location of the $p_{3/2}$, $p_{1/2}$ and $f_{5/2}$ orbitals is highly desirable. In order to address the issue, a study of the $^{51-53}\text{Ca}$ isotopes through the beta decay of mass selected $^{51-53}\text{K}$ nuclei was undertaken at the ISAC facility located at TRIUMF in Vancouver.

The neutron-rich $^{51-53}\text{K}$ isotopes were produced by spallation of a Ta target by 500 MeV protons, and extracted from a surface ionization source as singly-charged ions. The desired isotopes, following mass separation, were implanted into a moving tape collector located at the center of the 8π spectrometer, which comprises 20 Compton suppressed HPGe detectors. The SCEPTAR array of plastic scintillator detectors was used to detect the beta particles. The event-by-event coincidence data recorded for subsequent analysis included beta- γ and beta- γ - γ coincidences. Beta-gated, γ -single spectra and $\gamma\gamma$ coincidence matrices have been analyzed for all three cases ($^{51-53}\text{K}$). Figure I-21 is a spectrum obtained for ^{51}K . The detailed analysis is ongoing.

*Niewodniczanski Institute, Krakow, Poland, †Michigan State University, ‡TRIUMF, Vancouver, British Columbia, §University of Guelph, Ontario, ¶University of McMaster, Hamilton, Ontario, ||St. Mary’s University, Halifax, Nova Scotia, **Simon Fraser University, Burnaby, British Columbia, ††Greenville College.

¹M. Honma *et al.*, Phys. Rev. C **65**, 061301(R) (2002).

²R. V. F. Janssens *et al.*, Phys. Lett. **B546**, 55 (2002).

³D.-C. Dinca *et al.*, Phys. Rev. C **71**, 041302(R) (2005).

⁴S. Zhu *et al.*, Phys. Rev. C **74**, 064315 (2006).

⁵S. N. Liddick *et al.*, Phys. Rev. Lett. **92**, 072502 (2004).

⁶A. Gade *et al.*, Phys. Rev. C **74**, 021303(R) (2006), T. Otsuka, private communication.

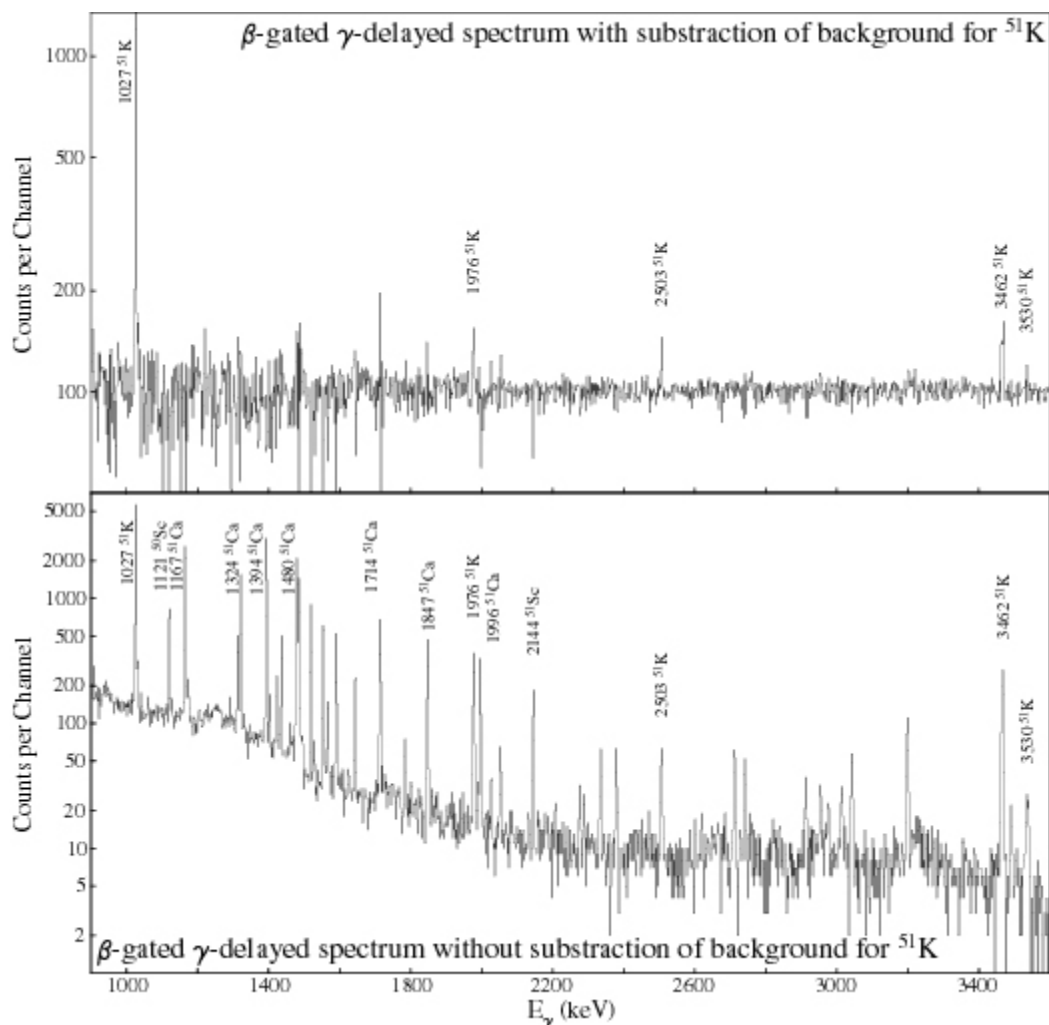


Fig. I-21. Sample spectra from the beta decay measurements on ^{51}K under the conditions given with the data.

d.1.3. Shell Model States in Neutron-Rich Potassium Isotopes (S. Zhu, R. V. F. Janssens, M. Carpenter, R. Broda,* W. Królas,* B. Fornal,* A. Gadea,† N. Marginean,† L. Corradi,† A. M. Stefanini,† J. Wrzesiński,* T. Pawłat,* S. Beghini,‡ G. DeAngelis,† F. Della Vedova,† E. Farnea,† E. Fioretto,† B. Guiot,† S. Lunardi,‡ P. Mantica,|| P. Mason,‡ G. Montagnoli,‡ D. R. Napoli,† R. Orlandi,† I. Pokrovskiy,† E. Sahin,† F. Scarlassara,‡ S. Szilner,¶ C. A. Ur,‡ M. Trotta,§ and J. J. Valiente-Dobon†)

We used the PRISMA spectrometer coupled with the CLARA gamma multi-detector array at the Legnaro National Laboratory to identify gamma rays in exotic neutron-rich nuclei produced in the $^{48}\text{Ca} + ^{238}\text{U}$ reaction. The spectrometer is able to provide the nuclear product A and Z identification. The precise determination of the product velocity vectors allowed to

correct properly for the Doppler shift of gamma rays emitted in flight and associated with a given isotope. The analysis focused on the neutron-rich ^{48}K and ^{49}K isotopes, and revealed a number of gamma transitions de-exciting states populated in each isotope. Figure I-22 displays the gamma spectrum obtained for ^{48}K .

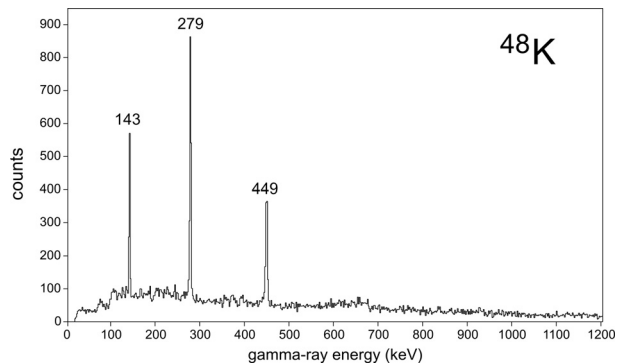


Fig. I-22. Gamma-ray spectrum measured by CLARA for ^{48}K .

The identified new gamma rays were used as the starting point in the analysis of the gamma coincidence data obtained for the same reaction in a thick target experiment performed earlier with the Gammasphere array at ANL in a series of experiments exploiting deep-inelastic heavy-ion reactions for the spectroscopy of neutron-rich nuclei.¹ In this experiment the identification of in-beam gamma transitions in exotic nuclei produced with very low cross-sections posed obvious difficulties, however, the presence of $^{48,49}\text{K}$ was clearly detected from the observed radioactive decays. The present PRISMA-CLARA results opened the way to establish the level schemes of both isotopes as shown in Fig. I-23. The assigned spins and parities are suggested based on the consideration of observed gamma decay features and simple shell model expectations.

The observed level structures of both isotopes contain essential information for improvements of the

quantitative shell model description in this region of nuclei. The ^{48}K levels arise from the corresponding proton-neutron couplings and provide information on the two-body effective interactions of the $p_{3/2}$ neutron with $s_{1/2}$, $d_{3/2}$ proton-holes and a $f_{7/2}$ proton-particle. An important conclusion is that the ^{48}K ground state spin/parity is 1^- rather than the earlier accepted 2^- values which require some reinterpretation of the beta decay to the ^{48}Ca daughter. In the ^{49}K level scheme, the extra pair of $p_{3/2}$ neutrons increases the complexity, but the 771 keV state is assigned as the most probable lowest lying $3/2^+$ state. This indicates that just as in the ^{47}K , the $s_{1/2}$ proton-hole state is the ground state, but the $d_{3/2}$ level is located at much higher energy. Thus, in the present study of nuclear structure evolution with increasing neutron richness, one observes the continuation of the reordering trend of these proton-hole states as seen in a series of lighter potassium isotopes.

*Institute of Nuclear Physics, Krakow, Poland, †INFN, Laboratori Nazionali di Legnaro, Italy, ‡INFN, Padova and Università, Italy, §INFN, Sezione di Napoli, Italy, ¶Ruder Bošković Institute, Zagreb, Croatia, ||Michigan State University.

¹R. Broda, J. Phys. G **32**, 151 (2006).

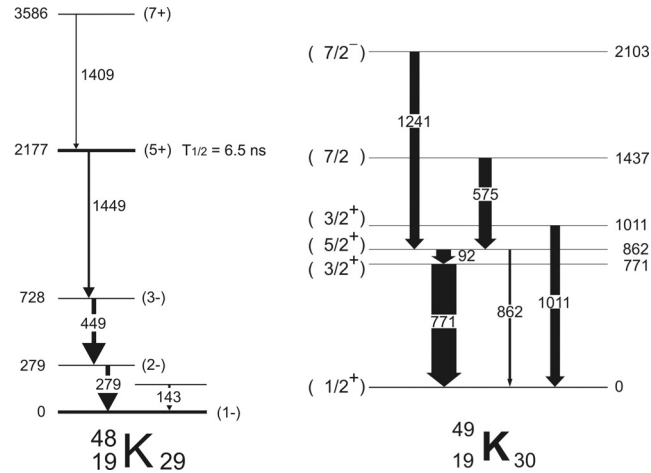


Fig. I-23. Established level schemes of ^{48}K and ^{49}K .

d.1.4. Yrast Structure of Neutron-Rich ^{51}Ca (R. V. F. Janssens, M. P. Carpenter, S. Zhu, B. Fornal,* R. Broda,* N. Marginean,† L. Corradi,‡ G. De Angelis,† F. Della Vedova,† E. Farnea,† E. Fioretto,† A. Gadea,† M. Honma,‡ W. Królas,* S. Lunardi,§ P. F. Mantica,¶ P. Mason,|| G. Montagnoli,|| D. R. Napoli,† T. Otsuka,** T. Pawlat,* F. Scarlassara,|| A. M. Stefanini,† S. Szilner,†† C. A. Ur,|| M. Trotta,‡‡ J. J. Valiente-Dobon,† and J. Wrzesiński*)

Around doubly-magic ^{48}Ca , the neutron $\nu p_{3/2}$, $\nu p_{1/2}$ and $\nu f_{5/2}$ orbitals are significantly separated in energy. As evidenced in earlier studies, a $N = 32$ subshell closure in neutron-rich nuclei occurs,¹⁻³ reflecting the presence of an energy gap between the $\nu p_{3/2}$ orbital and the two other neutron states. This closure disappears when going towards the stability line due to the strong proton $\pi f_{7/2}$ - neutron $\nu f_{5/2}$ monopole interaction, primarily governed by the tensor force, which causes a decrease in energy of the $\nu f_{5/2}$ single-particle orbital with respect to the $\nu p_{3/2}$ and $\nu p_{1/2}$ levels as protons are added to the $\pi f_{7/2}$ shell.^{4,5} It has been shown that the magnitude of this decrease is high enough to reduce a possible second gap, *i.e.*, between the $\nu p_{1/2}$ and $\nu f_{5/2}$ states, in the Ti and Cr isotopes.⁶⁻⁸ In Ca nuclei, however, the $\nu p_{3/2}$, $\nu p_{1/2} - \nu f_{5/2}$ splitting may be sufficient to produce a subshell closure also at $N = 34$, but this feature is difficult to detect, as the states involving the $\nu f_{5/2}$ orbital in such species like $^{51-54}\text{Ca}$ are hard to reach.

We investigated the yrast structure of ^{51}Ca by analyzing data from two complementary experiments. In the first measurement, γ - γ coincidence events, from neutron-rich species produced in deep-inelastic collisions of a ^{48}Ca

beam on a thick ^{238}U target, were collected with the Gammasphere array at Argonne. The production rate of the ^{51}Ca nucleus was, however, too low to locate unambiguously new γ rays that weakly appeared in coincidence gates on the known (from the $^{51,52}\text{K}$ β -decay studies)⁹ groundstate transitions in ^{51}Ca . In the second experiment the same system was investigated by employing the PRISMA spectrometer coupled with the CLARA γ -ray multi-detector array at the INFN, LNL Legnaro. A γ -ray spectrum from CLARA, gated on the ^{51}Ca products, showed a series of lines clearly belonging to ^{51}Ca (Fig. I-24). Out of those, three γ rays were known from the β -decay study.⁹ Subsequent analysis of γ coincidence data taken with Gammasphere allowed us to establish coincidence relationships between the observed lines and to construct an extended level scheme for ^{51}Ca (Fig. I-25). Of special interest is a state located at 4320 keV with a tentative spin-parity assignment of $9/2$ arising mostly from the $\nu p_{3/2}^2 f_{5/2}$ configuration, which involves an $f_{5/2}$ neutron. The energy of this state can be described quite well by shell-model calculations assuming a sizable energy gap between the $\nu p_{1/2}$ and $\nu f_{5/2}$ neutron orbitals at $Z = 20$.

*Institute of Nuclear Physics, PAN, Kraków, Poland, †INFN, Laboratori Nazionali di Legnaro, Italy,

‡University of Aizu, Japan, §Dipartimento di Fisica dell'Università di Padova, Italy, ¶Michigan State University, ||INFN, Sezione di Padova and Università di Padova, Italy, **University of Tokyo, Japan, ††Ruder Bošković Institute, Zagreb, Croatia, ‡‡INFN, Sezione di Napoli, Italy.

¹A. Huck *et al.*, Phys. Rev C **31**, 2226 (1985).

²R. V. F. Janssens *et al.*, Phys. Lett. **B546**, 55 (2002).

³A. Gade *et al.*, Phys. Rev. C **74**, 021301(R) (2006).

⁴T. Otsuka *et al.*, Phys. Rev. Lett. **87**, 082502 (2001).

⁵T. Otsuka *et al.*, Phys. Rev. Lett. **95**, 232502 (2005).

⁶S. Liddick *et al.*, Phys. Rev. Lett. **92**, 072502 (2004).

⁷B. Fornal *et al.*, Phys. Rev. C **70**, 064304 (2004).

⁸S. Zhu *et al.*, Phys. Rev. C **74**, 064315 (2006).

⁹F. Perrot *et al.*, Phys. Rev. C **74**, 014313 (2006).

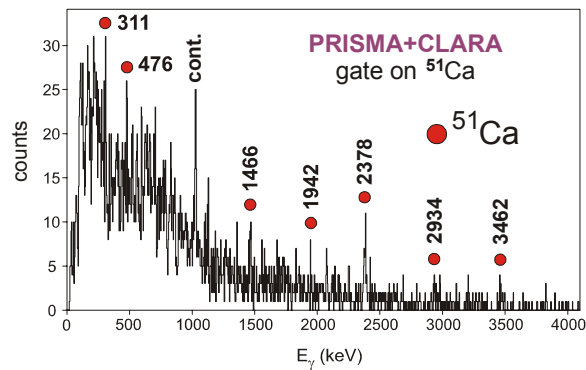


Fig. I-24. γ spectrum in coincidence with the ^{51}Ca products.

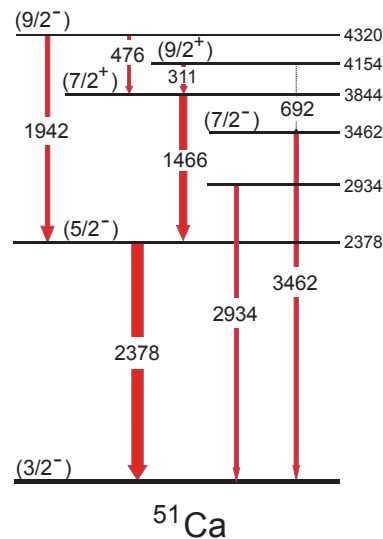


Fig. I-25. Proposed level scheme of ^{51}Ca .

d.1.5. One-Neutron Knockout in the Vicinity of the $N = 32$ Sub-Shell Closure:

${}^9\text{Be}({}^{57}\text{Cr}, {}^{56}\text{Cr} + \gamma)\text{X}$ (R. V. F. Janssens, M. P. Carpenter, S. Zhu, A. Gade,* D. Bazin,* B. A. Brown,* C. M. Campbell,* J. M. Cook,* A. N. Deacon,† D.-C. Dinca,* S. J. Freeman,† T. Glasmacher,* M. Horoi,‡ B. P. Kay,† P. F. Mantica,* W. F. Mueller,* J. R. Terry,* and J. A. Tostevin§)

The one-neutron knockout reaction ${}^9\text{Be}({}^{57}\text{Cr}, {}^{56}\text{Cr} + \gamma)\text{X}$ has been measured in inverse kinematics with an intermediate-energy beam. Cross sections to individual states in ${}^{56}\text{Cr}$ were partially untangled through the detection of the characteristic γ -ray transitions in coincidence with the reaction residues. The experi-

mental inclusive longitudinal momentum distribution and the yields to individual states were compared to calculations that combine spectroscopic factors from the full fp shell model and nucleon-removal cross sections computed in a few-body eikonal approach. The results of this study were published.¹

*Michigan State University, †University of Manchester, United Kingdom, ‡Central Michigan University, §University of Surrey, United Kingdom.

¹A. Gade *et al.*, Phys. Rev. C **74**, 047302 (2006).

d.1.6. One-Particle Excitations Outside the ${}^{54}\text{Ti}$ Semi-Magic Core: The ${}^{55}\text{V}$ and ${}^{55}\text{Ti}$ Yrast Structures

(S. Zhu, R. V. F. Janssens, M. P. Carpenter, F. G. Kondev, T. Lauritsen, C. J. Lister, A. Robinson, D. Seweryniak, X. Wang, B. Fornal,* S. J. Freeman,† M. Honma,‡ R. Broda,* A. N. Deacon,† B. P. Kay,† W. Króla,*§ J. Kozemczak,¶ A. Larabee,¶ S. N. Liddick,** P. F. Mantica,** T. Otsuka,†† T. Pawlat,* J. F. Smith,† D. Steppenbeck,† B. E. Tomlin,** and J. Wrzesiński*)

Our earlier work has clearly shown that the GXPF1 interaction is very successful in describing the yrast structure in the even-even ${}^{50,52,54}\text{Ti}$ isotopes and accounts for the $N = 32$ sub-shell closure, but fails in the case of ${}^{56}\text{Ti}$ ($N = 34$ sub-shell closure).^{1,2,3} This led to a modified GXPF1 interaction, labeled GXPF1A, with a narrower $\nu p_{1/2}$ - $\nu f_{5/2}$ gap in the effective single-particle energies. With five $T = 1$ matrix elements involving mainly the $\nu p_{1/2}$ and $\nu f_{5/2}$ single-particle orbitals modified, this interaction has provided a consistent description of the known low-lying structures along the entire chain of neutron-rich Ti isotopes, including ${}^{56}\text{Ti}$. In order to provide new tests of full pf -shell calculations with the GXPF1A interaction, the level structures of ${}^{55}\text{V}$ and ${}^{55}\text{Ti}$, the two nuclei with a single nucleon outside the semi-magic ${}^{54}\text{Ti}_{32}$ core, have now been investigated. The excited states in ${}^{55}\text{V}$ and

${}^{55}\text{Ti}$ have been populated by utilizing both fusion-evaporation and deep-inelastic reactions. The level schemes obtained from these studies can be found in Figs. I-26 and I-27. Shell-model calculations with the GXPF1A Hamiltonian account for the data reasonably well. The addition of a proton does not appear to affect the $N = 32$ shell gap significantly, although comparisons between calculations and experiment at high spins ($I^\pi \geq 21/2^-$) indicate the need for a larger model space for an accurate description of the data in this regime. The energy separation between the $\nu p_{1/2}$ and $\nu f_{5/2}$ orbitals in neutron-rich Ti isotopes is not large enough to result in an $N = 34$ shell gap. However, comparisons between the ${}^{55}\text{Ti}$ data and the calculations argue for the presence of a sizable $N = 34$ gap in ${}^{54}\text{Ca}$. The results of this study were published.⁴

*Institute of Nuclear Physics, Krakow, Poland, †University of Manchester, United Kingdom, ‡University of Aizu, Japan, §Joint Institute for Heavy Ion Research, ¶Greenville College, **Michigan State University, ††University of Tokyo, Japan.

¹R. V. F. Janssens *et al.*, Phys. Lett. **B546**, 22 (2002).

²B. Fornal *et al.*, Phys. Rev. C **70**, 064304(2004).

³D.-C. Dinca *et al.*, Phys. Rev. C **71**, 041302(R) (2005).

⁴S. Zhu *et al.*, Phys. Lett. **B650**, 135 (2007).

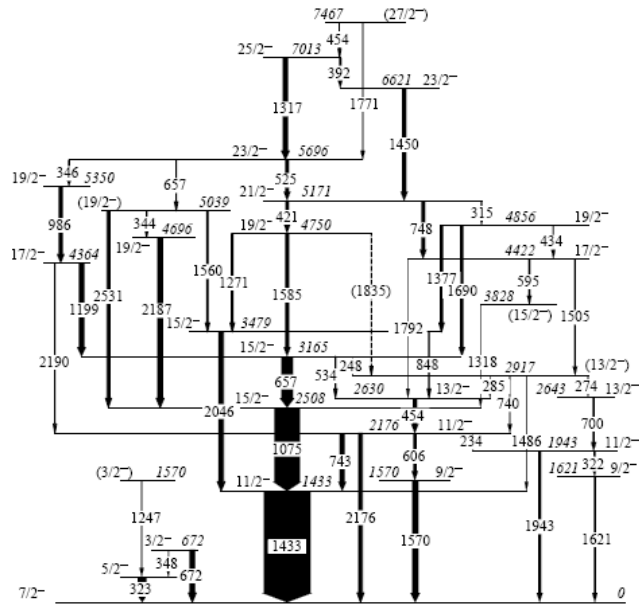


Fig. I-26. Proposed level scheme for ^{55}V .

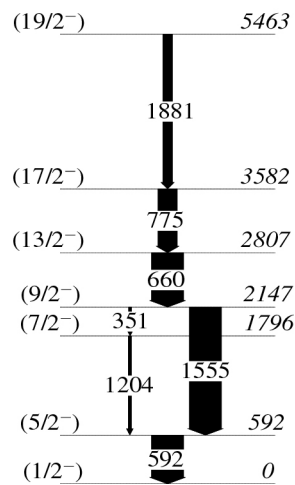


Fig. I-27. Proposed level scheme for ^{55}Ti .

d.1.7. Structure of the Even-Even Neutron-Rich ^{56,58,60}Cr Isotopes (S. Zhu, R. V. F. Janssens, M. P. Carpenter, F. G. Kondev, T. Lauritsen, C. J. Lister, D. Seweryniak, A. N. Deacon,* S. J. Freeman,* R. Broda,† I. R. Calderin,‡ B. Fornal,† J. F. Smith,* S. L. Tabor,‡ B. J. Varley,* M. Honma,§ F. R. Xu,¶ P. Chowdhury,** W. Króla,† S. N. Liddick,†† P. F. Mantica,†† B. E. Tomlin,†† and J. Wrzesiński†)

The existence of the $N = 32$ sub-shell above doubly-magic ⁴⁸Ca has been firmly established in a series of recent experiments.^{1,2} Shell model calculations with the GXPF1A effective interaction are able to account for this gap as resulting from a weakening of the $\pi 1f_{7/2}-\nu 1f_{5/2}$ proton-neutron monopole interaction as protons are removed from the $1f_{7/2}$ orbital, combined with a significant $\nu 2p_{1/2}-\nu 2p_{3/2}$ spin-orbit splitting.³ With the $\pi f_{7/2}$ shell half-filled, Cr isotopes are among the nuclei best suited for studying the possible role of collectivity in the region. Recent studies of odd, neutron-rich Cr isotopes above $N = 32$ indicate an increasing involvement of the shape-driving $g_{9/2}$ orbital in the low-lying structure of neutron-rich Cr isotopes.⁴ Experimental information on the excited states in the even-even, neutron-rich Cr nuclei provides further tests of the suitability of the fp shell-model space for the description of their level structure and of the possible shape-driving influence of the $vg_{9/2}$ orbital. The yrast states of the neutron-rich Cr isotopes were populated *via* two deep inelastic reactions of ⁴⁸Ca on 50 mg/cm² ²⁰⁸Pb and ²³⁸U targets at beam energies about 20% above the Coulomb barrier. Another approach used here for producing neutron-rich Cr isotopes involved fusion of ⁴⁸Ca projectiles with ¹⁴C radioactive targets (thickness 100 $\mu\text{g}/\text{cm}^2$, $\sim 90\%$ enrichment). The beam energy was selected as 130 MeV to optimize two-proton evaporation producing ⁶⁰Cr. Reaction products were dispersed according to their charge-to-mass (A/q)

ratio with the Fragment Mass Analyzer (FMA). An ion chamber behind the focal plane was used to provide Z resolution and separate ⁶⁰Cr residues from other isotopes with stronger yields.

The deduced level schemes of ^{56,58,60}Cr represent significant extensions over previous knowledge. Specifically, despite a low-spin structure reflecting the $N = 32$ sub-shell closure in ⁵⁶Cr, evidence was found at higher energy for a negative-parity sequence associated with prolate, collective rotation. This band exhibits striking similarities with those seen in the odd neighbors ^{55,57}Cr. The data collected for ⁵⁸Cr demonstrate unambiguously that the level scheme proposed recently by Marginean *et al.*⁵ from a PRISMA + CLARA experiment is in error, raising considerable doubt about an interpretation in terms of an E(5) dynamical symmetry proposed in the latter work. In addition, the lowest observed negative-parity state in ⁵⁸Cr is ~ 1.1 MeV lower than that in ⁵⁶Cr, a trend similar to that exhibited by the $9/2^+$ ($vg_{9/2}$) bandheads in the odd Cr neighbors. Furthermore, the properties of the sequence built on this negative-parity state differ significantly from those seen in ⁵⁶Cr, consistent with the spherical or slightly oblate shape proposed for ⁵⁹Cr by Freeman *et al.*⁶ The yrast sequence observed for the first time in ⁶⁰Cr is also consistent with an interpretation in terms of an oblate deformation. The results of this study have been published.⁷

*University of Manchester, United Kingdom, †Niewodniczanski Institute of Nuclear Physics, Krakow, Poland, ‡Florida State University, §University of Aizu, Japan, ¶Peking University, China, **University of Massachusetts, ††Michigan State University.

¹R. V. F. Janssens *et al.*, Phys. Lett. **B546**, 55 (2002).

²D. C. Dinca *et al.*, Phys. Rev. C **71**, 041302(R) (2005), and references therein.

³M. Honma *et al.*, Phys. Rev. C **65**, 061301 (2002).

⁴A. N. Deacon *et al.*, Phys. Lett. **B622**, 151 (2005).

⁵N. Marginean *et al.*, Phys. Lett. **B633**, 696 (2006).

⁶S. J. Freeman *et al.*, Phys. Rev. C **60**, 064301 (2004).

⁷S. Zhu *et al.*, Phys. Rev. C **74**, 064315 (2006).

d.1.8. Yrast Structures in the Neutron-Rich Isotopes $^{59,60}\text{Fe}$ and the Role of the $g_{9/2}$ Orbital
(R. V. F. Janssens, M. P. Carpenter, T. Lauritsen, C. J. Lister, D. Seweryniak, S. Zhu,
A. N. Deacon,* S. J. Freeman,* M. Honma,† P. Chowdhury,‡ J. F. Smith,* S. L. Tabor,‡
B. J. Varley,* and F. R. Xu¶)

Neutron-rich fp -shell nuclei have been the subject of much recent investigation. Primarily, such work has been motivated by the increasing evidence for unexpected modifications to the single-particle structures of these exotic systems due to aspects of the nucleon-nucleon interaction not immediately apparent in near-stable systems. In understanding these developments a great deal of synergistic effort is occurring on both the theoretical and experimental fronts.¹⁻⁹ The Fe isotopes, with $Z = 26$, represent the next logical step in the investigation of neutron-rich fp -shell nuclei. The structure of the neutron-rich isotopes $^{59,60}\text{Fe}$ has been studied with the Gammasphere detector array using fusion-evaporation reactions.

Level schemes for these nuclei have been extended to spins of $\sim 20 \hbar$. Both isotopes exhibit regular, near-yrast γ -decay sequences which are generated by the intrusion of the $g_{9/2}$ orbital into the fp shell-model space. The yrast and near-yrast structures have been compared with the results of shell-model calculations using the GXPF1A interaction in the full fp model space, and the role of the $g_{9/2}$ orbital in the experimental data was assessed by comparison with total Routhian surface calculations. In both cases, shell-model calculations reproduce the low-lying, natural-parity states satisfactorily. TRS calculations indicate a very soft shape, becoming softer as the rotational frequency increases.

*University of Manchester, United Kingdom, †University of Aizu, Japan, ‡University of Massachusetts, ‡Florida State University, ¶Peking University, China.

¹R. V. F. Janssens *et al.*, Phys. Lett. **B546**, 55 (2002).

²T. Otsuka *et al.*, Phys. Rev. Lett. **87**, 082502 (2001).

³M. Honma *et al.*, Phys. Rev. C **65**, 061301 (2002).

⁴B. Fornal *et al.*, Phys. Rev. C **70**, 064304 (2004).

⁵T. Otsuka *et al.*, Phys. Rev. Lett. **95**, 232502 (2005).

⁶D.-C. Dinca *et al.*, Phys. Rev. C **71**, 041302(R) (2005).

⁷A. N. Deacon *et al.*, Phys. Lett. **B622**, 151 (2005).

⁸A. Gade *et al.*, Phys. Rev. C **74**, 021301(R) (2006).

⁹S. Zhu *et al.*, Phys. Rev. C **74**, 064315 (2006).

d.1.9. Deep Inelastic Reaction Studies with Gammasphere: The Structure of ^{61}Fe

(R. V. F. Janssens, M. P. Carpenter, T. Lauritsen, D. Seweryniak, S. Zhu, N. Hoteling,*
W. B. Walters,* R. Broda,† B. Fornal,† A. A. Hecht,* M. Hjorth-Jensen,‡ W. Krolas,†§
T. Pawlat,† X. Wang,¶ A. Wöhr,¶ and J. Wrzesinski†)

The recent identification of lowered 2^+ energy trends near $N = 40$ below ^{68}Ni has given rise to much discussion of a possible new region of deformation. This would appear to result from a growing influence from the $g_{9/2}$ neutron orbital as the neutron pf orbitals are filled. One way to study the effect of this orbital is to identify and study the positive parity states in odd- A isotopes near $N = 40$, where the pf shell is full. The location in energy and the structure of these levels will yield important information about the evolution of these isotopes toward $N = 40$, and can be used to further characterize the general features of nuclei in this region. In ^{61}Fe , an isomeric $9/2^+$ state representing a single neutron excitation into the $g_{9/2}$ orbital has already been

identified, and characterized in terms of both magnetic and quadrupole moments. From the latter, a β_2 deformation of $+0.26$ or -0.24 has been suggested, indicating that this state is either prolate or oblate. To proceed further with such an interpretation, it is imperative that the bands and states above this isomer be established. Hence, in this experiment, data from the deep-inelastic reaction of $^{64}\text{Ni} + ^{238}\text{U}$ are used to identify new levels above the established isomer.

In this experiment, a pulsed beam of 450 MeV ^{64}Ni spaced by 410 ns was employed so that there would be time between pulses to allow for the decay of short-lived isomers, such as, for example, the $\sim 0.25 \mu\text{s}$ state

in ^{61}Fe . Thus, it is possible to construct triple-coincidence cubes which utilize the time with respect to the beam pulse in order to separate “prompt” events from “delayed” events. With this technique, four coincidence cubes were produced: prompt-prompt-prompt (PPP), prompt-prompt-delayed (PPD), prompt-delayed-delayed (PDD), and delayed-delayed-delayed (DDD). Since there are two known transitions that decay, in sequence, from the 861 keV isomeric state, a double coincidence gate in the PDD cube yielded new transitions above the isomer. Once this was established, the PPD cube could be used to identify weaker transitions at higher energies in the level scheme.

New levels and gamma rays are presented in the level scheme in Fig. I-28. Also shown is a comparison with the shell model in which the calculated levels compare favorably with those determined from experiment. Since this agreement could only be achieved upon the lowering of the $g_{9/2}$ single particle energy by 1.7 MeV, these results appear to support an oblate deformation, as opposed to prolate, where one would expect more of a rotational character that is unlikely to be so well reproduced by the shell model.

A paper summarizing these results is currently in preparation.

*University of Maryland, †Niewodniczanski Institute of Nuclear Physics, Krakow, Poland, ‡University of Oslo, Norway, §Oak Ridge National Laboratory, ¶University of Notre Dame.

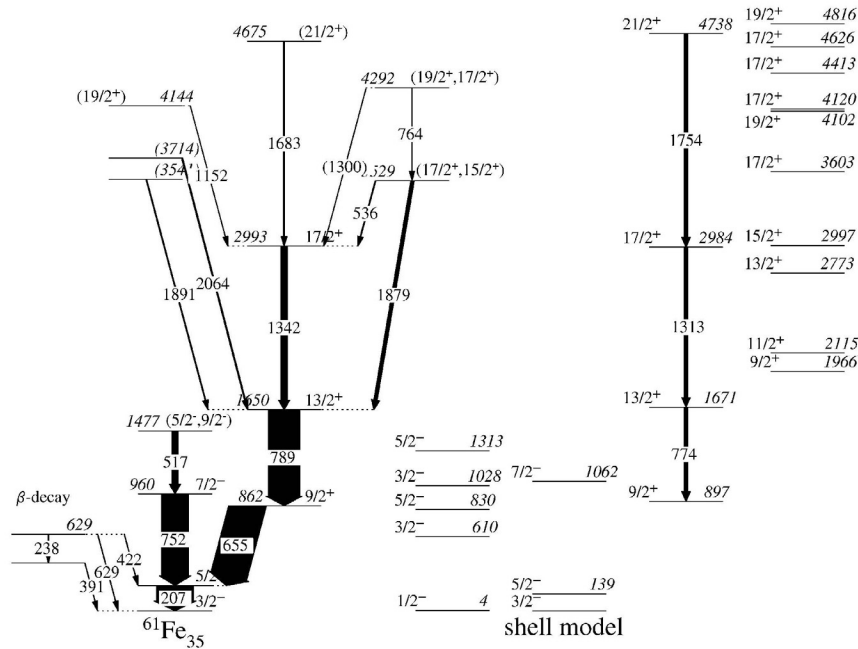


Fig. I-28. Level scheme determined for ^{61}Fe compared with shell model calculations.

d.1.10. Deep Inelastic Reaction Studies with Gammasphere: The Structure of ^{64}Fe

(R. V. F. Janssens, M. P. Carpenter, T. Lauritsen, D. Seweryniak, S. Zhu, N. Hoteling,* W. B. Walters,* R. Broda,† B. Fornal,† A. A. Hecht,* M. Hjorth-Jensen,‡ W. Krolas,†§ T. Pawlat,† D. X. Wang,¶ A. Wotr,¶ and J. Wrzesinski†)

The structure of ^{68}Ni and adjacent nuclei has been of considerable interest as neutron number 40 marks the filling of the $N = 3$ oscillator shell. Hence, there exists some remnant of a shell gap that has not been completely eroded away by the spin-orbit interaction, a fact that is evident in the 2^+ energy peak at $N = 40$ in

^{68}Ni . However, addition or subtraction of protons from the ^{68}Ni core leads to a very different behavior, as the 2^+ energies in, for example, the Fe isotopes, drops considerably as $N = 40$ is approached. Since such behavior is often associated with the onset of deformation, it is of special interest to investigate the

structure beyond the 2^+ energy in the Fe isotopes in this region. This additional data will, in turn, allow for a more complete and thorough analysis of the evolution of structure in this region, as well as a better understanding of the nucleon-nucleon interactions at play in these nuclei.

To investigate the neutron-rich Fe isotopes, an experiment was performed with the Gammasphere spectrometer in which the deep inelastic reaction of ^{64}Ni and ^{238}U was studied. A thick ^{238}U target was used so as to stop all reaction products at the target position centered in Gammasphere. Events were recorded under a three fold or higher condition. New levels in ^{64}Fe could be identified from a coincidence gate on the

known 746 keV, $2^+ \rightarrow 0^+$ transition. Additional gamma rays with energies 582, 687, 781, 1005, 1017, 1078, and 1079 keV were identified and placed in the level scheme shown in Fig. I-29, which was compared to shell model calculations. The shell model results compared well for the 2^+ energy, but the excitation energy of higher-lying levels were increasingly over-predicted. A larger model space, in which the $g_{9/2}$ neutron orbital was included, gave more favorable results, emphasizing the increased importance of this state near $N = 40$.

Results from this work have been published in Physical Review C **74**, 064313 (2006).

*University of Maryland, †Niewodniczanski Institute of Nuclear Physics, Krakow, Poland, ‡University of Oslo, Norway, §Oak Ridge National Laboratory, ¶University of Notre Dame.

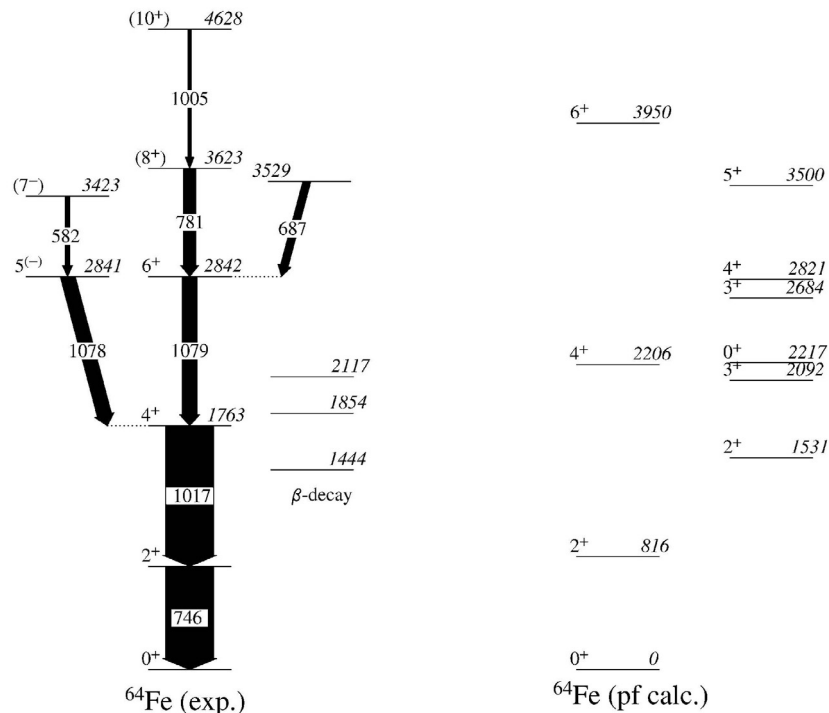


Fig. I-29. Level scheme adopted for ^{64}Fe , compared with shell model calculations.

d.1.11. Study of $N = 50$ Nuclei Near ^{78}Ni Using Deep Inelastic Reactions (M. P. Carpenter, F. G. Kondev, R. V. F. Janssens, N. Hoteling, T. L. Khoo, T. Lauritsen, C. J. Lister, D. Seweryniak, X. Wang, S. Zhu, R. Broda,* B. Fornal,* A. Galindo-Uribarri,† A. Ibanez,‡ E. Padilla-Rodal,†,§ and J. P. Ureggo-Blanco§)

The study of doubly- and semi-magic nuclei have historically proven to be important in establishing for example the interaction strengths for the shell model. Until recently, these parameters were set by nuclei

lying near the line of beta-stability, however, with the utilization of first and second generation radioactive beam facilities, studies of exotic neutron rich nuclei at and near closed shells have begun. What has motivated

many of these measurements from a nuclear structure standpoint is the fact that rearrangements of single-particle energies are observed in neutron rich systems. Such changes in the single-particle energies have been attributed to the attractive strength of the spin-isospin part of the effective nuclear interaction. As a result, one has observed the disappearance of certain magic numbers and the emergence of new closed shells.

While Gammasphere is not located at a traditional radioactive beam facility, one can still access neutron rich nuclei using techniques which do not require the acceleration of radioactive ions. For example, by studying the γ rays emitted after spontaneous fission of ^{248}Cm , important new information on excited states has been obtained for nuclei near ^{132}Sn . We have also studied neutron-rich nuclei using so-called deep inelastic reactions (DIC). In these studies, ^{208}Pb or ^{238}U targets are bombarded by a neutron rich stable beam at energies $\sim 25\%$ above the Coulomb barrier. By swapping protons and neutrons with the target, neutron-rich nuclei relative to the beam are produced, and their de-excitation by γ rays is studied with Gammasphere. Utilizing ^{48}Ca beams and DIC, we have studied the $N = 32$ and $N = 34$ isotopes $^{52,54}\text{Ti}$ to high spin and helped establish the presence of an $N = 32$ shell for $Z \leq 22$.^{1,2}

With the success of the Gammasphere experiments

utilizing a ^{48}Ca beam to explore the yrast sequences in the neutron rich Ti isotopes, we have extended our measurements into the region around $N = 50$ and $Z = 28$ (^{78}Ni). Neutron-rich nuclides in this region are of particular interest due to their role in the r -process, and in particular, their contribution to the peak in the solar elemental abundance near $A = 80$. While much is known with regards to the $N = 50$ isotones starting at ^{86}Kr and proceeding up towards ^{100}Sn , very little is known about the isotones approaching and including ^{78}Ni . In the Gammasphere measurement, data were collected using an ^{82}Se beam incident on both thick ^{208}Pb and ^{238}U targets. As a result, all products produced in these reactions are stopped in the target. Data were taken at two different beam energies - 525 and 630 MeV. In addition, the time between beam pulses was 400 ns allowing for the identification of isomers with lifetimes as long as several μsec .

One of the main purposes of this measurement was to identify the yrast structures for both ^{84}Se and ^{82}Ge to spins up to $\sim 12 \hbar$. In addition, we hoped to develop detailed level structures for ^{81}Se , ^{83}Se , ^{83}As , ^{81}Ge , and possibly ^{83}Ge . Two separate blue data bases have been created from the data taken at 630 MeV which correspond to the ^{208}Pb and ^{238}U targets, respectively. Current results include a more extensive level scheme for ^{84}Se up to $I = 12 \hbar$ and excited states in ^{82}Ge have been identified up to $I = 6 \hbar$ (see Fig. I-30).

*Niewodniczanski Institute of Nuclear Physics, Cracow, Poland, †Oak Ridge National Laboratory, ‡National Autonomous University of Mexico, Mexico City, Mexico §University of Tennessee.

¹R. V. F. Janssens *et al.*, Phys. Lett. **B546**, 55 (2002).

²B. Fornal *et al.*, Phys. Rev. C **70**, 064304 (2004).

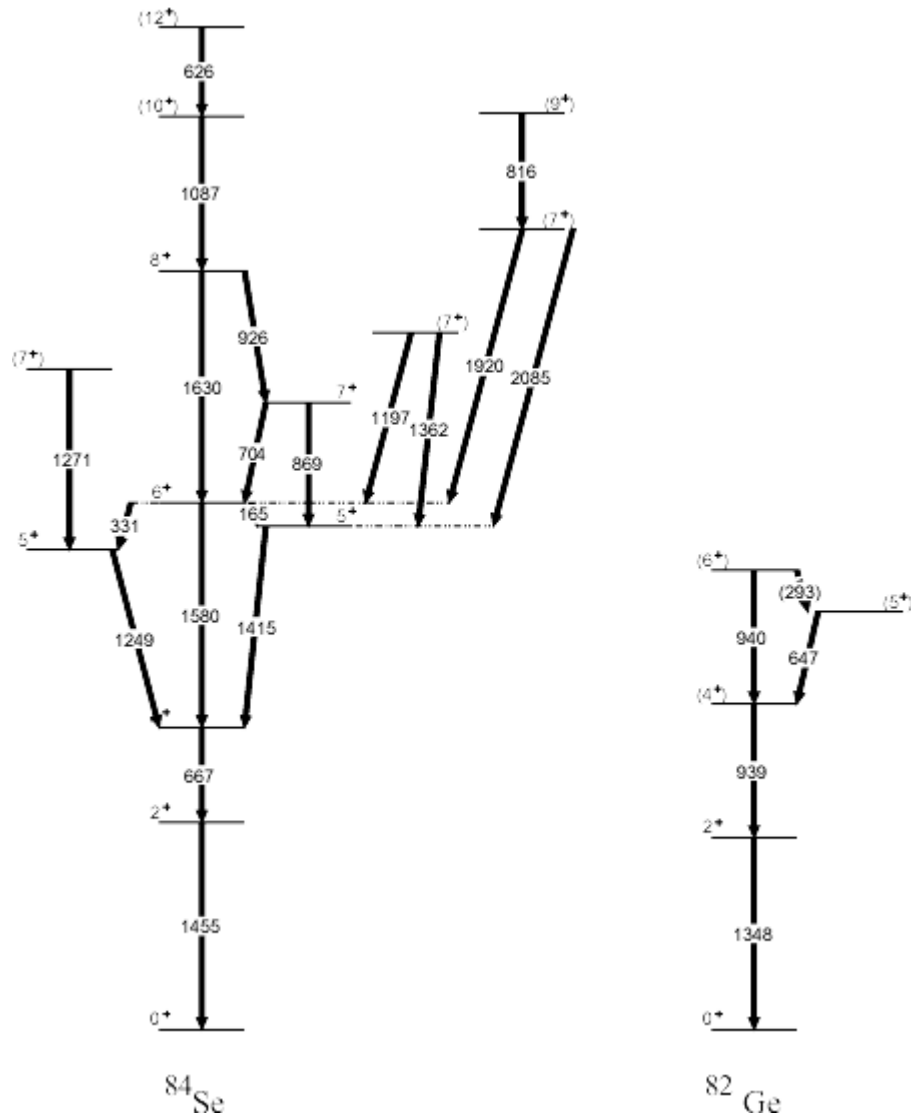


Fig. I-30. Partial level schemes for the $N = 50$ isotones deduced from this work.

d.1.12. Structure of Neutron-Rich Zn Isotopes (A. A. Hecht,* N. Hoteling,* M. P. Carpenter, R. V. F. Janssens, S. Zhu, F. G. Kondev, T. L. Khoo, T. Lauritsen, C. J. Lister, D. Seweryniak, X. Wang, W. B. Walters,† J. Stone,† R. Broda,‡ B. Fornal,‡ W. Krolas,‡ J. Wrzesinski,‡ A. Galindo-Uribarri,§ A. Ibanez,¶ E. Padilla-Rodal,§,|| J. P. Ureggo-Blanco,|| and A. F. Lisetskiy**)

The neutron rich region near doubly-magic ^{78}Ni is significant to both nuclear structure and nuclear astrophysics: as experimental input for models on shell structure far from stability and as the seed region for the beginning of the rapid neutron capture process of nucleosynthesis. This region is not easily accessible experimentally with most of the data on excited states coming from beta decay studies. Expanding this

knowledge to high spin states, deep inelastic scattering (DIS) experiments were performed at the ATLAS accelerator center at Argonne National Laboratory using pulsed beams of ^{82}Se and of ^{64}Ni impinged on thick targets of ^{238}U and ^{208}Pb . Gamma-rays were detected by the Gammasphere array consisting of 101 Compton-suppressed HPGe counters.

Focusing on Zn, excited states in the even-even nuclei $^{66-78}\text{Zn}$ were observed using $\gamma\text{-}\gamma\text{-}\gamma$ coincidence matrices. Several new levels were found for $^{66-76}\text{Zn}$, and many previously known levels were confirmed. Levels were tentatively identified up to 12^+ in ^{66}Zn , 14^+ in ^{68}Zn , 12^+ in ^{70}Zn , 12^+ in ^{72}Zn , 10^+ in ^{74}Zn and 6^+ in ^{76}Zn . Using the angular sensitivity of Gammasphere, angular correlations were studied in order to deduce the spins for several of the new states, and fix the spins of levels that were previously tentatively assigned. The variation in energy of the positive parity yrast levels as a function of neutron number for the even Zn isotopes is plotted in Fig. I-31.

Of particular interest are the tentative observation of two 6^+ states lying below the first excited 8^+ states in ^{74}Zn with the yrast intensity flowing largely through the upper 6^+ level. It was found in Ref. 1 and 2 that due to the enhanced two-body interaction in the $(g_{9/2})^2_{I=2}$ channel, there is an unusual ordering of seniority $s=4$ and $s=2$ states ($s=4$ is lower in energy than $s=2$) for both the $I=4^+$ and $I=6^+$ states in ^{72}Ni with the $s=2$

and $s=4$ $I=6^+$ levels lower than the $I=8^+$, $s=2$ state. The seniority symmetry imposes selection rules where $E2$ transitions between the states with the same seniority are strongly hindered. The apparent observation of two low lying 6^+ levels in ^{74}Zn is a direct consequence of the phenomena studied in ^{72}Ni and the seniority selection rules. By adding two protons to ^{72}Ni , the $\nu g_{9/2}$ content of the high-spin states does not change much, but stronger mixing of $(g_{9/2})^n$ configurations occurs with different n values and a breaking of the seniority symmetry. The shell model predicts almost the same $B(E2)$ value for the decay of the $I=8^+$ to $I=6^+_{1,2}$ for ^{74}Zn while experiment shows the larger intensity for the transition to the $I=6^+_2$ state. The shell model predicts a similar lowering of the $I=6^+_{1,2}$ in ^{76}Zn , but predicts different results for ^{78}Zn , where the small $B(E2)$ and small energy gap between the $I=8^+$ and $I=6^+_1$ states lead to an isomeric lifetime for the $I=8^+$ level.

A manuscript reporting both the experimental data and shell model calculations is currently under preparation.

*University of Maryland and Argonne National Laboratory, †University of Maryland, ‡Niewodniczanki Institute of Nuclear Physics, Cracow, Poland, §Oak Ridge National Laboratory, ¶Autonomous University of Mexico, Mexico City, Mexico ||University of Tennessee, **University of Arizona.

¹A. F. Lisetskiy, AIP Conference Proceedings **725**(1), 231 (2004).

²M. Horoi, AIP Conference Proceedings **764**, 170 (2005).

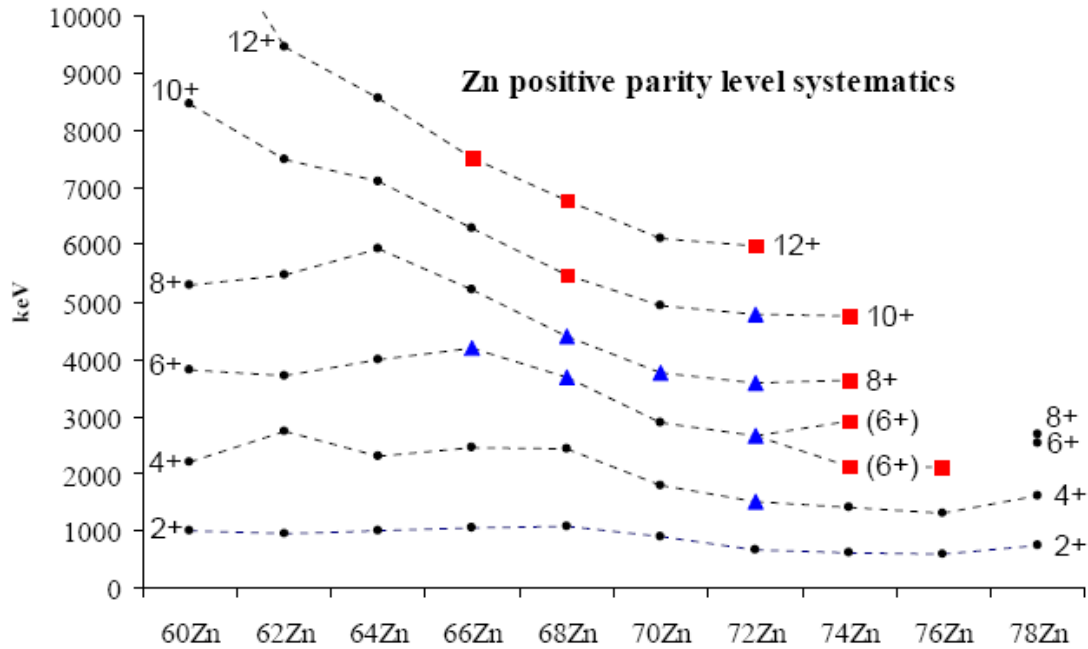


Fig. I-31. Even parity yrast level energies for Zn isotopes as a function of neutron number. Red squares represent new levels found in this work. Blue triangles represent levels with previously unsure level spins and parities which were fixed in this work.

d.1.13. Beta-Decay Studies of Neutron-Rich Fission Products for Advanced Fuel Cycle Applications (C. J. Lister, F. G. Kondev,*and P. Chowdhury†)

The DOE Office of Science issued a call for proposals for projects which allowed research into the physics of advanced fuel cycles while remaining inside the core mission of the Office. The call was entitled “Nuclear Physics Research and Development for the Advanced Fuel Cycles, LAB 07-05”. The physics division at ANL appears well positioned for this type of research, especially in the light of the CARIBU upgrade and the available equipment. A joint ANL/PHY, ANL/NE, University of Massachusetts-Lowell proposal was prepared and submitted. The proposals are expected to be reviewed in the summer of 2007 with funding from FY2008-2010.

The proposal abstract reads:

Beams of mass-separated neutron-rich isotopes that are important for Advanced Fuel Cycle (AFC) research will be extracted from the CARIBU source at the Argonne ATLAS accelerator and will be studied with our

existing suite of high quality spectroscopic tools (Penning Traps, the Fragment Mass Analyzer, Gammasphere, Total Absorption Gamma Spectrometer, the X-Array). The Nuclear Engineering program at Argonne will collaborate in this research and provide insight into the most important measurements for AFC and will rapidly disseminate results into the appropriate databases. The University of Massachusetts-Lowell will add their expertise in applied nuclear physics, and draw new young scientists into this research. Together, these resources offer a unique opportunity for significantly improved β -decay measurements of fission fragments that are relevant not only for AFC reactor design, but also for nuclear structure studies and astrophysics. We propose to strengthen the infrastructure for β -decay studies at ATLAS immediately, with short-term nuclear structure physics goals, and then start a program of detailed decay measurements on key isotopes for AFC research as soon as CARIBU is operational.

*Nuclear Engineering Division, Argonne National Laboratory. †University of Massachusetts-Lowell.

d.1.14. Multi-Quasiparticle K-Isomers in ^{174}Lu and Neutron-Rich $^{172,174}\text{Er}$ (M. P. Carpenter, F. G. Kondev, R. V. F. Janssens, T. Lauritsen, D. Seweryniak, S. Zhu, G. D. Dracoulis,* G. J. Lane,* A. P. Byrne,* R. O. Hughes,* P. Nieminen,* H. Watanabe,* P. Chowdhury,† and F. R. Xu‡)

Deep inelastic reactions on a series of rare earth targets have been performed at Gammasphere utilizing a ^{136}Xe beam with a beam energy of ~ 6 MeV/nucleon. The targets used have been thick in order that the excited nuclei are stopped in the target before they decay. Beam pulsing has also been utilized in order to search for high-K isomers which are plentiful in this mass region ($70 \leq Z \leq 82$). Two papers were published in 2006 reporting results from these measurements.

In the first publication, two-quasiparticle, isomeric states have been identified in the neutron rich isotopes $^{172,174}\text{Er}$. In the case of ^{172}Er , a candidate for the $K^\pi = 6^+$ two-quasineutron state is found at 1500 keV. In ^{174}Er , a nuclide whose level scheme was previously unknown, a long-lived isomer at 1112 keV decaying *via* an inhibited E1 transition and revealing the yrast sequence of ^{174}Er . This isomer is proposed to be a $K^\pi = 8^-$, two-quasineutron state, defining a sequence in the $N = 106$ isotones extending from the well-deformed neutron-rich isotope ^{174}Er to the neutron-deficient

isotope ^{188}Pb , where the presence of the isomer signifies a prolate minimum in an otherwise spherical well. Configuration-constrained potential-energy surface calculations are used to predict the excitation energy of the 6^+ and 8^- intrinsic states and as a basis for extracting the pairing force strength, G_n , in the $N = 104$ and $N = 106$ isotones. These results are published in Ref. 1.

The second publication reports on a $K^\pi = 13^+$, 280 ns four-quasiparticle isomer identified in the odd-odd nucleus ^{174}Lu . The isomer decays to both $K^\pi = 7^+$ and $K^\pi = 0^+$ rotational bands obtained from the parallel and antiparallel coupling of the proton $7/2^+[404]$ and neutron $7/2^+[633]$ orbitals. K mixing caused by particle-rotation coupling explains the anomalously fast transition rates to the 7^+ band but those to the 0^+ band are caused by a chance degeneracy between the isomer and a collective state, allowing the mixing matrix element for a large K difference to be deduced. Details can be found in Ref. 2.

*Australian National University, Canberra, Australia, †University of Massachusetts-Lowell, ‡Peking University, Beijing, China.

¹G. D. Dracoulis *et al.*, Phys. Lett. **B635**, 200 (2006).

²G. D. Dracoulis *et al.*, Phys. Rev. Lett. **97**, 122501 (2006).

d.2. Proton-Rich Nuclei

d.2.1. Single-Neutron States in ^{101}Sn (D. Seweryniak, M. P. Carpenter, S. Gros, R. V. F. Janssens, T. L. Khoo, T. Lauritsen, C. J. Lister, D. Peterson, A. P. Robinson, S. Zhu, X. Wang,* A. A. Hecht,† N. Hoteling,† G. Lotay‡, W. B. Walters†, and P. J. Woods‡)

Doubly-magic nuclei are the cornerstones of the nuclear landscape. Studying the properties of exotic doubly-magic nuclei such as ^{48}Ni , ^{78}Ni , ^{100}Sn and ^{132}Sn is essential for understanding the evolution of the nuclear structure far from the line of stability. Single-particle energies are important characteristics of doubly-magic nuclei. They provide a stringent test of nuclear mean field models and are essential ingredients in shell-model calculations of multi-nucleon configurations.

Due to low population cross sections the ^{100}Sn nucleus and its neighbors are not known very well. A search for

γ -ray transitions in ^{101}Sn , which contains only one neutron outside of the ^{100}Sn core, was carried out at ATLAS. ^{101}Sn nuclei were produced using the $^{46}\text{Ti}(^{58}\text{Ni},3n)^{101}\text{Sn}$ reaction with the cross section of only ~ 50 nb. Beta-delayed protons with energies and decay times consistent with previous ^{101}Sn decay studies¹ were observed at the focal plane of the FMA. In-beam γ rays were detected in Gammasphere and were correlated with the ^{101}Sn β -delayed protons using the Recoil-Decay Tagging method.

The resulting ^{101}Sn γ -ray spectrum is shown in Fig. I-32 (top) along with the spectrum of γ rays randomly correlated with long-lived β -particles (bottom). A γ -ray line at 172 keV can be seen in the ^{101}Sn spectrum,

which is absent in the background spectrum. Based on the systematics of $N = 51$ isotones this line was interpreted as a transition between the neutron $g_{7/2}$ and $d_{5/2}$ orbitals.

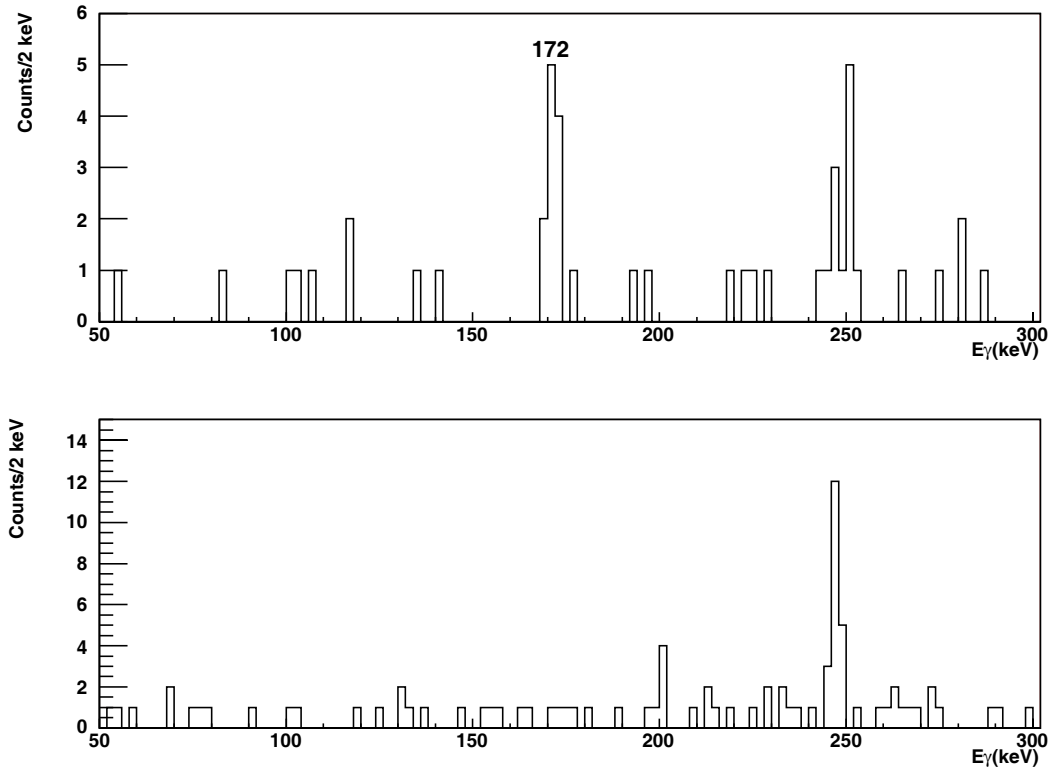


Fig. I-32. (top) Gamma rays tagged with ^{101}Sn β -delayed protons and (bottom) randomly correlated with long lived β emitters.

The separation energy between the $d_{5/2}$ and $g_{7/2}$ neutron states calculated using various mean-field potentials are widely spread and are on average larger than the measured value. Inclusion of tensor effects might help to reconcile the data and theory. The measured $d_{5/2}$ - $g_{7/2}$ energy difference was used to calculate excited states in light $^{102-109}\text{Sn}$ isotopes in the shell-model framework. Excellent agreement between the calculations and the data was obtained after attenuating the $(g_{7/2})_{0+}$ interaction by about 30%.

A search for core-excited states in ^{101}Sn is planned using the existing implantation station. The same method can be used to learn about proton-neutron interactions in the β -delayed proton emitter ^{100}In although a high granularity DSSD will be required in this case.

More experimental details and full discussion can be found in Ref. 2.

*Argonne National Laboratory and University of Notre Dame, †University of Maryland, ‡University of Edinburgh, United Kingdom.

¹O. Kavatsyuk *et al.*, Eur. Phys. J. A **31**, 319 (2007).

²D. Seweryniak *et al.*, Phys. Rev. Lett. **99**, 022504 (2007).

d.2.2. Isospin Symmetry of Odd-Odd Mirror Nuclei: Identification of Excited States in ^{48}Mn and a Comparison to the Mirror Nucleus ^{48}V (M. P. Carpenter, C. N. Davids, R. V. F. Janssens, C. J. Lister, D. Seweryniak, M. A. Bentley,* C. Chandler,† M. J. Taylor,* J. Brown,* J. Ekman,‡ S. J. Freeman,§ P. E. Garrett,¶ G. Hammond,† S. M. Lenzi,|| and R. du Rietz‡)

The fact that the attractive nuclear force acting between all neutrons and protons is approximately charge symmetric yields some startling and beautiful symmetries in nuclear behavior. The classic example is mirror symmetry, where two nuclei with interchanged numbers of protons and neutrons exhibit near-identical energy-level schemes. The Coulomb interaction lifts this degeneracy, and energy shifts result. However, the underlying spatial symmetry of the wave functions of these analogue states is generally preserved, and the resulting energy differences can be interpreted in terms of Coulomb phenomena. The long-range and well-understood Coulomb force, thus, has the potential to provide an extremely sensitive probe of spatial correlations and distributions of the protons in the nucleus.

Over the last decade, experimental advances have allowed for the study of the proton-rich members of mirror pairs in the $A \sim 40$ -60 region. Fortuitously, one of the most successful nuclear models - the large scale pf shell model - is now able to perform calculations in the whole pf shell, and has been applied to model Coulomb effects in this region. The differences in excitation energy [mirror energy differences (MED)] between analogue states have been shown to be remarkably sensitive to nuclear structure effects and, through detailed comparison with the shell model results, can now be interpreted with *quantitative* reliability. Mirror-pair spectroscopy in this region has so far been restricted to odd- A $T_z = \pm 1/2$ or even-even $T_z = \pm 1$ mirror pairs. We have recently measured for the first time a $T = 1$ odd-odd mirror pair with $A > 40$, namely, $^{48}\text{Mn}/^{48}\text{V}$ to high spin. The MED behavior is unlike any other observed in this region and, uniquely, is interpreted almost entirely in terms of a subtle shrinking of the nuclear radius as a function of angular momentum.

The experiment was performed at the ATLAS facility of the Argonne National Laboratory, where a beam of 110 MeV ^{40}Ca bombarded a self supporting ^{10}B target. The nuclei ^{48}Mn or ^{48}V were produced *via* the

evaporation of two neutrons or protons, respectively. The γ rays were detected with the Gammasphere array, which comprised 98 large-volume Compton-suppressed Ge detectors. The cross section leading to ^{48}Mn is expected to be a few tens of microbarns, a factor of $\sim 10^4$ weaker than the expected intensity of the mirror, ^{48}V , and, thus, unique identification of the recoils is essential. The recoiling nuclei were analyzed using the Fragment Mass Analyzer (FMA) which separates the residues as a function of M/q at the focal plane. Z identification is achieved using a split-anode isobutane-filled ionization chamber located behind the focal plane.

Figure I-33a shows the MED for the yrast positive parity sequence for the $^{48}\text{Mn}/^{48}\text{V}$ mirror pair along with the result of a full pf shell-model calculation based on the ANTOINE code¹ with Coulomb effects determined by the method described by Zuker *et al.*² In the odd- A and even-even mirror pairs of this region, the dominant Coulomb effect observed is a multipole effect associated with the angular-momentum recoupling of pairs of $f_{7/2}$ protons as a function of angular momentum. For these odd-odd nuclei, this effect is blocked by the occupation in both ^{48}Mn and ^{48}V of both $f_{7/2}$ protons and $f_{7/2}$ neutrons in the positive parity sequence. Despite the obvious restrictions placed on the shell model by limits on the valence space, and, hence, the need to assume a significant inert core, the full- pf shell model gives a remarkably accurate state-by-state account of the spin dependence of energy differences throughout the entire yrast sequence. In order to understand the behavior of the MED observed and calculated in Fig. I-33a, a single- j shell scenario, where only $f_{7/2}$ configurations are allowed is considered. The results of this calculation are shown in Fig. I-33b, and illustrates that the rise in MED results nearly entirely from radial effects, *i.e.* the shrinking of the nucleus with increasing spin.

A more complete account of these results can be found in a recent publication in Physical Review Letters.³

*University of York, United Kingdom, †Keele University, Staffordshire, United Kingdom, ‡Lund University, Sweden, §University of Manchester, United Kingdom, ¶University of Guelph, Ontario, ||INFN, Padova, Italy
¹E. Caurier *et al.*, Phys. Rev. C **50**, 225 (1994).

²A. P. Zuker *et al.*, Phys. Rev. Lett. **89**, 142502 (2002).

³M. A. Bentley *et al.*, Phys. Rev. Lett. **97**, 132501 (2006).

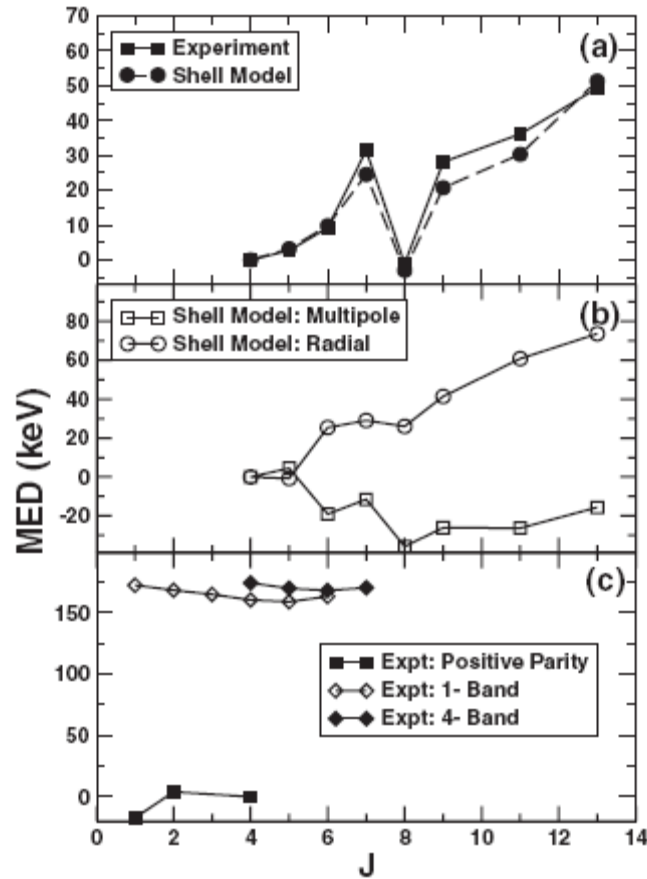


Fig. I-33. Mirror energy differences (MED) for the $T = 1$ states of $^{48}\text{M}/^{48}\text{V}$. (a) The experimental MED, along with the predictions of the shell model, for the positive-parity states. (b) The calculated multipole and radial contributions to the MED (see Ref. 3 for details). (c) The MED for the negative-parity structures based on the $J^\pi = 1^-, 4^-$ states and the MED for the non-yrast positive-parity states into which they feed.

d.2.3. Coulomb Shifts and Shape Changes in the Mass 70 Region (C. J. Lister, B. S. Nara Singh,* A. N. Steer,* D. G. Jenkins,* R. Wadsworth,* M. A. Bentley,* P. J. Davies,* R. Glover,* N. S. Pattabiraman,* T. Grahn,† P. T. Greenlees,† P. Jones,† R. Julin,† S. Juutinen,† M. Leino,† M. Nyman,† J. Pakarinen,† P. Rahkila,† J. Sarén,† C. Scholey,† J. Sorri,† J. Uusitalo,† P. A. Butler,‡ M. Dimmock,‡ D. T. Joss,‡ J. Thomson,‡ B. Cederwall,§ B. Hadinia,§ and M. Sandzelius§)

The odd-odd nucleus ^{78}Y was studied at ATLAS (using Gammasphere) and at Jyväskylä (using Juroball and RITU) by a York-ANL-Jyväskylä collaboration. $T = 1$ excited states were found for the first time in the Jyväskylä experiment, while the ANL data set was contaminated by reactions on light impurities. Even with the knowledge of the locations of the states, no

useful coincidence information could be extracted from the Gammasphere data set, despite lengthy investigation. The unusual negative Coulomb shifts were interpreted as arising from the nuclear shape smoothly increasing with spin.

This work has now been published.¹

*University of York, United Kingdom, †University of Jyväskylä, Finland, ‡University of Liverpool, United Kingdom, §Royal Institute of Technology, Stockholm, Sweden.

¹Phys. Rev. C **75**, 061301(R) (2007).

d.2.4. Shapes and Triaxiality of ⁷⁴Kr (C. J. Lister and S. M. Fischer)

Shape coexistence in light krypton isotopes is providing an exquisite test of current nuclear theories. Recently, Coulomb excitation of ^{74,76}Kr at GANIL has added detailed information on the shapes and their excitation modes. From a variety of “in-beam” Gammasphere experiments we have found relevant new additional information which compliments the inelastic excitation

studies. In particular, the role of triaxial shapes can be delineated. In fusion reactions producing ⁷⁴Kr, a triaxial shape band appears to be the main path for populating the known low-lying oblate shape isomer.

A paper is being written and will be submitted in FY2007.

d.2.5. $T = I$ States in ⁷⁴Rb and Their ⁷⁴Kr Analogs (S. M. Fischer,* C. J. Lister, N. J. Hammond, R. V. F. Janssens, T. L. Khoo, T. Lauritsen, E. F. Moore, D. Seweryniak, S. Sinha, D. P. Balamuth,† P. A. Hausladen,† D. G. Sarantites,‡ W. Reviol,‡ P. Chowdhury,§ S. D. Paul,¶ C. Baktash,¶ and C.-H. Yu¶)

⁷⁴Rb was investigated in connection with the issue of the strength of the np -pairing field and also because of its significance in testing the wavefunctions needed for inferring the structure-free decay rate of the superallowed ⁷⁴Rb - ⁷⁴Kr β -decay. The $T = I$ analogs of

the ⁷⁴Kr groundstate band were found, revealing rather small Coulomb shifts, but a candidate for the important low-lying $J = 0$ state was not found.

This work was published.¹

*DePaul University and Argonne National Laboratory, †University of Pennsylvania, ‡Washington University, §University of Massachusetts-Lowell, ¶Oak Ridge National Laboratory.

¹Phys. Rev. C **74**, 054304 (2006).

d.2.6. Mapping the Periphery of Deformation in the $A \sim 80$ Region: A Study of ⁸³Nb (S. M. Fischer, C. J. Lister, M. P. Carpenter, N. J. Hammond, R. V. F. Janssens, E. F. Moore, G. Mukherjee, D. Seweryniak, S. Sinha, S. J. Freeman,* J. Carney,† D. P. Balamuth,‡ and Y. Sun§)

The upper edge of the highly deformed region near $A \sim 80$ has been investigated at ATLAS using a conventional fusion-evaporation reaction. Large deformation was found for ⁸³Nb. Analysis suggests the conditions are right for K-isomers. The results have now been published.¹ This research has proven timely, as new experiments have recently revealed isomers in

$N = Z$ ⁸²Nb and ⁸⁶Tc and observed their decays. The isomers were produced at GSI following fragmentation experiments. The understanding of these isomers critically depends on the deformation inferred for ⁸³Nb. A possible interpretation is that they are two-quasiparticle K-isomers, relative to a $T = I$ np -paired vacuum groundstate.

*University of Manchester, United Kingdom, †DePaul University, ‡University of Pennsylvania, §University of Notre Dame.

¹S. M. Fischer *et al.*, Phys. Rev. C **75**, 064310 (2007).

d.2.7. Effect of a Triaxial Nuclear Shape on Proton Tunneling in ^{145}Tm (D. Seweryniak, C. N. Davids, M. P. Carpenter, N. Hammond, R. V. F. Janssens, T.-L. Khoo, G. Mukherjee, S. Sinha, S. J. Freeman,* A. Woehr,† A. Robinson,‡ P. J. Woods,‡ B. Blank,§ T. Davinson,‡ N. Hoteling,¶ Z. Liu,‡ J. Shergur,¶ A. A. Sonzogni,|| and W. B. Walters¶)

Proton decay is an important source of information on nuclear structure beyond the proton drip line. Transitional $^{145,146,147}\text{Tm}$ proton emitters are situated between spherical nuclei along the $N = 82$ shell closure and an island of prolate deformation. In fact, proton-rich $N = 76, 77, 78$ isotones are predicted to be triaxial or γ -soft. This offers a unique opportunity to shed light on the role of triaxiality on the proton emission. In order to learn more about the structure of the proton emitter ^{145}Tm , a search for in-beam γ rays with Gammasphere and the Fragment Mass Analyzer was carried out using the Recoil-Decay Tagging method. The ^{145}Tm ground-state rotational band was found to exhibit the properties

expected for a $h_{11/2}$ proton decoupled band. In addition, coincidences between protons feeding the 2^+ state in ^{144}Er and the 2^+-0^+ γ -ray transition were detected, the first measurement of this kind, leading to a more precise value for the 2^+ excitation energy of 329(1) keV.

As shown in Fig. I-34, calculations using the Particle-Rotor model indicate that the properties of the $\pi_{11/2}$ band are consistent with the presence of triaxiality with an asymmetry parameter $\gamma \sim 20^\circ$ if the calculated value of $\beta_2 = 0.25$ is used.

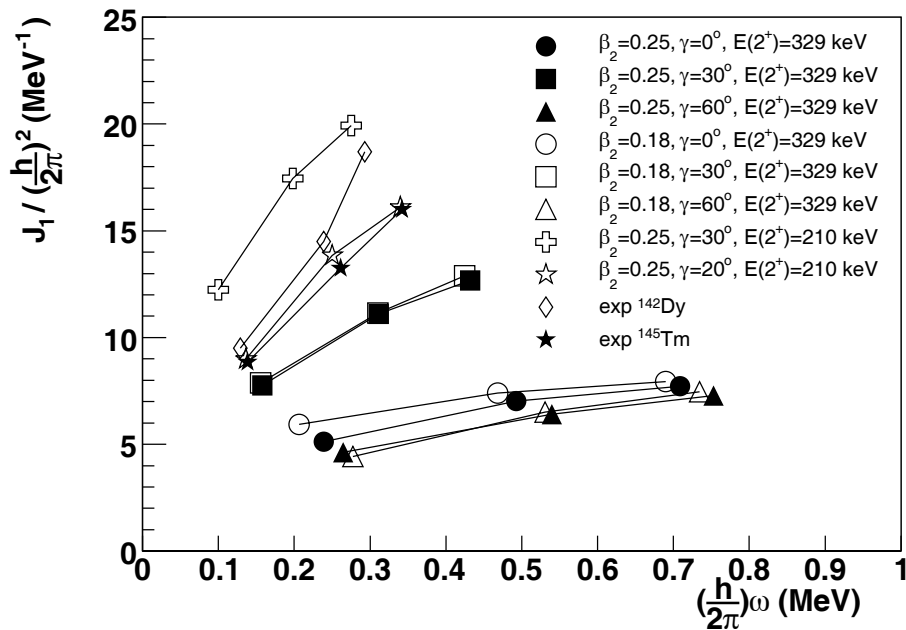


Fig I-34. The moment of inertia as a function of the rotational frequency extracted for the ^{145}Tm $\pi h_{11/2}$ band and the values calculated with the Particle Rotor model using different quadrupole deformations β_2 , asymmetry parameters γ , and moments of inertia (obtained from the 2^+ energies). Smaller $E(2^+) = 210$ keV takes into account increase in the moment of inertia as a function of the rotational frequency similar to the lighter $N = 76$ isotones. The moment of inertia for the even-even $N = 76$ isotope ^{142}Dy is plotted for comparison.

The ground state wave function components $0^+ \otimes h_{11/2}$ and $2^+ \otimes f_{7/2}$ calculated using the Core Quasi-Particle Coupling model for $\beta_2 = 0.25$ and $\gamma = 20^\circ$ are also consistent with that deduced from the proton decay rate and proton decay branching ratio to the 2^+ state in the

daughter measured for the ^{145}Tm ground state.

The experimental details and complete theoretical discussion can be found in Ref. 1.

*Argonne National Laboratory and University of Manchester, United Kingdom, †Argonne National Laboratory and University of Maryland, ‡University of Edinburgh, United Kingdom, §CEN Bordeaux-Gradignan, IN2P3-CNRS, France, ¶University of Maryland, ||Brookhaven National Laboratory.

¹D. Seweryniak *et al.*, Phys. Rev. Lett. **99**, 082502 (2007).

d.2.8. Multiple Band Structures in ¹⁶⁹Ta (M. P. Carpenter, R. V. F. Janssens, A. A. Hecht, T. Lauritsen, E. F. Moore, S. Zhu, F. G. Kondev, D. J. Hartley,* W. H. Mohr,* J. R. Vanhoy,* M. A. Riley,† A. Aguilar,† C. Teal,† M. K. Djongolov,‡ M. Danchev,‡ L. L. Riedinger,‡ G. B. Hagemann,§ G. Sletten,§ P. Chowdhury,¶ S. K. Tandel,¶ W. C. Ma,|| and S. W. Odegard**)

The intruder proton orbitals of the mass-170 region have recently drawn attention because of their anomalous behavior. Collective structures based on the $i_{13/2}$ proton orbital have been the focus of many studies of Lu nuclei, as wobbling excitations have been observed in ^{161,163,165,167}Lu. This collective mode indicates that stable triaxial deformation is present in these nuclei over a wide range of spin and energy. However, no examples of wobbling have been identified, thus far, outside the Lu nuclei, raising the following questions: Are these Lu nuclei unique? Or will stable triaxial deformation be observed in a broader region of nuclei? In order to answer this question, an investigation of the high-spin properties of ^{169,171}Ta was undertaken with the Gammasphere spectrometer.

Rotational structures in the ¹⁶⁹Ta nucleus were studied *via* the ¹²⁴Sn(⁵¹V, 6n) reaction, where the ⁵¹V beam was accelerated to 228 MeV by the Argonne Tandem-Linac Accelerator System (ATLAS) facility at Argonne National Laboratory. These data were obtained as a side channel of an experiment focusing on ¹⁷¹Ta,¹ but the sensitivity provided by the Gammasphere spectrometer proved sufficient for a significant

extension of the level scheme of this rare-earth nucleus. Over 170 new transitions and four new band structures were placed in ¹⁶⁹Ta, including the one associated with the [404]7/2 configuration. This sequence mixes strongly with the [402]5/2 band as should be expected for pseudospin partners. The intruder [660]1/2 sequence was also identified for the first time in ¹⁶⁹Ta. This configuration has drawn considerable attention recently as wobbling bands have been observed in Lu nuclei based on this orbital intruder.

As was the case for ¹⁷¹Ta, no wobbling structures were observed in ¹⁶⁹Ta. The moment of inertia and the band crossing behavior of the $i_{13/2}$ sequence indicate that it likely has enhanced deformation with respect to the other configurations. However, a lifetime measurement is required to verify this assertion. The new data allowed the excitation energies of all the configurations to be determined for the first time. In general, good systematic agreement is observed between the Ta bandhead energies and the calculated values of Ref. 2. The results of this study have recently been published in Physical Review C.³

*U. S. Naval Academy, †Florida State University, ‡University of Tennessee, §Niels Bohr Institute, Copenhagen, Denmark, ¶University of Massachusetts-Lowell, ||Mississippi State University, **University of Oslo, Norway.

¹D. J. Hartley *et al.*, Phys. Rev. C **72**, 064325 (2005).

²W. Nazarewicz, M. A. Riley, and J. D. Garrett, Nucl. Phys. **A512**, 61 (1990).

³D. J. Hartley *et al.*, Phys. Rev. C **74**, 054314 (2006).

d.2.9. Reflection-Asymmetric Tidal Waves in ²²⁰Th (M. P. Carpenter, R. V. F. Janssens, T. L. Khoo, T. Lauritsen, C. J. Lister, D. Seweryniak, S. Zhu, W. Reviol,* C. J. Chiara,* M. Montero,* D. G. Sarantites,* O. L. Pechenaya,* and S. G. Frauendorf†)

In a recent experiment at ATLAS, using the ²⁶Mg + ¹⁹⁸Pt reaction at 128 MeV, multiple octupole-type band structures in ²²⁰Th have been observed.¹ The

evaporation residues were selected with the HERCULES device and residue-gated γ rays were measured with Gammasphere. HERCULES is

particularly suitable for very asymmetric reactions and targets with thicknesses in excess of 0.5 mg/cm^2 .

The ^{220}Th level scheme has the following features: (1) The pattern of alternating-parity levels persists up to the highest spins observed ($s = +1$ simplex), but the nucleus exhibits a more vibrational-like behavior than the heavier thorium isotopes. (2) A rather large parity-splitting and a related staggering of the $B(E1)/B(E2)$ ratios is observed. (3) Two negative-parity, odd-spin sequences are present. (4) A short sequence of negative-parity states with even spins (presumably $s = -1$ simplex) is present as well.

As shown in Fig. I-35, the yrast states of ^{220}Th have an approximately constant rotational energy $\hbar\omega \sim E_\gamma$ (the transition energies fluctuate around $E_\gamma \sim 420 \text{ keV}$). The isotone ^{218}Ra shows a very similar behavior² (in contrast to the $N \geq 132$ isotones), a behavior that implies that the $N = 130$ nuclei do not rotate faster to acquire angular momentum. Multiple band crossings taking place over a broad range of spin values I , at the same value in two isotones, are considered to be a highly unlikely explanation of the described behavior and an interpretation in a "traditional" nuclear rotation

framework seems difficult. On the other hand, the near-equal spacing of transitions in the yrast structure cannot reflect the presence of spherical vibrational phonons either, as it extends over a large spin range. In Ref. 1, we propose a new approach which considers collectivity arising from reflection-asymmetric nuclear tidal waves with a constant angular velocity ω , hereby retaining the simplex structure. The nuclear shape in the rotating frame of reference is a combination of quadrupole and octupole deformations which both increase with I . The analogous I behavior was seen in "signature-partner" band structures built on K-isomers in $^{182,183}\text{Os}$,^{3,4} which the authors interpreted in terms of tidal waves⁵ on a triaxial nuclear surface. Another example may be the $K^\pi = 33/2^+$ band in ^{179}Re .

The concept of tidal waves accounts also for the staggering feature: the vibrational-like motion implies tunneling between the two shapes related to each other by the operation of space inversion which restores the parity. Nuclear tidal waves may well represent a common high-spin phenomenon in so-called transitional regions where the nuclear shape is deformation soft.

*Washington University, †University of Notre Dame.

¹W. Reviol *et al.*, Phys. Rev. C **74**, 044305 (2006).

²N. Schulz *et al.*, Phys. Rev. Lett. **63**, 2645 (1989).

³J. F. Smith *et al.*, Phys. Rev. Lett. **75**, 105 (1995).

⁴L. K. Pattison *et al.*, Phys. Rev. Lett. **91**, 182501(2003).

⁵D. M. Cullen, R. Glover, L. K. Pattison, P. M. Walker, S. Frauendorf, and D. Almeded, J. Phys. G **31**, S1709 (2005).

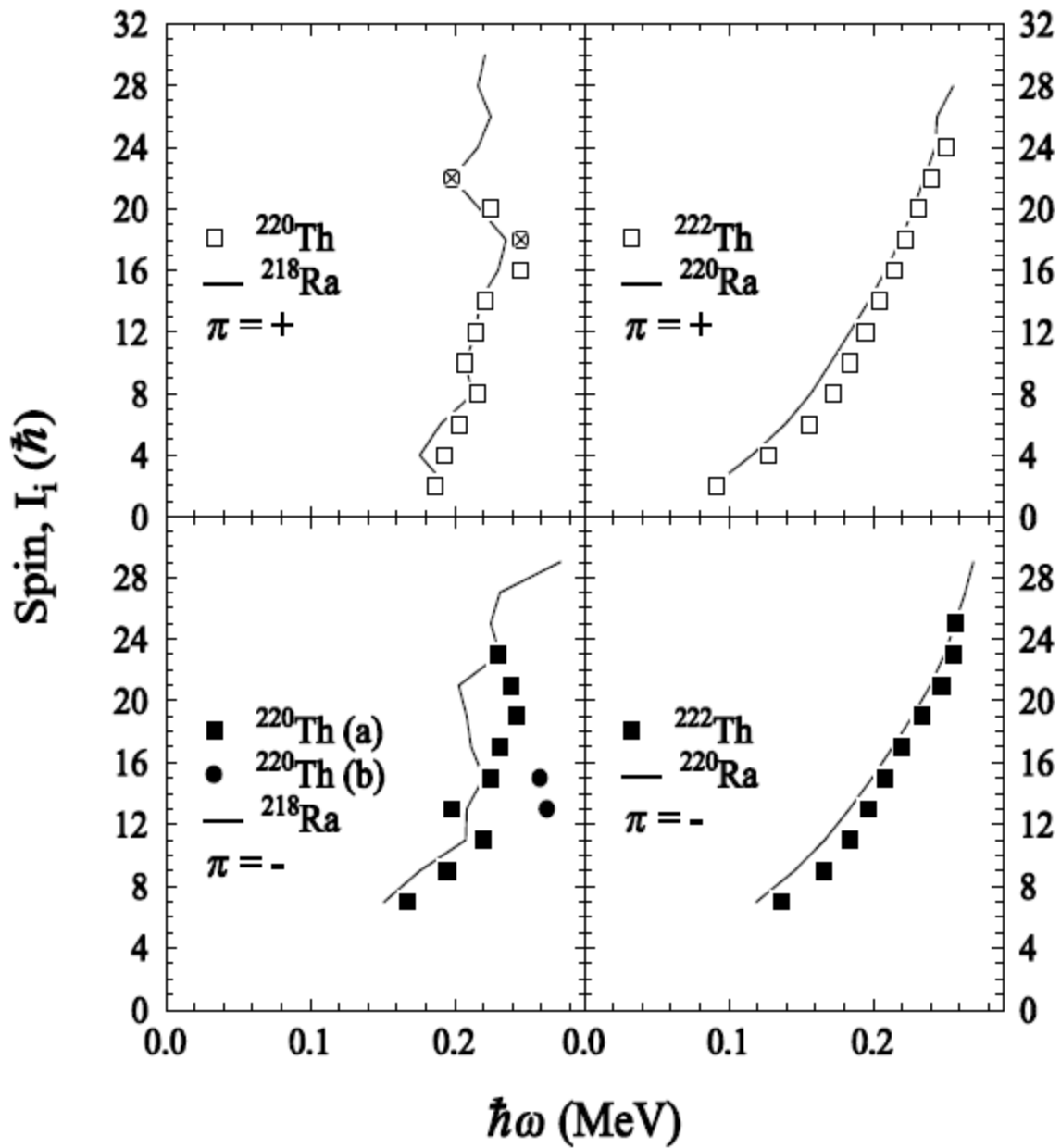


Fig. I-35. Spin I_i versus rotational energy $\hbar\omega$ for the yrast E2 transitions in $^{220}\text{Th}^1$ and $^{218}\text{Ra}^2$ (left panels) and in $^{222}\text{Th}^3$ and $^{220}\text{Ra}^3$ (right panels). The data points marked with crosses are derived from level-energy differences rather than from γ -ray energies. For ^{220}Th , both yrast (a) and yrare (b) states are shown.

E. OTHER NUCLEAR STRUCTURE RESEARCH

The efficiency of data collection with Gammasphere allows for studies of the gamma-decay pathways along excited, very high-spin superdeformed nuclei. These studies include the rotational damping observed in both the $A = 150$ and $A = 190$ region.

e.1. Rotational Damping, Ridges and the Quasicontinuum of γ Rays in ^{152}Dy

(T. Lauritsen, R. V. F. Janssens, T. L. Khoo, I. Ahmad, M. P. Carpenter, F. G. Kondev, C. J. Lister, D. Seweryniak, S. Zhu, P. Fallon,* A. O. Macchiavelli,* B. Herskind,† T. Døssing,† A. Korichi,‡ and A. Lopez-Martens‡)

The quasicontinuum of γ rays from the feeding and decay of superdeformed and normal bands in ^{152}Dy have been extracted in 1- and 2-dimensional spectra. The E_γ - E_γ correlations in the latter reveal strong ridges associated with superdeformed and normal states in this nucleus (see Fig. I-36). The entry distributions for normal and superdeformed bands have been extracted from measured fold and sum-energy distributions. A Monte Carlo model was developed to (simultaneously) describe all the quasicontinuum and ridge spectra as

well as the feeding intensity of the superdeformed bands. The rotational damping widths in the normal and superdeformed wells were derived based on a comparison of the data with model calculations of the continuum of γ rays at finite temperatures.

A comprehensive, detailed paper describing both the techniques used and results obtained has been published.¹

*Lawrence Berkeley National Laboratory, †Niels Bohr Institute, Copenhagen, Denmark, ‡C.S.N.S.M., IN2P3-CNRS, Orsay, France.

¹T. Lauritsen *et al.*, Phys. Rev. C **75**, 064309 (2007).

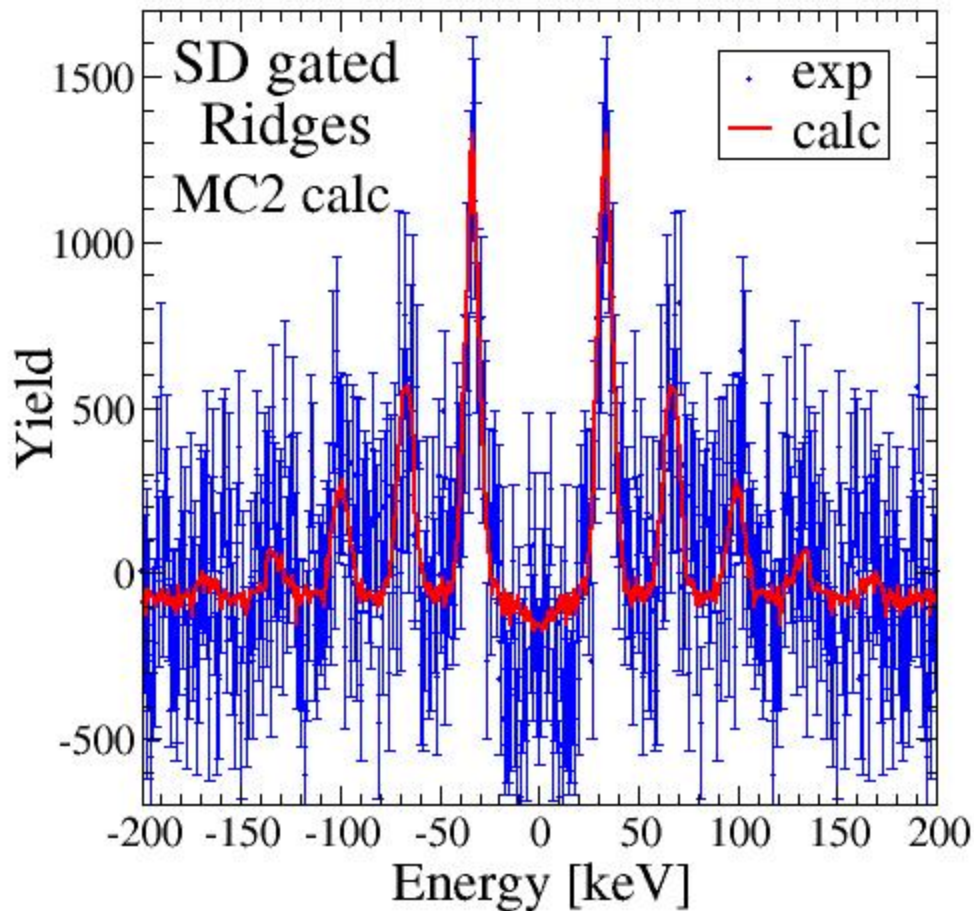


Fig. I-36. The ridges seen in a gamma-gamma matrix when double gates are placed on clean gamma rays of SD band 1 in ^{152}Dy .

e.2. Rotational Damping, Ridges and the Quasicontinuum of γ Rays in ^{194}Hg

(T. Lauritsen, T. L. Khoo, R. V. F. Janssens, I. Ahmad, M. P. Carpenter, F. G. Kondev, C. J. Lister, D. Seweryniak, S. Zhu, P. Fallon,* A. O. Macchiavelli,* B. Herskind,† T. Døssing,† A. Korichi,‡ and A. Lopez-Martens‡)

The ridges in gamma-gamma matrices, when double gates are placed on clean super-deformed (SD) transitions in ^{194}Hg , have been extracted. Ridges out to third order are clearly visible in Fig. I-37. These ridges, in conjunction with the quasicontinuum of gamma rays in ^{194}Hg that were extracted earlier,¹ will be used to determine the rotational damping parameters in ^{194}Hg in the same type of analysis that was performed recently for ^{152}Dy .²

The Monte Carlo code KL_sd/kla will be used to simultaneously reproduce the super-deformed ridges as well as the super-deformed area normal-deformed γ -ray quasi-continuum spectra. Via the renormalization of the rotational damping parameters necessary to reproduce the data, the strength of the rotational damping in the normal-deformed and super-deformed wells of ^{194}Hg will be inferred.

*Lawrence Berkeley National Laboratory, †Niels Bohr Institute, Copenhagen, Denmark, ‡C.S.N.S.M, IN2P3-CNRS, Orsay, France.

¹T. Lauritsen *et al.*, Phys. Rev. C **62**, 044316 (2000).

²T. Lauritsen *et al.*, Phys. Rev. C **75**, 064309 (2007).

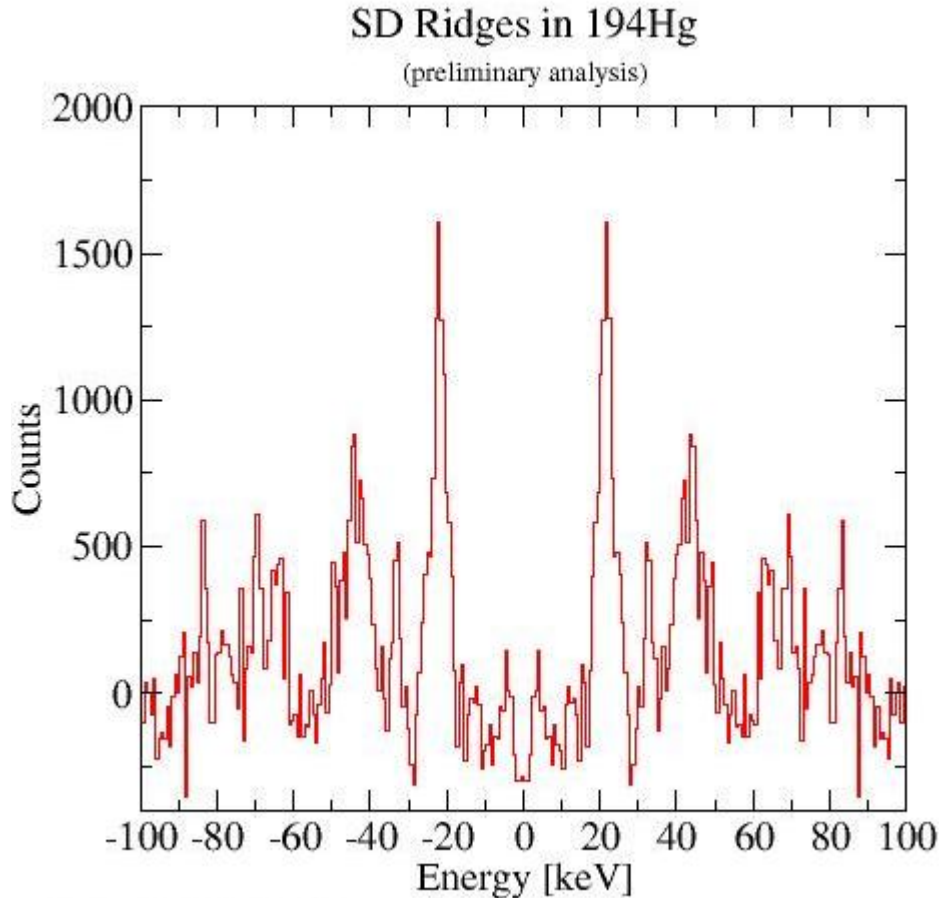


Fig. I-37. The ridges seen in a gamma-gamma matrix when double gates are placed on clean gamma rays of SD band 1 in ^{194}Hg .

e.3. Understanding the Origin of Ergodic Superdeformed Bands (T. L. Khoo, T. Lauritsen, A. Lopez-Martens,* T. Døssing,† M. Matsuo,‡ B. Herskind, and K. Yoshida§)

The excited states in the super-deformed (SD) potential well in ^{194}Hg exhibit a new phenomenon in nuclei. Very narrow ridges (FWHM ~ 10 keV) are observed in E_γ - E_γ matrices and fluctuations in the counts reveal that a large number of bands (~ 150) contribute. From the data, we can deduce that excited SD bands decay in almost the same manner as discrete bands, *i.e.*, an initial state with initial spin I decays to one final state with spin $I-2$. This occurs despite the fact that the ~ 150 excited bands represent complicated mixed states with 2-8 mean-field basis states. Thus, the γ transitions would be expected to have fluctuating transition strengths following Porter-Thomas distributions. Yet,

the collective flow remains almost intact, revealing the preservation of rotational coherence even in mixed chaotic states. In sharp contrast, normal deformed nuclei, which have smaller deformation, exhibit weak ($\sim 10\%$) narrow ridges with only ~ 30 bands, with the remaining collective strength spread over a very wide energy interval of ~ 200 keV.

The highly-correlated SD E2 flow was, in fact, predicted¹ by theory. We have sought to understand the origin of the new phenomenon by examining the results of this theory, with the assistance of new calculations. The narrowly confined E2 strength and the large

number of participating bands are found to be related. They arise due to two reasons: (a) the basis (mean-field) states in the SD well of Hg nuclei have an exceptionally small dispersion in rotational frequencies $\Delta\omega$ (~ 25 keV) and (b) the basis states mix through the 2-body residual interaction. (N.B. $2\Delta\omega = E_\gamma$). The onset of mixing ($n_{\text{mix}} \geq 2$, where n_{mix} is the number of components in the wave function) occurs at a lower heat energy ($U \sim 1.2$ MeV) than the onset of damping ($n_{\text{branch}} \geq 2$, where n_{branch} is the number of decay branches) at $U \sim 1.6$ MeV. When damping sets in the rotational strength normally becomes widely dispersed. In all other cases investigated so far, mixing and damping are simultaneous. Therefore, for excited SD Hg states, there exists a “golden” region, which sustains the unusually large number (~ 150) of rotational bands and where the dispersion in rotational strength Γ_{E2} remains exceedingly small (~ 10 keV). The spread Γ_{E2} (10 keV) is smaller than the estimated average spacing D (10-30 keV) between the excited levels, *i.e.*, $\Gamma_{E2} < D$. Mottelson² has pointed out that, when this condition is satisfied, rotational bands with unusual properties would arise, with exactly the characteristics

that we have now observed. Following Mottelson,² we call these ergodic bands. Figure I-38 shows the variation of n_{mix} and n_{branch} as a function of U for transitions from states with $I^\pi = 40^+$. It can be seen that n_{branch} remains close to 1 even after mixing occurs ($n_{\text{mix}} > 2$), before it gradually increases and then exceeds 2.

When $n_{\text{branch}} > 2$, damping sets in. For our excited SD states, the spread in E2 strength, usually called Γ_{rot} , is not expected to be as large as the ~ 200 keV normally observed in normal nuclei. The reason is that, as soon as mixing sets, motional narrowing also occurs, given by the condition $2\Delta\omega < \Gamma_\mu$; Γ_μ (40-55 keV) is the compound damping width. In this limit, $\Gamma_{\text{rot}} = 4\Delta\omega$ ($2\Delta\omega/\Gamma_\mu = 15$ -30 keV, which is reduced with respect to the usual value $4\Delta\omega$). There is no clear evidence in our data for this slightly broader damped component in the E_γ - E_γ ridge structure since the narrow ridge structure exhausts the full E2 strength. Motional narrowing, due to the small dispersion $2\Delta\omega$, is also responsible for the occurrence of these ergodic bands.

*C.S.N.S.M., Orsay, France, †The Niels Bohr Institute, Copenhagen, Denmark, ‡Niigata University, Japan, §Nara University, Japan, Lawrence Berkeley National Laboratory.

¹K. Yoshida and M. Matsuo, Nucl. Phys. **A636**, 169 (1998).

²B. R. Mottelson, Nucl. Phys. **A557**, 717c (1993).

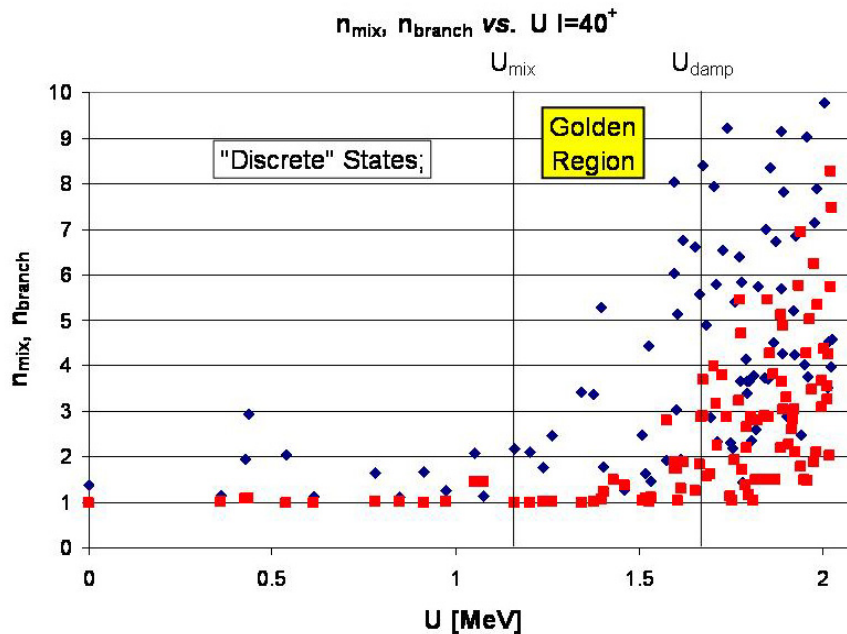


Fig. I-38. Variation of n_{mix} (blue diamonds) and n_{branch} (red squares) with U , the excitation energy above the yrast SD line for transitions from states with $I^\pi = 40^+$. Ergodic SD rotational bands occur in the golden region between the vertical lines, which mark the onset of mixing ($n_{\text{mix}} \geq 2$) and damping ($n_{\text{branch}} \geq 2$).

e.4. Triaxial Strongly Deformed Bands in ^{163}Tm (R. V. F. Janssens, E. F. Moore, M. P. Carpenter, N. J. Hammond, T. Lauritsen, G. Mukherjee, D. Seweryniak, S. Zhu, X. Wang,* U. Garg,* Y. Gu,* S. Frauendorf,* T. Li,* B. K. Nayak,* N. S. Pattabiraman,† S. S. Ghugre,† R. S. Chakrawarthy,‡ M. Whitehead,‡ and A. O. Macchiavelli§)

Triaxiality in nuclei has been a longstanding prediction of theory, but has proved very difficult to establish experimentally. Triaxial strongly deformed (TSD) bands in the region of $A \sim 160$ -175, predicted by theory,^{1,2} have been observed in Lu, Hf and Ta nuclei.³⁻¹² Further, some of these observed TSD bands have been identified as so-called "wobbling bands". This wobbling mode of excitation is generally considered as one of the most unambiguous fingerprints for nuclear triaxiality. Nevertheless, the fact that wobbling bands have only been observed in several ($A = 161, 163, 165, 167$) Lu isotopes,⁸⁻¹² but not in any other element remained somewhat of a puzzle until very recently. A possible resolution of this issue has been proposed in our work of exploring the TSD band structures in the ^{163}Tm nucleus.¹³

A "thin" target experiment and a DSAM lifetime measurement were carried out with the reaction $^{130}\text{Te} (^{37}\text{Cl}, 4n)$ using Gammasphere at LBNL and at ANL, respectively. As can be seen in Fig. I-39, the level scheme resulting from our data analysis indicates four bands of interest: two known yrast bands and two proposed TSD bands. The structure of key transitions connecting the two TSD bands in ^{163}Tm is distinctly different from the one expected for wobbling bands. The measured quadrupole moments (Q_t) of TSD bands in ^{163}Tm (~ 7.5 eb) are essentially the same as the ones (of wobbling bands) in ^{163}Lu , while such values in Hf

nuclei are larger by 4-6 eb (see Table III in Ref. 14), possibly pointing to a different nature. There is a discrepancy (~ 20 -30%) between data and calculations for the Q_t moments of the TSD bands.¹⁴ However, this seems to be a general feature in the region and requires further investigation.

The two new bands observed in the ^{163}Tm nucleus have been identified to be the TSD bands built on a TSD minimum: $\varepsilon_2 = 0.39$, $|\gamma| = 17^\circ$. It has been confirmed that these two TSD bands are associated with a larger deformation than the yrast (ND) bands, *i.e.*, Q_t (TSD) ~ 7.5 eb and Q_t (ND) ~ 6.4 eb. Within the framework of present calculations, the deformation of the TSD bands is driven mainly by a large neutron gap at $N = 94$ (see Fig. 5 in Ref. 14). The TSD bands in ^{163}Tm have been interpreted as structures associated with particle-hole excitations in a TSD well.¹³ It is worth pointing out that the Tilted Axis Cranking (TAC)¹⁵ calculations performed in the present work provide a natural explanation for the presence of wobbling bands in the Lu isotopes and the absence of such bands in all neighboring Tm, Hf and Ta nuclei. The explanation is related to: (I) the shape driving effects of the $i_{13/2}$ proton orbital; (II) the presence of a strong shell gap at $N = 94$; and (III) the level density around the Fermi surface. The results of this study have been published.^{13,14}

*University of Notre Dame, †UGC-DAE Consortium for Scientific Research, Kolkata, India, ‡University of Manchester, United Kingdom, §Lawrence Berkeley National Laboratory.

¹H. Schnack-Petersen *et al.*, Nucl. Phys. **A594**, 175 (1995).

²R. Bengtsson, <http://www.matfys.lth.se/~ragnar/TSD-defsyst.html>.

³W. Schmitz *et al.*, Phys. Lett. **B303**, 230 (1993).

⁴S. Törmänen *et al.*, Phys. Lett. **B454**, 8 (1999).

⁵H. Amro *et al.*, Phys. Lett. **B506**, 39 (2001).

⁶M. K. Djongolov *et al.*, Phys. Lett. **B560**, 24 (2003).

⁷D. J. Hartley *et al.*, Phys. Lett. **B608**, 31 (2005).

⁸P. Bringel *et al.*, Eur. Phys. J. A **24**, 167 (2005).

⁹S. W. Ødegård *et al.*, Phys. Rev. Lett. **86**, 5866 (2001).

¹⁰D. R. Jensen *et al.*, Phys. Rev. Lett. **89**, 142503 (2002).

¹¹G. Schönwaßer *et al.*, Phys. Lett. **B552**, 9 (2003).

¹²H. Amro *et al.*, Phys. Lett. **B553**, 197 (2003).

¹³N. S. Pattabiraman *et al.*, Phys. Lett. **B647**, 243 (2007).

¹⁴X. Wang *et al.*, Phys. Rev. C **75**, 064315 (2007).

¹⁵S. Frauendorf, Nucl. Phys. **A677**, 115 (2000).

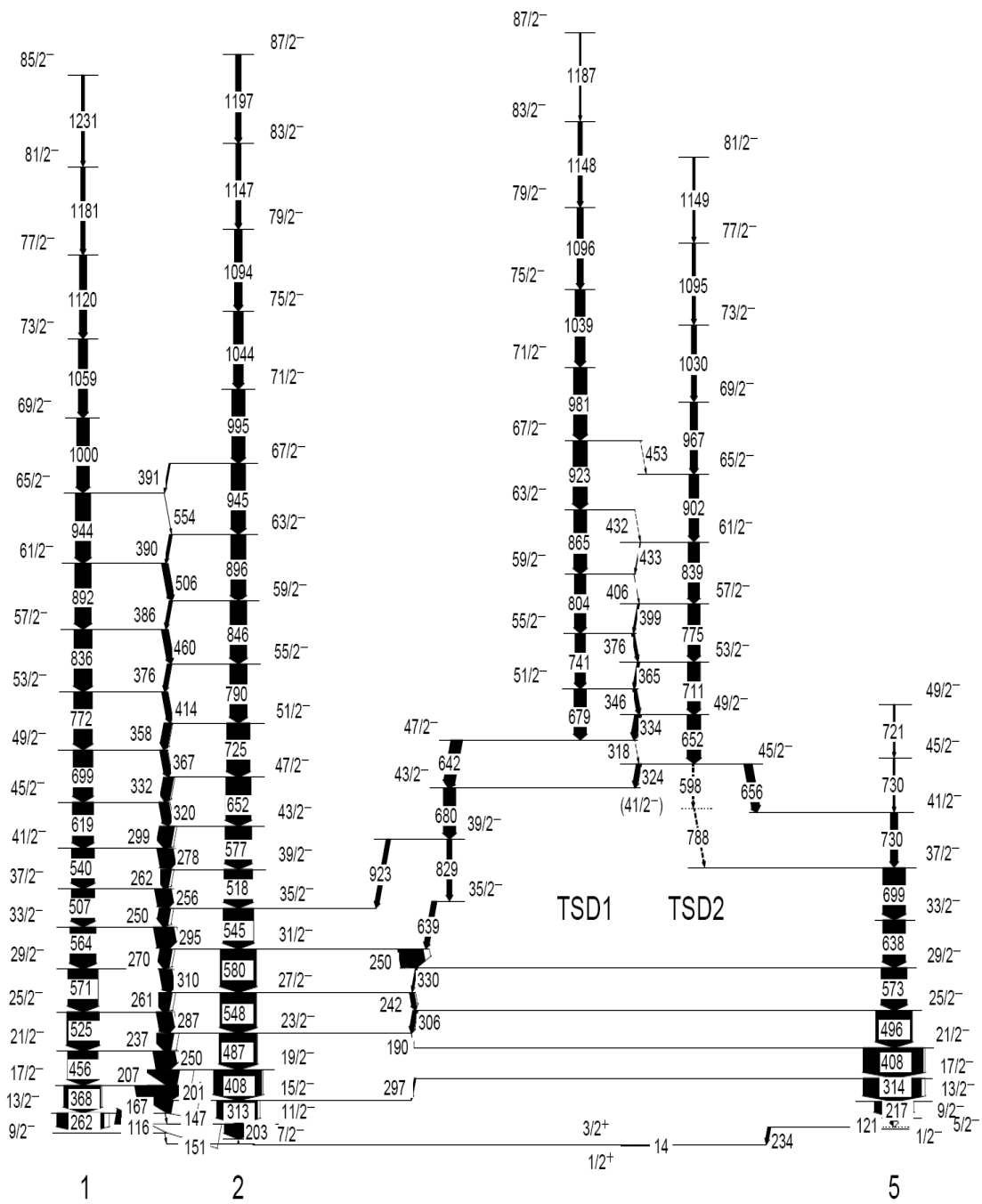


Fig. I-39. Partial level scheme of ^{163}Tm .

e.5. Quantifying the Level of Isospin Mixing in the $A = 31$ Mirror Nuclei (C. J. Lister, M. P. Carpenter, R. V. F. Janssens, T. L. Khoo, T. Lauritsen, D. Seweryniak, S. Zhu, N. S. Pattabiraman,* D. G. Jenkins,* M. A. Bentley,* R. Wadsworth,* G. Lotay,† P. J. Woods,† and Krischichayan‡)

One of the outstanding questions in nuclear physics is the extent to which isospin symmetry is violated as a function of increasing Z and A . The focus of the present work is on isospin mixing and its impact on electromagnetic transition rates but such an investigation is not straightforward as the role of isospin mixing has to be disentangled from other nuclear structure effects. Stringent selection rules apply in $N = Z$ nuclei making them an excellent focus for searching for isospin mixing. Despite few striking examples, our knowledge of isospin mixing and its effect on electromagnetic decays is rather limited at the present time.

A new approach to the issue was recently highlighted by Ekman *et al.*, who studied the $T = 1/2$ mirror nuclei, ^{35}Ar and ^{35}Cl .¹ They found that the decay branching of the lowest $7/2^-$ level was very different in the two nuclei. They found that in ^{35}Ar an E1 transition was present, while in the well-studied stable nucleus ^{35}Cl , the analogous transition was almost completely absent. Importantly, both $7/2^-$ states are particle bound, which rules out a lot of possibilities for perturbing the transition strengths. In general, it is expected that such E1 transitions in conjugate nuclei would be of very similar strength. Ekman *et al.*, advanced the explanation that the cancellation of the E1 matrix element in ^{35}Cl arose from isospin mixing, in this case between the dominant $T = 1/2$ and a weak $T = 3/2$ component.¹ They were unable, however, to quantify this suggestion since absolute transition strengths were not available for ^{35}Ar .

Recently, similar behavior to that reported for $A = 35$ was found in the $T = 1/2$ mirror nuclei, ^{31}S and ^{31}P (see Fig. I-40). Again, the decay pattern of the first $7/2^-$ state was found to change dramatically between the mirror nuclei. In this case, a 2195 keV E1 transition clearly present in ^{31}P was found to have no counterpart in the decay scheme of ^{31}S . It is very difficult in the

absence of lifetime measurements, and hence, absolute transition strengths, to speculate on the role that different mechanisms such as isospin mixing might have on the E1 transition strengths. Lifetimes are well known for states of interest in the stable isotope ^{31}P , but prior to the present work, lifetimes were only known for a few low-lying states in ^{31}S .

Lifetimes in ^{31}S were obtained using the Doppler Shift Attenuation Method (DSAM). The earlier study of the mirror nuclei ^{31}S and ^{31}P used the $^{20}\text{Ne} + ^{12}\text{C}$ reaction. It was found that it was difficult to get a reliable adhesion between a carbon foil and a thick target backing which was appropriate for a DSAM measurement. It was, therefore, decided to change to the $^{16}\text{O} + ^{16}\text{O}$ reaction and use metal oxide on metal targets. A ^{16}O beam at an energy of 29 MeV bombarded a target of nickel monoxide of $530 \mu\text{g}/\text{cm}^2$ thickness backed by $3.5 \text{ mg}/\text{cm}^2$ nickel. The resulting gamma radiation was detected using the Gammasphere array consisting of 100 high-purity germanium detectors. Lineshape spectra were obtained by gating in an all detector versus specific angle matrices. The program "lineshape" was employed, in which the shell-corrected Northcliffe and Schilling stopping powers for the recoil nucleus in the target and backing material was used. The mean lifetime of the transition of interest 1166 keV in ^{31}S was estimated as 0.98(20) ps. Figure I-41 shows the lineshape of the 1166 keV transition at 70° , 90° and 110° .

Having obtained a lifetime for the $7/2^-$ level in ^{31}S , we are now able to calculate $B(\text{E1})$ transition rates for the transitions de-exciting both $7/2^-$ states in ^{31}S and ^{31}P (see Table I-6). In the case of the 2195/2215 keV mirror E1 transitions, it is striking that the latter is relatively much weaker. Theoretical analysis is underway to probe whether isospin mixing is responsible for this difference.

Table I-6. B(E1) transition rates obtained for ^{31}S from lifetimes measured in the present work and ^{31}P from the literature.

Nucleus	E_γ (keV)	$I_i \rightarrow I_f$	B(E1) W.u.
^{31}S	1166	$7/2^- \rightarrow 5/2_2^+$	5.9×10^{-4} W.u.
	2215	$7/2^- \rightarrow 5/2_1^+$	$<2.0 \times 10^{-6}$ W.u.
^{31}P	1136	$7/2^- \rightarrow 5/2_2^+$	$4.5(8) \times 10^{-4}$ W.u.
	2195	$7/2^- \rightarrow 5/2_1^+$	$8.2(6) \times 10^{-5}$ W.u.
	1481	$11/2^- \rightarrow 9/2_2^+$	$1.0(5) \times 10^{-3}$ W.u.

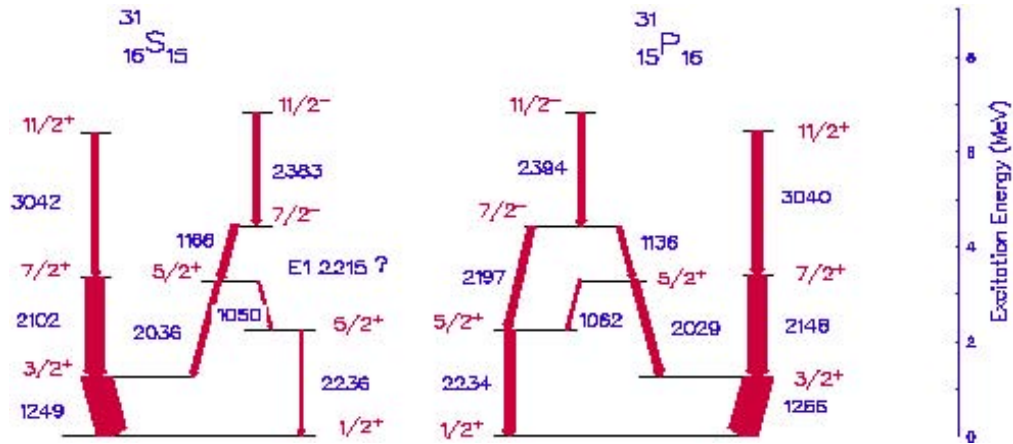


Fig. I-40. Comparison of the mirror level schemes for ^{31}S and ^{31}P . In ^{31}S , the transition between the $7/2^-$ state and the first excited $5/2^+$ state is missing, leading to the present investigation of isospin breaking in these nuclei.

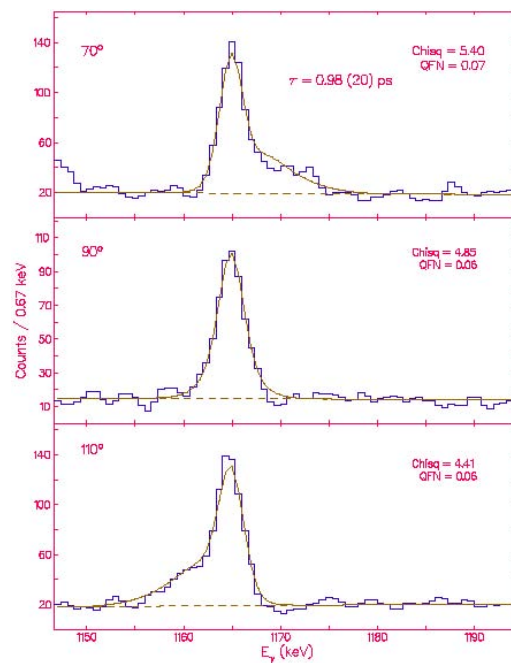


Fig. I-41. DSAM fit to the line shapes of the 1166 keV gamma ray from $7/2^-$ state in ^{31}S measured at three different angles.

*University of York, United Kingdom, †University of Edinburgh, United Kingdom, ‡UGC-DAECRSR, Calcutta, India.

¹J. Ekman *et al.*, Phys. Rev. Lett. **92**, 132502 (2004).

²D. G. Jenkins *et al.*, Phys. Rev. C **72**, 031303(R) (2005).

F. THE PHOBOS EXPERIMENT AT RHIC

Having completed its planned research program after six years of successful operation, the PHOBOS experiment at RHIC was disassembled in the fall of 2005. As one of the two “small” RHIC experiments, PHOBOS has played a disproportionately large role in the RHIC physics program with a main focus on charged particle multiplicity measurements, but also with central contributions to studies of flow, particle spectra, particle correlations, and anti-particle to particle ratios.

Although the PHOBOS data taking has been completed, a significant body of data is still under analysis. Recent results have been obtained including system size dependence of elliptic flow,¹ elliptic flow fluctuations in Au + Au collisions,² transverse momentum spectra of identified hadron spectra,³ and an analysis of cluster properties seen in two-particle correlations in pp collisions at 200 and 410 GeV.⁴

Further analyses of PHOBOS data will be carried out and published over the next few years. Also, longer papers that summarize the PHOBOS results in more general categories will be written and published.

f.1. The PHOBOS Experiment at RHIC (B. B. Back for the PHOBOS Collaboration)

f.1.1. System Size, Energy, Pseudorapidity, and Centrality Dependence of Elliptic Flow

The elliptic flow, v_2 , observed in relativistic heavy-ion collisions, provides important information on the hydrodynamic properties of the hot and dense medium formed in the participant region of such collisions. Until recently, the eccentricity of this region has been derived by using simple geometry such that the short

transverse axis is assumed to coincide with the impact parameter. In recent studies of Cu + Cu collisions, surprisingly large values of v_2 were observed in near-central collisions, for which the geometrical model predicts very small values of the overlap eccentricity, Fig. I-42.

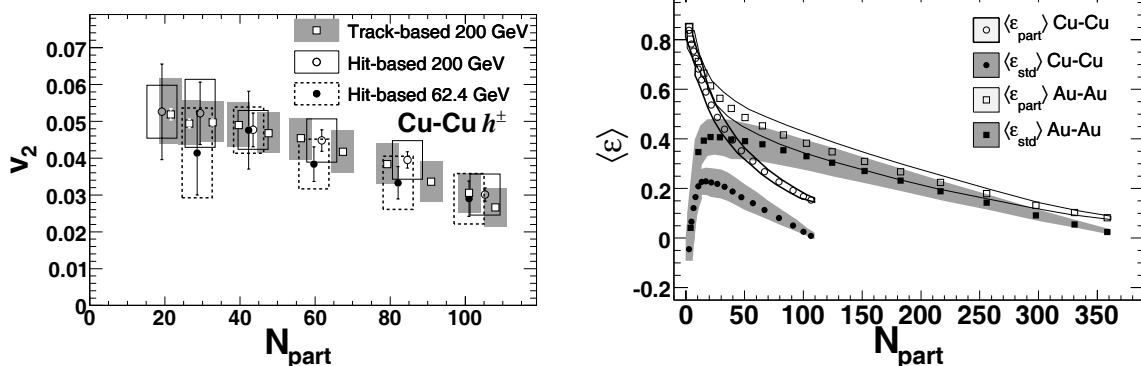


Fig. I-42. Left: The elliptical flow signal, v_2 obtained from a hit-based analysis in the $-1 < \eta < 1$ range is shown as a function of N_{part} for 0-40% central CuCu collisions at 62.4 (solid points) and 200 (open circles) GeV and compared to results for a track-based analysis for the 200 GeV data. The boxes show 90% C.L. systematic errors whereas the error bars represent 1σ errors. Right: Glauber Monte Carlo calculations of the average eccentricity $\langle \epsilon \rangle$ calculated by including (open symbols) or excluding (solid symbols) the co-variance term σ_{xy} of Eq. 1 for both CuCu and AuAu collisions at 200 GeV.

In a simple geometrical representation of the participant region one expects that v_2 approaches zero for the most central events. This discrepancy has been understood as event-by-event fluctuations of the orientation of the participant region because of the small number of nucleons involved for this system. Using the probabilistic distribution of nucleon-nucleon interaction points in a Glauber Monte Carlo calculation one may compute the “participant eccentricity” in the transverse x-y plane

$$\varepsilon_{part} = \frac{\sqrt{(\sigma_y^2 - \sigma_x^2)^2 + 4\sigma_{xy}^2}}{\sigma_y^2 + \sigma_x^2}, \quad (1)$$

f.1.2. Elliptic Flow Fluctuations in Au + Au Collisions at 200 GeV

A new analysis method for elliptic flow in heavy-ion collisions has recently been developed on the basis of a maximum likelihood method. This analysis is found to

which corresponds to a principal component transformation that maximizes the eccentricity for each event. Here σ_x^2 , σ_y^2 , and σ_{xy} are the associated (co)variances of the participant region consisting of nucleon-nucleon interaction points. In Fig. I-42 (right panel) this quantity, obtained in Glauber Monte Carlo simulations, is compared to the standard method of calculating the eccentricity, ε_{std} , in which the covariance term, σ_{xy} was excluded. We observe that for the light CuCu system the omission of the co-variance term has a substantial effect on the computed eccentricity of the participant region.¹

agree well with both the track-based and hit-based methods employed previously,² Fig. I-43 (left top panel).

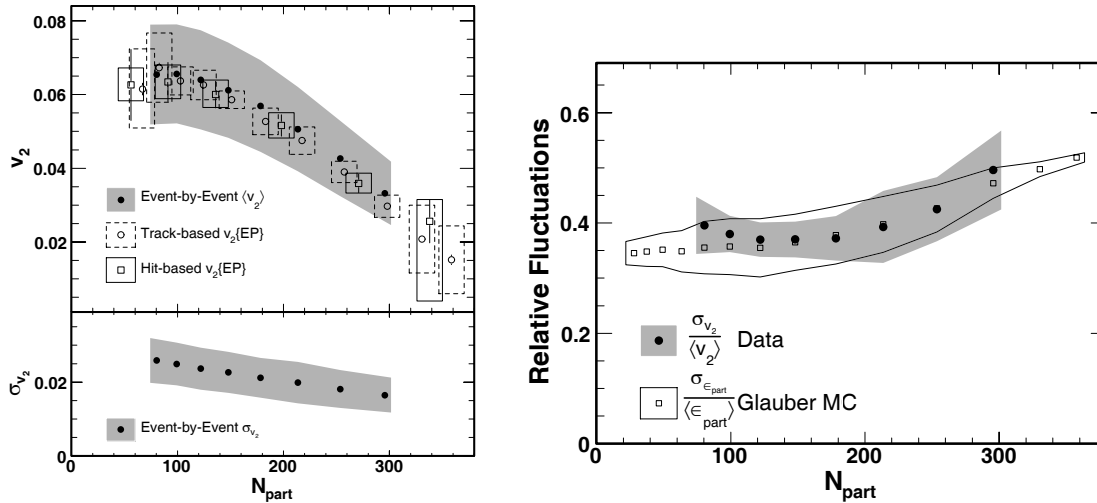


Fig. I-43. Left panel: The average elliptic flow $\langle v_2 \rangle$ (top) and its standard deviation σ_{v_2} (bottom) is plotted vs. the number of participants, N_{part} for 200 GeV Au + Au collisions. Results of the present event-by-event analysis technique (solid points) are compared with previously published data (open symbols). Right panel: The normalized elliptic flow fluctuation $\sigma_{v_2}/\langle v_2 \rangle$ (solid points) is plotted as a function of N_{part} and compared to the normalized eccentricity fluctuation $\sigma_{\varepsilon_{part}}/\langle \varepsilon_{part} \rangle$ obtained from Glauber Monte Carlo simulations (open squares).

The event-by-event method allows for the determination of the fluctuation of the elliptic flow signal, σ_{v_2} , for events of a certain centrality class as shown in Fig. I-43 (left bottom). The relative size of

these fluctuations for AuAu collisions is found to depend only weakly on centrality, solid points in Fig. I-43 (right) in agreement with Glauber Monte Carlo simulations (open squares).³

f.1.3. Identified Hadron Transverse Momentum Spectra in AuAu Collisions at 62.4 GeV

Particles emitted in AuAu collisions at 62.4 GeV have been identified on the basis of their (1) time-of-flight, (2) energy-loss, and (3) residual energy of particles stopped in the first Si detector layers of the PHOBOS spectrometer. This analysis allows for the accumulation of identified particle spectra (pions, kaons and protons) over a wide range of transverse

momentum with unique coverage for low p_T particles over a range of collision centralities. The resulting spectra were fit with the blast-wave model⁴ which simulated thermal emission from a radially expanding source is shown in Fig. I-44 for the 0-15% centrality bin.

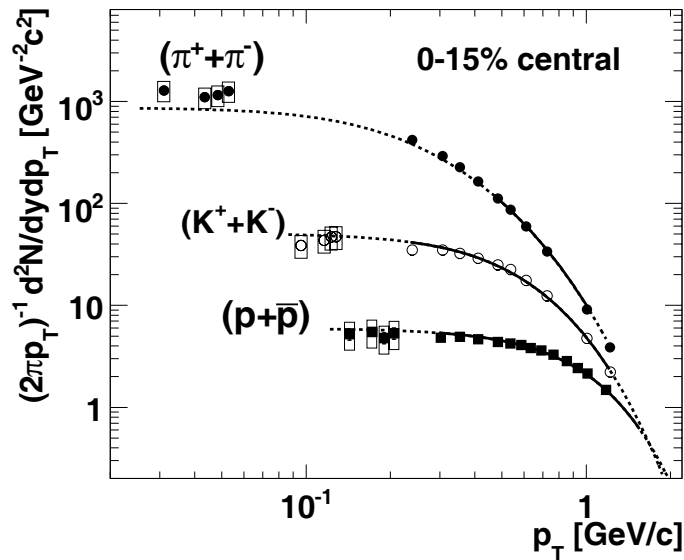


Fig. I-44. Blast-wave fits to identified spectra of pions (solid circles), kaons (open circles) and (anti)-protons (solid squares) for 0-15% central AuAu collisions at 62.4 GeV. The low p_T data obtained by the stopped particle method are shown with systematic errors (boxes).

The parameters obtained from the blast-wave fits vary only slightly with collision centrality, with the temperature at kinetic freeze-out $T = 103$, 102 , and 101 MeV and the radial expansion velocity $\beta_s = 0.78$, 0.76 , and 0.72 (fraction of c), for the 0-15%, 15-30%, and 30-50% centrality bin, respectively. Here,

a linear velocity profile is assumed, namely $\beta(r) = \beta_s(r/R)$, where $R = 10$ fm is the radius of the fireball at kinetic freeze-out. These fits were derived by excluding the stopped particle data points. Including these points into the fit changes the values of T and β_s by less than 6 MeV and 0.02, respectively.

¹B. Alver *et al.*, accepted for publication in Phys. Rev. Lett.

²B. B. Back *et al.*, Phys. Rev. Lett. **95**, 122303 (2005).

³B. Alver *et al.*, submitted to Phys. Rev. Lett.

⁴E. Schnedermann, J. Sollfrank, and U. Heinz, Phys. Rev. C **48**, 2462 (1993).

G. REACTION MECHANISM STUDIES

Studies of the heavy-ion fusion reaction have recently experienced a renaissance with the discovery at Argonne of a substantial reduction of the fusion cross section at deep sub-barrier energies. Both systematic evaluations of the effect based on published data as well as the measurements in new systems are carried out.

g.1. Radius-of-Curvature of the S Factor Maximum in Sub-Barrier Fusion Hindrance

(C. L. Jiang, B. B. Back, R. V. F. Janssens, and K. E. Rehm)

It has recently been demonstrated that the appearance of sub-barrier fusion hindrance in heavy-ion fusion reactions is associated with a maximum in the astrophysical S factor.¹ The energy corresponding to the maximum is denoted E_s and the corresponding logarithmic derivative of the cross section is denoted L_s .

It was found that the S factor can be expressed approximately by the second-order Taylor expansions of $\ln S(E)$ around the maximum

$$S = S_0 e^{-(E-E_s)^2/2\rho}, \quad (1)$$

where S_0 is the value of the S factor at its maximum and ρ is the radius-of-curvature, which can be formulated as

$$\frac{1}{\rho} = \left| \frac{d^2 \ln S}{dE^2} \right| = \left| \frac{dL}{dE} - \frac{d(\pi\eta/E)}{dE} \right| \text{ at } E = E_s. \quad (2)$$

i.e., ρ is determined by the difference of derivatives from the logarithmic derivative of the experimental cross section, $L(E)$, and that corresponding to a constant S factor, $L_{cs}(E) = \frac{\pi\eta}{E}$.

Previously, we have found² that E_s follows an overall systematics over a wide range of projectile-target combinations as a function of the parameter $\zeta = Z_1 Z_2 \sqrt{\mu}$ where μ is the reduced mass number. In addition, E_s appears to depend sensitively on the nuclear structure of the interacting nuclei. Following this approach, we have examined the radius-of-curvature of the S factor maximum for a number of systems for which the fusion cross sections have been studied down to small cross sections. The radius-of-curvature is in all cases derived from the difference in logarithmic derivatives between the data and the constant S factor expression according to Eq. (2), either for which an S factor maximum has been observed, or where extrapolation methods have been used to obtain the slopes of the logarithmic derivatives near E_s .

The radius-of-curvatures, thus obtained, are shown in

Fig. 45a as a function of the parameter ζ . With the aid of some other curves from systematics, a fit curve of ρ was obtained as the dashed curve shown in Fig. 45a (see Ref. 3 for details). There is a maximum of ρ , appearing at around $\zeta = 1000$, near the data point for the system $^{16}\text{O} + ^{76}\text{Ge}$, *i.e.*, in a region where the data were mostly obtained by extrapolation. It would, therefore, be of interest to perform more detailed experimental studies of some systems with the parameter ζ in the range $\zeta < 1000$ to determine whether a maximum value of ρ occurs in this region.

In Fig. 45b we show the same data, but normalized to the energy E_s . For the light fusion systems, from $^{10}\text{B} + ^{10}\text{B}$ to $^{16}\text{O} + ^{16}\text{O}$, the value of ρ is rather large relative to its centroid value E_s . Furthermore, the ratio ρ/E_s decreases by more than one order of magnitude, from about 0.35 to about 0.015 for heavier systems. If this ratio is large, the S factor maximum is not easily recognized visually. Thus, the determination of the sub-barrier hindrance effect in light systems represents a significant experimental challenge. An S factor representation is shown in Fig. 45c for the system $^{12}\text{C} + ^{13}\text{C}$. The solid curve is obtained with the description of the radius-of-curvature given by Eq. (1). In this case, it is difficult to recognize the S factor maximum. This is an important result with consequences for studying the extrapolation of the S factors to very low energies for reactions of astrophysical interest.⁴

Aside from the general trend discussed above and displayed in Fig. 1-45a, large fluctuations of ρ around the average trend, represented by the dashed curve are seen for systems of colliding nuclei of the same element, but with different masses. In particular, the systems highlighted by vertical bands, namely $^{58}\text{Ni} + ^{58}\text{Ni}$, $^{58}\text{Ni} + ^{60}\text{Ni}$, $^{58}\text{Ni} + ^{64}\text{Ni}$, $^{64}\text{Ni} + ^{64}\text{Ni}$ and $^{90}\text{Zr} + ^{90}\text{Zr}$, $^{90}\text{Zr} + ^{89}\text{Y}$, $^{90}\text{Zr} + ^{92}\text{Zr}$, $^{90}\text{Zr} + ^{96}\text{Zr}$, show large deviations from the overall general trend. These systems range from "stiff" to "soft" colliding nuclei.

These deviations emphasize a strong dependence of ρ on nuclear structure.

The detailed result of the present study has been published in Ref. 3.

¹C. L. Jiang, H. Esbensen, B. B. Back, R. V. F. Janssens, and K. E. Rehm, Phys. Rev. C **69**, 014604 (2004).

²C. L. Jiang, B. B. Back, H. Esbensen, R. V. F. Janssens, and K. E. Rehm, Phys. Rev. C **73**, 014613 (2006).

³C. L. Jiang, B. B. Back, R. V. F. Janssens, and K. E. Rehm, Phys. Rev. C **75**, 057604 (2007).

⁴C. L. Jiang, K. E. Rehm, B. B. Back, and R. V. F. Janssens, Phys. Rev. C **75**, 015803 (2007).

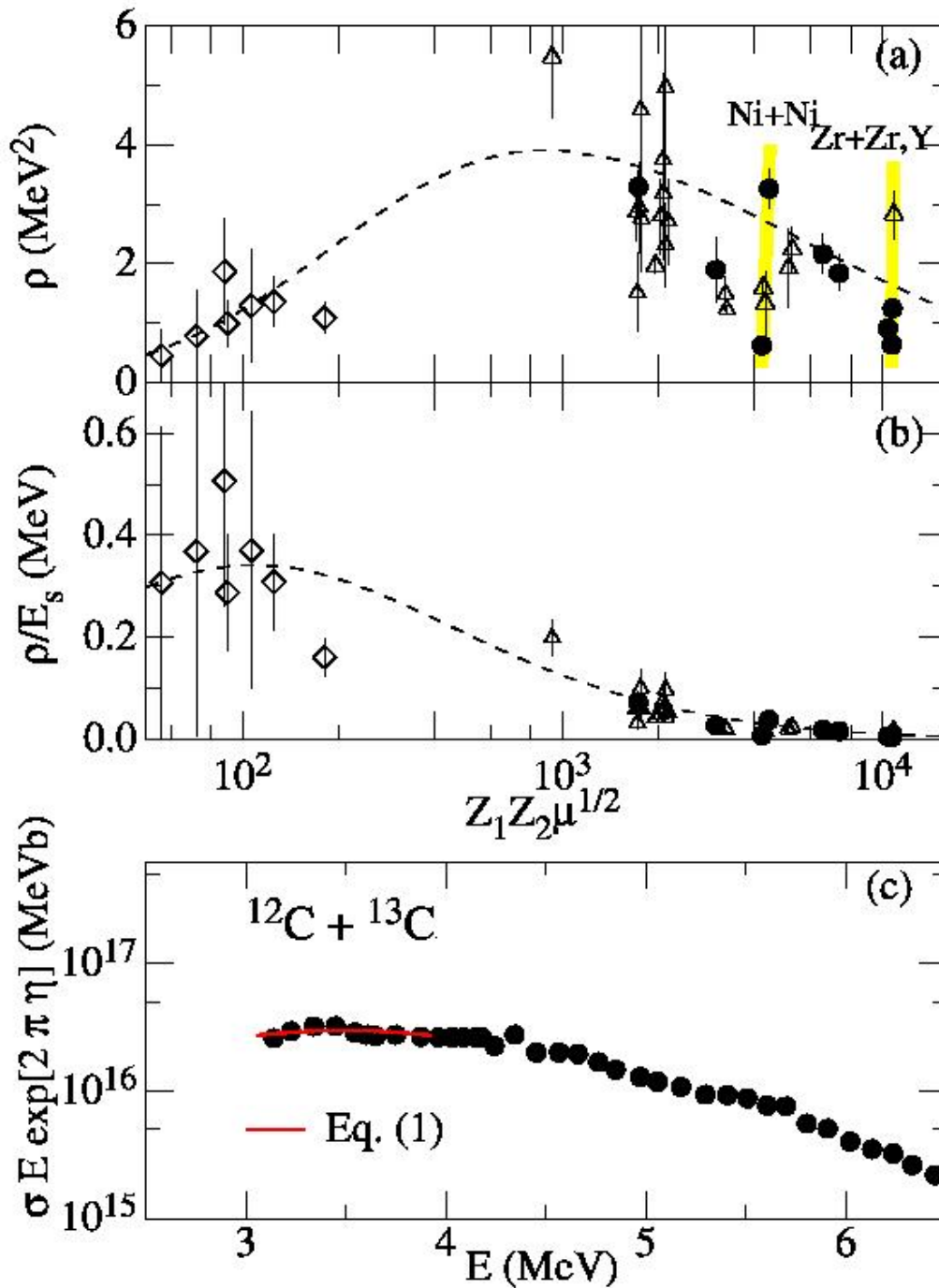


Fig. I-45. (a) Systematics of the radius-of-curvature of the S factor maximum. The value of the radius-of-curvature ρ is plotted versus $Z_1 Z_2 \mu^{1/2}$. The vertical bands highlight the location of the Ni + Ni and Zr + Zr, Y systems. (b) Same as (a) but the ordinate has been divided by the value E_s . (c) S (E) factor for the system $^{12}\text{C} + ^{13}\text{C}$. The solid curve was obtained from Eq. (1). See text for details.

H. HIGH-PRECISION AND HIGH-SENSITIVITY EXPERIMENTS

High precision measurements of nuclear masses for select systems of high importance for fundamental decay processes and astrophysical reactions remain a central focus of the research program at ATLAS.

h.1. High-Precision Q -Value Measurements on Superalloyed Fermi Emitters

(G. Savard,^{*}[†] S. Caldwell,^{*}[†] J. Fallis,[¶]^{*} A. A. Hecht,^{*}^{**} D. Lascar,^{*}^{††}, A. Levand,^{*}
N. D. Scielzo,^{*} H. Sharma,^{*}[¶] K. S. Sharma,^{*}[¶] I. Tanihata,^{*} A. C. C. Villari,^{*}^{‡‡}
F. Buchinger,[‡] J. A. Clark,[§] J. E. Crawford,[‡] S. Gulick,[‡] J. C. Hardy,^{||} J. K. P. Lee,[‡] and
R. Segel^{††})

Superalloyed $0^+ \rightarrow 0^+$ decays provide the most precise value for the weak vector coupling constant and the up-down mixing matrix element V_{ud} , and play a critical role in the test of the unitarity of the top row of the Cabibbo-Kobayashi-Maskawa (CKM) quark mixing matrix. The data on the superalloyed Fermi decays used to obtain the most precise value of V_{ud} involves Q -value, lifetime and branching ratio measurements and comes from over 100 different experiments. And although they contribute less than 20% of the total uncertainty on V_{ud} , the remainder come from the small theoretical corrections that must be applied to the data. The recent measurement on ^{46}V performed at the CPT yielded a significant shift in that data set and resulted in

a first statistically significant shift of the corrected Ft value from the mean value used to determine V_{ud} . To see if this is an isolated case or a first sign of a general trend, it is necessary to apply the high precision available with ion trap measurements to others emitters. This work was continued this year with precision Q -value measurements on the superalloyed emitters ^{10}C and ^{38}K to complement the recent work we did on ^{14}O , ^{42}Sc , $^{26\text{m}}\text{Al}$ and ^{34}Cl . The results of these measurements, compared to the most recent tabulation on superalloyed emitters (J. C. Hardy and I. S. Towner, Phys. Rev. C **71** 055501 (2005)), are shown in Fig. I-46.

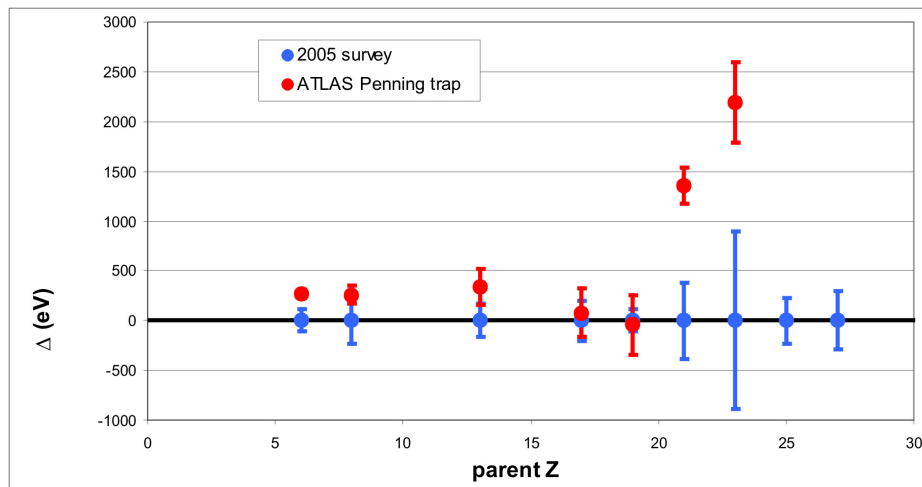


Fig. I-46. Q -values obtained at the CPT for the high-precision superalloyed Fermi emitters compared to the tabulation of all previous precision measurements.

As can be seen from Fig. I-46, the precision obtained at the CPT equals or exceeds the combined precision of all previous measurements and our measurement of the

Q -value in the decay of ^{10}C in particular has reached an accuracy below 40 eV, a record for Penning trap measurements on short-lived isotopes. Our

measurements were performed in triplets where possible systematic errors can be tested directly on-line and no effect outside of the stated error bars was observed. We find excellent agreement with the Chalk River Q -value difference measurements that are considered the most reliable components of the high-precision reaction Q -value data, but conclude that the experimental error bars on many single threshold or reaction measurements must have been underestimated. For the five lightest emitters measured we find fairly good agreement with previous results although our results are typically slightly higher. For the heavier emitters ^{42}Sc and ^{46}V , we find large shifts to higher Q -values which raise the corresponding Ft values

accordingly. If all other inputs (lifetimes, branching ratios and theoretical corrections) are taken at face value, this would considerably worsen the CVC test and the limit on scalar currents obtained from superallowed decays. This first clear deviation from the CVC test is instead most likely an indication of a problem with the nuclear structure dependent corrections for these heavier cases where core excitations can play a more important role. Measurements on the remaining two cases in the high-precision set and complementary measurements of the excitation energy of the long-lived isomers in these nuclei should soon determine the extent of this effect.

*Argonne National Laboratory, †University of Chicago, ‡McGill University, Montreal, Quebec, §Yale University, ¶University of Manitoba, Winnipeg, Manitoba, ||Texas A&M University, **University of Maryland, ††Northwestern University, ‡‡GANIL, Caen, France.

h.2. Mass Measurements of Heavy Fission Fragments Using the CPT Mass Spectrometer (H. Sharma,^{*,†} G. Savard,^{*,‡} S. Caldwell,^{*,‡} J. Fallis,^{*,†} L. Gang,^{*,§} A. A. Hecht,^{*,||} D. Lascar,^{*,**} A. Levand,^{*,*} N. D. Scielzo,^{*,*} I. Tanihata,^{*,*} A. C. C. Villari,^{*,††} Y. Wang,^{*,†} K. S. Sharma,[†] F. Buchinger,[§] L. Blomeley,[§] J. A. Clark,[¶] J. E. Crawford,[§] S. Gulick,[§] J. K. P. Lee,[§] and R. Segel||)

With the addition of the new isobar separator to the CPT system, it was possible to extend the previous measurements on heavy fission fragments from ^{252}Cf with 17 new mass measurements. Of these, 8 are new measurements and the remainder are improvements to our previous results. The new data extend our knowledge of the masses of neutron rich nuclides to $N = 93$ for La and Ba isotopes, $N = 94$ for Ce isotopes and $N = 95$ for Pr isotopes, the farthest excursion from

stability for these elements so far. The data analysis for these cases is now completed. Our results are in good agreement with the 2003 Atomic Mass Evaluation (AME 2003) in regions where it is anchored by previous experimental data. However, they reveal a trend for these neutron-rich isotopes to be less bound than the results of the AME 2003 as the neutron number increases (see Fig. I-47).

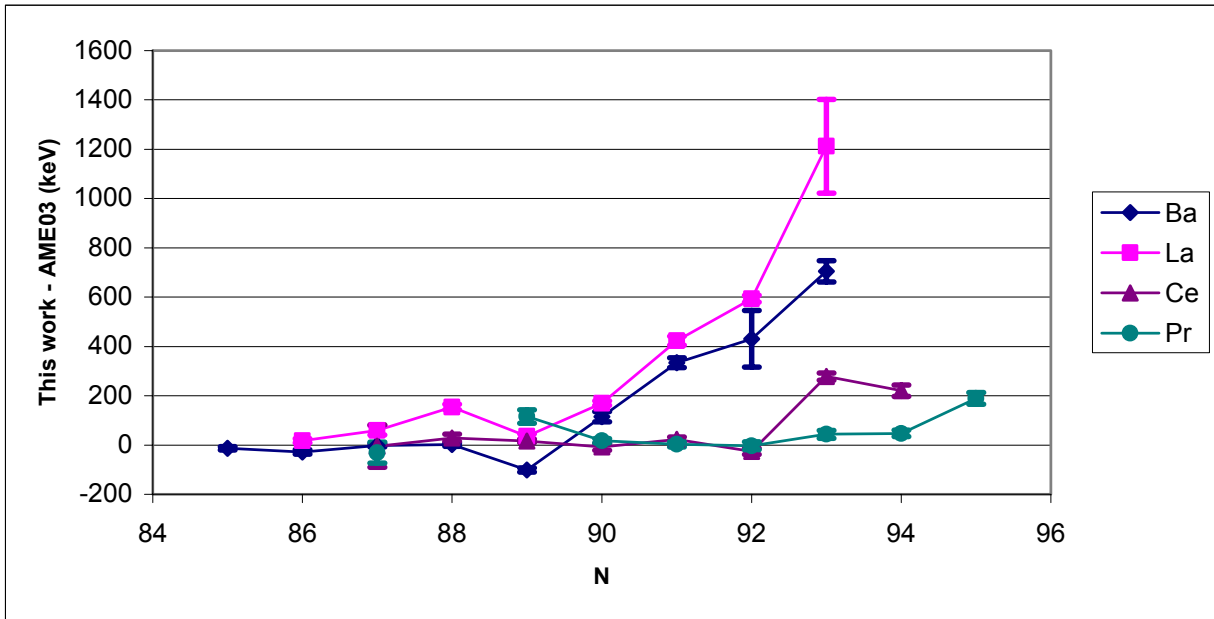


Fig. I-47. Comparison of the data from this work with the results of the AME2003.

Trends in the two-neutron separation energies for these nuclides are shown in Fig. I-48. The dotted lines show the results of the AME 2003 while the solid lines show the values calculated entirely from the results of our

measurements. The plot clearly shows that the region of deformation starting at $N = 90$ for the Pr, Nd and heavier nuclides terminates with Ce and is not present for the Ba and La isotopic chains.

*Argonne National Laboratory, †University of Manitoba, Winnipeg, Manitoba, ‡University of Chicago, §McGill University, Montreal, Quebec, ¶Yale University, ||University of Maryland, **Northwestern University, ††GANIL, Caen, France.

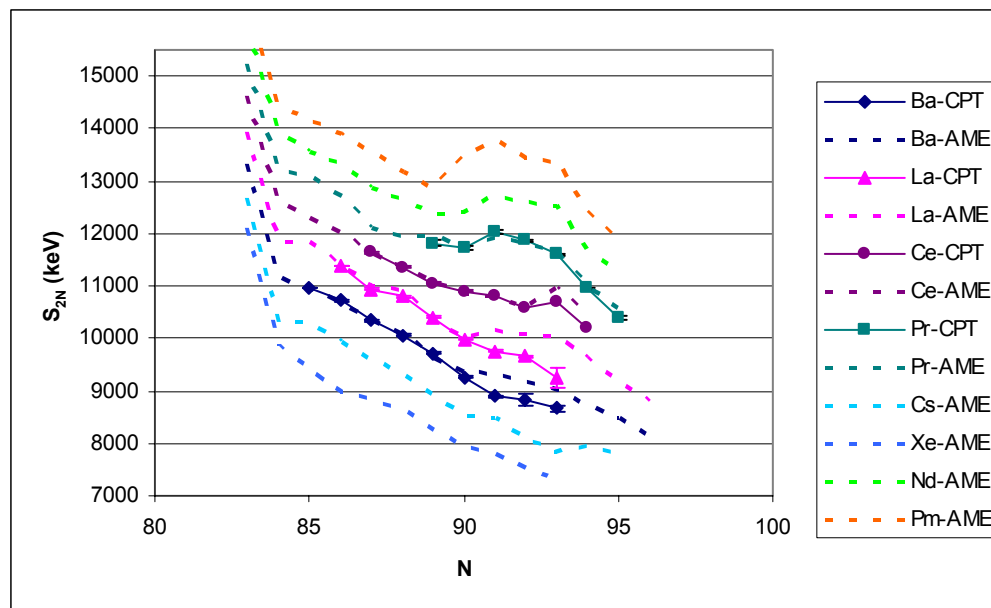


Fig. I-48. Two-neutron separation energies from this work and the AME 2003.

h.3. A Bragg Scattering Method to Search for the Neutron Electric Dipole Moment (M. Peshkin, M. Arif,[¶] T. W. Dombeck,^{*} D. S. Hussey,[¶] D. Jacobson,[¶] H. Kaiser,[†] D. Koetke,[‡] and R. K. Smither[§])

The goal of this experiment is to search for the neutron electric dipole moment by observing the precession of the neutron's spin polarization in the atomic electric fields when neutrons are Bragg reflected from a perfect silicon crystal. The anticipated rotation in a single reflection is a few microradians. By causing the neutrons to undergo some 20,000 successive reflections as they drift down a slot cut into the crystal, we anticipate achieving a sensitivity of a few times 10^{-27} e-cm, comparable with the sensitivity sought in the next round of ultra-cold-neutron experiments, but with significantly different systematic errors. Our experiments are being carried out at the reactor at the NIST Center for Neutron Research, in Gaithersburg, MD.

In 2006, NIST commenced construction of a dedicated beam line and experimental area for this experiment. That construction is expected to be completed in early summer 2007. At that time, we will measure the reflectivity and geometrical properties of an improved slotted silicon crystal currently being prepared at Argonne. We have previously shown experimentally that the reflectivity of a properly prepared silicon surface is greater than 0.9999. In 2007, we plan to measure the reflectivity or raise its lower bound.

We are currently preparing for an experiment to measure the interaction of the neutron's magnetic dipole moment (MDM) with the atomic electric fields by the same technique, making use of the Schwinger interaction between an electric field and a moving MDM, the latter appearing as an effective EDM. The MDM experiment will serve as a proof of principle and exploration of systematic errors for the EDM experiment, and it will also serve as a necessary calibration of the effective electric fields experienced by the neutrons in the EDM experiment. Technical details of the MDM experiment will be given in a NIST report "Technical Report on the Status of the Measurement of Neutron Schwinger Scattering in Silicon," to be published in 2007. The MDM experiment is being done in collaboration with F. Wietfeldt of Tulane University.

We are currently procuring a set of Helmholtz coils to achieve the magnetic field quality needed for the Schwinger experiment. We have on hand, or on order, all of the necessary polarization handling equipment (polarizer, Heusler analyzer crystal, spin rotation coils, etc.). We expect to use these in 2007 to investigate the effects of neutron penetration into the crystal in Bragg scattering and begin preliminary measurements and

calibrations.

^{*}University of Hawaii, [†]University of Indiana, [‡]Valparaiso University, [§]APS User Program, Argonne National Laboratory, [¶]National Institute of Standards and Technology.

I. DEVELOPMENT OF NEW EXPERIMENTAL EQUIPMENT

A vital program of development of new instrumentation and methods is carried out at ATLAS. Most prominent among these is the development of the HELIOS spectrometer to study transfer reactions in inverse kinematics and the development of the CARIBU facility, which will provide exotic neutron-rich beams of high quality for these and other studies. In addition, other existing instrumentation is being augmented and improved to increase the sensitivity and reach of the experimental program.

i.1. HELIOS – A Solenoidal Spectrometer for Inverse Reactions (B. B. Back, C. J. Lister, R. Pardo, K. E. Rehm, J. P. Schiffer, S. J. Freeman,* and A. H. Wuosmaa†)

The effort to design and build a spectrometer based on a large superconducting solenoid, HELIOS (HELical Orbit Spectrometer), is progressing rapidly. The spectrometer provides automatic particle identification and a very large solid angle for detecting light low-energy particles emitted in inverse kinematics reactions while preserving the energy dispersion corresponding to

the center-of-mass system. The physics aim is to study single particle transfer, pick-up or inelastic scattering reactions on light targets (H, He) with heavy radioactive beams produced either at the ATLAS in-flight facility or at the future CARIBU radioactive ion injector. Details on the spectrometer concept and performance simulations are given in Ref. 1.

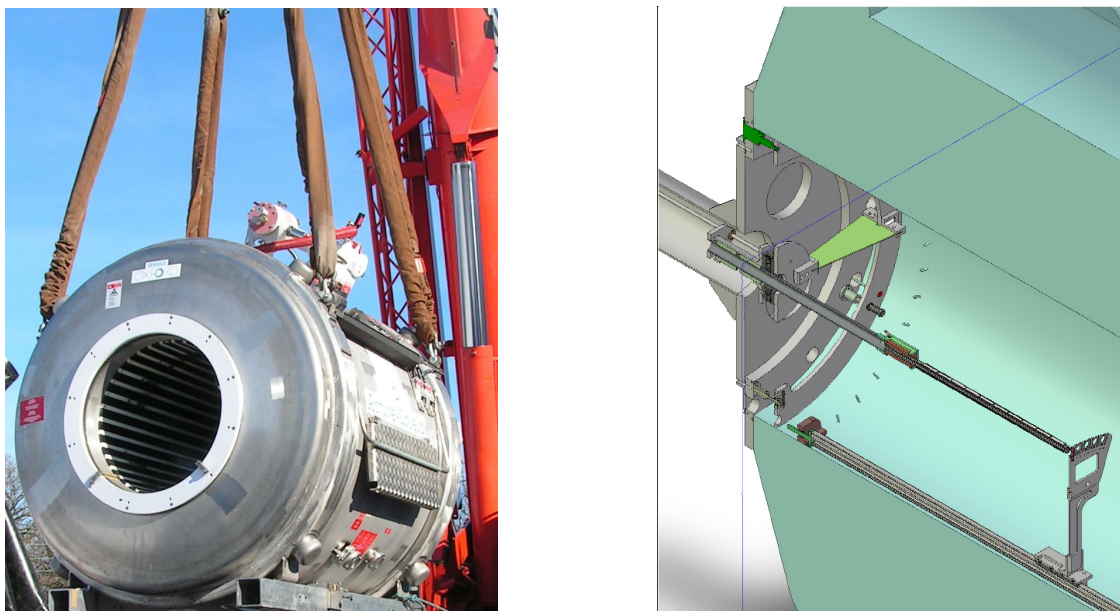


Fig. I-49. Left: Arrival of the Siemens solenoid at Argonne, December 8, 2006. Right: Cut-away schematics of the HELIOS spectrometer showing the target mechanism, the Piezo-electric cooled square cross section Si detector array, the alignment and positioning mechanism as well as the end-flanges that serve to make the solenoid bore into a vacuum chamber.

A superconducting solenoid magnet from a decommissioned MRI scanner was acquired from Siemens Medical. The magnet parameters, namely 3 T magnetic field strength in a 90 cm bore of length ~2 m,

is well suited for the spectrometer design. The solenoid was transported from Tübingen, Germany to Argonne (Fig. I-49 left) at the end of 2006 and installed on a custom-designed support stand in its final location in

the former general purpose area at ATLAS. The mechanical design of end-flanges and the support structures for the Si-detector array and target mechanism is complete (Fig. I-49 right) and the components are presently at various stages of manufacturing. A jig for field mapping using a three axis Hall probe has been fabricated and is ready for use. It is planned to power up the magnet to a 2 T field and

to carry out the field mapping late summer 2007. A set of legacy Si detectors have been tested. They will be mounted and wire-bonded to custom-designed PC boards, and incorporated into the 2×2 cm hollow detector array that will detect particles emitted into the backward hemisphere. First source tests are planned for the fall and the first stable beam test experiment will be carried out in the beginning of CY2008.

*University of Manchester, United Kingdom, †Western Michigan University.

¹A. H. Wuosmaa, J. P. Schiffer, B. B. Back, C. J. Lister, and K. E. Rehm, Nucl. Instrum. Methods A.

i.2. A High Resolution Isobar Separator for the CARIBU Project (C. N. Davids and D. Peterson)

A high-resolution isobar separator for the CARIBU project has been designed. Its properties are: high transmission ($> 95\%$), high first-order mass resolution (22,400:1), and compact size. The isobar separator uses only magnetic dispersive elements and all focusing elements are electrostatic.

electrostatic quadrupoles, sextupoles, and multipole using the ion-optical program SIMION. From these we have obtained the physical lengths of the various electrodes, as well as realistic fringe-field distributions. The two 60° bending magnets have been ordered. Design of the focusing elements is proceeding, and they will be fabricated locally.

3-dimensional simulations have been performed for the

i.3. GRETINA Progress (C. J. Lister, J. Anderson,* and the GRETINA Collaboration)

Good progress was made in many areas of the GRETINA gamma-ray tracking project. In the physics direction, workshops were held at St. Louis (to discuss auxiliary detectors and interface issues), Berkeley (to discuss electronics) and Florida State University (to discuss science strategy and produce a white paper in preparation for the NSAC Long Range planning process).

made in better understanding electronic cross talk.

In the hardware domain, the first “quad” module of tracking crystals was delivered. The mechanical design was refined and modified to be incorporated at various operation sites. The 10-channel primary digitizers were prototyped. In signal processing, great strides were

At Argonne, responsibility was taken for the trigger design, the signal routers and clock distribution system. John Anderson (ANL/HEP) has taken the lead role in this area. A Memorandum of Understanding (MOU) was signed between LBNL and ANL, and the first Statement of Work (SOW) issued. John has started design of the prototype board with a goal of integrating with digitizers by May 2007.

Kim Lister has continued on the GRETINA steering committee, which meets weekly for telephone conference calls.

*High Energy Physics Division, Argonne National Laboratory.

i.4. Polarization Experiment at Lawrence Berkeley National Laboratory (S. Gros, C. J. Lister, J. Pavin,* and I. Y. Lee*)

Using planar germanium detectors for linear polarization measurements of gamma rays has proven promising, with very high “Figure of Merit”, Q .¹ The alpha-gamma fine structure decays from heavy nuclei

provide a good method of calibration of polarization sensitivity “offline”.² To date, our studies have been with analog electronics. However, digital pulse processing should allow better position determinations

of the interaction points, and thus, even higher polarization sensitivity.

In order to investigate this possibility, the ANL polarization setup was transferred to the 88" cyclotron at Berkeley, where the GRETINA data acquisition system was used. Figure I-50 shows the truck being

loaded with equipment for shipping. Figure I-51 shows the experiment installed at LBNL. Data were collected for two weeks, amassing 1.5 Tbytes of digital data. A steep learning curve has been experienced in digital data analysis, due to formats which are very different from their analog counterparts, but generation of spectra has now started.

*Lawrence Berkeley National Laboratory.

¹N. Hammond, C. J. Lister, and G. D. Jones, Argonne National Laboratory Physics Division Annual Report 2003, Section h.13, page 106 (<http://www.phy.anl.gov/div/ar04/index.html>).

²G. D. Jones, Nucl. Instrum. Methods **A491**, 452 (2002).



Fig. I-50. Loading the germanium strip detector for shipping, along with its polarization setup and electronics.



Fig. I-51. The polarization experiment installed and running at LBNL. The rack of GRETINA digital electronics is on the left of the picture.

i.5. Digital Waveform Analysis of Signals from the Twin-Ionization Chamber (N. Patel, X. D. Tang, A. Lauro, and K. E. Rehm)

As was shown in our previous ^{16}N experiment, a twin-ionization chamber provides energy information as well as the emission angle for a particle is emitted from the cathode foil located in the center of the ionization chamber. The angle information is normally obtained from the shape of the Frisch-grid signal. In order to improve the angle resolution and collect information about multi-particle decays (*e.g.*, from the decay of ^{12}C into three alphas), we started to study the signals from a waveform digitizer.

A LeCroy 2262 Waveform digitizer was used to store the digitized signals from the grids and anodes on the computer. Figure I-52 shows some typical waveforms

from the anode and Frisch grid for alpha particles produced *via* $^{10}\text{B}(n,\alpha)^7\text{Li}$ and $^6\text{Li}(n,\alpha)t$ reactions with neutrons from a Pu-Be source. The signal on the left side of Fig. I-52 corresponds to alphas emitted perpendicular to the cathode, while the right side corresponds to alphas emitted parallel to the cathode. Using a trapezoidal digital filter for the anode signal (see red curve in Fig. I-52), an energy resolution of 1.35% was obtained, which is very close to the value achieved with a standard ORTEC shaping amplifier. The blue curves show the digitized grid signals, whose shapes are close to what is expected for alphas emitted perpendicular (left) or parallel (right) to the cathode.

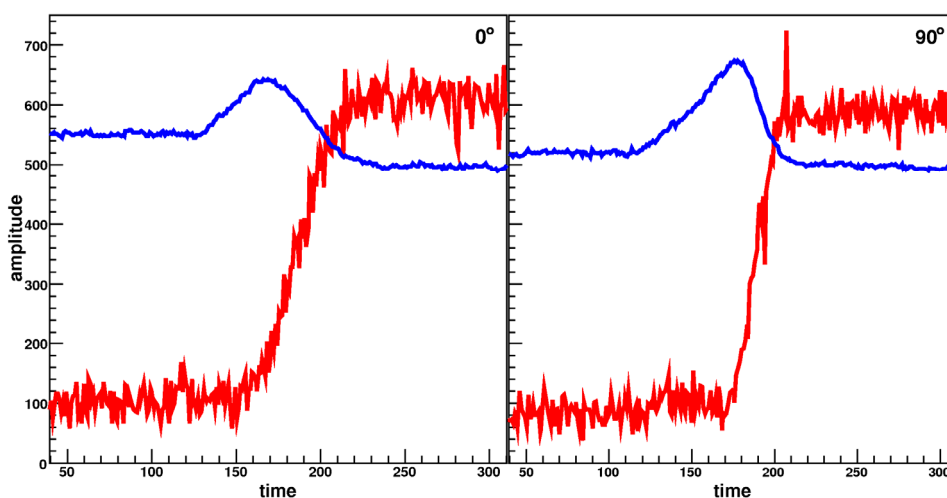


Fig. I-52. Grid (blue) and anode (red) waveform of alpha particle emitted at two different angles. Left: $\sim 0^\circ$ (perpendicular to cathode) and right: $\sim 90^\circ$ (parallel to cathode).

It is interesting to note that the rise time of the anode signal also shows an angle dependence, with the left signal exhibiting a longer rise time τ_r than the right signal. This correlation is shown in more detail in Fig. I-53 in a plot of τ_r^2 vs. the amplitude of the anode signal. For comparison, angle (grid) vs. the amplitude

of the anode is also shown in Fig. I-53. This correlation allows us to obtain energy and angle information from an analysis of the anode signal alone. Improvements by using the digitized waveform from the Frisch grid are underway.

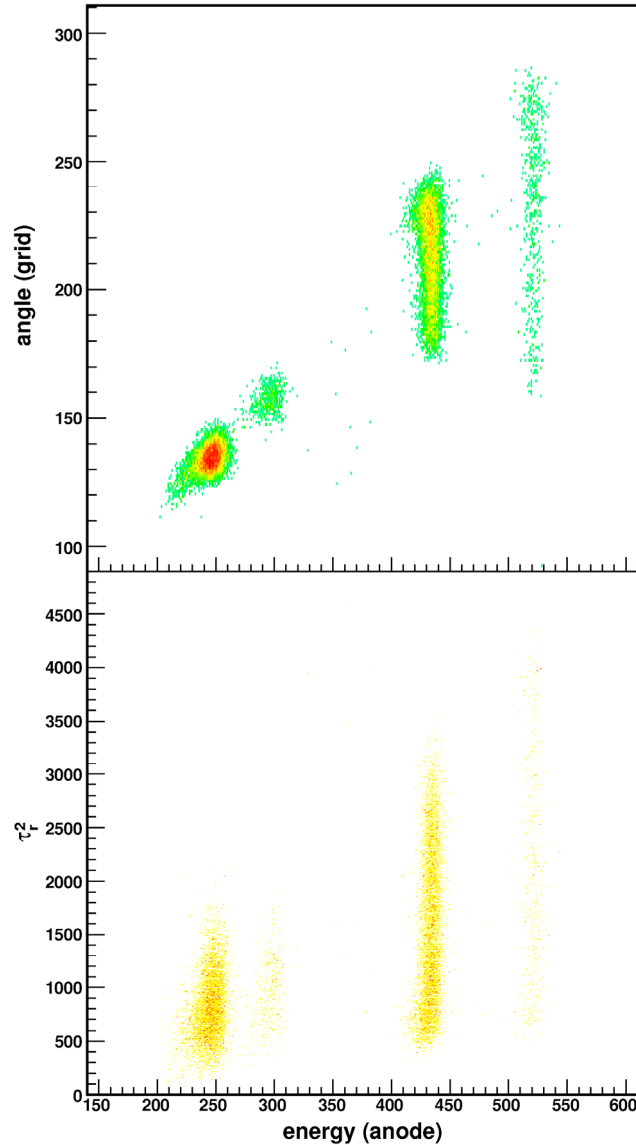


Fig. I-53. Top plot shows the angle (grid) vs. energy (anode) while the bottom plot shows the anode rise time squared, τ_r^2 , vs. the energy (anode) signal.

i.6. Argonne Implantation-Decay Array – Status Report (D. Seweryniak, B. Shumard, D. Henderson, and A. P. Robinson)

In order to facilitate coincidence measurements between a Double-Sided Si Strip detector and the X-Array of Ge clover detectors a new thin and compact vacuum chamber was designed and built to house the

DSSD behind the FMA focal plane. The chamber, together with one of the clover detectors and a LEPS, is shown in Fig. I-54.

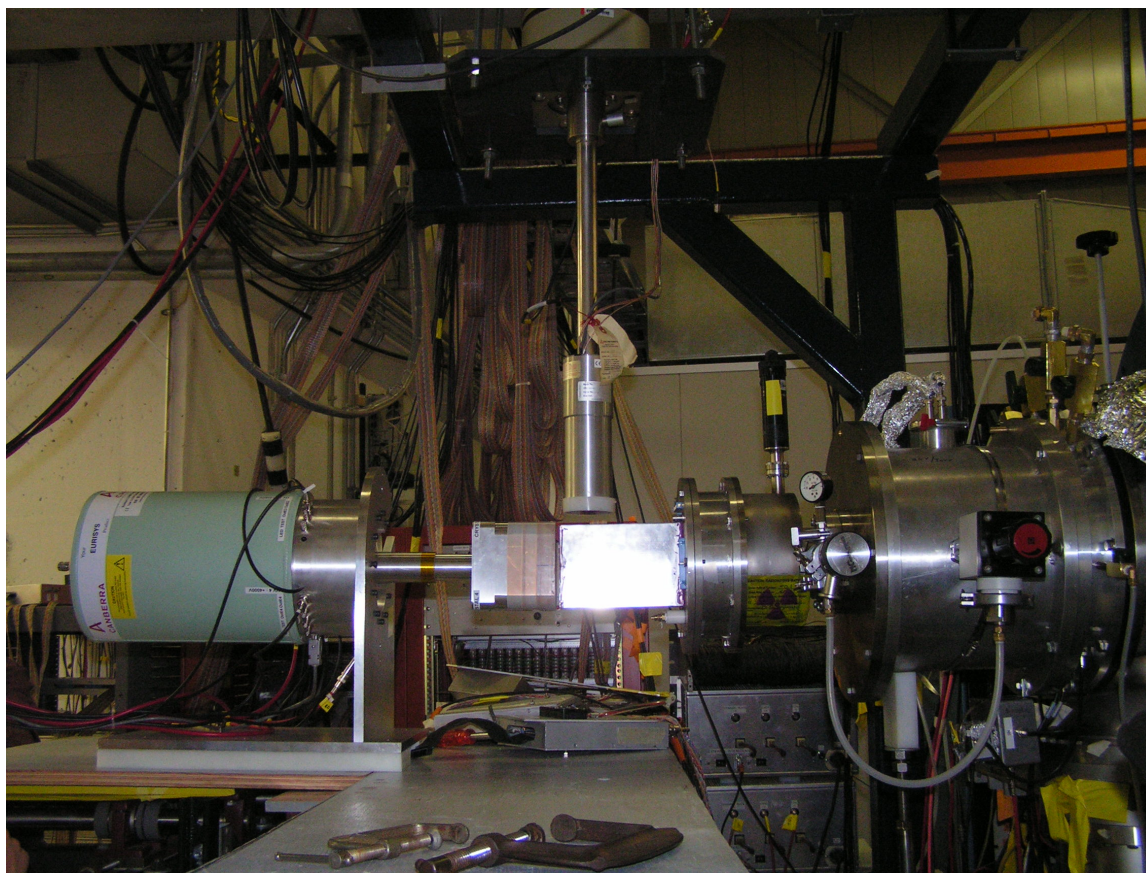


Fig. I-54. The compact DSSD chamber together with one of the clover detectors and a LEPS.

Figure I-55 contains a picture of the DSSD inside the chamber. The chamber walls are only 1/16" thick. Thanks to the small size of the chamber, the DSSD can be surrounded by 5 clover detectors in "box" geometry.

The chamber was already used in several experiments with the 40×40 and 80×80 DSSDs. The frame which will support the 5 clover detectors is currently under construction.

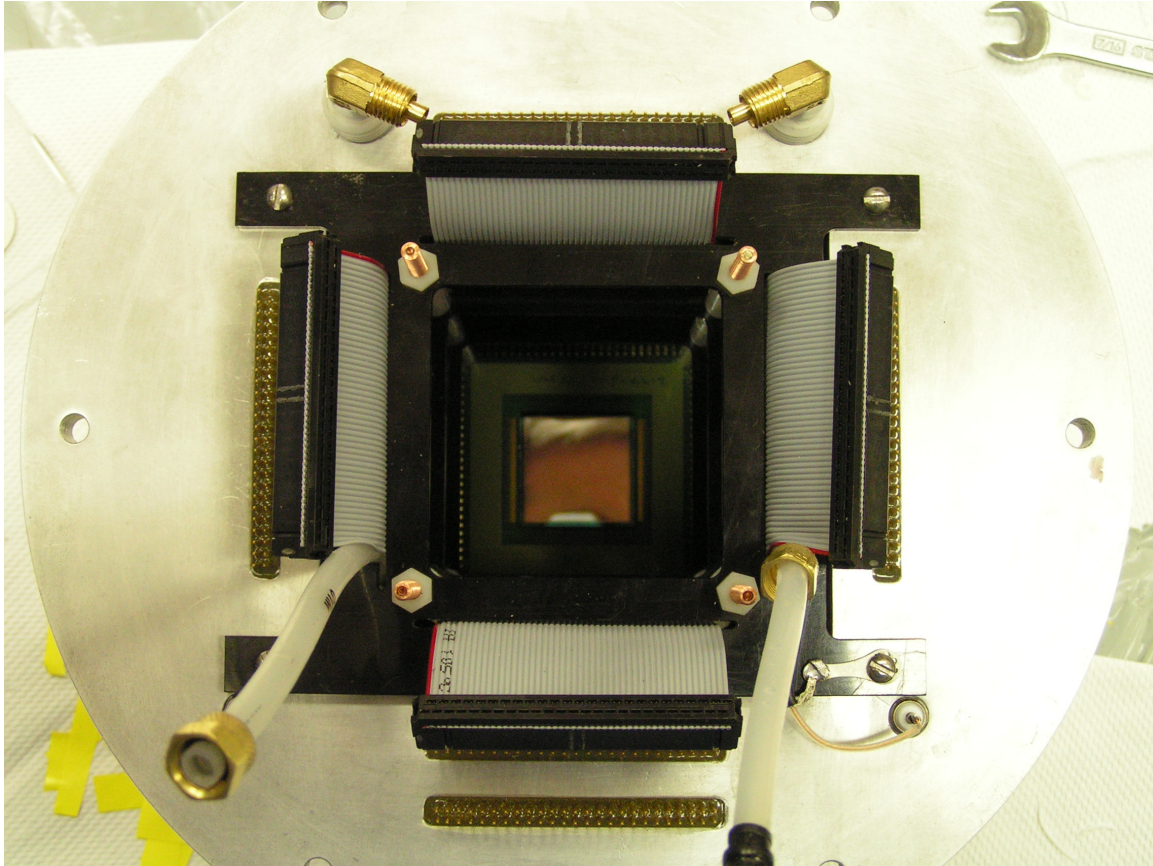


Fig. I-55. The 80×80 DSSD inside the chamber.

i.7. A Comparison of Performance of High Purity Germanium (HPGe) DSSDs with Different Electrode Technologies (S. Gros, C. J. Lister, N. Hammond, S. Fischer, S. Freeman,* and P. Chowdhury†)

Segmented planar Germanium (Ge) detectors are used in various nuclear sciences applications such as molecular imaging, gamma-ray telescopes on board satellites, detection of hidden radioactive material for national security and nuclear structure studies. Despite their excellent energy resolution, current planar Ge counters suffer from charge collection inefficiencies and cross talk induced between neighboring electrodes. These shortcomings arise particularly when the detectors are used in “multiple correlated” counting mode; for example, in the case of Compton cameras and γ -ray polarimeters. In these regards, the performance of these detectors could greatly be improved. Moreover, their extreme fragility and limited portability still restrict most of their operation to the safe laboratory environment. Recent advances in contact technology and electrode processing could potentially resolve some of these shortcomings and

increase the robustness and longevity of planar HPGe detectors.

In order to identify the causes of charge collection inefficiencies and pinpoint the origin of cross talk, we tested and compared the performance of two planar HPGe DSSDs. Both detectors offered different crystal dimensions, electrode technologies and front-end electronics. The first prototype (MARK4) was manufactured by Ametek (ORTEC) with their traditional L.E.P.S. technology. The second detector (NP1) was acquired through an SBIR collaboration with PhDs Co. and was produced with new ultra thin sputtered amorphous germanium contacts. The dimensions and characteristics of the detectors are summarized in Table I-7.

The project also aimed to evaluate the properties of the

new amorphous germanium contacts. Although the initial energy resolution values were acceptable, the AC electrodes were subject to large random and microphonic noise, and the whole detector was oscillating when more than a few contacts were connected on either side. This behavior was found to result from improper grounding occurring at different sites (cryostat, signals connections, preamplifiers mother boards) and from a strong coupling of the preamplifiers through their bias voltage lines. The oscillatory problem was solved by perfecting the grounding of the detector casing, and decoupling the preamplifiers. An improved preamplifier design was also used, which reduced significantly the magnitude of the AC noise to an almost usable signal quality.

The comparison tests were identical for both detectors: a ^{137}Cs source was placed at ~ 20 cm from the center of the Ge crystal, illuminating the strips connected to the DC preamplifiers. Data consisting of time and energy, measured for each strip, were acquired through analog instrumentation with the SCARLET data acquisition system. A sorting algorithm extracted events with multiplicity 1 and 2, and the data analysis focused on comparing the energy distribution from the Compton scattering of 662 keV γ -rays for double hits between neighbor and next neighbor strips.

Figure I-56 shows a set of example energy distributions between 2 strips (sum energy vs. energy difference). Figure I-56a, b and c present the results for neighbor hits between Boron (B), Lithium (Li) and amorphous Germanium (a-Ge) strips respectively, while Fig. I-56b, d and f show the energy response for interactions between 2 next-neighbors in B, Li and a-G strips. For all cases involving interactions in neighbor strips (Fig. I-56a, c and e), the sum energy is higher than the incident photon energy. When next neighbor interactions are considered (Fig. I-56b, d, and f), the shift in sum energy is smaller, and in the case of 2nd next neighbor interactions (not shown here), the sum energy peak is almost at the right incident gamma-ray energy. This deviation in sum energy demonstrates the existence of cross talk in the detector. The capacitive coupling between the strips is large enough to induce a positive shift of the baseline for the B, Li and a-Ge electrodes signals. As the coupling between electrodes decreases with distance, the shift in sum energy reduces from interactions between neighbors to interactions between next neighbors, and becomes undetectable for events between electrodes separated by more than 2 strips. The cross talk is the largest between Li electrodes, and is of similar magnitudes between B and amorphous-Ge strips.

Figure I-57a shows a detailed energy distribution from 2 neighbor strips in the NP1 prototype (Fig. I-56c). Two regions are delimited by colored polygons. The top linear region corresponds to full energy events (FEE) having constant sum energies. The lower region with a curved shape corresponds also to FEE, but the amount of charges generated from the photon absorption is not recovered. The projections of intensity on the energy difference axis for both regions, shown in Fig. I-57b and c, help determine the origin of the second curved region. The intensity observed in the constant sum energy region shows two maxima at energies corresponding to forward scattering angles around 60° , which follows the Compton intensity profile expected for 662 keV γ -rays. The intensity projection observed for the second type of events does not follow the expected Compton profile. It peaks instead at small energy sharing – which mainly corresponds to single hits FEE, interacting either near a strip boundary or close to the gap separating the strips. At larger energy sharing, we believe that the loss of charges results from either the incident or scattered photon, interacting in an active region of the crystal that favors trapping and recombination, thus, reducing the lifetime of the charge carriers. These low electric field regions are usually located near the sides of the Ge crystals, or close to the gap between neighbor strips. We believe that a reduction of the inter-strip gap would reduce the amount of lost charges. We studied altering the bias voltage from 650 V to 800 V, but did not observe any improvement in charge collection efficiency.

Overall, the performance of the B strips compared to thick Li contacts and to the new a-Ge technology shows that thin contacts with a small inter strip gaps provides the best combination to limit the loss of charge and the amount of cross talk between strips. Despite the problems we had with the NP1 detector, it appeared that this detector has an electrode technology that is robust and that amorphous-Ge contacts are stable even after many thermal cycles. We have discussed some issues with the detector manufacturer regarding the design of the detector's cryostat, the scheme of grounding the electronics, and the design of the front-end preamplifiers, and have emphasized the need for a smaller gap between the strips. This should improve the performance of the NPX type of detectors. We anticipate that the present counter will be re-mounted in a superior cryostat and will be returned to us for further testing in FY2008.

A paper presenting some results is being prepared for Nucl. Instrum. Methods.

Table I-7. Characteristics of the MARK4 and of the NP1 Prototype Detectors.

<i>Detector</i>	<i>Crystal Dimensions</i>	<i>Depletion Voltage</i>	<i>Bias Voltage</i>	<i>Strips Width</i>	<i>Guard Ring Width</i>	<i>Anode Technology</i>	<i>Anode Strip Gap</i>	<i>Anode Readout</i>	<i>Cathode Technology</i>	<i>Cathode Strip Gap</i>	<i>Cathode Readout</i>
<i>Mark 4</i>	88 × 88 mm ² 20 mm thick	2 kV	2.2 kV	5 mm	5 mm	0.6 mm Lithium diffused	0.5 mm saw cut	AC coupled CSP/ warm FET	0.1 mm Boron ion implanted	0.15 mm	DC coupled CSP/ cold FET
<i>NP1</i>	100 mm ∅ 14 mm thick	500 V	-650 V	5 mm	2~5 mm	Sputtered a-Ge/ Al contacts	0.5 mm	DC coupled CSP/ warm FET	Sputtered a-Ge/ Al contacts	0.5 mm	AC coupled CSP/ warm FET

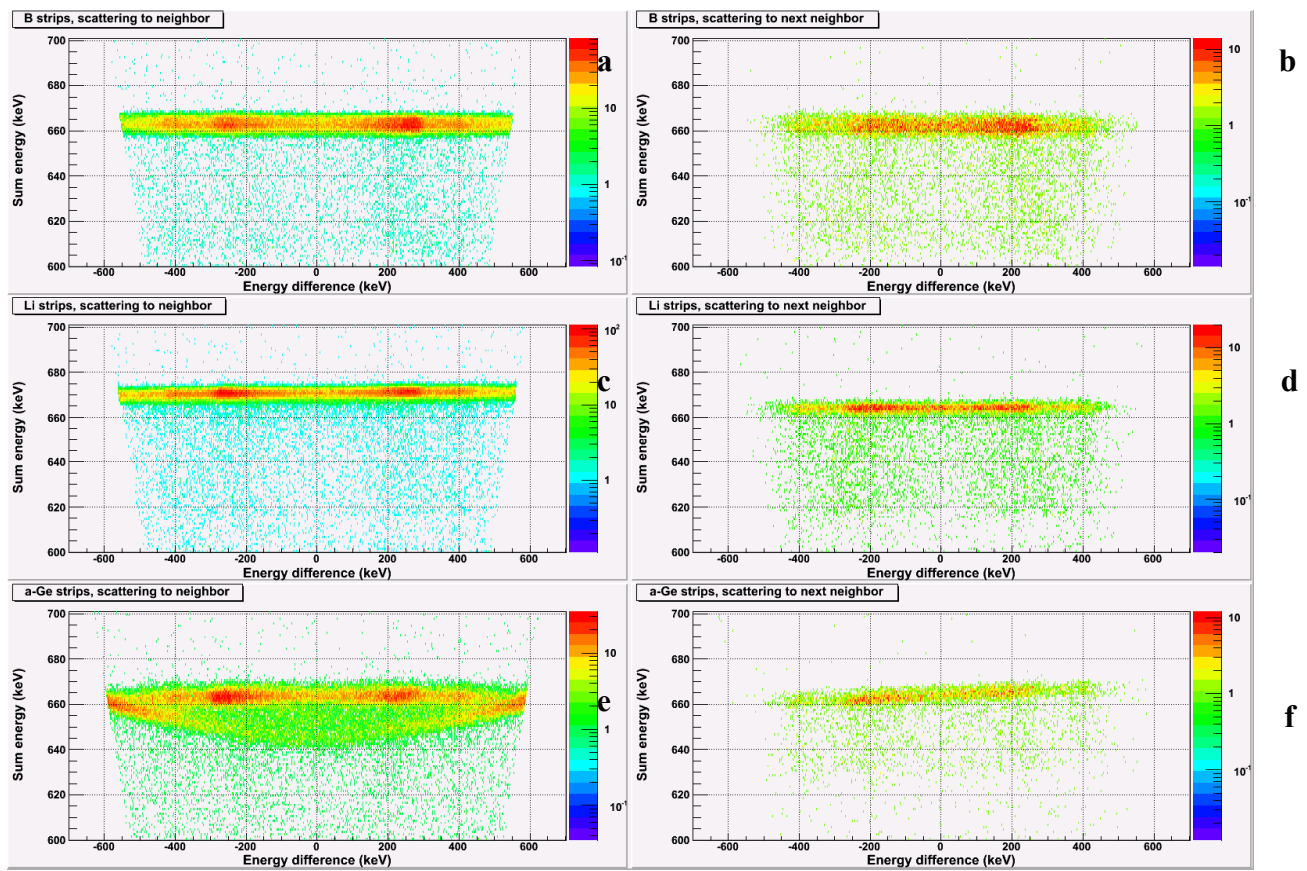


Fig. I-56. Example energy distributions for double hit interactions: between a) two neighbor and b) two next neighbor Boron strips; between c) two neighbor and d) two next neighbor Lithium strips; between e) two neighbor and f) two next neighbor for amorphous Germanium strips.

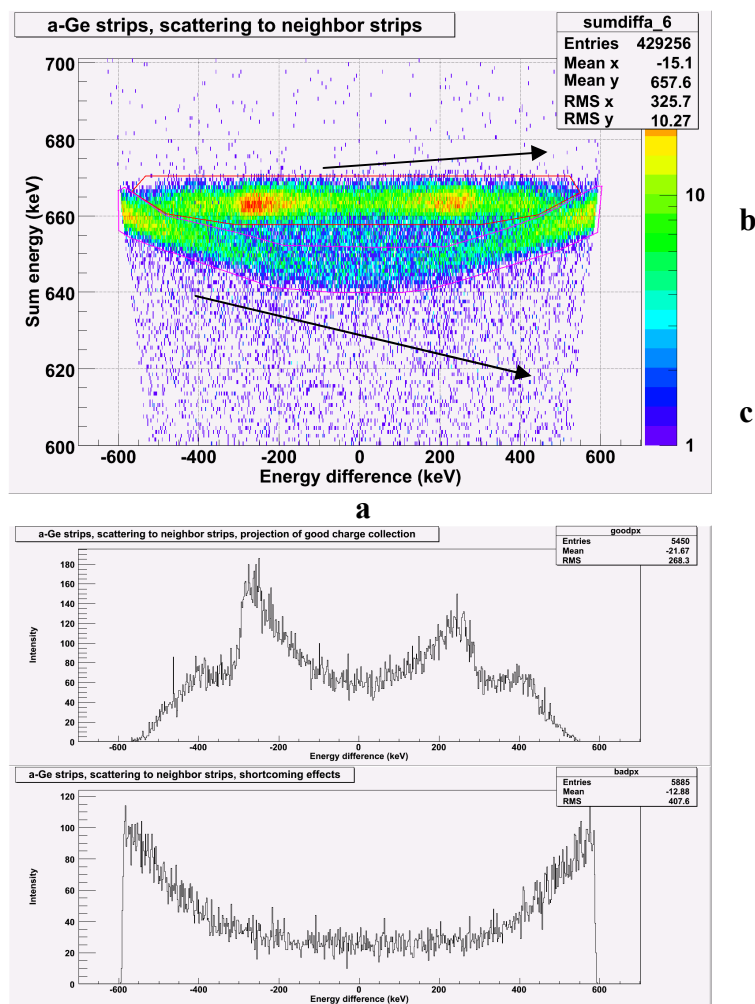


Fig. I-57. Energy distribution for neighbor *a*-Ge strips (a) and intensity projections of energy distributions for: b) good events with full collection of charge carriers; c) events with energies distorted by cross talk or charge losses.

*University of Manchester, United Kingdom, †University of Massachusetts-Lowell.

i.8. Development of a Portable Gamma Array, MISTI, for Homeland Security Use (C. J. Lister and B. Philips*)

The Domestic Nuclear Detection Office (DNDO) in the Department of Homeland Security (DHS) issued a call for proposals for an advanced technology demonstrator for “stand-off radiation detectors systems” DNDO-BAA07-010FP-018. The specification called for the detection, identification and location of a caesium-137 source at 100 m. An NRL/ANL collaboration has been formed to design and build a portable device with this capability.

At Argonne, we are involved in the design and

procurement of the germanium array. This will consist of ~28 large volume hyper-pure p-type counters mounted in “Pop-Top” capsules, and attached to a purpose-built liquid nitrogen Dewar. We are initially involved in investigating the issue of mechanical ruggedness. A test will be made at NRL using a vibration stand usually employed for evaluating the robustness of satellites being prepared for rocket launches.

This work is expected to be carried out in FY2007-2008

and be completed early in FY2009.

*Naval Research Laboratory.

i.9. Gammasphere Operations (M. P. Carpenter, C. J. Lister, R. V. F. Janssens, T. L. Khoo, T. Lauritsen, J. Rohrer, E. F. Moore, D. Seweryniak, P. Wilt, S. Zhu, and F. G. Kondev*)

As reported last year, Gammasphere was moved in 2006 back to the FMA beam line in area IV allowing for measurements requiring Gammasphere to run in conjunction with the FMA to be performed. The move took place in the first week of March and experiments resumed by the end of the month. Even though the device was unavailable for approximately 1 month due to the move, twenty-four PAC approved experiments were performed with Gammasphere in 2006 which is 20% larger when compared to the number of experiments performed in 2005. Twenty of these experiments were performed on the FMA beam line.

By the end of 2006, Gammasphere had been operating at ATLAS for nearly four years, and it appears that the device will operate at our facility for the foreseeable future. In 1997, 2000 and 2002, Gammasphere was moved after approximately two years of operation at the host facility. In each instance, all Ge detectors were annealed and optimum energy resolution was restored to the array. Since Gammasphere is not scheduled to move from Argonne, we have undertaken a policy to anneal a detector once its resolution has degraded beyond 3 keV at 1.33 MeV.

Due to failures of resistors along the bias chain, we continue to see breakdowns on the BGO PMT bases. This results in a non-responsive channel. The PMT can be repaired by locating the failed resistor and replacing it, however, this is a very time consuming operation. While it is our plan to replace all of these bases with new components in the long run, we continue to repair the bases as they fail and as the schedule allows. For example, whenever a Ge detector is removed for

annealing, its corresponding BGO shield is removed and repaired. A prototype replacement for the BGO bases has been constructed and is currently being tested for both gain stability and long term reliability.

The new data acquisition system has been commissioned and is now utilized in all Gammasphere experiments. With the new system, one is able to record the data to a hard drive. In this way, experimenters are able to bring their own USB hard drives to record data on and take with them at the end of an experiment. Along with the new acquisition system, a new online analysis program, GSSort, has been developed using the Root package from CERN. GSSort is rapidly replacing both the SCANU and DAPHNE sorting programs which were used previously. Detailed information about GSSort can be found on the Gammasphere web page.

It had been planned to modify the board in order to allow for the BGO energies to be available for readout ~ 2 μ sec after they were hit by a γ ray. This same modification had been done for the Ge energies and times and the BGO times in 2003. This modification will allow for the BGO energy information to be available for FMA experiments where the recoiling residues have flight times greater than 1 μ sec. This modification for each board will take 1 1/2 months to perform and has been postponed until 2007 when ATLAS will be down for upgrades and maintenance.

*Nuclear Engineering Division, Argonne National Laboratory.

i.10. Nuclear Target Development (J. P. Greene)

The Physics Division operates a target development laboratory that produces targets and foils of various thicknesses and substrates, depending on the requirements for experiments performed at the ATLAS and dynamitron accelerators. The targets are prepared

from both naturally occurring materials and stable isotopes that are supplied either in pure, elemental form or as stable compounds. In addition to ATLAS experiments, targets and foils are provided for all staff members whether working within the Physics Division

or undertaking experiments at other facilities. Whenever possible, support is provided to other ANL divisions and, in particular, to requests from researchers at the University of Chicago as well as other universities (e.g., Yale and Notre Dame).

In the past year, numerous targets were fabricated either as self-supporting foils, on various substrates or as "sandwich" targets. Targets produced included Al, ^{243}Am , Au, ^{10}B , Ba, ^{138}BaO , Be, ^{12}C , ^{40}Ca , CD_2 , Ce, ^{140}CeO , ^{252}Cf , ^{50}Cr , Cu, Formvar, C/Ti/Gd, ^{76}Ge , Havar, HfH, ^{113}In , Kapton, $^{6,7}\text{LiF}$, ^{24}Mg , MgO , ^{92}Mo , Mylar, ^{15}N (ammonium salt), ^{150}Nd , $^{142}\text{Nd}_2\text{O}_3$, ^{58}Ni , NiO, Os, Parafilm, ^{208}Pb , phosphor, Pt, SiC, ^{149}Sm , ^{120}Sn , Ta, Ta^{18}O , Ta_2O_5 , $^{126,130}\text{Te}$, $^{120,124,128}\text{TeO}_2$, Teflon, ^{229}Th , ^{46}Ti , TiC, TiCl_4 , TiD, UC_2 , UF_4 , W and WC. Many of these target foils have been fabricated by mechanical rolling using our small rolling mill. A large fraction of these targets were prepared for experiments carried out at Gammasphere.

Beyond target development, thin plastic films and foils are produced for various detector systems used for experiments at ATLAS as well as energy degraders and windows for the Advanced Penning Trap. New materials and mounting technologies are being implemented with the gas cell needed for the CARIBU project and for astrophysics research using in-flight radioactive beams at SPS III and for gas targets at the FMA.

As part of ATLAS support, the target lab routinely produces carbon stripper foils of $2\ \mu\text{g}/\text{cm}^2$ for use in the tandem as well as other thickness for additional stripping throughout the accelerator. For the production of enriched beams at ATLAS, there continues to be a need for the preparation of various dilutions of isotopic source material into suitable form for introduction into the ion sources.

The target development laboratory includes state-of-the-art equipment used for thin-film fabrication. The addition of a new, multi-purpose, computer-controlled vacuum evaporation system extends our capabilities and provides a stable platform for the continued production of accelerator targets. The available techniques consist of multiple resistive heating, focused ion beam sputtering, ion assisted deposition, electron beam and electron bombardment evaporation, carbon arc evaporation, electrodeposition and mechanical rolling. The evaporators are maintained under high vacuum and each vessel contains a quartz-crystal film-thickness monitor with deposition rate indicators. Also

included are movable shutters, quartz-lamp substrate heaters and thermocouple temperature sensors, allowing for complete process monitoring during target deposition.

Other auxiliary equipment used for target development includes electrodeposition apparatus, a small rolling mill, an alpha particle counting chamber, inert atmosphere glove box, laminar flow clean bench, pellet press, a reduction furnace, and a variety of precision balances. A turbo-pumped target storage facility is in operation for maintaining, under high vacuum, those targets that readily oxidize in air. This system utilizes computer-controlled circuitry to prevent targets from exposure to atmosphere during power interruptions. A second storage system employing a bank of vacuum desiccators and connected to a mechanically pumped manifold is available for use by individual experimenters. An additional set-up, consisting of two large plastic desiccator boxes, evacuated using a small turbo-pump system, is in operation for long-term material storage. This allows a separation of material storage from target storage, hence eliminating repeated exposure when transferring and retrieving targets.

A low-level radioactive source and target preparation laboratory exists at a separate location within the division that is dedicated to the production of these sources and targets. Available preparation techniques include multiple resistive heating employing a diffusion-pumped vacuum evaporator. A second, smaller evaporator system was constructed for close proximity evaporations of higher activity materials, to be used as targets as well as radioactive sources. Preparation and handling of actinide targets by electrodeposition as well as fission sources (mainly ^{252}Cf) has been done using this lab as well as high activity samples for source experiments at Gammasphere and EDM search experiments using $^{225,226}\text{Ra}$.

An area of increased research effort has been toward development of ISOL targets for the RIA proposal involving a uranium compound production target. Toward this end, direct measurements of the thermal conductivity of uranium carbide have been made using a method developed at ANL. Sample material of small grain size uranium carbide has been obtained from several sources for these measurements and is being studied for radioactive release properties in collaboration with ORNL. This work is still in progress.

J. ATLAS USER PROGRAM

j.1. ATLAS User Program (E. F. Moore and R. V. F. Janssens)

During FY2006 ATLAS hosted strong “campaigns” involving radioactive beams, the CPT, and, of course, Gammasphere. In the spring of 2006, Gammasphere was moved back from its "stand alone" position to its location in front of the FMA.

Many of the experimental programs were driven by outside Users, and in all programs, there was considerable outside User involvement. Over 97% of all experiments performed in FY2006 included one or more outside Users and roughly 60% of the approved experiments had an outside User as the Principal Investigator. In July 2005, Frank Moore moved over to the Argonne SCD Division to work full time for the U.S. Department of Energy, Radiological Assistance Program (RAP). Nevertheless, he continued to provide limited assistance with scheduling, with essential User services and with the ATLAS web page. However, a large portion of the in-house scientific staff and members of the technical support staff spent substantial amounts of their time in experiment setup, preparation, and assistance for the many different experiments performed at ATLAS.

A total of 213 Users from 56 different institutions were present at ATLAS for experiments in FY2006. A total of 61 Users came from U.S. universities, while 77 originated from foreign universities, mostly from Canada and Europe. The number of Users from U.S. national laboratories was 55, while that for scientists from foreign similar institutions was 20. There were 75 students at ATLAS for experiments in FY2006, of which 13 were based at Argonne long-term.

The Program Advisory Committee met twice during the FY2006, on January 20-21 and on September 15-16 to recommend experiments for beam time allocation at ATLAS. In January 2006, the Program Advisory Committee members were:

j.2. Experiments Involving Outside Users

All experiments in which outside Users directly participated during FY2006 are listed below. The spokesperson for each experiment is given in square

Ani Aprahamian, University of Notre Dame
 Birger Back, Argonne National Laboratory
 Art Champagne, Univ. of North Carolina-Chapel Hill
 Augusto Macchiavelli, Lawrence Berkeley Nat. Lab.
 David Radford (*Chair*), Oak Ridge National Laboratory
 Gene Sprouse, Stony Brook University
 Piet Van Duppen, University of Leuven, Belgium

By the time of the September meeting, the term of two committee members had expired and the composition of the PAC was as follows:

Birger Back, Argonne National Laboratory
 Sean Freeman, University of Manchester, U.K.
 David Radford, Oak Ridge National Laboratory
 Hendrik Schatz, Michigan State University
 Gene Sprouse, Stony Brook University
 Krzysztof Starosta (*Chair*), Michigan State University
 Piet Van Duppen, University of Leuven, Belgium

At the January meeting, a total of 103 days of beam time were approved. The corresponding number for the September meeting is 127. In each instance, the request for beam time far exceeded the amount available: in January the total demand was for 273 days, while 253 days were requested in September. Due to the large demand for beam time, the PAC was asked to prioritize experiments into two categories; those that must be run at any cost (*priority I*), and those that should be granted beam time if at all possible (*priority II*). For each of the two PAC meetings, roughly 20% of the accepted proposals were ranked as priority II.

In FY2006, the ATLAS User Group Executive Committee consisted of Ani Aprahamian (University of Notre Dame), Krzysztof Starosta (Chair, Michigan State University), Ingo Wiedenhöver (Florida State University), and Alan Wuosmaa (Western Michigan University). The term of this committee expired at the end of calendar year 2006.

brackets after the title, and the collaborators are given below each entry.

1. Investigation of the Ionization Density Limit of a Large Accelerated Gas Cell System [Savard]
G. Savard, J. Clark, A. Levand, Z. Zhou, J. Wang, W. L. Trimble, M. Portillo, J. Vaz, B. Blank, L. Blomeley, D. J. Peng, D. Mackay, J. J. Letcher, N. D. Scielzo, H. Sharma, J. Fallis, D. Lascar, R. Segel, A. A. Hecht, S. Caldwell, G. Li, T. Sun, M. Sternberg, and J. van Scholt
2. Electromagnetic Decay Properties of the $T_z = \pm 1/2$ $A = 67$ Mirror Pair: Isospin Symmetry From E1 Amplitudes [De Angelis]
G. De Angelis, D. V. Tonev, D. R. Napoli, S. Lunardi, E. Farnea, C. A. Ur, D. G. Sarantites, C. J. Chiara, W. Reviol, O. Pechenaya, M. P. Carpenter, C. J. Lister, G. Mukherjee, N. Hammond, R. Orlandi, S. F. Gadea Raga, J. J. Valiente-Dobon, F. Della Vedova, A. Bracco, S. Leoni, S. M. Lenzi, R. Wadsworth, D. Seweryniak, S. Zhu, and S. N. S. Bondili
3. Request for Exploratory Time: The $k_{17/2}$ Orbital in the Heaviest Elements [Freeman]
S. J. Freeman, R. Chapman, J. F. Smith, B. P. Kay, C. J. Lister, R. V. F. Janssens, M. P. Carpenter, S. Zhu, and X. Wang
4. Studies of Excited States in ^{101}Sn . Phase I: Search for ^{101}Sn β -Delayed Protons [Seweryniak]
D. Seweryniak, S. Zhu, R. V. F. Janssens, C. J. Lister, M. P. Carpenter, N. Hammond, D. Henderson, A. A. Hecht, W. B. Walters, D. A. Peterson, C. Vaman, G. Lotay, K. Starosta, P. J. Woods, S. Gros, and N. Hoteling
5. The $^{44}\text{Ti}(^3\text{He},p)$ Reaction and the Question of $T = 0$, $T = 1$ Pairing in $N = Z$ Nuclei [Macchiavelli]
A. O. Macchiavelli, R. M. Clark, P. Fallon, M. Wiedeking, K. E. Rehm, R. V. F. Janssens, S. Zhu, C. N. Davids, and C. J. Lister
6. Identification of Excited States in ^{107}Te with Recoil Decay Tagging Measurement [Starosta]
K. Starosta, C. Vaman, D. Seweryniak, A. P. Robinson, D. A. Peterson, K. B. Lagergren, P. J. Woods, C. N. Davids, W. B. Walters, A. A. Hecht, S. Zhu, S. Gros, D. Henderson, G. Lotay, and N. Hoteling
7. The First Spectroscopic Study of the Odd-Odd $N = Z \pm 2$ Mirror Pair $^{44}\text{V}/^{44}\text{Sc}$ [Bentley]
M. A. Bentley, J. R. Brown, M. J. Taylor, E. K. Johansson, L. L. Andersson, P. E. Garrett, D. Seweryniak, C. J. Lister, M. P. Carpenter, T. Lauritsen, and R. V. F. Janssens
8. Transient-Field g Factor Measurements of Excited States in Fission Fragments [Smith]
A. G. Smith, B. J. Varley, A. L. M. Thallon, G. S. Simpson, S. J. Freeman, B. P. Kay, R. Orlandi, I. Ahmad, M. P. Carpenter, R. V. F. Janssens, C. J. Lister, T. Lauritsen, and J. Greene
9. DSAM Lifetime Measurements for Fission Fragments using Hercules [Reviol]
W. Reviol, D. G. Sarantites, C. J. Chiara, O. Pechenaya, S. A. Komarov, D. Seweryniak, M. P. Carpenter, R. V. F. Janssens, S. Zhu, T. L. Khoo, J. Greene, and M. Montero Diez
10. The Structure of Neutron-Rich sdf -Shell Nuclei using Multi-Nucleon Transfer Reaction Studies at Gammasphere [Fallon]
P. Fallon, I.-Y. Lee, E. Rodriguez-Vieitez, M. Descovich, C.Y. Wu, D. Cline, S. Zhu, D. Seweryniak, M. P. Carpenter, R. V. F. Janssens, A. O. Macchiavelli, and M. Wiedeking
11. Beyond the $N = Z$ Line: A Study of the $T_z = -1$ Nucleus ^{70}Kr [Wadsworth]
R. Wadsworth, M. J. Taylor, S. N. S. Bondili, P. E. Kent, P. J. Davies, C. J. Lister, D. Seweryniak, M. P. Carpenter, S. Zhu, S. M. Fischer, D. G. Sarantites, and W. Reviol
12. High Spin States in the $N = Z - 3$ Nucleus ^{49}Fe - Coulomb Effects at Large Proton Excess [Bentley]
M. A. Bentley, J. R. Brown, P. E. Kent, M. J. Taylor, R. Wadsworth, D. G. Jenkins, L. L. Andersson, E. K. Johansson, D. Rudolph, D. Seweryniak, S. Zhu, T. Lauritsen, C. J. Lister, M. P. Carpenter, R. V. F. Janssens, and M. B. Gomez-Hornillos

13. Identification of the Mixed-Symmetry One-Phonon $2_{1,ms}^+$ State of ^{136}Ce and ^{134}Xe in Inverse-Kinematics Coulomb Excitation [Ahn]
T. Ahn, G. I. Rainovski, A. Costin, C. J. Lister, R. V. F. Janssens, M. P. Carpenter, S. Zhu, and N. Pietralla
14. Study of Excited States in ^7He through the $d(^8\text{Li}, ^3\text{He})^7\text{He}$ Reaction [Wuosmaa]
A. H. Wuosmaa, R. H. Siemssen, L. Jisonna, J. C. Lighthall, S. T. Marley, N. J. Goodman, D. Patel, K. E. Rehm, R. V. F. Janssens, R. C. Pardo, J. Greene, D. Henderson, J. P. Schiffer, and C. L. Jiang
15. Re-Examination of the $^{32}\text{S} + ^96\text{Ru} \rightarrow ^{128}\text{Nd}^* \rightarrow ^{123}\text{Pr} + p4n$ Reaction Using the Fragment Mass Analyzer: Was Proton Decay Observed at Dubna in 1970? [Perajarvi]
K. Perajarvi, H. T. Penttila, J. Cerny, A. P. Robinson, C. N. Davids, and D. Seweryniak
16. Accelerator Mass Spectrometry of ^{59}Ni at High Sensitivity [Paul]
M. Paul, I. Ahmad, P. Collon, D. J. Robertson, C. J. P. Schmitt, D. Henderson, J. Greene, C. L. Jiang, R. C. Pardo, K. E. Rehm, X. Tang, N. Patel, R. H. Scott, R. Vondrasek, and L. Jisonna
17. Test of Nuclear Chirality in ^{104}Rh - Study of Electromagnetic Transitions and the Chiral Selection Rules via Lifetime Measurements using the Recoil Distance Method in Inverse Kinematics [Rainovski]
G. I. Rainovski, A. Costin, T. Koike, R. Wadsworth, M. T. Danchev, A. Dewald, R. V. F. Janssens, M. P. Carpenter, C. J. Lister, S. Zhu, C. Vaman, and N. A. Pietralla
18. Distortion of Mirror Symmetry: The Special Case of $A = 71$: $T_z \pm 1/2$ Mirror Nuclei ^{71}Br and ^{71}Kr [Fischer]
S. M. Fischer, C. J. Lister, D. G. Sarantites, C. J. Chiara, O. Pechenaya, D. Seweryniak, S. Zhu, S. Gros, D. A. Peterson, R. A. Kaye, W. A. Yemington, D. J. McLaughlin, W. Reviol, D. P. Robinson, X. Wang, and Y. K. Ryu
19. Proton Decay below the ^{100}Sn Double Shell Closure [Robinson]
A. P. Robinson, D. Seweryniak, P. J. Woods, C. N. Davids, S. Gros, S. Zhu, G. Lotay, A. A. Hecht, and B. Shumard
20. Measurement of the β -Delayed α Spectrum of ^{16}N with a New Technique-4 [Rehm]
X. Tang, M. M. Notani, N. Patel, C. L. Jiang, J. P. Schiffer, J. Greene, S. Henderson, B. Shumard, K. E. Rehm, R. V. F. Janssens, L. Jisonna, R. E. Segel, D. M. Kahl, C. Brune, A. H. Wuosmaa, M. Paul, A. E. Champagne, A. A. Hecht, and G. Savard
21. Sub-Barrier Fusion of the Closed Shell $^{48}\text{Ca} + ^{48}\text{Ca}$ System [Back]
B. Back, C. L. Jiang, C. J. Lister, R. V. F. Janssens, C. N. Davids, D. Seweryniak, K. E. Rehm, A. P. Robinson, X. Tang, S. Zhu, X. Wang, and D. A. Peterson
22. Structure of the Neutron-Rich Fe Isotopes via Deep-Inelastic Reactions [Walters]
W. B. Walters, J. R. Stone, N. Stone, J. Wrzesinski, W. A. Krolas, R. J. Broda, B. Fornal, A. A. Woehr, N. Hoteling, A. A. Hecht, S. Zhu, M. P. Carpenter, R. V. F. Janssens, D. Seweryniak, C. N. Davids, and X. Wang
23. Precision Measurement of the Q-Value of the Superallowed Decays of ^{42}Sc , ^{50}Mn , ^{54}Co , ^{34}Cl , and ^{26m}Al with the CPT Mass Spectrometer [Savard]
G. Savard, J. A. Clark, A. Levand, J. Fallis, H. Sharma, Y. Wang, N. D. Scielzo, A. C. Villari, P. J. Sloan, I. Tanihata, S. L. Gulick, R. E. Segel, A. A. Hecht, K. S. Sharma, J. C. Hardy, D. Lascar, M. Sternberg, C. L. Wrede, C. M. Deibel, D. Danaher, and C. Riviere
24. Quantifying the Level of Isospin Mixing in the $A = 31$ Mirror Nuclei [Pattabiraman]
N. S. Pattabiraman, R. Wadsworth, D. G. Jenkins, R. Glover, Krishichayan, C. J. Lister, S. Zhu, M. P. Carpenter, C. J. Barton, P. E. Kent, P. J. Woods, T. Davinson, G. Lotay, R. V. F. Janssens, T. L. Khoo, T. Lauritsen, and D. Seweryniak

25. Gammasphere and Fragment Mass Analyzer Upgrades [Lister]
C. J. Lister, S. M. Fischer, D. Seweryniak, S. Zhu, S. Gros, A. P. Robinson, T. L. Khoo, A. A. Hecht, M. P. Carpenter, B. Shumard, N. Hoteling, R. V. F. Janssens, and C. N. Davids
26. Effects of Heavy Ion Irradiation on Phase Transitions of the Vortex Matter in High Temperature Superconductors [Kwok]
W. K. Kwok, U. Welp, L. Paulius, and R. Xie
27. Neutron-Proton Correlations in Odd-Odd $N = Z$ ^{86}Tc : Characterization of the 1.6 ms Isomer [Regan]
C. J. Lister, P. H. Regan, D. Henderson, I. J. Cullen, N. J. Thompson, G. D. Jones, A. B. Garnsworthy, S. J. Williams, Z. Liu, B. Blank, and B. Shumard
28. Lifetimes of Astrophysical Resonances in ^{19}Ne [Woods]
P. J. Woods, G. Lotay, D. Seweryniak, D. G. Jenkins, T. Davinson, M. P. Carpenter, R. V. F. Janssens, A. P. Robinson, S. Gros, and S. Zhu
29. Lifetimes of Chiral Bands in ^{135}Nd [Garg]
U. Garg, T. Li, S. Mukhopadhyay, F. G. Kondev, S. Zhu, M. P. Carpenter, T. Lauritsen, D. Seweryniak, X. Wang, R. V. F. Janssens, S. Gros, and A. A. Hecht
30. High-Spin Spectroscopy of ^{224}U [Reviol]
W. Reviol, C. J. Chiara, O. Pechenaya, D. G. Sarantites, K. Hauschild, A. P. Lopez-Martens, T. L. Khoo, M. P. Carpenter, C. J. Lister, D. Seweryniak, and S. Zhu
31. Search for a High-K Isomer in ^{252}No [Khoo]
T. L. Khoo, D. Seweryniak, A. P. Robinson, S. Gros, D. A. Peterson, I. Ahmad, B. Back, M. P. Carpenter, C. N. Davids, J. Greene, A. A. Hecht, R. V. F. Janssens, F. G. Kondev, T. Lauritsen, C. J. Lister, S. Zhu, P. Chowdhury, S. K. Tandel, U. S. Tandel, A. M. Heinz, J. Qian, X. Wang, R.-D. Herzberg, G. D. Jones, and S. Eeckhaudt
32. Search for Deformed States in ^{185}Pb [Carpenter]
M. P. Carpenter, F. G. Kondev, R. V. F. Janssens, C. J. Lister, A. P. Robinson, S. Zhu, D. Seweryniak, T. L. Khoo, T. Lauritsen, X. Wang, N. Hoteling, A. A. Hecht, A. J. Larabee, W. Reviol, S. Gros, and M. Asai
33. High Spin States in the $T = 3/2$ Mirror Nuclei ^{37}Ca and ^{37}Cl , and the $T = 1/2$ Mirror Nuclei ^{37}K and ^{37}Ar [Williams]
S. J. Williams, A. B. Garnsworthy, S. J. Steer, I. J. Cullen, G. A. Jones, P. E. Kent, J. R. Brown, M. J. Taylor, D. Rudolph, P. E. Garrett, G. A. Demand, D. Bandyopadhyay, M. A. Phillips, and K. L. Green
34. The Study of (p,p), (p, α) and (α ,p) Reactions Using MUSIC and the Thick Target Technique-2 [Tang]
X. Tang, K. E. Rehm, M. M. Notani, N. Patel, L. Jisonna, C. L. Jiang, D. Henderson, B. Shumard, and J. P. Schiffer
35. The Spin of the 2.643 MeV State in ^{20}Na , Studied via the $^{19}\text{Ne}(^3\text{He},d)^{20}\text{Na}$ Reaction [Jisonna]
L. Jisonna, X. Tang, M. M. Notani, N. Patel, C. L. Jiang, J. Greene, D. Henderson, B. Shumard, R. E. Segel, A. H. Wuosmaa, J. P. Schiffer, K. E. Rehm, R. C. Pardo, G. Zinkann, and J. O. Fernandez-Niello
36. A Study of np Interactions in Odd-Odd $N = Z + 2$ ^{112}Cs [Smith]
J. F. Smith, S. J. Freeman, A. N. Deacon, B. P. Kay, D. Steppenbeck, E. S. Paul, A. N. Grint, B. M. McGuirk, M.-K. Petri, and C. J. Chiara

37. The Branching Ratio of the Subthreshold 1- State in the β -Decay of ^{16}N [Rehm]
X. Tang, K. E. Rehm, M. M. Notani, C. J. Lister, M. P. Carpenter, R. V. F. Janssens, C. L. Jiang, J. P. Schiffer, G. Savard, N. Patel, L. Jisonna, R. E. Segel, A. H. Wuosmaa, and S. Zhu
38. Precision Measurement of the Q-Value of the Superaligned Decays of ^{10}C , ^{34}Cl , $^{38\text{m}}\text{K}$, ^{50}Mn and ^{54}Co , and the Unitarity of the CKM Matrix [Savard]
G. Savard, A. Levand, H. Sharma, A. A. Hecht, D. Lascar, J. A. Clark, J. Fallis, N. D. Scielzo, S. Caldwell, R. E. Segel, F. Buchinger, C. L. H. Wrede, and C. M. Deibel
39. K-Isomers in Trans-Plutonium Nuclei via Deep-Inelastic and Transfer Reactions [Chowdhury]
S. K. Tandel, U. S. Tandel, C. Wilson, A. J. Knox, P. Chowdhury, M. P. Carpenter, C. J. Lister, S. Zhu, D. Seweryniak, T. Lauritsen, T. L. Khoo, F. G. Kondev, R. V. F. Janssens, A. P. Robinson, J. Greene, I. Ahmad, S. Gros, D. A. Peterson, and X. Wang
40. The p-Process ^{146}Sm Nuclide: Half-Life and Production [Paul]
M. Paul, K. E. Rehm, R. C. Pardo, R. Vondrasek, R. H. Scott, P. Collon, D. Henderson, C. J. P. Schmitt, M. M. Notani, N. Patel, Y. Kashiv, N. Kinoshita, L. Jisonna, J. Greene, D. Robertson, and C. L. Jiang
41. Evolution of the One-Phonon Mixed-Symmetry $2_{1,ms}^+$ State from U(5) to O(6) Dynamical Symmetry Limits in Xe Isotopes from Inverse-Kinematics Coulomb Excitation [Pietralla]
N. A. Pietralla, T. Ahn, L. Bettermann, W. Rother, V. R. Werner, M. T. Chamberlain, R. V. F. Janssens, C. J. Lister, M. P. Carpenter, and S. Zhu
42. Neutron Excitations at the Fermi Surface above the N = 32 Shell Gap: Structure of ^{55}Ti [Zhu]
R. V. F. Janssens, S. Zhu, M. P. Carpenter, T. Lauritsen, A. P. Robinson, D. Seweryniak, B. Fornal, S. J. Freeman, A. N. Deacon, J. F. Smith, B. P. Kay, D. Steppenbeck, and A. J. Larabee
43. The Structure of ^{13}B [Schiffer]
J. P. Schiffer, C. L. Jiang, X. Tang, R. C. Pardo, M. M. Notani, A. H. Wuosmaa, K. E. Rehm, D. Patel, R. E. Segel, I. Tanihata, J. C. Lighthall, and S. T. Marley
44. Preliminary Measurement of the β -v Correlation in ^{14}O [Scielzo]
N. D. Scielzo, G. Savard, H. Sharma, I. Tanihata, A. A. Hecht, A. Levand, J. A. Clark, K. S. Sharma, S. Caldwell, D. Lascar, J. Fallis, R. E. Segel, T. Wang, D. Donaher, and G. Li
45. Study of ^{92}Pd Through $^{40}\text{Ca}(^{54}\text{Fe},2n)$ [Sarantites]
D. G. Sarantites, W. Reviol, C. J. Chiara, O. Pechenaya, W. L. Mason, C. J. Lister, R. V. F. Janssens, D. Seweryniak, M. P. Carpenter, S. Zhu, and T. Lauritsen

j.3. Renovation of the ATLAS Data Room (C. J. Lister and J. Rohrer)

After 20 years, the ATLAS data room was looking tired. Moreover, the functionality of the room had changed over the years, with most experiments now having their electronics and acquisition computers located at the beam lines near the equipment. Finally, a new high speed data acquisition network needed to be installed, and the old VAX-based systems decommissioned.

During spring shutdown in 2006 a renovation took

place. Redundant racks were removed, along with old cables, patch panels, furniture and computers. New partition walls were installed and new furniture acquired. The new data network came online, and new workstations running “Root” visualization packages became available to users. A new conference area was created (see Fig. I-58) with a refrigerator, chilled water, and a microwave oven. Wireless network access was installed. This has all proven very popular with the outside Users of our facility.



Fig. I-58. The conference area in the renovated data room.

II. OPERATION AND DEVELOPMENT OF ATLAS

OVERVIEW



Operational performance, work on improvement projects, and related accelerator physics R&D projects for the Argonne Tandem Linear Accelerator System (ATLAS), a DOE national user facility, are described in this chapter. ATLAS is funded to provide heavy-ion beams for basic research in nuclear physics but also serves other areas of research and development, including material science. In addition, ATLAS has a long-standing program in developing the tools of accelerator mass spectroscopy (AMS) applied to wide ranging research programs such as oceanography, nuclear physics, astrophysics, and geology. Over half of the beam time is allocated to experiments for which the spokesperson is an outside user. Recent ATLAS operating performance and related development projects are described in this section. ATLAS personnel are also involved in developing technology in support of a future advanced facility, based on ATLAS technologies, for beams of short-lived nuclei.

ATLAS continued to operate on a 5.3 day schedule through FY2006 and into FY2007 with some limited 7-day operation to accommodate runs approved for longer operation that would be disadvantaged by breaking into segments. Although not efficient use of the facility, this schedule has been brought about by budgetary constraints. In December 2006, ATLAS began a long maintenance period focused on replacing our smallest refrigerator with a larger unit to provide improved cooling capacity. This increased capacity will improve overall operation but will also improve the performance of the new resonators that are part of the Energy Upgrade project expected to be online in 2008. Construction of a new cryostat and resonators for a major energy upgrade of the facility, which will increase the overall voltage of ATLAS by ~25%, nears completion. Construction of the final six resonators is complete and electropolishing and surface preparations are underway.

For FY2006, ATLAS provided 38 beams of different isotopes to users. A total of 5358 hours of research beam time was provided for the research program, while the total scheduled operating hours for FY2006 was 5568 including startup time.

Since FY1995, ATLAS has made beams of short-lived rare isotopes (RIBs) available for nuclear physics research. A total of 19 different radioactive beams have been developed over those years and are generally available for use. Further development of RIBs is planned as required by the nuclear physics and nuclear astrophysics programs at ATLAS.

The proposal to create neutron-rich beams from fission fragments and accelerate those beams with the ATLAS accelerator, now known as CARIBU – Californium Rare Ion Beam Upgrade –

was approved and the project began on January 1, 2006. The total project cost is \$4.6M and the first beam is planned for the second quarter of FY2009.



Table II-1. Summary of ATLAS experiments and user statistics.

	<u>FY2006</u> (actual)	<u>FY2007</u> (extrap.)	<u>FY2008</u> (pred.)	<u>FY2009†</u> (pred.)
<u>Beam Use for Research (hr)</u>				
Nuclear Physics	5202	3370	4450	4350
Accelerator R&D (CARIBU & ATLAS)	31	*350	200	300
Accelerator Mass Spectroscopy	75	85	100	100
Other	<u>50</u>	<u>45</u>	<u>50</u>	<u>50</u>
Total	5358	3850	4800	4800
Number of Experiments Receiving Beam	46	36	40	41
Number of Scientists Participating in Research	411	311	368	368
<u>Institutions Represented</u>				
Universities (USA)	21	15	18	18
DOE National Laboratories	3	3	3	3
Other	32	20	26	27
<u>Usage of Beam Time (%)</u>				
In-House Staff	36	35	35	35
Universities (USA)	36	40	40	40
Other DOE National Laboratories	5	5	5	5
Other Institutions	<u>23</u>	<u>20</u>	<u>20</u>	<u>20</u>
Total	100	100	100	100

*Includes tests of the prototype RIA gas catcher system.

†Does not include stopped beam experiments.

A. OPERATION OF THE ACCELERATOR

a.1. Operations Summary (R. C. Pardo, D. Barnett, L. Carlquist, A. Deriy, G. Devane, R. Jenkins, A. Krupa, E. Lindert, S. McDonald, F. H. Munson, Jr., D. R. Phillips, M. Power, A. Ruthenberg, R. H. Scott, S. Sharamentov, P. Strickhorn, R. C. Vondrasek, and G. P. Zinkann)

ATLAS provided a total of 5358 hours of beam available to the research program in FY2006 and 5714 hours were scheduled for all operational activities during that period. The facility ran with a reliability factor of 94.3% for the fiscal year. The beam time exceeded the planned value for this year because of a delay in a planned major maintenance shutdown to install a new cryogenic refrigerator, a project described in more detail below. This shutdown did not occur until FY2007 and regular operation continued instead.

A record total of 38 different isotopes were provided during this period; the species distribution is shown in Fig. II-1. The focus of the research program continues

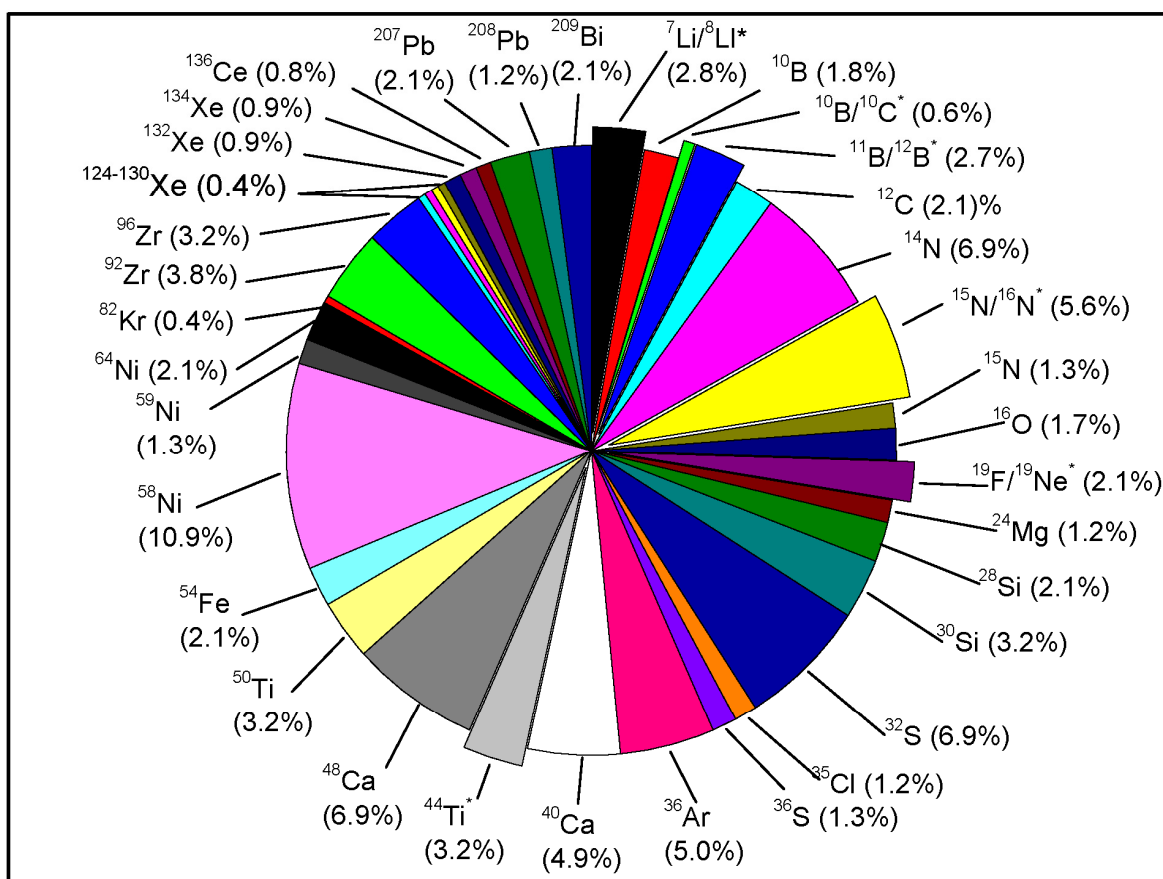
to be on the lighter elements with $A \leq 58$ accounting for ~80% of all beam time.

In-flight beams used in research for the first time included ^{12}B and ^{19}Ne . In FY2006, in-flight radioactive beams of ^8Li , ^{10}C , ^{12}B , ^{16}N , and ^{19}Ne as well as the longer-lived ^{44}Ti were provided. The total radioactive beam time provided for the year was 910 hours. Significantly improved transmission from the negative ion source to the Tandem allowed the available beam current for ^{44}Ti to increase to 2×10^6 ions/s reliably. Work continues on the development of an RF chopper for improved beam purity of in-flight RIBs with installation of that system planned for late 2006.

The CARIBU project, a major new initiative for the facility, will provide a wide array of far-from-stability neutron-rich beams. The project is now into its second year and has made excellent progress in all major areas. It is discussed in more detail in another section of this report. Although the project will draw on a large

number of ATLAS operations personnel to implement the project, we do expect normal ATLAS operations to continue, largely unaffected, until FY2008 when time will be required for early tests. A larger amount of time will be required when commissioning activities begin in FY2009.

ATLAS Beams for FY2006



* Radioactive Beams comprised 17% of running time

Fig. II-1. Distribution of beam time by isotope provided by ATLAS in FY2006. A record total of 38 different isotopes were provided to the research program. Radioactive beams (indicated by an asterisk) comprised 17% (910 hours) of all beam time in the fiscal year.

B. DEVELOPMENTS RELATED TO ATLAS

b.1. Status of the ECR Ion Sources (R. C. Vondrasek and R. H. Scott)

b.1.1. Refinement of the Sputter Technique

The sputter technique, which has been in use on the ATLAS ECR ion sources since 1994, has an inherent limiting factor in that it requires a relatively high gas pressure in the plasma chamber for adequate sputter yield. The high pressure limits the production of high-charge state ions as well as intense beams of the mid-charge states. When operating with the sputter probe for large beam currents (100 μA of Pb^{23+}) the pressure increases to 3.0×10^{-7} due to the higher sputter yield required, and this higher pressure negatively impacts overall source performance. When optimizing for high charge state production, the operating pressure is

typically 1.0×10^{-7} Torr, but then the sputter yield decreases due to an insufficient amount of gas in the region of the sputter probe and large beam currents ($>10 \mu\text{A}$ of Pb^{37+}) cannot be achieved. To mitigate this limitation, a technique has been developed to lower the overall pressure in the plasma chamber by introducing the working gas at the tip of the sputter sample. This has the effect of introducing the gas in the region it is most needed for a good sputter yield as opposed to diffusing throughout the entire plasma chamber.

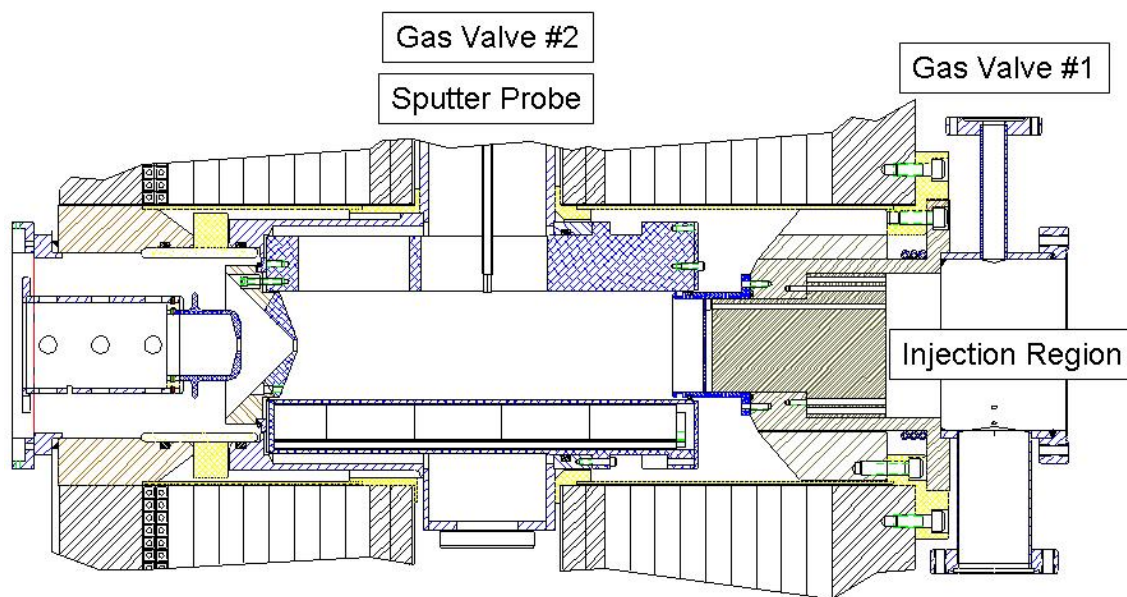


Fig. II-2. Sputter probe configuration on ECR2. The gas from Valve #1 diffuses into the plasma chamber via the injection region. The gas from the Valve #2 flows into the plasma chamber directly from the sputter probe.

In operation, the main plasma support gas is introduced through a valve mounted on the injection region tank. The sputter support gas is then introduced directly at the sputter probe tip using a second gas valve. This has the effect of decoupling the plasma support gas (Valve #1) and sputter support gas (Valve #2) levels and providing an increased local pressure at the probe tip where it is needed for an adequate sputter yield. The gas flows through a stainless steel tube which holds the

sputter sample and is introduced into the plasma chamber through a 0.5 mm diameter hole in the sputter sample, shown in Fig. II-2.

The source was run in two-frequency heating mode ($14 + 10.85$ GHz) with the total RF power level kept constant at 500 W. The extraction voltage was 14 kV, and the solenoid coil currents were not varied between runs. A natural lead sample was used with the sputter

voltage kept constant at -0.28 kV (0.1 mA drain).

The results from the two operating modes are shown in Table II-2. With the gas flowing in only through the injection region (Valve #1), the total source drain current was 1.07 mA with a vacuum of 1.0×10^{-7} Torr. With the gas flowing in only through the sputter sample

(Valve #2), the total drain current decreased to 0.83 mA, reflecting the decrease in the amount of gas within the plasma chamber, and the vacuum increased to 1.4×10^{-7} Torr in the plasma tank. This measurement is outside of the plasma chamber and at this level may not accurately reflect what is occurring within the plasma chamber itself.

Table II-2. Beam Intensities for ^{208}Pb .

Charge state	Intensity (μA) using Valve #1	Intensity (μA) using Valve #2
31+	6.75	9.67
32+	6.00	8.36
33+	4.88	6.88
34+	3.95	5.59
35+	3.00	4.22
36+	2.08	3.04

As can be seen in the table, the beam currents for the highly charged ions (HCI) of lead increased on average by 42%. This demonstrates that the technique of lowering the base pressure within the plasma chamber

by introducing the working gas at the sputter sample location improves the HCI production. More tests are scheduled to determine the effect on the mid-charge state production.

b.1.2. Source Liner Development

The measurement of ^{39}Ar in ocean water samples has been an ongoing process hampered by the prevalence of potassium in the ion source. The potassium problem was addressed by installing a quartz liner in the ion source, thus, reducing the background level by a factor of 130. But this also had the detrimental effect of reducing the beam intensity due to the inadequacies of quartz as a plasma chamber material. In collaboration with a group at Princeton University, a new ultra-pure aluminum liner was fabricated with a measured bulk potassium contaminant of <10 ppb.

First, a baseline measurement of source performance for $^{40}\text{Ar}^{8+}$ was performed. After a few days of conditioning, $490 \mu\text{A}$ of $^{40}\text{Ar}^{8+}$ was extracted from the source without a liner in place. Then the ultra-pure aluminum liner was installed and conditioned for several days. At 250 W of power, $340 \mu\text{A}$ of $^{40}\text{Ar}^{8+}$ was achieved. This is a factor of 4 higher than the previous best beam current with a quartz liner. It is hoped that the potassium level in the source will be reduced by either the same amount or greater as when the quartz liner is in use.

b.2. ATLAS Control System (F. H. Munson and M. Power)

b.2.1. ATLAS Operations Databases and Communication Improvements

A project to provide a web-based ATLAS “bulletin board” is underway. With one of its planned primary displays located in the ATLAS control room, this bulletin board will be used to convey instructions and generally distribute information primarily regarding ATLAS operations to the ATLAS operators.

ATLAS maintains a relational database management system called Hercules. The system is comprised of three separate databases. These include the “operator shift log”, an “equipment maintenance log”, and a

“mechanical and electrical drawing index”. As part of an on-going project to retire this system, the functionality of the mechanical and electrical drawing index portion of the system has been replaced by a web-based application that interfaces to the open source MySQL relational database management system. This system has the added advantage of being able to link to the actual drawing indexed in the database for viewing if the drawing file exists. This feature was not available in the older Hercules system.

b.2.2. ATLAS Hardware Upgrade Project

CAMAC (Computer Automated Measurement and Control) is the I/O (Input-Output) hardware subsystem architecture historically used at ATLAS. Acquiring CAMAC modules used at ATLAS that provide a GPIB (General Purpose Interface Bus or IEEE488) interface or a Serial Line (RS-232) interface has become cost prohibitive. One solution is to replace the functionality of these particular CAMAC modules with an Ethernet “gateway” that provides a connection between the ATLAS control system LAN (Local Area Network) and devices that use the GPIB or RS-232 interface. Prototype software that interfaces this gateway to Vsystem has been written to test the feasibility of this approach.

In addition to the GPIB and RS-232 CAMAC modules mentioned previously, CAMAC modules in use at ATLAS in general are becoming unavailable from manufacturers, or are becoming too costly to acquire and repair. Motivated by the new CARIBU (Californium Rare Ion Breeder Upgrade) project, it has been decided that a CAMAC alternative should be found. The overall goal is to limit or eliminate the need for purchasing new CAMAC equipment except for some unexpected special need. This would be accomplished by replacing CAMAC equipment with alternatives in those systems that can be isolated, and operated more or less independently, retaining the replaced CAMAC equipment (crates and modules) as spares.

A significant amount of time has been devoted to researching an alternative. After much consideration it has been decided that one or more of the three architectures or bus structures that will be used for CARIBU, and future ATLAS projects, include a commercially available IOC (Input Output Controller), VME64x (Versa Module Eurocard 64-bit Extension), and cPCI (Compact PCI). Initial focus has been on the IOC and the VME64x approach. Both of these bus structures (as well as cPCI) support the pseudo IP (Industry Pack) standard.

Industry packs are self contained modules providing several different I/O options and typically come in two sizes. The size being considered for use at ATLAS is the standard 1.8 × 3.9 inch module.

The IOC is a 1U (1.75”) high rack mount unit that employs a PC/104 CPU (Central Processing Unit) module that provides all of the typical SBC (Single Board Computer) features, such as an Ethernet controller, USB (Universal Serial Bus) controller, HDD (Hard Disk Drive) controller, graphics adapter controller, and keyboard and mouse interfaces. The IOC has provisions for supporting up to as many as six industry packs. This is approximately one third the I/O capability of the standard CAMAC crate currently used at ATLAS.

The VME64x approach utilizes a standard PC mounted in a 1U high rack mount chassis configured with a PCI module capable of interfacing to a VME64x crate controller. Through the use of “carrier modules” a single slot in a VME64x crate can accommodate up to four industry packs. With one slot being devoted to the crate controller, a seven slot crate could support up to four times the number of industry packs provided for by the IOC. This is almost equal to the I/O capability of the standard CAMAC crate currently used at ATLAS.

The current plan is to use IOCs in those applications where space is at a premium and required I/O is minimal, and use VME64x crates where use of the IOC is not suitable.

An IOC and a VME64x crate have been acquired. Analog I/O, digital I/O, RS-232 I/O, and stepper motor controller IPs have been acquired as well. Prototype software to interface to Vsystem for testing and evaluation purposes has been written. To date, Vsystem software handlers have been written to test monitoring or controlling devices requiring 16-bit ADC I/O, 16-bit DAC I/O, 48-bit digital I/O, RS-232, and stepper motors.

b.3. ATLAS Electronics (S. Sharamentov)

b.3.1. RF Amplifier Replacement

Sixteen new RF amplifiers (see Physics Division Annual Report 2005, page 113) were built and installed in two Booster RF racks, bringing the total number of modified RF racks to 3. Three more racks, one in the Booster and two in ATLAS, will be modified in 2007-2008. Additional improvement was the

installation of 97 MHz band pass filters in the resonator's pick-up lines. These filters suppress the 104 MHz split ring resonator mode and the easing process of locking the self-exciting resonator oscillations to a master frequency.

b.3.2. Tandem Electronics Upgrade

The old electronics for the Tandem multi-harmonic buncher was replaced with new I and Q RF controller systems identical to the previously installed (see Physics Division Annual Report 2004, page 142) PII multi-harmonic buncher system.

A new four channel high voltage power supply chassis, replacing old power supplies, was designed and built. Each channel is based on Ultravolt A – 25A series high voltage DC-DC converters, covering the output voltage

range positive or negative polarity from 0 to 25 kV, and up to 30 W of output power. This power supply features a flexible channel configuration design allowing for independent control of all four channels, two pairs of precisely tracking each other master-slave channels or combination of two independent channels and one pair of master-slave outputs, of plus or minus polarity. Figure II-3 shows the new chassis with four output channels

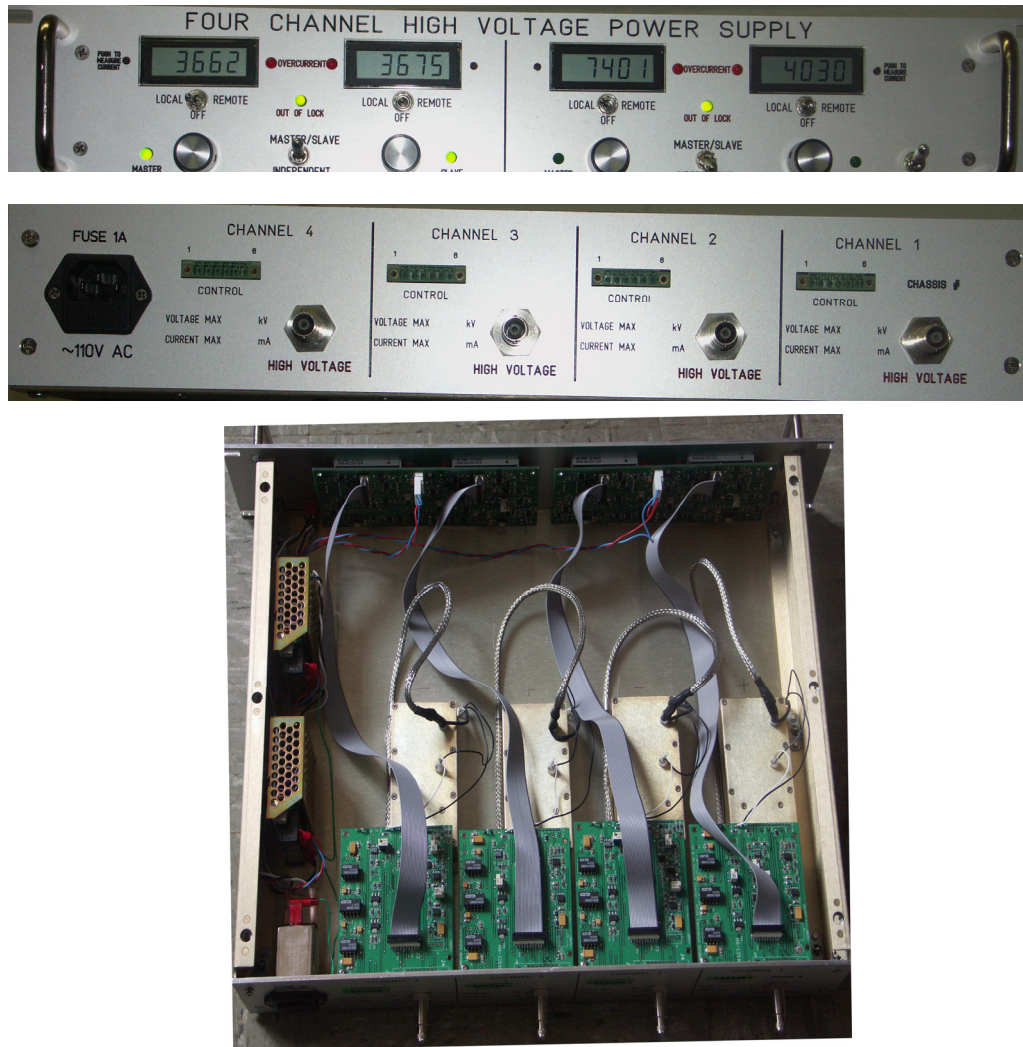


Fig. II-3. Front, rear and top view of the four channel power supply. The power supply was installed in the Tandem area as the QET002 quadrupole power supply.

b.4. Slow Tuner System with High Slew Rate (G. Zinkann and S. Sharamentov)

The Argonne Tandem Linear Accelerator System (ATLAS) superconducting cavities use a pneumatic system to maintain the cavity eigenfrequency at the master oscillator frequency. The present pneumatic slow tuner control has a limitation in the tuning slew rate. In some cases, the frequency slew rate is as low as 30 Hz/sec. The total tuning range for ATLAS cavities varies from 60 kHz to as high as 450 kHz depending on the cavity type. With the present system, if a cavity is at the extreme end of its tuning range, it may take an

unacceptable length of time to reach the master oscillator frequency. We have designed a new slow tuner control system that increases the frequency slew rate by a factor of three hundred in the most extreme case.

A single channel slow tuner prototype system was developed two years ago. The single channel system was tested on an on-line superconducting cavity. The results of this test were used to develop a six channel

unit. This six channel unit, shown in Fig. II-4, is capable of controlling six SC cavities in one ATLAS cryostat.

six channel slow tuner system on the A-cryostat and a portion of the B-cryostat resonators, and we plan to expand this to the remainder of the system in subsequent years.

In January 2007 we will install the final version of the



Fig. II-4. The electronic control system for the six channel control unit.

b.5. ATLAS Cryogenic System (S. MacDonald and R. Jenkins)

b.5.1. Installation of an Additional 2800 Refrigerator

An Accelerator Improvement Project (AIP) to increase the refrigeration capacity and improve reliability and overall performance of the ATLAS cryogenic system was undertaken in late 2006. The \$173k project planned to use a CTI Model 2800 cold box that was acquired from Lawrence Livermore National Laboratory in late 2001. The project was to replace the Model 1630 refrigerator with this unit, which will increase the overall capacity of the cryogenic system by approximately 100 watts and to make other improvements to the helium distribution system for added reliability and capacity. This increase in capacity will allow the operation of the ATLAS upgrade cryostat

at planned fields, as well as provide an increased operating margin which should decrease cryogenic downtime.

The refrigerator was removed from storage in April 2006 and found to have incurred extensive damage during shipment. This refrigerator was also found to have many leaks caused by poor fabrication techniques and corrosion. The repairs of these leaks consumed a period of seven months that was not planned for. Eventually, all leaks were repaired. The refrigerator was then rewired and outfitted with a remote wet engine operation device, a JT valve controller, new

thermometry readouts and a redesigned liquid nitrogen control system. The rebuilt refrigerator, shown in Fig. II-5, was then successfully tested using local

utilities and one of the spare RS compressors in November and December 2006.



Fig. II-5. CTI Model 2800 – 300 Watt liquid helium refrigerator shown after installation in the ATLAS facility.

Engineering and planning of the 2800 installation was completed during the refrigerator repair period. Integration designs were finalized, the cold lines were fabricated and the procurement of high lead-time items was accomplished. A vacuum break to separate the PII and booster sections was also designed. This break, along with the 2800 installation, would effectively separate the insulating vacuum portions of the three accelerator sections. This separation will allow each of the sections to be warmed independently, allowing

greater flexibility in maintenance, upgrades and operating.

In late December 2006 the facility entered a long maintenance period for the final installation. The first operation of the installed system began in February and ATLAS returned to operation in March. In the end, the installation was highly successful and the cryogenics system is operating extremely well.

b.6. A 50-kV RF Chopper for In-Flight RIB Beams (J. Bogaty, R. C. Pardo, and S. I. Sharamentov)

Work has continued on the RF Chopper project whose goal is to improve the in-flight RIB beam cleanliness by removing the primary beam tails. The vacuum chamber for the chopper is complete and work is now

proceeding on completion of the RF control electronics and the resonant tuning circuits for the chopper. The system is expected to be ready for installation by November 2007.

b.7. Californium Rare Ion Breeder Upgrade Project (CARIBU) (R. Pardo, G. Savard, S. Baker,* C. Davids, T. Levand, D. Phillips, F. Munson, M. Power, A. Ruthenberg, S. Sharamentov, T. Sun, R. Vondrasek, B. Zabransky, and G. Zinkann)

The Californium Rare Ion Beam Upgrade (CARIBU) for the ATLAS facility is under construction. The facility will use ^{252}Cf fission fragments thermalized and collected into a low-energy particle beam by a helium gas catcher, mass analyzed by an isobar separator, and charge bred to higher charge states for acceleration in ATLAS. In addition, unaccelerated beams will be available for trap and laser probe studies. A $1\text{Ci } ^{252}\text{Cf}$ source will provide sufficient yield to deliver accelerated beams of up to $\sim 5 \times 10^5$ (10^7 to traps) far-from-stability ions per second on target.

The CARIBU Project Implementation Plan was signed on December 23, 2005 and the project began formally on January 3, 2006. The project can be thought of as consisting of seven major activities, that in early stages largely can progress independently. Those activities are:

1. Source and shield cask
2. Gas catcher and RFQ system
3. Isobar separator
4. High voltage platform
5. Electron cyclotron resonance (ECR) charge breeder ion source
6. Weak beam diagnostics
7. Building enhancements required by the CARIBU project

This year the dominant effort has focused on design and engineering of these major components, safety reviews that provide input to the design and engineering effort, and R&D activities associated with designing a gas catcher system that can handle larger space charge forces than has been required in previous applications. The building footprint is being expanded by the construction of a new space (a separate project that is not part of CARIBU). Activities this year also include designing, procuring and installing enhancements to that space required by the CARIBU project. Good progress has been made in all of these major subsystems and we are now entering an intense construction and procurement phase for most of these systems.

A total of ten project milestones were scheduled to be met during the past year and 8 of those have been achieved. The remaining outstanding milestones are associated with completion of the design of the gas catcher, source holder, and cask. These reviews are planned to take place by late February 2007.

We are now entering a period of major procurement activity. Bids for two major procurements, the isobar separator dipole magnet systems and the high voltage platform, are now beginning solicitation. In addition, procurements associated with the ECR charge breeder (CB) project and the building facilities enhancements are well advanced.

Detailed Discussion of the Major Components of CARIBU

ECR Charge Breeder

This major activity institutes modifications to change an existing ECR ion source (ECR-I) into a charge breeder ECR source. Modifications include changes to the "injection region" iron, RF waveguides and other

components to provide a pathway into the plasma for the low-charge-state ions from the isobar separator. The ions are then decelerated and trapped in the plasma, charge bred and extracted at higher charge states,

sufficient for acceleration in ATLAS. In addition to these changes, new 1+ stable beam sources are being constructed to serve as a source of stable beams for development and setup of the ECR CB. In addition, the beam transfer from the CARIBU isobar separator has been modeled and the beam deceleration optics into the CB has been studied resulting in a final design for ion transfer into the CB.

Early in the project a major change in the preliminary plans was made regarding source operating voltage. After significant internal review, discussion and preliminary tests, it was decided to redesign ECR-I with the goal of operating the source at 50 kV. By operating the source at this potential, a significantly simpler gas-catcher isobar-separator beam optics is possible. All

Source and Shield Cask Assembly

The source and shield cask assembly provide shielding to the ^{252}Cf source as well as mechanisms to manipulate the source to move it from a storage position to the operating position at one end of the gas catcher system. In addition, the shield cask is designed to function as an on-site transportation cask for movement of the source from the Building 200 M-wing hot cell area over to the CARIBU facility. The design of the shielding system is intended to allow personnel access to the CARIBU building area and the area around the cask on the high-voltage platform.

The activity on this major subsystem has focused on understanding the safety requirements that must be met in order to handle a 1 Ci ^{252}Cf source and the design of the shielding and handling system. A laboratory ALARA review of the CARIBU Project was conducted on October 28, 2005. This was done at a very early stage before the project was approved by DOE. The trigger for the review was the concern that an airborne release of ^{252}Cf could result in a large radiation dose to an individual, primarily by inhalation. The maximum credible incident or worst case accident scenario was discussed and the mitigation measures were considered to prevent a large dose. The ALARA Committee Chair issued a memo with recommendations and with concurrence for specification of a sheet-metal building addition to the ATLAS accelerator. Local source shielding will be used rather than a concrete building.

High Voltage Platform

In order to accelerate ions in the ATLAS linac, an ion must have a velocity of $\sim 0.008c$ to match the velocity profile of the first resonator. This is achieved by

tests indicate operation at this voltage should be possible. This decision is supported by noting that two other ECR source projects are operating at 60 kV bias voltage.

This year, the final design for the system was finalized and a design and safety review of the system was held on August 3-4. Comments from the review committee were incorporated into the final plans and procurement and construction activity was initiated. It appears that the rebuilt source will be able to turn on in a normal operating mode in May 2007 and charge breeder tests with stable beams should be initiated by summer 2007, approximately 3-4 months ahead of the project schedule.

This review was followed by an Integrated Safety Review of the project in January 2006 by an ad-hoc committee appointed by the Physics Division Director in response to a recommendation of the TCMS project review. The resulting report gave overall concurrence to the preliminary cask and shield design ideas and provided other recommendations giving guidance concerning various important issues to address as the design went forward.

In the ensuing months up to the present, the designs of the source mount and shielding cask have gone forward. That design effort is essentially finished with final design drawings for most of the system available. The system is now ready for a final design and safety review. This review is now planned for late February 2007.

In addition to the cask and source holder design, a storage can for the shipping cask to hold the source when it is shipped from Oak Ridge to ANL has been designed. The design has been reviewed by ORNL personnel. Although certification is not required, a can must be fabricated and pass ASME-specified testing. Fabrication and testing is planned for the second quarter of 2007. Preliminary plans and procedures have been developed for transfer of the ^{252}Cf source from the shipping cask to the local shield cask.

mounting the ECR ion source on a high voltage platform. For fission fragments from CARIBU, a maximum total voltage of 250 kV is required. This

requirement means that the ^{252}Cf source and all associated equipment must also be biased to that voltage. Thus, the source, shield cask, isobar separator and associated equipment are mounted on a new HV platform designed for a maximum operating voltage of 200 kV (50 kV comes from the local additional bias of the ^{252}Cf source and the ECR charge breeder ion source). This new HV platform design is based on the design of the existing platforms, but the dimensions are set by the equipment required (shield cask, gas catcher, isobar separator and associated equipment). The platform height is constrained by the facility beamline height of 69" and the shielding requirements of the source. Thus, although the basic platform design was easily specified, the exact dimensions were strongly coupled to the designs of the other equipment occupying the platform. This was largely due to the large amount of shielding needed around the source constraining the platform elevation and the large space needed by the gas catcher system and isobar separator

Gas Catcher System

The gas catcher system must stop and thermalize the fission recoils and transform them into a cooled low-energy ion beam for injection into the isobar separator. The gas catcher must operate at large ionization density (similar to those that will be present at RIA/AEBL) and a major thrust early in the project was the completion of a (out of project but emphasized by the TCMS review) high-intensity test demonstrating operation under such conditions. The test was performed on a new beamline in experimental area II at ATLAS that was completed and commissioned during the year and performed using a gas catcher with RF focusing along the full body and the extraction cone. The gas catcher used had a length of 85 cm, similar to what will be used for the CARIBU gas catcher, an inside diameter of 25 cm, and was operated at pressures of 100-200 mbar as required for CARIBU. The activity extracted from the device was monitored as a function of primary beam current and showed essentially no loss in efficiency up to 10^8 incoming ions per second followed by a slow decrease with further increase in intensity and still about 10% efficiency at 10^9 ions per second. These tests, performed from October to December 2006, demonstrated successful efficient operation at 3 to 4 orders of magnitude higher intensity than previously achieved and confirmed the validity of the approach being developed for the CARIBU gas catcher. The high-intensity gas catcher used for these tests had

which made it desirable to build the platform without significant extra space.

Therefore, finalizing the platform design was delayed into December, beyond the anticipated date, when the final overall dimensions of the other equipment, including elevation, were agreed upon. In order to accommodate the necessary radiation shielding and the required diameter of the gas catcher, the platform floor is only 26.5" off the building floor, but this will be sufficient for the required 200 kV bias and is well within the rated standoff voltage of 275 kV for the insulated feet.

The design of the platform is now complete and is in the procurement process. The forecast for completion of the platform is early August 2007. Following completion of the platform, electrical distribution, chilled water and other utilities must be supplied to the platform.

additional features to improve the outgassing of the device and the uniformity of the RF fields and those are being implemented in the final design of the CARIBU gas catcher. Detailed simulations were performed to find the optimum size for the CARIBU gas catcher and we settled for the 85 cm stated above and a larger diameter of 50 cm. This yields sufficient stopping range to limit the number of required degraders to 3 to cover all fission fragments. Transfer of the source from the cask to the gas catcher will take place through an all-metal valve using a UHV compatible shielding plug that will not compromise the vacuum requirements. Transport of the radioactive ions extracted from the gas catcher must be performed through focusing structures to remove the remaining gas and form a low emittance beam. Simulations of this section were performed by a new CARIBU post-doc, Dr. Tao Sun, that started with the project in October 2006. Using two sections of RFQ separated by microRFQs, followed by acceleration to 50 keV and focusing through a 1 mm aperture, yields enough differential pumping to remove most of the gas before acceleration and form a low-emittance beam with properties suitable for the operation of the isobar separator. The whole RFQ-acceleration-focusing section is just under 1 m long and feeds directly into the matching section at the entrance of the isobar separator.

Isobar Separator

The isobar separator design relies on the extremely low transverse emittance expected from the gas catcher/RFQ system as well as the corresponding low energy spread for ions extracted. Because of these excellent beam properties it is possible to design a relatively simple, single stage, isobar separator which still is expected to achieve a mass resolution of approximately 1/20,000 without energy compensation.

The activity associated with the isobar separator this year has been to finalize the beam optics design of the separator, present that design in a design review corresponding to Project Milestone 8, and begin the procurement of the long lead-time dipole magnets. In addition, the detailed design of the multipole high-order correctors has been initiated and work on the vacuum chamber is now underway.

A design review of the isobar separator took place on October 11, 2006. This review focused on the detailed beam optics design of the system and the detailed choices made regarding focusing elements and corrector elements. Most importantly, the decision to use electrostatic quadrupoles for first order focusing and high order electrostatic multipole elements was

Weak Beam Diagnostics/ATLAS Facility Enhancements

We plan to install two tape stations in the low-energy region of the CARIBU facility to identify the isotopic species selected by the isobar separator. One tape station is planned on the unaccelerated beamline, after the isobar separator, and a second station will be installed after the ECR charge breeder to allow species confirmation at that location as well. No work on these systems has begun, but we plan to modify an existing design developed for the CPT existing trap facility.

In order to efficiently develop accelerated beams through the ATLAS facility, we plan to perform initial setups using similar m/q stable beams with intensities that allow use of existing diagnostics. After scaling to the desired beam, weak beam diagnostics are required to check that the correct species has been selected, to optimize transmission, and to check operating conditions periodically throughout a run. The planned diagnostics include weak beam profile monitors, particle counters, and energy and time detectors.

This year work has progressed by exploring diagnostics options and developing prototypes of those options. A secondary electron emission, MCP amplifier, and

endorsed.

The procurement specifications for the dipole magnets, power supplies and NMR gaussmeters were finalized in December and the procurement process has now been initiated. Delivery of the magnets is forecast for June 2008.

The beam optics into and out of the separator design use electrostatic focusing elements. Electrostatic quadrupoles form the entrance waist into the system and set the beam divergence into the dipole magnets as shown in Fig. II-6. A symmetric set of lenses reform the exit waist where the mass selection is made. Sextupoles in the entrance and exit region and a 48-element electrostatic high-order multipole corrector control aberrations sufficiently to achieve the design mass resolution. A design for the electrostatic quadrupole and sextupole systems has been developed and cost estimates for constructing these devices in local machine shops are being obtained. The design of the high order correcting multipole element between the two dipoles is continuing at this time. A final design for the multipole is expected by February 2007.

scintillator coupled to a CCD digitized camera previously developed at ATLAS has been installed and re-commissioned. The device, shown in Fig. II-7, had been demonstrated in live time down to approximately 1000 ions/s and is now being interfaced into a computer to allow signal integration and averaging to improve its sensitivity even further. This device has also been modified to provide a direct pulse for every ion detected to allow a rate to be extracted without computer analysis and provide live time response at almost any rate.

An alternative system, replacing the scintillator/CCD detector with a resistive-division two-dimensional anode to provide the X-Y beam profile, has been ordered for evaluation from Quantar Technology. This system will be very similar to one in use at Oak Ridge National Laboratory developed by D. Shapiro.

In addition, a simple phosphor screen coupled to an extremely sensitive CCD camera (without an MCP amplifier) will be tested for maximum sensitivity. This system has been purchased and will be tested when ATLAS resumes operation in February.

In addition to these weak beam diagnostics, silicon detectors will be mounted throughout the system to determine the energy and timing properties of the beam. A simple prototype diagnostics chamber has been designed and is under construction to be installed in the spectrograph beamline for testing in February.

We plan to finalize our diagnostic choices for the ATLAS system in the next 9 months and begin procurement and construction of all diagnostics in FY2008. The total procurement budget for this activity is \$200k.

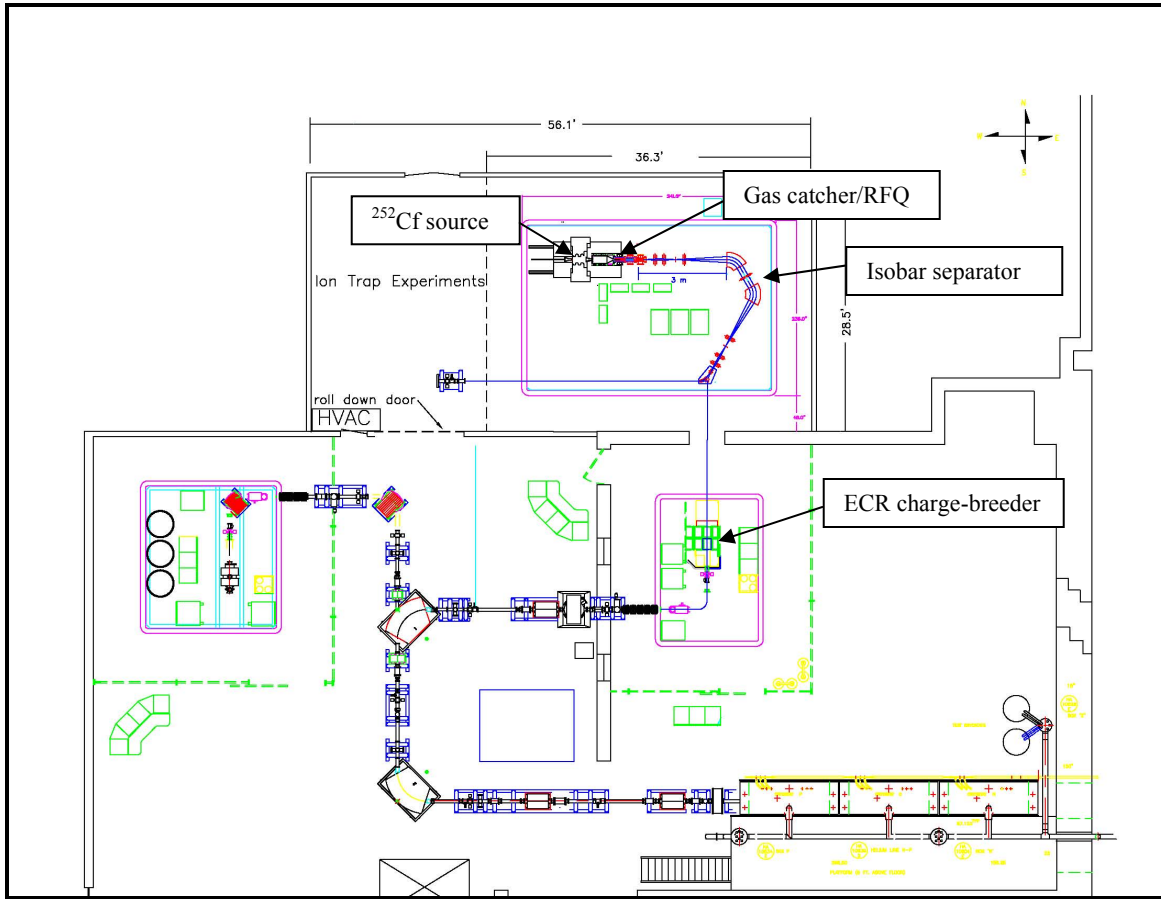


Fig. II-6. Layout of the major components of the CARIBU project. The relationship between the source and shielding, gas catcher/RFQ cooler, isobar separator, and ECR charge breeder is indicated. Not shown are the unaccelerated-beam trap equipment and the stable beam 1+ platform and sources that are used to develop the charge breeder performance.

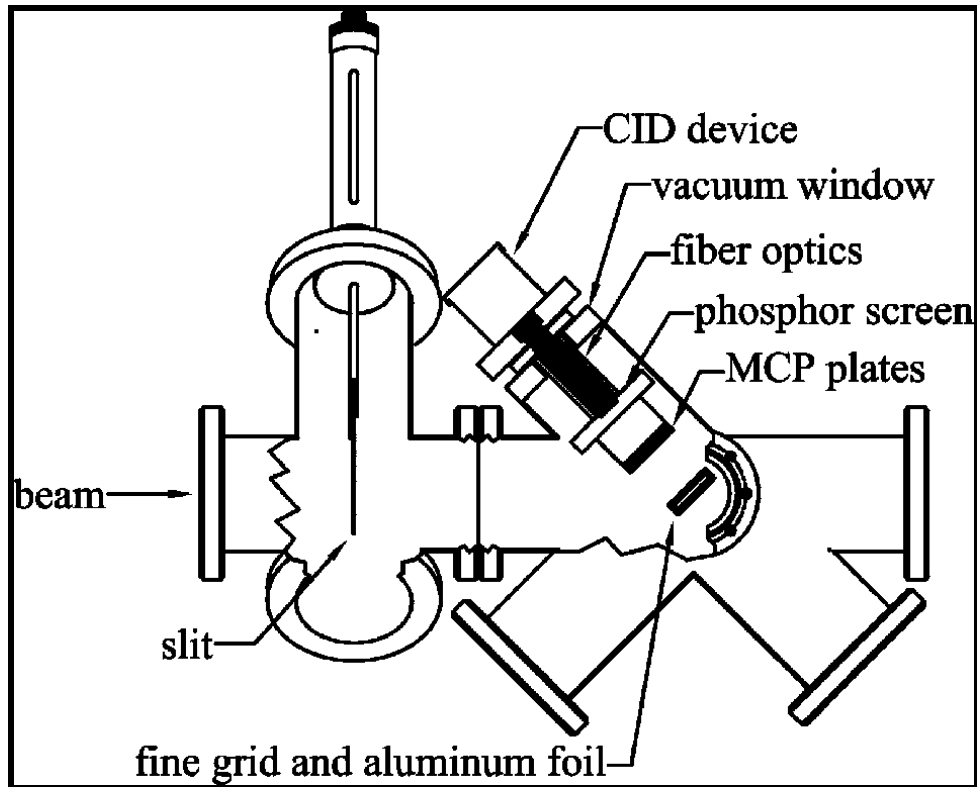


Fig. II-7. Sketch of the main components for a weak-beam diagnostics profile detector and beam counter under evaluation for CARIBU.

Building Expansion and Facility Enhancements

The californium source and other equipment on the new high-voltage platform will be housed in a new building addition, not part of the CARIBU project, which also will provide a small experimental area for the unaccelerated beam experiments. Certain facility enhancements are required in the new building for the operations of CARIBU. These enhancements include a 2-ton crane, additional electrical service of approximately 100 kVA, a HEPA exhaust and filter system, a roll-up door for room isolation, and a hole in the existing concrete wall for the connecting beamline between the CARIBU platform and the ECR charge breeder. The building is now complete and all of the facility enhancements are expected to be in place by February 15.

The building, shown in Fig. II-8, was largely completed by late November, approximately six weeks later than planned originally, but the remaining enhancements are delayed by approximately three additional months due to a variety of procurement snafus. The final feature, additional electrical power needed by the CARIBU,

will be installed in January 2007. These delays have not caused any significant delay in the project, partly because of our own delays in finalizing the specifications for the high-voltage platform as previously discussed.

Safety reviews of the building expansion and facility enhancements have included considerations of possible scenarios associated with a worst case release of radioactive materials from the californium source. These reviews and analyses have included a NEPA analysis, fire hazard analysis, and a maximum credible incident analysis which envisioned the release of materials due to a plane crash into the building. The results of these analyses have been incorporated into the design of the various components surrounding the source – the shielding cask, the HEPA exhaust system, high voltage isolation and room isolation design.

Thus, the room containing the californium source will remain generally isolated from the rest of the ATLAS facility. A negative pressure will be maintained in the

new space. The space will be exhausted by the 1500 CFM HEPA exhaust system filtering out most radioactive particulates from the stack effluent. The

HEPA exhaust stack is 30 feet high assuring adequate dispersal of radioactive noble gases as well as any accidental release.

*EQO Division, Argonne National Laboratory.



Fig. II-8. Building addition for the CARIBU facility. The addition is funded as a separate laboratory project.